Development of a microRNA Delivery Scaffold System for Bone Tissue Engineering

AUTHOR(S)

Irene Mencía Castaño

CITATION

Castaño, Irene Mencía (2015): Development of a microRNA Delivery Scaffold System for Bone Tissue Engineering. Royal College of Surgeons in Ireland. Thesis. https://doi.org/10.25419/rcsi.10808552.v1

DOI

10.25419/rcsi.10808552.v1

RCSI

2015

Development of a microRNA Delivery Scaffold System for Bone Tissue Engineering

A thesis submitted to the School of Postgraduate Studies, Faculty of Medicine and Health Sciences, Royal College of Surgeons in Ireland, in fulfillment of the degree of

Doctor in Philosophy

Irene Mencía Castaño, BPharm, MSc

Department of Anatomy

Supervisors:

Dr. Caroline M. Curtin, Dr. Garry P. Duffy, Prof. Fergal J. O'Brien

Declaration

I declare that this thesis, which I submit to RCSI for examination in consideration of the award of a higher degree is my own personal effort. Where any of the content presented is the result of input or data from a related collaborative research programme this is duly acknowledged in the text such that it is possible to ascertain how much of the work is my own. I have not already obtained a degree in RCSI or elsewhere on the basis of this work. Furthermore, I took reasonable care to ensure that the work is original, and, to the best of my knowledge, does not breach copyright law, and has not been taken from other sources except where such work has been cited and acknowledged within the text.

Signed _____

Student Number 11112158_____

October 2015

Abstract

Although bone has an intrinsic capacity for self repair, the healing of large bone defects that typically present in humans often involves complications which result in failure to heal, leading to delayed or non-union of the defect. Due to limitations of current therapeutic approaches of autografting and allografting, the use of tissue engineered scaffolds has emerged. Despite some success with this approach, these scaffolds often require a further stimulus to promote complete healing of large bone defects. microRNAs (miRNAs) have recently emerged as promising therapeutics to stimulate bone repair, owing to their ability to intercept entire gene cohorts. However, the development of a safe and efficient localised delivery system is required for successful clinical translation of miRNA therapeutics to bone tissue engineering (TE). The overall goal of the research presented in this thesis was to determine the potential of using in-house synthesised nano-sized hydroxyapatite particles (nHA) to act as non-viral vectors for the delivery of a series of miRNAs to human (h)MSCs and to determine the combination leading to optimal osteogenesis and angiogenesis before ultimately producing miRNA-activated scaffolds capable of mediating enhanced osteogenesis by human MSCs.

In the study presented in Chapter 2 of this thesis, nHA particles combined with reporter miRNAs demonstrated potential as highly efficient and minimally cytotoxic non-viral vectors for the delivery of miRNA enhancers and inhibitors (miR-mimics and antagomiRs) to human MSCs. Single administration of low miRNA doses rendered very pronounced silencing activities to a level comparable to viral and lipid-based vectors and ultimately, a 20 nM dose was brought forward for further study. In Chapter 3, efficient nHA-based delivery of antagomiR-133a, antagomiR-16 and a miR-210 mimic, three targets identified to have particular therapeutic potential, enhanced osteogenesis by human MSCs. AntagomiR-133a emerged as the optimal osteo-therapeutic, while both antagomiR-16 and the miR-210 mimic were deemed worthy of further investigation.

In Chapter 4, the coll-nHA scaffolds demonstrated significant potential for the efficient localised delivery of both miR-mimics and antagomiRs to human MSCs, representing the first non-viral, non-lipid, ‘off-the shelf’ 3D system developed in the field. Additionally, antagomiR-133a activated scaffolds upregulated Runx2 and orchestrated accelerated calcium deposition, thus showcasing the osteo-therapeutic potential of this innovative strategy for bone TE applications. In Chapter 5, while the miR-210 mimic showed a limited pro-angiogenic therapeutic efficacy, the combinatorial delivery of the miR-210 mimic with antagomiR-16 demonstrated significant potential to simultaneously enhance the angiogenesis and osteogenesis capabilities of human MSCs. This dual formulation presents the first combinatorial miRNA approach harnessing these two processes and sits within seminal reports on the recently emergent field of combinatorial miRNA delivery.

Collectively, this thesis has demonstrated that nHA particles are able to deliver miRNAs with superior efficiency than that reported for other non-viral systems. When applied in 3D, a miRNA-activated coll-nHA scaffold with significantly enhanced therapeutic potential was achieved. Together with the demonstration of successful combinatorial miRNA delivery to harness both angiogenesis and osteogenesis, this underlines the immense potential of extending this platform to different fields of TE beyond osteogenesis and bone repair.

Table of contents

Acknowledgements

First and foremost, I would like to thank Dr. Garry Duffy and Prof. Fergal O'Brien for taking me on as a PhD student, it's been a privilege. I sincerely appreciate all of your guidance in getting me to this stage and the careful and committed reviewing in every aspect of this thesis. The enthusiasm in the progress of this project and the opportunities you offered while working here have been invaluable to me. I extend my sincere gratitude to Dr. Caroline Curtin for the continuous guidance and support from day one in all things lab related and of course for the many corrections that were invaluable to this work. It was a pleasure to work with you and I wouldn't have made it this far without your advice, positive energy and encouragement throughout the course of my PhD.

A special thanks to all in the Tissue Engineering Research Group, a genuinely nice and brilliant multicultural team who made working in RCSI the most fun: Amos, Tanya, Andrew, Janice, Johnny, Greg, Sara, Alan Ryan, Tijna, Will, Rukmani, Rob, Christina, David, Nicola, Conor, Paula, Emily, Amro, Orlaith, Cathal, Tatiane, Amir, Laura, Eduardo, Claire, Tommy and Kai. Past people: Tara, Ryan, Alan H, William Whyte, Mike, Adolfo, Emmet, Ash, Conn, Cai and Caroline Herron. Special thanks to the GC-4life clubbers and the 'Fabliss' girls for chats, laughs and all the very entertaining outings! A huge thanks goes especially to the office girlies past and present: Erica, Elaine, Rosie and Arlyng. Sharing office time with you meant daily inspiritment, and I also appreciate you not kicking me out for ranting too much and asking too many writing questions - specially Rosie! I also appreciate the help of Moose & Quinny for proof-reading in the final writing stage. I extend my gratitude to the students that helped out at the beginning of this research: Cáoimhe, Áine and Éanna. I am also grateful to Sadaf during the last months in the lab, for motivating me with a fresh scientific perspective and engaging in very interesting discussions. Special thanks to Adolfo and Eduardo for insight and discussion in pharma-related research. Thanks to the colleagues in the Trinity Centre for Bioengineering, to Clodagh and Niall in CMA Trinity for helping with SEM and TEM, and also huge thanks to Brenton for beautiful confocal imaging.

I would like to thank the BioAT RCSI bunch: Valerio, Ross, Éanna, Tádgh, Hugh, Cian, Cormac, Claire and Sinéad. Thanks for welcoming me from day one of the start of the PhD program and make PhD life very interesting to say the least! In this amazing experience I also have thank for their friendship and being there at all good and bad times to Natalia, Elena and Alba – Salá I'm going to miss your face in that lab! To the rest of the RCSI crew I've met through these years, and in particular to Eugenia, for making me discover DYDC and from there return to the joys of dance performing and whatever might come next! I am also grateful for all Spaniard buddies I found in Dublin, in and out of work, for being my home away from home. To the 'Gazpachos', for providing excellent distraction and super fun times and just for being there while I was writing this thesis. The understanding and support of my lifelong friends back home has also kept me writing, and now I'm ready for some serious catching-up!

Lastly, I am incredibly grateful for the never-ending love and support of my family. To my wonderful parents thanks so much for having my back during this experience and no matter what I do in life. Thanks for absolutely everything you have done for me in your life, all your hard work taught me to be who I am so this PhD is dedicated to you. To my grandparents, all cousins, and all the 'in-law' family, thanks for bringing me back to reality. Special thanks to my big little sister Alicia, you are the most talented and determined person I know, and have been also a big inspiration for me to pursue my dreams and goals in life. By extension thanks to Jon Lartey, el hoyo-man, for so many laughs, showtimes and a powerful and contagious life motto! Finally, to Pablo, thank you for betting for me and for holding my hand into and along this amazing journey. You have been my strength to go through this whole process and your confidence and grounding never failed to make things easier.

I also gratefully acknowledge financial support for this work provided by the BioAT PhD Programme, funded through the Programme for Research in Third Level Institutions Cycle 5 and the European Regional Development Fund, part of the European Union Structural Funds Programme 2007–2013.

Publications, Prizes and Presentations

Journal publications

I. Mencía Castaño, C.M. Curtin, G. Shaw, M.J. Murphy, G.P. Duffy, F.J. O'Brien (2015), A novel collagen-nanohydroxyapatite microRNA-activated scaffold for tissue engineering applications capable of efficient delivery of both miR-mimics and antagomiRs to human mesenchymal stem cells. *Journal of Controlled Release* 200:42-51.

I. Mencía Castaño, C.M. Curtin, G.P. Duffy, F.J.O'Brien (2015), Scientifically Speaking: Nanohydroxyapatite-based microRNA delivery on collagen-nanohydroxyapatite scaffolds for bone tissue engineering. *Controlled Release Society Newsletter* 32(4):eprint.

I. Mencía Castaño, C.M. Curtin, G.P. Duffy, F.J.O'Brien (2015), Next generation bone grafting: non-viral inhibition of miR-133a using collagen-nanohydroxyapatite microRNA-activated scaffolds rapidly enhances osteogenesis by human mesenchymal stem cells. *Manuscript submitted.*

R.M.Raftery, **I. Mencía Castaño,** David P. Walsh, S.A. Cryan, F.J. O'Brien (2015), Materials Science in Ireland: Delivering nucleic-acid based nano-medicines on biomaterial scaffolds: challenges, progress and future perspectives. *Manuscript in preparation for invited contribution to Advanced Materials.*

Prizes

RCSI Alumni Travel Award to attend Orthopaedic Research Society Annual Meeting (2015): ORS 2015 Annual Meeting, Las Vegas, Nevada, US, microRNA-activated scaffolds for enhancing bone formation by mesenchymal stem cells through the regulation of osteogenic genes.

Travel Award to attend Controlled Release Society Annual Meeting (2014): 41st Annual Meeting & Exposition of the Controlled Release Society Meeting, Chicago, Illinois, U.S., Nanohydroxyapatite-based microRNA delivery on collagen-nanohydroxyapatite scaffolds for bone tissue engineering.

First Prize for Best Overall Post-graduate Student Poster Presentation (2013): RCSI Annual Research Day, Dublin, Ireland, Nano-hydroxyapatite particles as novel non-viral microRNA delivery vectors for bone tissue engineering applications.

International Conferences

I. Mencía Castaño, C.M. Curtin, G.P. Duffy, and F.J. O'Brien (2015). Regulation of osteogenic genes using microRNA-activated scaffolds to enhance mesenchymal stem cell osteogenesis.
42nd Annual Meeting & Exposition of the Controlled Release Society, Edinburgh, Scotland.

I. Mencía Castaño, C.M. Curtin, G. Shaw, M.J. Murphy, G.P. Duffy, and F.J. O'Brien (2015). microRNA-activated scaffolds for enhancing bone formation by mesenchymal stem cells through the regulation of osteogenic genes.
ORS 2015 Annual Meeting, Las Vegas, Nevada, U.S.

I. Mencía Castaño, C.M. Curtin, G.P. Duffy, and F.J. O'Brien (2014). miRNA-activated scaffolds for enhancing mesenchymal stem cell osteogenesis.
8th UK Mesenchymal Stem Cell Meeting and International Conference On Stem Cell Translation, Galway, Ireland.

I. Mencía Castaño, C.M. Curtin, G.P. Duffy, and F.J. O'Brien (2014). Nanohydroxyapatite-based microRNA delivery on collagen-nanohydroxyapatite scaffolds for bone tissue engineering.
41st Annual Meeting & Exposition of the Controlled Release Society Meeting, Chicago, Illinois, U.S.

I.Mencía Castaño, C.M.Curtin, G.P. Duffy and F.J. O'Brien (2014). Collagen-nanohydroxyapatite scaffolds as delivery platforms for microRNA-based bone tissue engineering.
UK & Ireland Controlled Release Society Annual Symposium, Cork, Ireland.

I.Mencía Castaño, G.P. Duffy, C.M.Curtin and F.J. O'Brien (2013). Use of nanohydroxyapatite particles for microRNA delivery in bone tissue engineering.

6th European Chapter of the Tissue Engineering and Regenerative Medicine Society (TERMIS-eu) Meeting, Istanbul, Turkey.

I.Mencía Castaño, G.P. Duffy, C.M.Curtin and F.J. O'Brien (2013). Efficient microRNA delivery using non-viral nanohydroxyapatite particles for bone tissue engineering applications.
125th Anatomical Society Summer Meeting, Dublin, Ireland.

National Conferences

I. Mencía Castaño, C.M. Curtin, G.P. Duffy, and F.J. O'Brien (2015). Rapid enhancement of human mesenchymal stem cell osteogenesis using collagen-nanohydroxyapatite scaffolds for non-viral inhibition of miR-133a.
4th BioAnalysis and Therapeutics (BioAT) PhD Programme Research Day Meeting, Dublin, Ireland.

I. Mencía Castaño, C.M. Curtin, G.P. Duffy, and F.J. O'Brien (2015). Enhanced mesenchymal stem cell osteogenesis using microRNA-activated scaffolds.
RCSI Annual Research Day, Dublin, Ireland.

I. Mencía Castaño, C.M. Curtin, G.P. Duffy, and F.J. O'Brien (2015). miRNA-activated scaffolds enhance human mesenchymal stem cell osteogenesis.
21st Annual Conference of the Bioengineering Section of the Royal Academy of Medicine in Ireland, Carton House, Maynooth, Ireland.

I. Mencía Castaño, C.M. Curtin, G.P. Duffy, and F.J. O'Brien (2014). Functionally efficient microRNA-activated scaffolds to enhance human MSC differentiation for tissue engineering applications.
3rd BioAnalysis and Therapeutics (BioAT) PhD Programme Research Day Meeting, Dublin, Ireland.

I. Mencía Castaño, C.M.Curtin, G.P. Duffy, and F.J. O'Brien (2014). Use of Collagen-nanohydroxyapatite scaffolds as delivery platforms for microRNA-based tissue engineering.
36th All Ireland Pharmacy Schools Conference, Dublin, Ireland.

I. Mencía Castaño, C.M.Curtin, G.P. Duffy, and F.J. O'Brien (2014). Collagen-nanohydroxyapatite scaffolds for microRNA delivery in bone tissue engineering. *RCSI Annual Research Day, Dublin, Ireland.*

I. Mencía Castaño, C.M.Curtin, G.P. Duffy, and F.J. O'Brien (2014). Nanohydroxyapatite particles and collagen-nanohydroxyapatite scaffolds as microRNA delivery systems for bone tissue engineering.
Innaugural Human Disease Mapping 2014 Meeting, Dublin, Ireland.

I.Mencía Castaño, C.M.Curtin, G.P. Duffy, and F.J. O'Brien (2014). microRNA activation of collagen-nanohydroxyapatite scaffolds for bone tissue engineering. *20th Annual Conference of the Bioengineering Section of the Royal Academy of Medicine in Ireland, Co. Limerick, Ireland.*

I.Mencía Castaño, G.P. Duffy, C.M.Curtin and F.J. O'Brien (2013). Nanohydroxyapatite particle-mediated microRNA delivery for bone tissue engineering applications.
2nd BioAnalysis and Therapeutics (BioAT) PhD Programme Research Day Meeting, Maynooth, Ireland.

I.Mencía Castaño, G.P. Duffy, C.M.Curtin and F.J. O'Brien (2013). Nano-hydroxyapatite particles as novel non-viral microRNA delivery vectors for bone tissue engineering applications.
Annual Royal College of Surgeons Research Day, Dublin.

I.Mencía Castaño, G.P. Duffy, C.M.Curtin and F.J. O'Brien (2013). Nano-hydroxyapatite particles as microRNa delivery vectors to enhance osteogenesis for bone tissue engineering applications.
19th Annual Conference of the Bioengineering Section of the Royal Academy of Medicine in Ireland, Co. Meath, Ireland.

I.Mencía Castaño, G.P. Duffy, C.M.Curtin and F.J. O'Brien (2012). Development of a collagen-nanoHA microRNA delivery scaffold system for tissue engineering applications.
1st BioAnalysis and Therapeutics (BioAT) PhD Programme Research Day Meeting, Dublin, Ireland.

List of Figures

List of Tables

List of Equations

Nomenclature

°C	degrees Celsius
2D	two-dimensional
3D	three-dimensional
AcvR	activin receptor
ALP	alkaline phosphatase
AM	acetoxymethyl
ANOVA	analysis of variance
BCL2C2	C-2 clon of B-cell lymphoma -2 protein
BLAST	basic local alignment sequence tool
BM	bone marrow
BMP	bone morphogenetic protein
BBP	BMP binding protein
BSA	bovine serum albumin
Ca	calcium
CaP	calcium phosphate
CM	conditioned media
COL	collagen
coll	collagen
Ct	cycle threshold
cel	caenorhabditis elegans
DAPI	4’, 6- diaminido-2-phenylindole
DH	hydrodynamic diameter
DLS	dynamic light scattering
Dlx5	distal-less homeobox 5
DMEM	Dulbecco’s modified Eagle’s medium
DNA	deoxyribonucleic acid
ds	double-stranded
dopa	dihydroxyphenylalanine
ECM	extracellular matrix
EDAC	1-ethyl-3-(3’-dimethylaminopropyl)carbodiimide
EDTA	ethylenediaminetetraacetic acid
EFNA3	ephrinA3 ligand

ELISA	enzyme-linked immunosorbent assay
EPHB4	ephrin receptor B4
ESCs	embryonic stem cells
FBS	foetal bovine serum
FDA	Food and Drug Administration
FGF	fibroblast growth factor
g	gram
g	relative centrifugal force
GAM	gene-activated matrix
GF	growth factor
GFP	green fluorescent protein
h	hour
HA	hydroxyapatite
HCl	hydrochloric acid
HIF	hypoxia inducible factor
HOXA10	homeobox A10 protein
hsa	homo sapiens
HUVEC	human umbilical vein endothelial cells
IGF	insulin-like growth factor
iv	intravenous
kV	kilovolt
lncRNA	long non-coding RNA
LPA4	lysophosphatidic acid receptor 4
luc	luciferase
M	molar
MC3T3-E1	mouse calvarial osteoblast cell line
min	minute
miR	microRNA
miRNA	microRNA
ml	millilitre
mm	millimetre
mM	millimolar
mmu	mus musculus
MPa	megapascal

mRNA	messenger RNA
MSC	mesenchymal stem cell
MTA1	metastasis-associated protein 1
mTOR	mammalian target of rapamycin
MTS	sodium (3-(4,5-dimethylthiazol-2-yl)-2,5-diphenyltetrazolium bromide)
mV	millivolt
mW	millwatt
nHA	nanohydroxyapatite
NHS	N-hydroxy-succinimide
nm	nanometre
nM	nanomolar
nt	nucleotide
OB	osteoblast
OCN	osteocalcin
OPC	osteogenic progenitor cells
p21	cyclin-dependent kinase inhibitor-1A coding p21 gene
PBS	phosphate buffered saline
PCL	polycaprolactone
PDGF	platelet derived growth factor
pDNA	plasmid DNA
PEG	polyethylene-glycol
PEI	polyethyleneimine
pH	potential for hydrogen ion concentration
piRNA	Piwi-protein associated RNA
PCR	polymerase chain reaction
PLGA	polylactic-co-glycolic acid
PMMA	polymethylmethacrylate
pre-miRNA	precursor miRNA
pri-miRNA	primary miRNA transcript
PTH	parathyroid hormone
PTHrP	PTH related peptide
qRT-PCR	quantitative real time polymerase chain reaction
®	registered trademark

RISC	RNA-induced silencing complex
RM	regenerative medicine
RNA	ribonucleic acid
RNAi	ribonucleic acid induced interference
rno	ratus norvergicus
rpm	revolutions per minute
rRNA	ribosomal RNA
RT	reverse transcription
Runx2	runt-related transcription factor 2
scr	scrambled
siRNA	small interfering RNA
shRNA	short-hairpin RNA
Smad	similar to mothers against decapentaplegic proteins
Std	standard
ST2	cloned stromal-cell line from mouse bone marrow
STAT3	signal transducer and activator of transcription 3
TE	tissue engineering
TERG	Tissue Engineering Research Group
TGF	transforming growth factor
™	trade mark
tRNA	transfer RNA
Twist1	twist basic helix-loop-helix transcription factor 1
µm	micrometre
µM	micromolar
µg	microgram
µl	microlitre
UTR	untranslated region
UV	ultraviolet
VEGF	vascular endothelial growth factor
vs	versus
Wnts	wingless-related integration site proteins

Chapter 1. Introduction and Literature Review

1.1.Tissue engineering and regenerative medicine: an overview

The term "tissue engineering" (TE) originated in 1985 (1) and was first defined in a scientific paper by Langer and Vacanti in 1993 as an ‘interdisciplinary field that applies the principles of engineering and the life sciences toward the development of biological substitutes that restore, maintain, or improve tissue function or a whole organ’ (2). This definition encompasses the use of living cells and/or their extracellular products to regenerate tissues inside the patient’s body and for the purpose of drug discovery or diagnostics. Subsequently, the term “regenerative medicine” (RM) was coined to refer to a vast medical area with surgical connotation, within which TE was viewed as one amongst many strategies to treat tissues requiring repair due to dysfunction, disease, injury, age or congenital disorders (3, 4). Today, both TE and RM are used interchangeably (1) and in combination (TERM), and have emerged as a very significant field with a growing global market estimated to reach $89.7 billion by 2016 (5).

Traditional approaches to replace damaged tissue involve the use of allografting and autografting, which is widely regarded as the gold standard procedure. Respectively, these techniques consist of re-implanting cells or tissue harvested from patients themselves or from same-species donors, at the site of damage. Although both techniques display clinical success, they also present many constraints generally associated with the requirement for additional surgical procedures, limited donor tissue, donor-site morbidity and chronic pain (6). Moreover, allografting has the added risk of rejection by the patient’s immune system, graft-versus-host-disease, as well as risk of disease transmission from donor to patient (7). Furthermore, there is a widening gap between the amount of tissue/organ donors available to meet the growing demands of an increased aging population (8). Another approach commonly used in some tissues including hip, knee and heart valve replacement is the use of prosthesis, which are artificial devices to substitute a missing or impaired part of the body. Inherent shortcomings to the use of prosthesis include the induction of scar

tissue formation, loosening and deterioration of the prosthesis limiting the half-life of the implant, and mobility reduction in the case of joint replacement (9). Hence, the field of TE aims to provide alternative treatment prospects by typically introducing the use of three major components: biomaterials (scaffolds), cells and external stimuli. These three factors compose what has been coined as the 'tissue engineering triad' and can be applied individually or as part of multiple combinations (10) (Figure 1.1). In particular, scaffolds provide structural, morphological and biological cues to the cells to facilitate required tissue formation and external stimuli direct cells to produce tissue (2). The focus of this thesis will be on the use of bone biomimetic scaffolds incorporating microRNA delivery as an external stimulus to direct human mesenchymal stem cells to produce bone tissue and thus mediate bone repair.

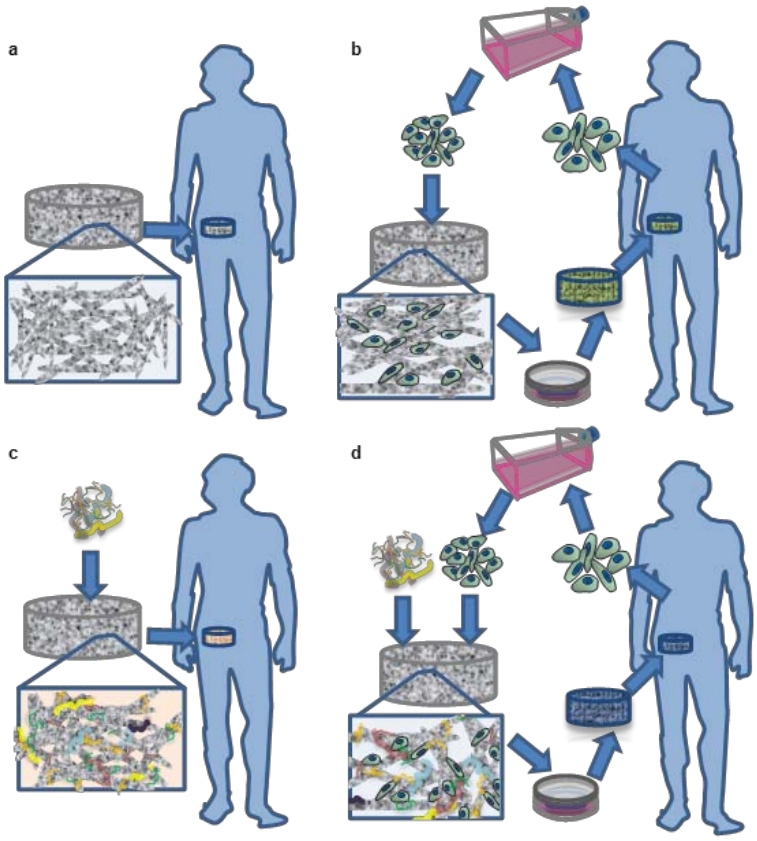

Figure 1.1 Overview of strategies applied in TE adapted from (10). a) Direct implantation of cell-free scaffold (grey). **b)** Cells are harvested, expanded and cultured *in vitro* using scaffolds, then constructs (green) are implanted at a defect site. **c)** Direct implantation of cell-free bio-activated scaffold (orange) for localised delivery of bio-stimuli to promote tissue regeneration. **d)** Cells are harvested, expanded in culture, combined with biological cues and cultured *in vitro* using scaffolds, then constructs (blue) are implanted at a defect site.

1.2.Bone function, structure and composition

Bone is a highly dynamic tissue, with remarkable remodelling and repair capabilities, which functionally provides biomechanical support to the whole body whilst permiting locomotion as well as formation of new blood cells and promotion of calcium homeostasis (11). Within bone, there are two distinct regions that differ in density and structural organisation (Figure 1.2). Firstly, a hard and highly dense outer layer is found, denominated compact or cortical bone, which accounts for 80 % of the total bone mass of an adult skeleton. Secondly, a spongy internal structure named trabecular or cancellous bone is found, which accounts for the remaining 20 % skeletal bone mass. In humans, trabecular bone has nearly ten times the surface area of the compact bone and an ultimate compressive strength ranging from 5 to 15 MPa (12). It is through this interconnected porous network of trabecular bone that a network of vasculature is present. Within the interstices of this porous structure the medullary cavity is also found enclosing the bone marrow, which is responsible for the production of blood cells.

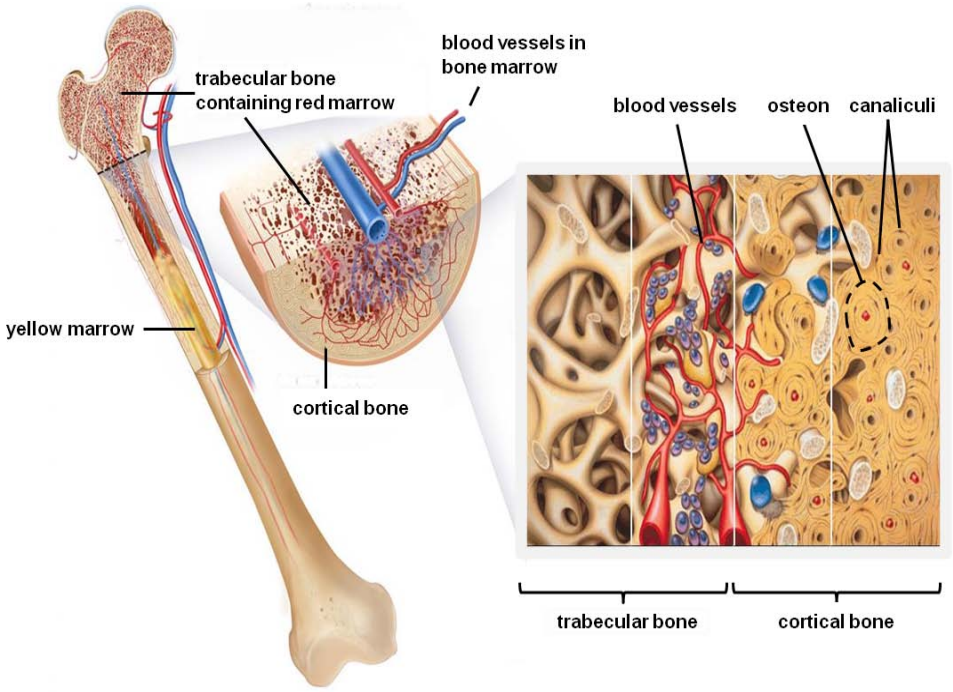

Figure 1.2 Microstructure of bone adapted from (13) and (14). Cortical bone comprises the outer layer and is a highly dense structure of osteons and interconnected canaliculi. Trabecular bone is less dense and overall displays higher porosity in an interconnected network. Its pores allow perfusion by blood vessels and the intersticial space of trabecular bone contains the bone marrow.

Bone tissue comprises of organic and inorganic phases of an extracellular matrix (ECM) in conjunction with a cellular component. The organic phase of the ECM is composed of collagen type I fibres in a 95 % and the remainder 5 % encompasses proteoglycans as well as other non-collagenous proteins. With regards the inorganic or mineral phase, this accounts for almost 2/3 of the total bone tissue weight, and nano-sized crystals of hydroxyapatite (nHA) are the major characteristic component (70 %). A range of salts including calcium carbonate, fluoride, magnesium and sodium are combined with these crystals to complete de total inorganic phase of bone. The combination of both the organic and inorganic ECM phases results in a composite with high mechanical strength: the network of collagen fibres imparts elasticity and permits twisting and bending, whereas nHA is hard although brittle, and hence imparts a high compressive modulus to the tissue. Overall, this results in a stabilised framework which provides the mechanical strength and relative elasticity to this tissue, making bone able to resist impact loading (11).

The cellular component of bone is estimated to be 2 % of the total bone mass; however, such a small mass is essential for bone metabolic function and homeostasis. There are four key cell types within bone: osteoprogenitor cells, osteoblasts, osteocytes and osteoclasts. Osteoprogenitor cells and preosteoblasts are immature cells committed towards differentiation into the osteogenic lineage, representing ~ 1 % of the bone marrow cell population (15). Osteoblasts and osteocytes are fully differentiated cells that populate the bone matrix. Osteoblasts are responsible for the deposition of new bone matrix involving the secretion of collagen type I and other non-collagenous proteins such as alkaline phosphatase, osteocalcin and osteopontin to form the so-called osteoids. nHA crystals are then deposited in alignment to the osteoid, forming a nucleation site that leads to tissue mineralisation and progression to mature bone (16). When osteoblasts become confined within the mineralised bone matrix they transform into osteocytes, which are mechanosensory cells with a pivotal role in the functional adaptation of bone and bone turnover (17). Finally, osteoclasts are multinucleated cells derived from monocyte and macrophage precursor cells located in the haematopoietic stem cell niche. They function as

resorptive cells by breaking down bone through a catabolic process called osteolysis (11, 18).

1.3.Bone formation, remodelling & repair

The cellular component of bone works globally to maintain a dynamic balance between the processes of bone formation and resorption, which is collectively referred to as bone remodelling (Figure 1.3) The equilibrium between bone formation and remodelling is critical to maintaining a healthy and functional tissue and is also a fundamental part of the bone repair process.

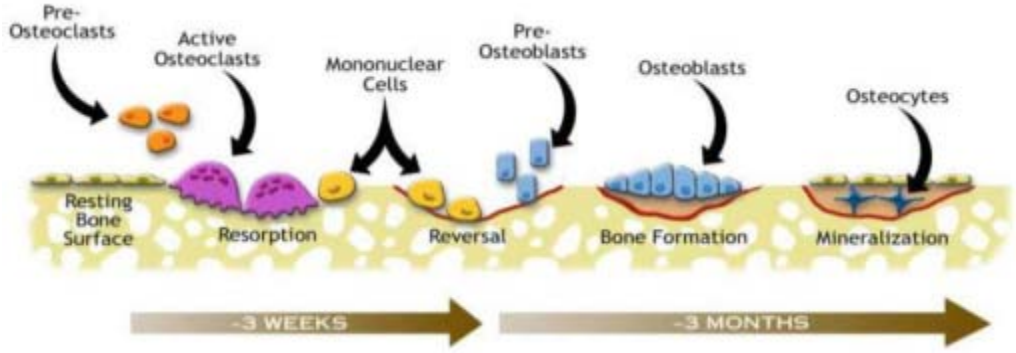

Figure 1.3 The bone remodelling cycle, taken from (11). Schematic representation of the concerted function of every cellular component of the bone in the remodelling process, in order to maintain the mineral homeostasis and healthy bone turnover.

Two main bone developmental processes can be distinguished: intramembranous ossification and endochondral ossification. The process of intramembranous ossification takes place in the formation of flat bones, such as skull bones, and involves the direct differentiation of mesenchymal stem cells (MSCs) into osteoblasts, which is defined as osteogenesis (19). On the other hand, endochondral ossification, the process responsible for long bone formation and elongation, implies an initial MSC condensation process to form a temporary cartilaginous template that is ultimately transformed into bone (20).

1.3.1.Osteogenesis

The process of osteoblast differentiation and bone formation is referred to as osteogenesis and the complex signalling mechanisms underlining this process

are summarised in Figure 1.4. Activation of osteogenesis is extracellularly triggered by several anabolic factors such as bone morphogenetic proteins (BMPs) and wingless-related integration site proteins (Wnts). Additionally, interplay with transforming growth factor beta (TGFβ), fibroblast growth factor (FGF) and insulin-like growth factor (IGF) signalling pathways also modulate the osteogenesis process (21). These extracellular signals are transduced to ultimately activate transcription factors of osteogenesis including runt-related transcription factor-2 (Runx2), the major driver that induces characteristic patterns of osteogenic gene expression.

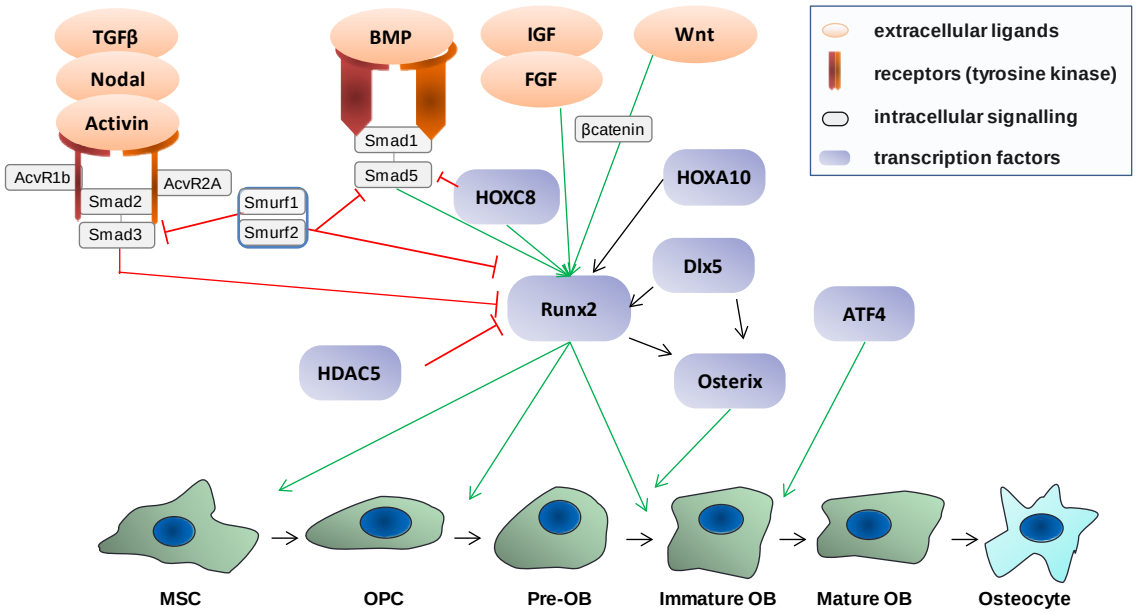

Figure 1.4 Molecular mechanisms of osteogenesis. MSCs differentiate along the osteogenic lineage to become osteogenic progenitor cells (OPC) and then osteoblasts (OB) in progressive maturity stages. This process is initiated by extracellular ligands and transduced to the transcription factors by the intracellular signalling molecules. The transcription factors drive osteogenesis by orchestrating the gene expression of the cells. Red brake symbols (⊣) indicate signalling pathways inhibitory for osteogenesis. Arrows designate activation of osteogenesis.

MSC mediated osteogenesis can be divided in 3 distinct stages, each of them associated with particular gene expression profiles (Figure 1.5): (i) proliferation, (ii) ECM deposition and (iii) mineralisation (22). During the proliferative phase, genes such as activator protein-1, histone H4 and collagen type I are upregulated, which then decrease during the following stage of ECM production, for which alkaline phosphatase (ALP) is a pivotal marker. When

ALP expression declines osteocalcin and osteopontin simultaneously increase, which are late stage markers of mineralisation and maturation (23).

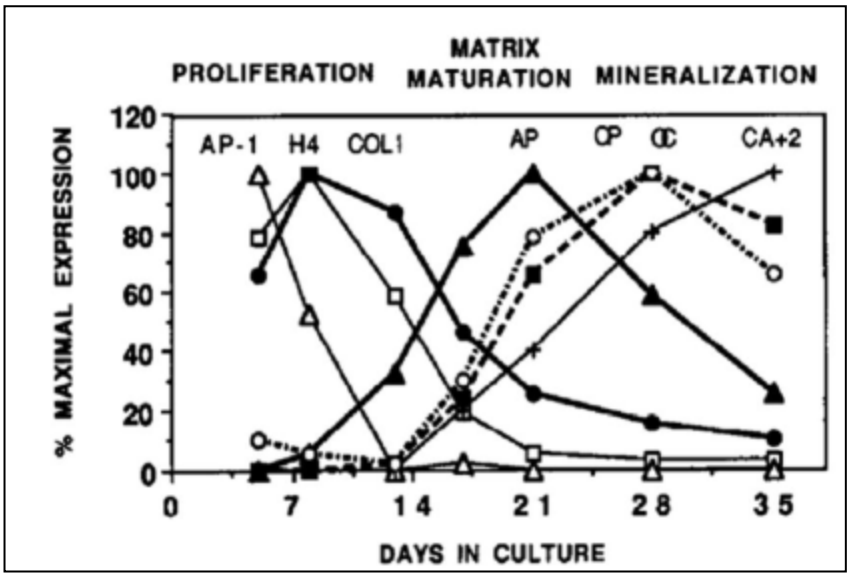

Figure 1.5 Expression of bone formation markers over time, taken from (24). AP-1, H4 and COL I are measures of proliferation. Activator protein-1 (AP-1) represents c-fos and c-jun which are cell growth regulated genes. H4 histone is a cell cycle gene which reflects DNA synthesis. COL I is collagen type I. Alkaline phosphatase (AP) is expressed during matrix maturation. During the mineralisation phase, osteopontin (OP) and osteocalcin (OC) are expressed and calcium (Ca2+) is deposited.

1.3.2.Bone repair and the role of angiogenesis

Bone tissue has regenerative potential owing to the natural activation of a number of mechanisms immediately following tissue damage. The majority of bone fractures heal via a process involving callus formation (Figure 1.6;(11)). This process is initiated by the bleeding associated to the disruption of blood vessels resident in the bone. The augmented presence of blood components at the injure site begins an inflammatory reaction, in which a series of growth factors concentrate. These recruit osteoprogenitors and angioprogenitors to the damaged area. Consecutively, the second and third stages involve the formation and maturation of both an external soft callus and an internal hard callus to stabilise the fracture. Finally, during the late stage of bone repair an intensive remodelling activity takes place to revert both calli to the physiological size and structure of the pre-existing bone over a period of 6 to 8 weeks.

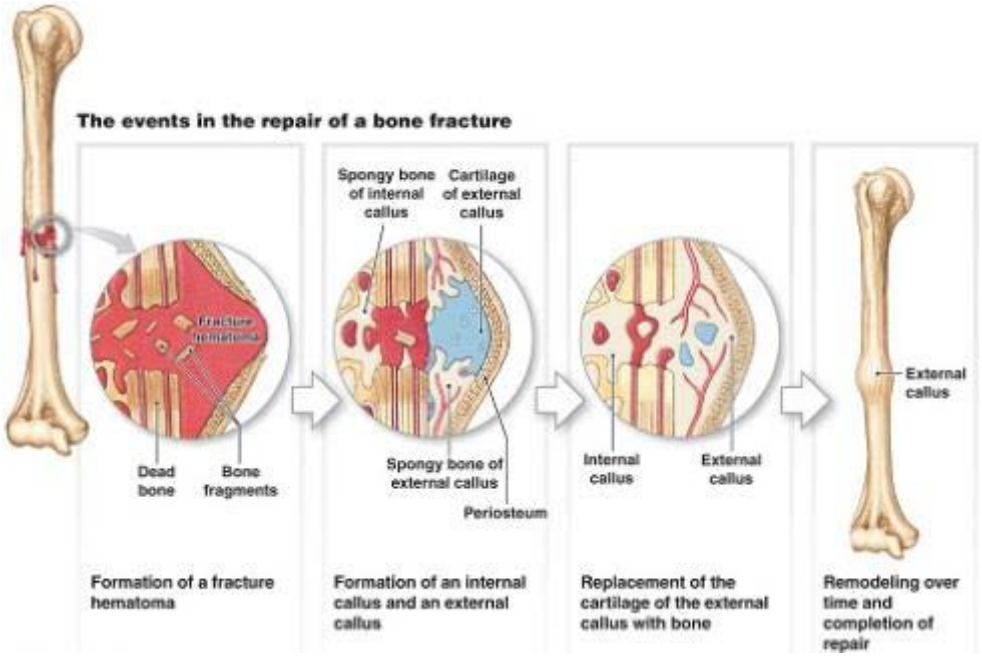

Figure 1.6 Diagram of the events in the course of repair of a bone fracture, adapted from (11). Initially a blood clot or fracture haematoma forms. The internal and external callus form to stabilise the edges of the defect and intensive remodelling takes place to complete the bone repair process.

Another critical process within bone repair is the generation of a new microvascular network, mediated by angiogenesis and vasculogenesis. Both processes are guided by the morphogen vascular endothelial growth (VEGF) (11). Ultimately, the new vasculature surrounding the bone defect site allows the transport of oxygen, nutrients, growth factors and cells which are necessary and essential to support the osteogenic role of MSC as well as to promote bone formation and remodelling (11, 25).

1.3.3.Bone defects and current clinical interventions

Although bone has an intrinsic capacity for self repair, the healing of large bone defects that typically present in humans often involves complications, leading to delayed or non-union of the defects in roughly 10 % of all fractures which ultimately require surgical intervention (26). This renders bone as the second most transplanted tissue worldwide, next to blood, with approximately 2.2 million conventional bone grafting procedures carried out globally every year (27) and a market value in excess of $2.5 billion only in the US (28). Specifically, surgical interventions commonly address the treatment of trauma-

induced critical-size fractures or replace disease-related bone voids. The latter result from primary tumour resection, spinal fusion and dental surgery, as well as weakened and fractured bone associated to osteoarthritis. Failure rates as high as 30 % have been documented following the use of the current gold standard, that is, autologous bone grafting (26). Thus a substantial and unmet need for the development of tissue-engineered bone grafts still exists.

In bone TE, focus is placed on the regenerative potential of several cell types to lay down bone tissue as well as in designing a biomaterial scaffold that upon implantation in the defect site is capable of both housing those cells and withstanding the mechanical loading typical of native bone tissue. The pre-requisites to the development of TE scaffolds for bone repair and current types of materials relevant for this application are described in detail in following sections of this chapter. Although a number of commercially available tissue-engineered bone grafts exist (29), incorporation of external stimuli within the scaffold is frequently needed to achieve optimal therapeutic potential required for successful repair of large bone defects (30). In that frame of mind, efforts have concentrated in the incorporation of several types of biomolecules which will also be reviewed in following sections of this chapter.

1.4.Cells for bone Tissue Engineering

By definition, bone TE encompasses the use of living cells and/or their extracellular products (2). Cell-based bone TE approaches involve the re-implantation at the defect site of *in vitro*-cultured cells, which may be autologous or allogeneic. Regardless of their origin, cells used in TE can be expanded to provide sufficient numbers for tissue repair, or, on the other hand, they can be ‘engineered’ or modified to enhance their regenerative capacity. This can be done by utilising a range of culture regimes and/or bio-stimuli *in vitro.* Furthermore, a plethora of immortalised cell lines and primary cells have been used *in vitro* to evaluate different aspects of bone TE biomaterials designed for prospective cell-free application. Overall, cell lines offer a suitable environment for *in vitro* testing, due to their accessible sourcing and long-term maintenance up to high passage numbers. However, primary cells are of greater use in TE research since they have good *in vitro-in vivo* correlation (31). The ST2 and

MC3T3-E1 cell lines are examples of clonal, non-transformed stromal and pre-osteoblastic cells respectively. Both cell lines show the ability to produce calcified bone tissue *in vitro* (32, 33). In contrast, primary cells are directly expanded in culture following extraction from a donor, meaning that they are non-clonal and not immortalised. Of interest to bone repair, human umbilical vein endothelial cells (HUVECs) are a mature endothelial cell type regarded as an excellent tool to analyse angiogenic function in culture with different angiogenic cues (34). As angiogenesis is crucial for bone repair, the angiogenic potential of bone TE therapies is an important parameter to examine and this will be explored in Chapter 5 of this thesis.

Stem cells are an attractive cell type for bone repair applications, given their vast regenerative potential. Many sources of adult stem cells can be found in the body (35), which are preferred to embryonic stem cells (ESCs) due to ethical concerns. Among the different types of adult stem cells, those derived from the mesenchyme (MSC) have been widely explored for several TE applications (4, 36), and their remarkable success in both pre-clinical and clinical trials over the last decade has highlighted their therapeutic value (37). Of note, over 490 clinical trials have been conducted or are underway involving MSCs (38). The term ‘mesenchymal stem cell’ was coined by Caplan *et al.* (39), who modified the initial-sharing terminology of ‘marrow stromal cells’ which was in practice at the time to designate this cell type (36, 40). This is because their work demonstrated the multipotency of these cells. Particularly, these cells were shown to be able to both self-renew and give rise to all mesenchymal tissue types, including osteoblasts, chondrocytes, adipocytes and myocytes (Figure 1.7; (39)). Currently, it is accepted that MSCs function to maintain organ integrity (35); hence MSC-like cells have been proposed to reside in virtually all tissues and organs in the body (36). MSCs can be found within the bone marrow (BM), umbilical cord (41), adipose tissue (42), peripheral blood (43), amniotic fluid (44), dental pulp (45) and placenta (46).

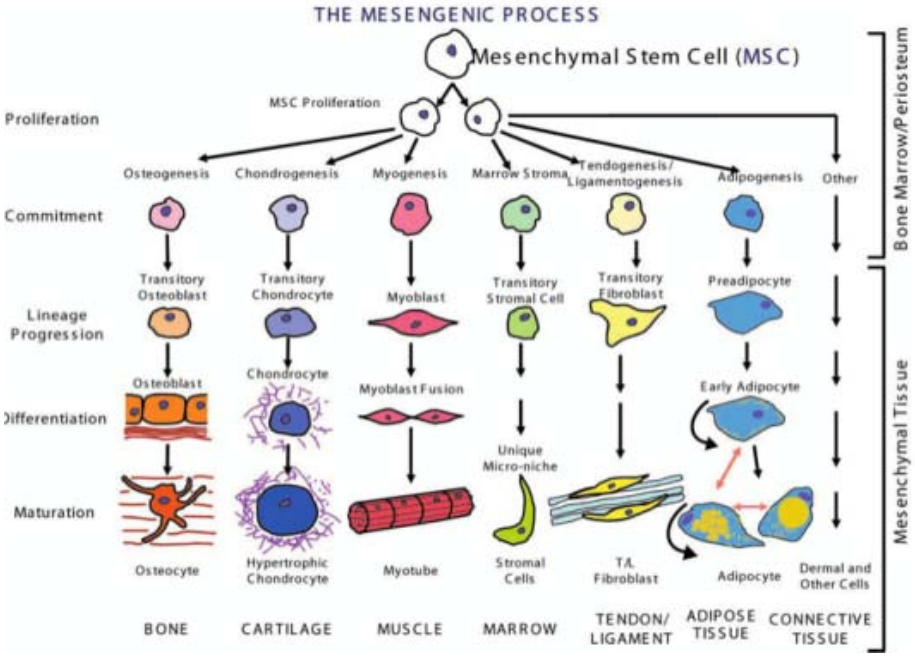

Figure 1.7 Diagram representing the differentiation of MSCs into various mesenchymal lineages, adapted from (47).

MSCs are considered a promising cell source for TE strategies due to their aforementioned multipotency as well as because of their relative ease of harvest and immunosuppressive capacities (36, 47-49). The process of harvesting and isolating MSCs is aided by their plastic-adherence ability (40). In order to fully characterise MSCs, a number of markers need to be assessed (50, 51) in addition to their tri-lineage potential, namely the ability to differentiate into osteogenic, adipogenic and chondrogenic lineages (52). With regards the immunosupresive potential of MSCs, it has been shown that they control a low-state of local immune surveillance of the damaged tissue, which benefits the process of tissue repair (47, 53-55). Additionally, pro-chondrogenic treatments are also of interest in approaches that recapitulate the process of endochondral bone formation (56). Addition of dexamethasone, β-glycerol phosphate and ascorbate-2-phosphate to the growth culture medium is considered a standard technique to drive MSCs towards the osteogenic pathway (57). In particular, BM-MSCs are the cell type of interest to this thesis, as they have shown enormous potential for bone regeneration when used *in vivo* in rats, mice, dogs and sheep (58), and have progressed to a Phase 2 clinical trial for the treatment of non-union fractures by direct administration in the defect site (38).

1.5.Biomaterials for bone TE

Biomaterials research is a major field and influences the medical device, TE and drug delivery industries, with a global market value estimated at $200 billion dollars annually (59, 60). Overall, biocompatibility, bio-resorbability and ease of fabrication are key pre-requisites of biomaterials for use in TE applications (61). A biomaterial must be well tolerated upon implantation into the recipient, without generating rejection or an excessive immune reaction. The bio-resorbability of the material should allow native tissue to fully replace the defect site and prevents the need for subsequent surgical procedures. This implies that degradation of biomaterials must generate non-toxic and non-immunogenic by-products in order to avoid undesired effects in the long term. Additionally, biomaterial fabrication should involve ease of sterilisation, stability and long term storage (62), highly important from the perspective of clinical applicability.

For specific application as bone graft substitutes, biomaterial scaffolds must meet two additional key requirements: osteointegration and mechanical strength. Osteointegration refers to the ability of the construct to support cellular interaction, adhesion and proliferation, as well as ECM deposition. The mechanical strength relates to the ability of the construct to allow clinical handling as well as to withstand mechanical loading. Additionally, mechanical properties can stimulate the residing cells to enhance bone repair (63). Importantly, porosity and pore interconnectivity affect both the osteointegration and mechanical properties of the scaffold. Porosity can be defined as the percentage of void space within a scaffold (64) and is inversely proportional to mechanical strength or stiffness (65, 66). However, a highly porous, interconnected structure is beneficial for osteointegration and furthermore prevents core necrosis of the scaffold (67). Thus a compromise in the level of porosity must be reached to balance mechanical properties and osteointegration. In addition, the inclusion of nano-features in the internal structure of a scaffold may provide improved properties for cell interaction (Figure 1.8). Hence nanotechnology is increasingly influencing the design of TE scaffolds (68, 69). Taking into account all the aforementioned criteria, the development of the ideal off-the-shelf scaffold remains a challenge (69) and the

biomaterial composition of the scaffold also greatly influences the potential for success. Four distinct types of biomaterials are typically used in the field of bone TE: synthetic and natural polymers, ceramics and composites (70, 71).

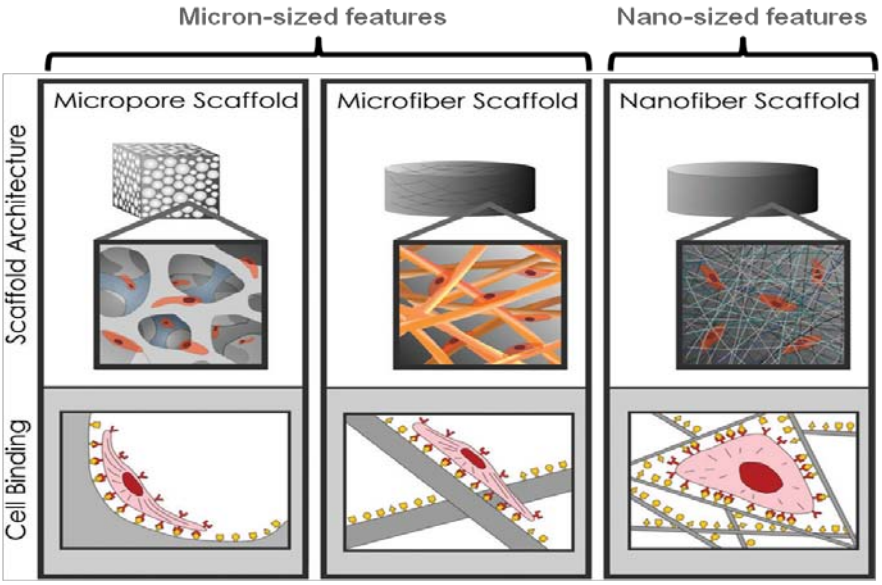

Figure 1.8 Cell-scaffold interaction varies depending on micron or nano-sized pores and features within the scaffold architecture, adapted from (68). Cells binding to scaffolds with microscale architectures flatten and spread as if cultured on flat surfaces, whereas larger surface area is available for contact on scaffolds that present their binding motifs on nano-scale pores and features, therefore improving cell attachment and cellular interactions.

1.5.1.Synthetic polymers

A range of synthetic polymers have shown promise in bone TE due to their versatility, which allows for tailoring and manipulation of their architectural and mechanical properties. These include polyethylene-glycol (PEG), polymethylmethacrylate (PMMA), polycaprolactone (PCL), and co-polymers of polyglycolide and polylactide (PLGA) (72, 73). The tailoring of their properties, in terms of strength, stiffness, porosity and degradation rates, is controlled by altering chain lengths and proportions of the components in case of mixtures. Although these materials hold Food and Drug Administration (FDA) approval for TE purposes, frequently their degradation generates acidic by-products which trigger inflammation responses (74-77) that exert an inhibitory effect on tissue formation (75).

1.5.2.Natural polymers

Polymers of natural origin applied to TE typically involve components of natural ECM and hence present natural ligands that provide active sites for cell chemotaxis and adhesion, which make them bioactive. Commonly used natural polymers include collagen, elastin, gelatine, alginate, silk fibrin, chitosan, glycosaminoglycans and hyaluronic acid (70, 78-86). An alternative approach to the use of natural bulk polymers as scaffolds involves decellularisation of natural ECMs from tissue extracted from different sources. Overall, natural materials possess high biocompatibility and bioactivity, however their mechanical properties tend to be poor unless chemically or physically reinforced by a stiffer filler material or by applying cross-linking methods (87).

Collagen is of particular interest for TE applications as it is the most abundant protein found in the ECM of all body tissues (88-90). More specifically, collagen type I is a key component of the ECM of skin, blood vessels, tendon, cartilage and bone (91, 92). Although collagen type I has demonstrated capabilities of conducting osteogenesis *in vitro* (93), it is also susceptible to rapid degradation rates. Thus, the development of a number of hybrid collagen-based constructs, which show superior physical properties in comparison to collagen alone, has been the focus of research for over a decade in the bone TE field. This includes intensive efforts in our Tissue Engineering Research Group (TERG) at RCSI that led to the development of a series of collagen-based constructs which display a highly porous architecture (7, 94-97). From these, a composite scaffold containing a ceramic of particular interest for bone repair, namely nano-sized hydroxyapatite (nHA;(97)), is described in further detail below as it represents a key component of the work presented in this thesis.

1.5.3.Ceramics

Ceramics are inorganic crystalline structures made up from inorganic materials, with characteristically high melting points and high hardness. However, their brittleness and difficulties in reproducible fabrication limit their applicability in TE. Within this group of biomaterials the following types are used in bone TE: bioactive glasses, calcium carbonates and coral as well as calcium sulphates

and calcium phosphates. Bioactive glasses and calcium carbonates are able to enhance bone mineral deposition (98, 99), however they tend to very brittle (100). The more applicable ceramics for bone TE are calcium sulphates and more importantly calcium phosphates (CaPs), both of which are highly bioactive and, depending on the phase used, resorbable (99, 101). Specifically, CaPs are the most ubiquitous group of bioceramics in nature and they exhibit excellent bone-bonding properties. CaPs exist in different forms, including brushite, tri-calcium phosphate and hydroxyapatite (HA; (102-108)), which differ mainly in the stoichiometric proportion of calcium to phosphate. HA is also found in the mineral component of teeth and bone (69, 109), and its detailed properties are described below, owing to the central role of nHA particles to the research presented in this thesis.

1.5.3.1.Hydroxyapatite

Hydroxyapatite ($Ca_{10}(PO_4)_6(OH)_2$) is a type of CaP that belongs to the class of minerals termed apatites. The main common feature of apatites is the disposition of the crystals in a hexagonal structure, first described in 1930 (Figure 1.9; (110, 111)). Moreover, HA constitutes 70 % of the bone mineral phase in its crystalline structure (69, 109), and its bioactive properties are widely recognised. HA is clinically approved and is found commercially in a variety of forms including granules, pastes, cements and porous blocks, all of which are collectively used as bone fillers, in dental surgery or as coatings for the implantation of synthetic prosthesis (112). Furthermore, HA osteo-conductive and osteo-inductive properties have previously been demonstrated *in vitro* and *in vivo* as reviewed by Habibovic *et al.* (113). Nano particulate HA (nHA) has proven to have enhanced osteointegration properties compared to micro and macro scale HA particles (114-119). This is because it displays high surface grain size and roughness, which leads to decreased brittleness and improved resorbability properties (120, 121). Additionally, the nano-features of HA also have a positive effect on cell proliferation and reduce cell apoptosis (122). Much ongoing research in the nHA area focuses on the development of improved methods for nHA particle synthesis and the subsequent incorporation of nHA into composite scaffolds involving synthetic and natural polymers.

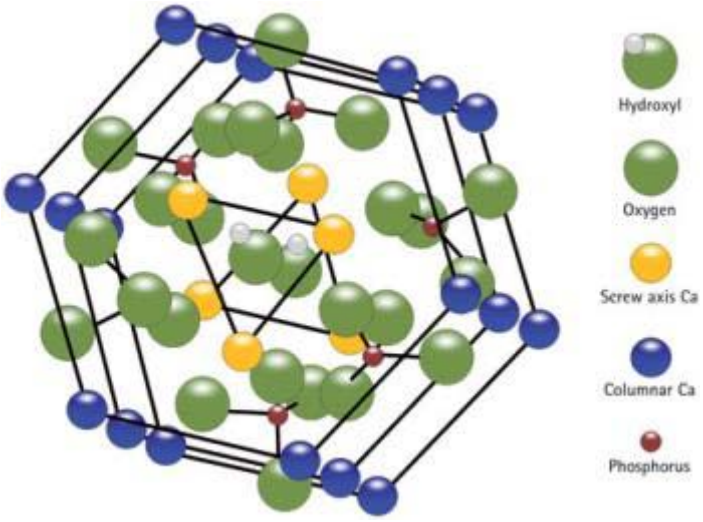

Figure 1.9 Diagram of the three-dimensional (3D) structure of crystalline hydroxyapatite. Hydroxyapatite single unit crystals adopt hexagonal spatial organisation as typical of the apatite family of minerals. Calcium atoms are positioned within the screw axis (yellow) or at the vertexes of the hexagon (blue), while phosphorus atoms (magenta) are located in an intermediate position between the screw axis-calcium and the oxygen atoms, represented in green, distributed throughout the hexagon.

1.5.3.2.Synthesis of HA and nHA

Significant advances in HA and nHA synthesis have been based on wet chemical precipitation methods due to the simplicity and low cost of these techniques, which also allow for the modification of conditions which control HA stability. These conditions include the pH, solvent, temperature, pressure, nature of precursors and the complexing agents used for controlling the reaction kinetics (123). Two main routes of wet chemical synthesis of HA have been exploited using phosphoric acid as a key precursor. However, these reactions are limited by the formation of toxic by-products, which lead to the development of an alternative and more biocompatible technique by Kumta *et al.* (123), which was based on $CaCl_2$, Na_3PO_4 and NaOH precursors (Equation 1.1).

Equation 1.1

$$10CaCl2 \cdot 2H2O + 6Na3PO4 \cdot 12H2O + 2NaOH \rightarrow Ca_{10}(PO_4)_6(OH)_2 + 20NaCl + 92H_2O$$

The reaction proposed by Kumta *et al.* was the focus of recent work in our laboratory which developed a novel synthesis technique for nHA particles

involving the use of low concentrations of a commercial solution of sodium polyacrylate, Darvan 821A®, as a dispersing agent (124). This synthesis technique prevents particle aggregation during the synthesis by wet precipitation (124, 125) and has been utilised in our laboratory for the development of composite collagen-nHA based scaffolds (97) and the use of nHA particles as non-viral vectors for plasmid deoxyribonucleic acid (pDNA) delivery for gene therapy in bone TE (126, 127).

1.5.4.Composite scaffolds of polymers and ceramics

The combination of ceramics with either synthetic or natural polymers represents a logical approach in the development of bone graft substitutes with enhanced therapeutic potential compared to scaffolds composed of either individual phase alone (128-132). The mechanical properties of scaffolds based on synthetic polymers can be enhanced when reinforced with nHA particles (133). The biological performance and *in vivo* bone healing potential of composite scaffolds have also been improved when incorporating nHA particles into collagen-PLGA and gelatine based scaffolds (76, 134, 135). Additionally, the potential of collagen-HA scaffolds for bone repair can be enhanced by varying the fabrication method and particle size of the HA phase (136, 137).

A collagen (coll)-nHA composite scaffold has been developed in our laboratory, which meets all requirements for bone-grafting (Figure 1.10). It is fabricated using a lyophilisation process previously implemented in our laboratory (94, 138, 139). This involves the growing of ice crystals within a collagen solution during the freezing process which subsequently sublimate during the drying phase, ultimately leaving the collagen fibres arranged in a continuous and highly porous network. The final freezing temperature determines the pore size of the resulting material which can range from 85 - 325 μm (94, 138, 139). In addition, physical and chemical crosslinking methods have been established, to structurally reinforce these scaffolds and reduce their degradation rates. These coll-nHA scaffolds have demonstrated significant osteogenic potential *in vitro* and *in vivo* (7, 97) and have since been successfully applied in our laboratory as bioactive depots for gene delivery. Collectively this previous research

illustrates the immense potential of the coll-nHA scaffolds to serve as depots for the localised delivery of microRNAs, which is the primary aim of this thesis.

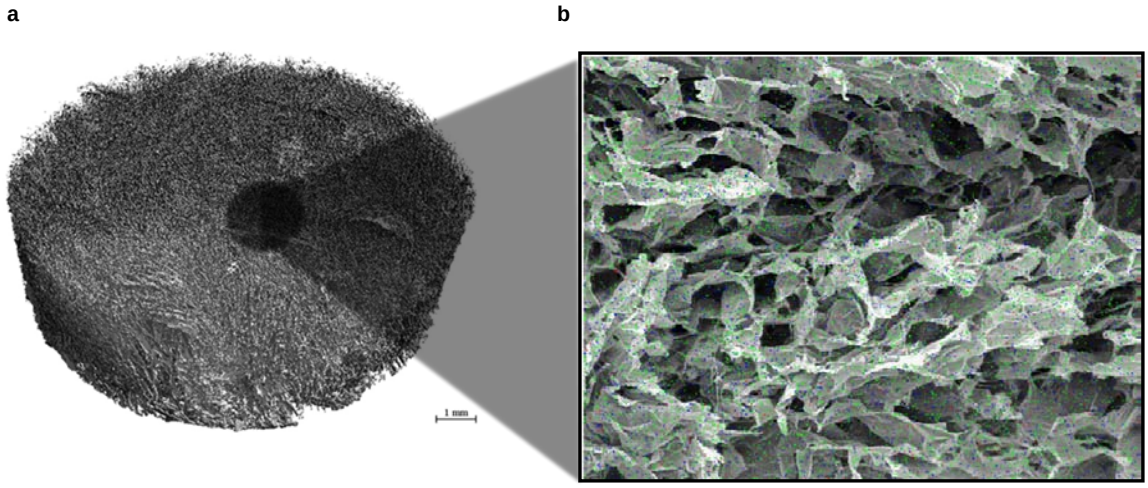

Figure 1.10 Coll-nHA scaffold synthesised in RCSI TERG, adapted from (125). a) Representative micro-computed topography image, scale bar 1 mm. **b)** Representative Energy Dispersive X-Ray map of a coll-nHA scaffold showing the widespread distribution of calcium (green), phosphate (blue) and sodium (red) overlying a corresponding scanning electron microscopy (SEM) image.

1.6.Biomolecule delivery to enhance healing in bone TE

The administration of biomolecules to progenitor cells is a frequent strategy to direct the cells towards enhanced matrix production and *de novo* tissue formation. From this perspective, several types of biomolecules may be incorporated as extra agents in bone TE strategies to enhance tissue healing. Intensive research efforts over the last 15 years have focussed on advancing the application of growth factors (140) and gene therapy (141), while the application of ribonucleic acid induced interference (RNAi) has started to emerge within the overall TE field over the last five years (142, 143).

1.6.1.Growth factors

Growth factors (GF) are large polypeptide molecules that play a pivotal role in the information transfer between cells and their microenvironment during morphogenesis and tissue repair (Figure 1.11). The multi-faceted effects of GFs can be divided in the following: (i) mitogenic; stimulating cell division, (ii)

chemotactic; triggering cell migration, (iii) morphogenic; instructing cell differentiation, (iv) apoptotic; inducing cell death and (v) metabolic; modulating cell metabolism (144-146).

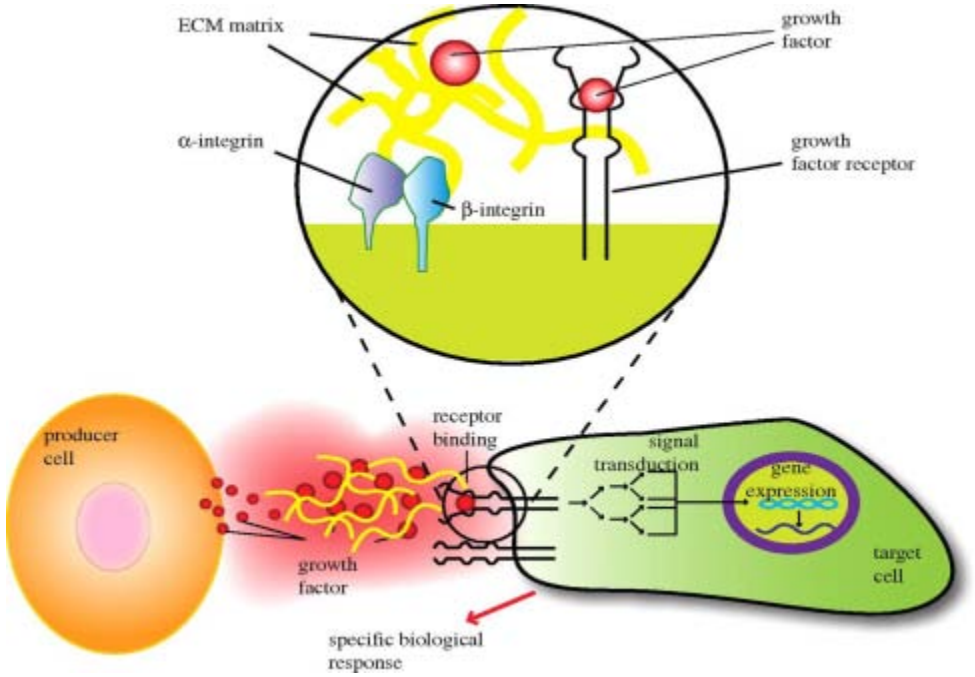

Figure 1.11 Cross talk between cells mediated by growth factors (GFs) and ECM, taken from (147). GFs secreted by producer cells bind transmembrane receptors and the signal is transmitted into the cell through complex signal transduction machinery to elicit a specific biological response. The ECM can also influence this process by releasing GFs upon degradation or influencing cell migration towards gradients of GFs.

The GF concentration and GF exposure duration are critical factors that dictate the eventual cell fate. In the case of morphogen GFs, concentration gradients are known to regulate embryonic development as well as tissue regeneration (148). Of particular interest, MSC osteogenesis can be modulated by altering the GF availability (149). The GFs most widely applied in bone TE as osteo-inductive factors are BMPs (150) and VEGF (151-153), detailed in subsections below. Alternatively, the application of additional GFs involved in the bone repair process has also been approached. FGFs (154, 155), TGF-βs (156-158) and platelet-derived growth factors (PDGFs) (159, 160), as well as parathyroid hormone (PTH) (161, 162) and PTH related peptide (PTHrP) (163, 164) have reported stimulation of bone healing *in vivo*. More recently, the application of GFs in a combinatorial manner has emerged as an attractive avenue of research. Multiple combinations have proven beneficial compared to the effect

of the single GFs, including combinations of (i) BMPs with VEGF, FGF-2, PDGF, IGF-1, PTH, TGF-β3 and BMP binding protein (BBP), (ii) VEGF with FGF-2 or PDGF, (iii) FGF-2 with PDGF, IGF-1 or PTH, and (iv) PDGF with IGF-1 or TGF- β1 (165).

The major drawback associated with the application of GFs for bone repair is their sort half-life, which ranges from minutes to hours *in vivo* due to enzymatic degradation. Hence difficulties arise with achieving the local bioactive concentrations for the sustained time period needed to improve tissue repair. Frequently this results in the application of high doses with the associated increased cost, which may be prohibitive to widespread clinical use (166).
Of relevance, an indirect route of administering the selected GFs surfaced more than a decade ago, which consists on the use of gene therapy to introduce GF-encoding genetic material to progenitor cells, as discussed in further detail in the next section.

1.6.1.1.Bone morphogenetic proteins (BMPs)

The significance of BMPs to direct bone formation was first discovered in 1965 (167). To date, over 30 BMPs have been discovered (144, 168), among which BMP-2, -4, and -7 are able to stimulate new bone formation *in vivo* in critical-sized defects (25). Importantly, BMP-2 and -7 delivery from collagen type I sponges has been approved by the FDA for restricted clinical use (169) and commercialised as Medtronic's INFUSE® and Olympus Biotech's Osigraft™ respectively (30). However, both products have reported numerous side effects and complications associated with the uncontrolled release of the BMPs from the collagen sponges (166). Such reports have emphasised the need for alternative strategies capable of controlling the localised release of GFs at the defect site.

1.6.1.2.Vascular endothelial growth factor (VEGF)

VEGF, originally denominated *vascular permeability factor*, was first identified in 1983 (170). Subsequently the importance of several VEGF family ligands and receptors in cardiovascular, haematopoietic and lymphatic development was shown (171, 172). Although the primary function of VEGF is the stimulation and migration of endothelial cells, it has also a demonstrated essential role in intramembranous and endochondral bone formation (173, 174). However, precise control over the levels of VEGF available to the cells is a pre-requisite that limits its clinical applicability (175), as supraphysiological VEGF levels lead to uncontrolled vessel formation, which is in high association with tumour growth (176). This makes local confinement of VEGF at the defect site of critical importance for VEGF-based bone repair strategies (146, 177).

1.6.2.Nucleic-acid based therapy: Gene & RNA interference

Nucleic-acid based therapy entails the introduction of genes or RNA interference (RNAi) to elicit a therapeutic effect on cell fate and metabolism and has been considered the medical treatment of the future (178). The number of nucleic-acid based therapy trials currently underway affirms the continued interest in the promise of its application (179). Originally, gene therapy emerged as a strategy to transform the target cells into producing factories of therapeutic protein. With this frame of mind, genes encoding a number of GFs and proteins have successfully been applied to bone repair including BMPs (71, 180), Runx2 (181), IGFs and TGFs (182), PDGF (183-185), FGFs (186, 187) and VEGF (183, 184, 188). Currently, gene therapy has slowly progressed as a mature area of medicine (189) and the classical paradigm of genes as mere encrypted messages for protein production (190) has shifted to the interpretation of genes as ‘units of genetic information that code for proteins but also for RNA molecules with transcriptional, regulatory and/or other functional activities’ (Figure 1.12; (191, 192)). This implies that gene therapy can be used with objectives beyond inducing protein production. This is the case of harnessing RNAi therapy (193), where different RNAi molecules ultimately result in

inhibition of protein synthesis. The process of protein-silencing mediated by RNAi is presented later in further detail.

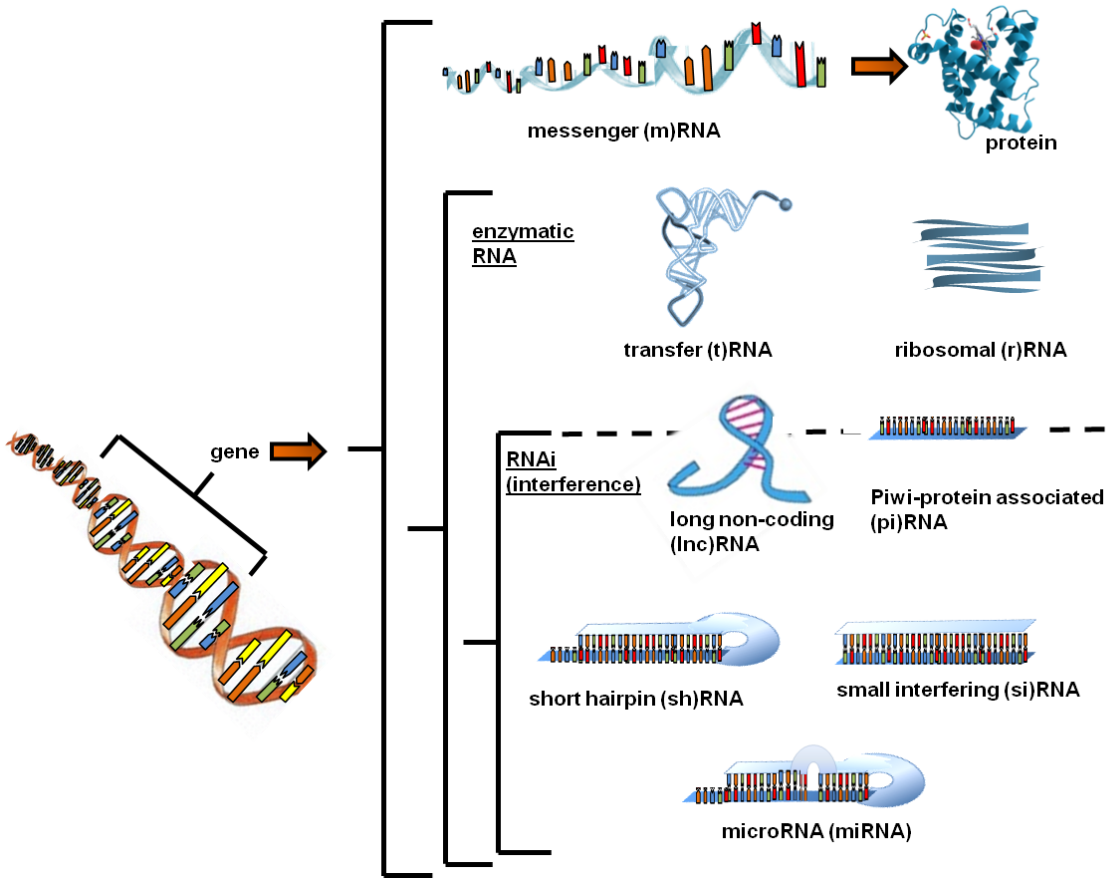

Figure 1.12 Types of genetic information that may be encoded in a gene. A gene contains information that generates messenger (m)RNA or enzymatic RNAs. The final port of stable mRNA is the production of protein, with the cooperation of transfer (t)RNA and ribosomal (r)RNA and controlled by the RNA interference (RNAi) molecules. Long non-coding (lnc)RNAs and Piwi-protein associated (pi)RNAs are involved in additional enzymatic functions.

A key accessory to nucleic-acid based therapy is pDNA, a stable nucleic acid structure naturally found in bacteria, which replicates independently of the core genome and thus serves as an endogenous route for the transfer of genetic information during the process of bacterial conjugation (194). pDNA can be engineered to incorporate a gene of interest and introduced to bacterial cells; bacteria then act as factories of pDNA copies and these copies are later extracted and purified to generate the pDNA that will be administered as a therapeutic. In classical gene therapy the gene of interest is protein-coding (195), but genes encoding short hairpin (sh)RNA or precursors of microRNA (miRNA) can also be incorporated into the plasmid in RNAi therapy.

Nucleic-acid delivery presents an opportunity to overcome the drawbacks associated with GF delivery, such as detrimental bolus effects (26, 196) as it offers the ability to engineer cellular protein production for a sustained time frame that mirrors the physiological response (Figure 1.13). While the sustained time frame of action is highly beneficial in TE applications, it is also crucial that the therapeutic effect comes to an end by the time that the tissue repair process is completed. In this context, the application of nucleic-acid based therapeutics to TE seeks to temporarily increase the ability of the target cells to produce tissue while avoiding to permanently modify their behaviour and regenerative potential, thus preventing undesired effects derived from permanent genome modification such as pathological tissue overgrowth.

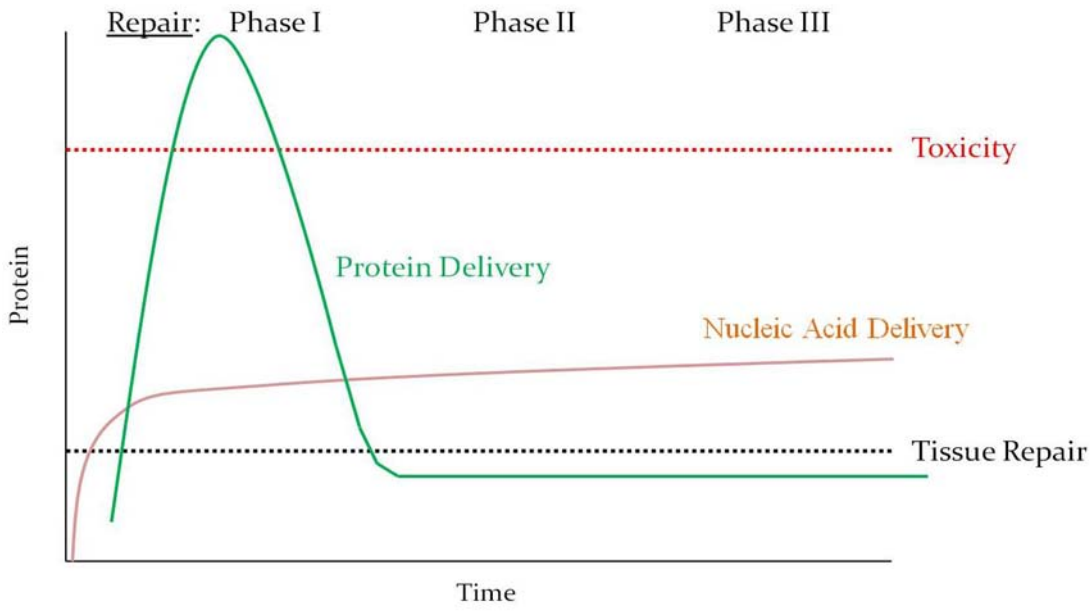

Figure 1.13 Nucleic acid delivery versus protein delivery, adapted from (195). With protein delivery, a large bolus release of the protein detrimental to healing is seen in the initial phases, which quickly subsides to levels that are inconsequential to tissue repair. In comparison, nucleic acid based therapy strategies do not cause an initial damaging bolus release of protein and the level remains constant to enhance the therapeutic effect over the relevant timeframe.

1.6.3.Gene expression control by RNAi

RNAi plays a pivotal function as an intermediary controller of gene expression. When the expression of a protein-coding gene is activated, the transcription process takes place (192). Transcript messenger (m)RNA copies are generated from the template DNA strand, which locate to the cytosol. Here the translation process ultimately leads to synthesis of amino-acid chains which conform the coded protein (192). Prior to the translation process, mRNAs can encounter the mature RNAi molecules in the cytosol and undergo RNA-induced silencing (197-204).

The RNA-induced silencing pathway (Figure 1.14) involves the processing of long double-stranded (ds)RNA, naturally or artificially found within the cell, into smaller RNAs such as shRNA, small interfering (si)RNA and miRNAs, that become incorporated into the RNA-induced silencing complex (RISC; (199, 205-209)). shRNAs are single strands of RNA ~ 60 nt, that adopt a duplex conformation with perfect complementarity and the bent area generating a loop. Although they generally are further processed into siRNAs, recent evidence indicates that shRNAs may also present silencing activity (210-213). siRNAs are complementary perfect duplexes of 2 RNA strands ~22 nt generated from longer precursors, one of which elicits silencing activity. Both shRNAs and siRNAs bind to mRNA targets displaying perfect base-pair complementarity (205, 206). Finally, miRNAs may also be found prior to incorporation into the RISC as duplexes of 2 RNA strands ~22 nt generated from longer precursors, but these duplexes present imperfect base-pair interactions and their silencing activity is also associated with imperfect complementarity binding to the target mRNA (205, 206). With regards to the interaction with target mRNAs, a small sequence found within their untranslated region (UTR) is recognised by the RISC complexes based on perfect (or near perfect) complementarity. Although the 3'UTR region is regarded as the main area prone to interact with RISC, it has been shown that 5' UTR regions are also capable of this interaction with miRNAs (214). Finally, the interaction of the target mRNA with RISC directs for mRNA cleavage or repression of its translation, resulting in a decrease in target and/or protein levels (215).

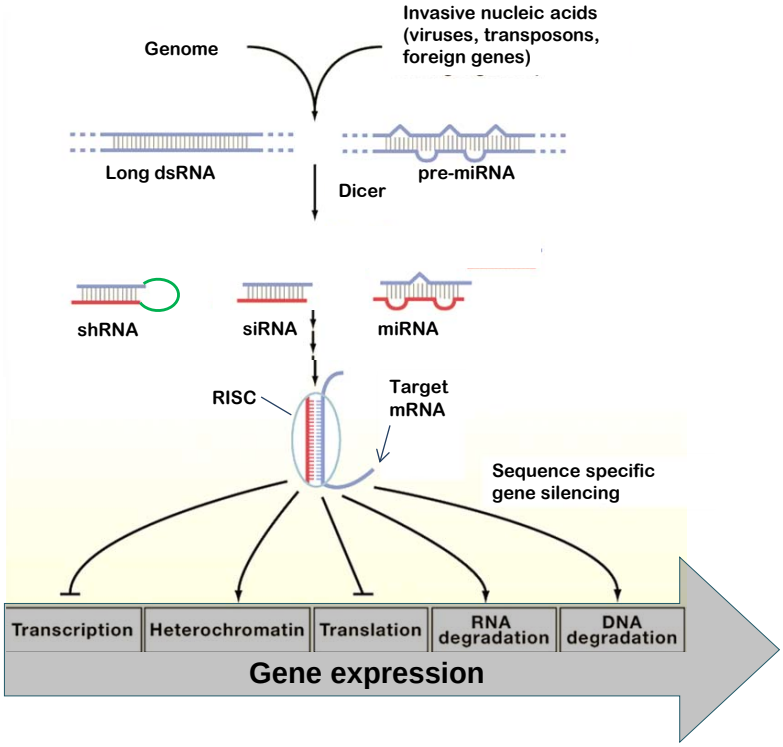

Figure 1.14 Pivotal role of RNAi in the control of gene expression, adapted from (216). Cellular entry and pre-processing of dsRNA into shRNA, siRNA and miRNA is followed by incorporation in the RISC. Target mRNAs interact with these complexes based on perfect or near-perfect sequence complementarity to the RNAi seed region. This interaction induces the mRNA degradation or translational repression among other more complex functions such as transcriptional repression, DNA degradation and alterations in heterochromatin.

1.6.4.RNAi therapy and Stem Cell differentiation

The application of RNAi therapy has potential to promote the differentiation of pluripotent, multipotent and progenitor cells, in addition to accelerating differentiation (217). In comparison with gene therapy, advantages of RNAi therapy facilitate some aspects of successful intracellular delivery, nowadays considered the limiting factor to realising the full potential of nucleic-acid based therapies. These include the smaller size of the molecules and their cytoplasmic activity, meaning that vectors can carry higher amounts of RNAi cargo than pDNA copies and do not need to enter the nucleus. Moreover, each type of RNAi cargo offers distinct therapeutic advantages: shRNAs and siRNAs display stringent complementarity on single messenger targets, eliciting a focalised regulatory effect, whereas miRNAs display a multi-targeting function towards several messenger targets, simultaneously controlling complex signalling pathways (218, 219). Thus, using miRNAs presents the advantage of increasing

the number of targets that can be manipulated simultaneously and intercept entire gene cohorts. In this way, a robust and widespread biological response, ideal to harness numerous tissue repair processes, is expected from the therapeutic delivery of miRNAs. Consequently, out of the different RNAi strategies, the application of miRNA therapeutics for TE purposes has begun to garner the most attention in recent years (220-224). Another interesting aspect of miRNAs, detailed in the following sections, is the possibility to inhibit or block their function, therefore providing a bidirectional regulation of gene and protein expression.

1.6.4.1.siRNA-mediated stem cell differentiation

Successful application of siRNA-mediated stem cell differentiation was first showcased by Hribal *et al.* with the administration of pan-Foxo siRNA to induce myogenic conversion (225). However, the field evolved slowly and siRNA-mediated induction of osteogenesis was not reported until 2008, when chordin silencing demonstrated increased 4 fold ALP activity and 2 fold calcium deposition in hMSCs (226). Following this development, intensive research begun in the field, with reports of siRNA-mediated increases in *in vitro* osteogenesis by silencing BCL2C2 (142), LPA4 (227), MTA1 (228), mTOR (229), p21 (230), STAT3 (217) and Twist1 (231). All of these reports demonstrated an homogeneous ~ 4 fold increase in ALP activity in comparison with the control group while using MSCs of mouse and human origin.

1.6.4.2.miRNA-mediated stem cell differentiation

miRNAs have a pivotal role in regulating embryonic development (215), and it has been shown that they can induce similar levels of myogenic differentiation in ESCs as those seen with siRNA (232, 233). In particular, the miRNA-based induction of osteogenesis can be approached by either mimicking a panel of positive miRNAs, such as miR-29b (234), miR-148b and miR-489 (235), miR-210 (236), miR-196a (237) and miR-2861 (238), or inhibiting a panel of negative miRNAs, including miR-30a-d (239), miR-31 (240), miR-100 (241), miR-133a and miR-135 (242), miR-141 (243) and miR-214 (244). Due to heterogeneity in

the methodology applied, widely variable outcomes in osteogenesis have been reported in these studies. These are further discussed in Chapter 3 of this thesis where three miRNAs were assessed as osteo-therapeutics, namely miR-133a, miR-16 and miR-210.

1.7.microRNA discovery, biogenesis & nomenclature

miRNAs are an abundant and evolutionary conserved class of non-coding single-stranded RNA molecules averaging 22 nucleotides (nt) length in their mature form. Lin-4 RNA, discovered in 1993, is recognized as the foundation member of this class of RNAs in animals (245-247). A number of seminal studies in the field progressively unravelled the mechanism of action of miRNAs (248-252) and by 2001 over one hundred miRNAs had been identified among human, fly and 11 additional species (245-247). The field of miRNA research has since evolved at an accelerated pace, and there are over 2500 human miRNAs known to date (253), regulating up to 60% of the protein-coding genome (254). The importance of miRNA-directed gene regulation is coming into focus with increasing numbers of studies unravelling their biological effects. Some examples of miRNA function involve (i) the regulation of developmental stages of a cell, (ii) lineage commitment, (iii) differentiation, (iv) proliferation and (v) apoptosis, as well as (vi) inflammation, immune response events and related diseases including asthma and cystic fibrosis, (vii) tumour formation and (viii) the progression of viral infections (219, 220, 255-258).

The biogenesis process of miRNAs can be divided in three main phases: transcription, maturation and RISC assembly (Figure 1.15). Initially miRNAs are transcribed either as intronic regions of protein-coding genes, separated from the exons during the splicing process, or directly as long primary transcripts from miRNA genes, termed pri-miRNAs, which can contain clusters of miRNA stem loops (259). Next, during the process of miR maturation a precursor miRNA (pre-miRNA) is generated in the nucleus by Drosha, which cleaves both strands of the pri-miRNA leaving a 60–70 nt stem loop intermediate (259, 260) with 5’ phosphate and ~2 nt 3’ overhang ends (261, 262). This pre-miRNA is actively transported to the cytoplasm by Ran-GTP and Exportin-5 (263, 264) to subsequently undergo processing by Dicer (202, 265)(24). Dicer cuts both

strands at the proximity of the stem loop, producing an imperfect duplex, termed miRNA:miRNA* (266). The half-life of this duplex is short and the two strands separate to yield the mature miRNA single strand and the opposing arm of the former duplex, that is designated miRNA*. The miRNA* fragment is more unstable and as such it is detected at much lower frequencies than the counterpart mature miRNA (267, 268). Finally, the mature single stranded miRNA is assembled into the RISC in a pathway that shares many characteristics with siRNAs, as earlier depicted in Figure 1.16. It has been proposed that the strand that presents the less tightly paired 5' is directed for entry into the RISC (269, 270), and the formation of this complex has been coined as miRISC (271). Downstream from the formation of miRISC the interaction with the target mRNA takes place, which subsequently leads to mRNA cleavage or translational repression (215, 254).

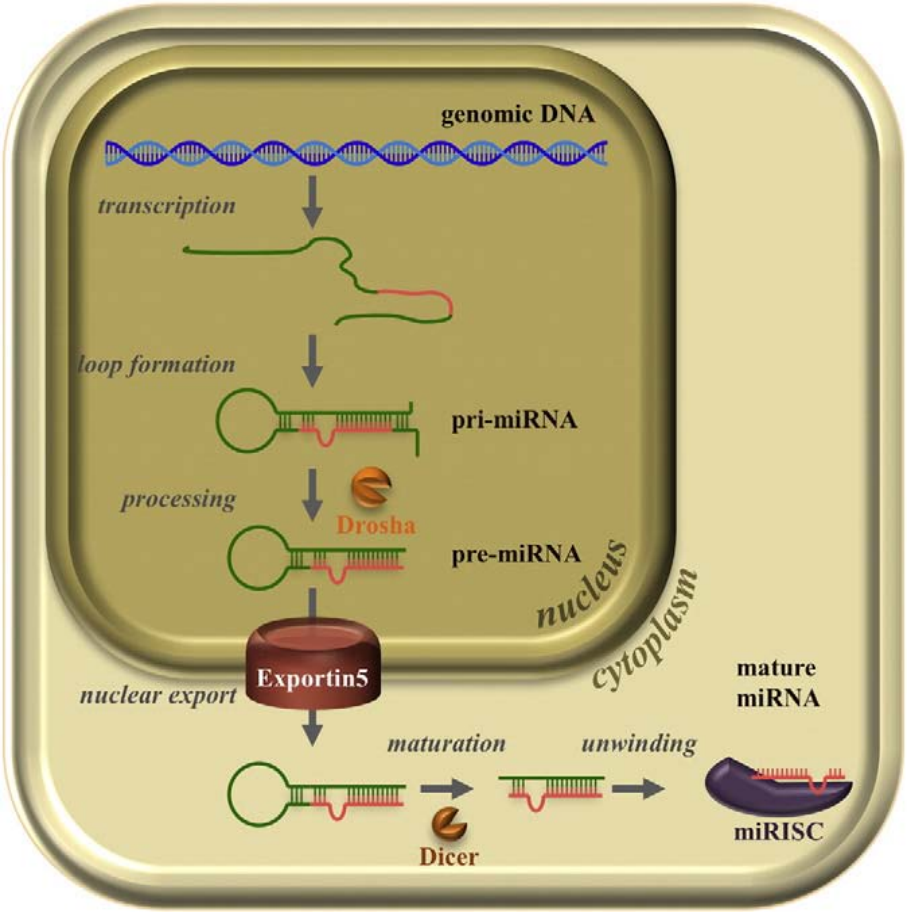

Figure 1.15 miRNA biogenesis taken from (272). A miRNA gene is transcribed generating the primary (pri)-miRNA. In the nucleus, Drosha cleaves the pri-miRNA to produce the precursor (pre)-miRNA. Exportin-5 transports the pre-miRNA into the cytoplasm, where it is cleaved by Dicer, releasing the miRNA:miRNA* duplex. The miRNA strand (red) is loaded into the RISC complex, whereas the miRNA* strand (green) is typically degraded.

From the discovery of the first miRNA, great lengths have been taken to establish a uniform nomenclature system to designate the different biogenic stages and variants, summarised in Table 1.1. This nomenclature system also maintains an orderly organisation of newly discovered miRNAs based on sequencing data and prevents overlapping in the denomination of new miRNAs (273). Specific nomenclature has also been established to designate the different types of base-pairing interaction that can take place between a miRNA and its target. In general, any miRNA is designated by using the prefix ‘miR’ followed by a number of 1 to 4 figures which is set based on order of discovery while taking into account sequence similarity or homology with previously known miRNAs. Moreover, based on evolutionary conserved sequences certain miRNA families have been established whose members present a high degree of homology, in particular in relation with their seed region on the 5’- end.

Table 1.1 Nomenclature established for designating miRNAs and their types of interaction with the target mRNAs.

Term	Definition
miR-XX	miRNA coding gene
mir-XX	precursor hairpins (lower case)
spp – miR-XX	mature sequence miR-XX designated for a determined species
miR-XX-1; miR-XX-2	mature identical sequences proceding from different genes (i.e. distinct pri-miRNA loci)
miR-XXa/b	closely related mature sequences differing in only 1 or 2 nucleotides
miR-XX-5p/3p	different mature miRNA sequences excised respectively from 5’- and 3’-arms of the same pre-miRNA (new nomenclature replacing miRNA and miRNA*)
miRNA::mRNA	Interaction of a miRNA and its target mRNA
6mer-1A	An exact match to positions 2-6 of the mature miRNA (the seed) followed by an adenine (‘A’)
6mer	An exact match to positions 2-7 of the mature miRNA (the seed)
7mer-1A	An exact match to positions 2-7 of the mature miRNA (the seed) followed by an 'A'
7mer-m8	An exact match to positions 2-8 of the mature miRNA (the seed + position 8)
8mer-1A	An exact match to positions 2-8 of the mature miRNA (the seed + position 8) followed by an 'A'

1.7.1.Exogenous control of miRNA

Synthetic molecules have been developed for either mimicking or inhibiting the function of endogenous miRNAs (299). On the one hand, miR-mimics act in the same manner as the endogenous miRNA, that is, binding to a target mRNA and subsequently causing suppression of protein synthesis by degrading the mRNA or inhibiting the translation into protein. Modifications for enzymatic stability and improved cellular uptake are limited for the “guide” strand to be suitable for incorporation into the RISC (303). On the other hand, miRNA inhibitors prevent the activity of miRNAs inside the cell, thus leading to an increase in mRNA and protein expression (274). Among the alternatives to pursue miRNA inhibition, antimiRs or antagomiRs can be chemically modified for improved binding affinity to the target miRNA strand and enhanced enzymatic stability (218). Some of these modifications include methylations to bridge the ribose in a locked postion, generating locked nucleic acids, and replacement of the phosphate backbone with methylations, thiolations or morpholino groups. In addition to the development of antagomiRs, “blockmiRs”, miRNA sponges and small chemical inhibitors have also been developed to abrogate miRNA-induced silencing (218), which offer high pharmacodynamic control but also present with drawbacks: blockmiRs limit the simultaneous multiple targeting of miRNAs, miRNA sponges are delivered as pDNA (275) and small chemicals present decreased specificity towards particular miRNA targets (276).

1.7.2.miRNA therapeutics

miRNA therapy accounts for a subset of miRNAs currently found in the pipeline as clinical candidates for the treatment of fibrosis (miR-21), inflammation (miR-155), atherosclerosis (miR-33), heart failure (miR-208), cardiac repair (miR-15) and neoangiogenesis (miR-92a), as well as hepatitis C treatment (miR-122) and liver cancer treatment (miR-34) (223). A miR-122 inhibitor commercialised as Miravirsen - by Santaris Pharma -, has progressed to Phase IIa clinical trials, with successful results to date (277), and a miR-34 mimic (MRX-34 - by Mirna Therapeutics -) is currently in Phase I clinical trials, undergoing patient recruitment and with unreported results to date (278). The trends in miRNA patent filing capture the dramatic scientific progress in the field and forecast the

fast-paced advance towards commercial development in this field: the number of filed patents related to miRNA-based therapeutics surpassed 350 in the US by 2009 (223) and currently accounts for over 1500 patent applications (279). Nearly half of the filed patents were related to medicinal preparations, of which efforts in delivery vehicles and preparations represented 14 %, in close position with TE-related applications (Figure 1.16). These TE-related applications focus on bone, muscular, ocular and cardiovascular disorders as well as in wound healing, and accounted for 13 % of the total patent filing distribution. This underlines the high interest in developing advanced delivery systems for miRNA therapeutics and their incorporation in the field of TE (280, 281).

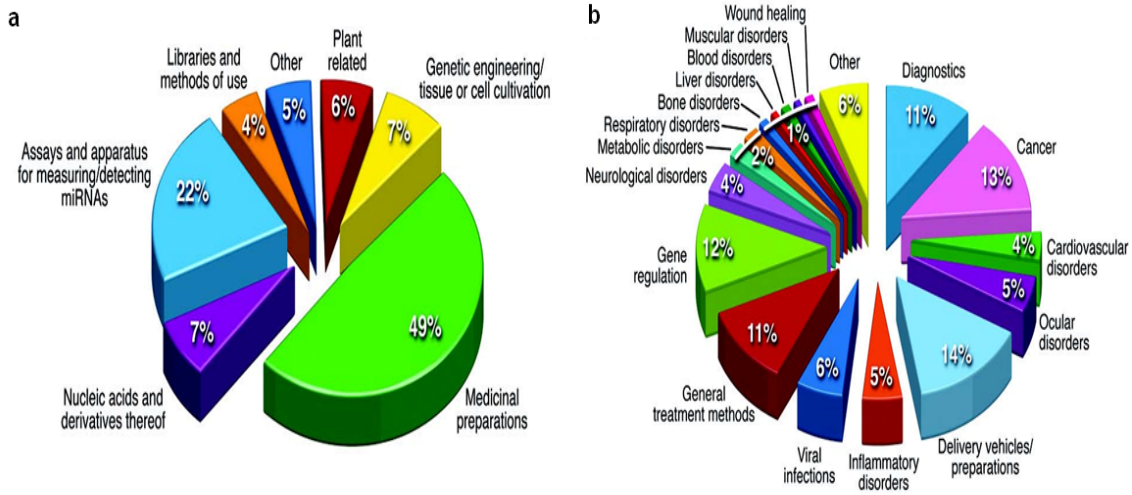

Figure 1.16 miRNA-related patent distribution in the United States, taken from (303). a) The distribution of different technological fields as determined by International Patent Classification codes. **b)** Distribution of filed patents related to miRNA-based medicinal preparations divided by particular indications.

1.8.Vectors for gene & RNAi delivery

The delivery of naked nucleic acids, both *in vitro* and *in vivo,* has demonstrated limited success to-date (282). Due to the negatively charged phosphodiester backbone of these molecules and the susceptibility to nucleases their ability to enter into the cells is restrained, and once inside the cells they ultimately locate in endolysosomal compartments that degrade their content (283). Therefore, an important aspect of successful nucleic acid delivery involves the ability of the molecules to effectively escape this cellular digestion process, also known as endolysosomal escape (284). Hence the use of a delivery vector to carry the nucleic acids into the cells and aid the endolysosomal escape is necessary.

Different vector types are available that permit gene and RNAi transfer, which are broadly divided into two major categories, viral (285-289) and non-viral (290-292). By consensus in the field a number of pre-requisites have been established (293), summarised in Table 1.2, and the need to develop an ideal safe and effective vector that meets all these requirements has not been fulfilled to-date (284). Thus effective delivery remains as the greatest challenge to unleashing the vast potential of both gene and RNAi therapy.

Table 1.2 Pre-requisites of nucleic acid delivery vectors.

Fabrication	Safety	Stability	Functionality
Ease of fabrication	Safe administration route	Robustness/stability (chemical)	Internalisation
Inexpensive	Non-pathogenic	In physiologic fluids, including serum	Endolysomal escape
Facile purification	Non-toxic	For storage and administration	Entry in non-dividing cells
Targetability (to specific cells/tissue)	Non-immunogenic	Protection of cargo	Nuclear transport (generally not RNAi)
		Packaging sufficient amount of cargo	Efficient un/packaging

1.8.1.Viral vectors

A wide range of viral vectors may be used for nucleic acid delivery including retroviruses, adenoviruses and lentiviruses. By their very nature, viruses are excellent at gaining cellular and nuclear entry, which contributes to high levels of transfection of the target cells. Retroviruses are highly efficient at entering dividing cells, while lentiviruses and adenoviruses can enter both dividing and non-dividing cells (294). The first *in vivo* study using adenoviruses to deliver siRNA showed specific target silencing in brain and liver tissue (295). Interestingly, dose –dependent toxicity of adenoviral- miRNA delivery is reduced in comparison to the use of shRNA and siRNA (296). Additionally, enhanced osteogenesis has been shown following viral delivery of miR-424 and miR-31 inhibitors (297, 298) as well as miR-346, miR-26a, miR-29b, miR-148b and miR-196a enhancers (299). In spite of the interest generated by the highly efficient nucleic acid transfer that viruses mediate, multiple issues, generally related to safety concerns, are associated with the use of these vectors. The key issue is the risk of insertional mutagenesis associated with retroviruses and

lentiviruses, which may affect host genes, such as was the case in initial fatalities within clinical trials (57). Other major drawbacks with viral vectors, include immunogenicity, inflammation, limited loading capacity of large size plasmids and large scale manufacturing issues (57). Finally the high and permanent transfer achieved with these vectors may result in pathological over-expression of the introduced gene, as documented by cases of ectopic bone formation following viral delivery of BMP pDNA (300, 301). In summary, the use of viral vectors is very efficient but entails a compromise with regards to their safety (302). For this reason, non-viral vectors have become increasingly more attractive as safe and valid alternatives (303).

1.8.2.Non-viral vectors

The advantages of non-viral gene transfer methodologies widely relate to increased safety, as they exhibit low immunogenicity and low toxicity. Another beneficial factor is that they incur a low production cost and simplified large scale production in comparison with viral vectors (304). Although non-viral methodologies are sometimes regarded as a minority pursuit in nucleic acid transfer, they permit high cargo loads and a temporary release of the RNAi cargo or the synthesised protein (280, 305). In TE applications a temporary release of the cargo is beneficial to promote tissue regeneration, as this reduces the risk of undesired bolus effects at the initial stages while avoiding permanent activation of the tissue repair process once the tissue has been regenerated. Hence, the temporary effects characteristic of non-viral vectors poses a significant advantage for TE applications over the permanent effects observed with viral-based delivery (4, 304). Another important consideration in applying non-viral delivery vectors is that their transfection efficiencies vary depending on the cell type targeted (284, 293, 304), and primary stem cells have been deemed more difficult to transfect than immortalised cell lines (306). Considering the beneficial prospect of applying MSCs for bone repair over other cell types (4, 36, 58), developing non-viral vectors to deliver nucleic acids to MSCs remains a major unmet need in TE.

Within the different non-viral approaches for nucleic acid delivery, physical and chemical techniques can be distinguished. Physical techniques are based on temporary disruption of the cell membrane, and involve electroporation, hydrodynamic pressure, magnetofection, microinjection and ultrasound microbubbles (282). Current developments in chemical non-viral technologies include the use of synthetic nanoscale complexes, mainly categorised in (i) cationic lipid-based vectors and (ii) synthetic cationic polymers. Numerous cationic polymers have been synthesized for DNA and/or siRNA delivery in different research fields (307, 308). However, the use of polymer-mediated miRNA delivery is rarely reported in the field of TE (309) and in turn, the use of cationic lipid-based vectors is widely popular, as summarised in Table 1.3.

Table 1.3 Representative lipid-based miRNA delivery systems for TE, taken from (298).

Vector	miRNA delivered	Approach (effect on miRNA)	Cell type	Potential application
HiPerFect	miR-146b-5p miR-23b miR-99a	Enhancement	neural stem cells	Neurogenesis
DharmaFECT®	miR-198	Enhancement	Keratinocytes	Wound healing
SiPORT™ NeoFX™	miR-1 miR-499	Enhancement	Cardiomyocyte Progenitor cells	Cardio-myogenesis
	miR-21 miR-335-5p MiR-17	Enhancement	MSCs Primary calvarial osteoblasts	Osteogenesis
Lipofectamine® RNAi-MAX	MiR-720	Enhancement	hDPCs	Osteogenesis
	MiR-682	Inhibition	Myogenic progenitor cells	Myogenesis
Lipofectamine® 2000	MiR-375	Inhibition	3T3-L1 adipocytes	Adipogenesis
	MiR-1	Inhibition	ESCs	Osteogenesis

Lipid vectors are frequently formulated as liposomes, many of which have progressed to commercial formulations, including FuGene®, HiPerFect, DharmaFECT®, SiPORT^{TM} NeoFx ^{TM}, DOTAP® and Lipofectamine® 2000 (303, 310). Advantages of liposomes include versatility, ease of large scale production and an unlimited cargo loading capacity (311), however they generate toxicity and immunogenicity, which represents a significant concern when translating to clinical applications (311-313). Polyethyleneimine (PEI) is a frequently used alternative synthetic cationic polymer popular due to its

relatively high nucleic acid transfer efficiency (174, 314), however its application has also been associated with high cytotoxicity and significant cell damage (315). Thus, research efforts have recently turned to the exploration of natural non-viral vectors such as chitosan and CaPs. Chitosan is a biodegradable, biocompatible and non-toxic polymer proceeding from crustacean shells which has recently shown potential for pDNA mediated bone regeneration (316). Furthermore, a number of groups have assessed chitosan particles as RNAi and miRNA delivery vectors. The major drawback of this vector is perhaps its variable transfection efficiency, which is highly dependent on the cell type (312).

1.8.3.Calcium phosphate (CaP) and hydroxyapatite (HA) as non-viral nucleic acid delivery vectors

The use of CaP nanoparticles as non-viral vectors for nucleic acid delivery was first documented by Graham and van der Erb in 1973 (317) and they are renowned for their remarkable biocompatibility, low toxicity and good biodegradability as well as being relatively easy to fabricate and use (126). Additionally CaPs are associated with a non-immunogenic response and non-toxic degradation products (318, 319), and have also been explored as delivery vectors for a range of drug cargos, including therapeutics such as insulin and cisplatin as well as contrast agents for imaging-based diagnostics, such as lanthanide ions (Figure 1.17; (320)). An interesting feature of CaPs is their pH-dependent solubility in association with their physico-chemical nature. CaPs are chemically inert and structurally maintained by electrostatic interactions (321). This triggers their dissolution in the presence of an acidic pH found in intracellular compartments (322), which in turn prevents extracellular liberation of their cargo. Another interesting feature is their ability for immediate complexation with nucleic acids, due to the affinity towards their phosphate backbone chain, which is also an effective and easy approach to limit the size growth of CaP crystals (318, 322, 323). These beneficial properties have resulted in the development of commercial CaP transfection kits and in the field of siRNA delivery, CaP-based particles have demonstrated significant luciferase and green fluorescent protein (GFP) reporter silencing efficiencies (324-327).

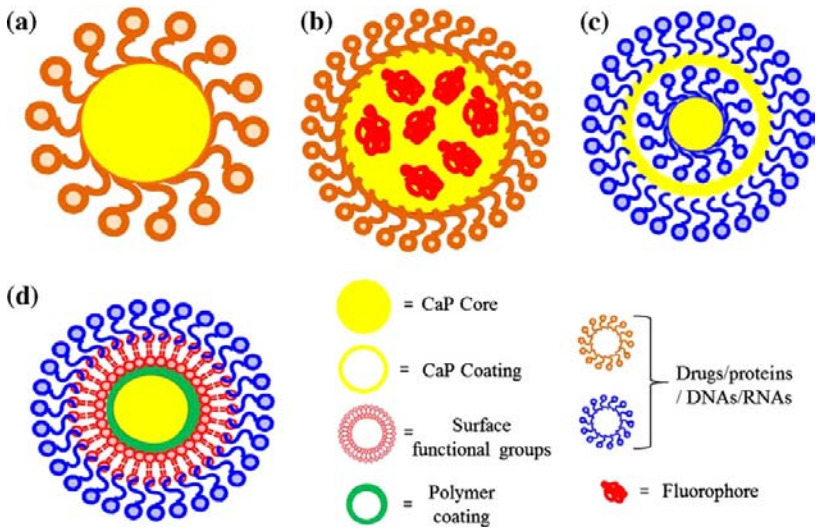

Figure 1.17 Schematic of CaP NPs for drug delivery applications, taken from (318). a) single shell CaP for nucleic acid transfection. **b)** single shell entrapping or dopping the CaP core with fluorophore agents for imaging-based diagnostics. **c)** multi-shell functionalisation for nucleic acid transfection. **d)** Surface functionalisation by polymer coating approach, beneficial for drugs or biomolecules that are poorly adsorbed on CaP.

Hydroxyapatite (HA), besides being the mayor CaP phase found in bone also has the ability to complex with nucleic acids and serve as a safe transfection reagent (319). The advantageous dual function of these nHA particles as bone mineral biomimetics and vectors for nucleic acid delivery has led to intensive research of nHA-based pDNA delivery in our laboratory. As a result of that work, nHA particles were optimised to achieve greater transfection efficiency than a commercial CaP transfection kit in hMSCs (126); which further translated in enhanced osteogenesis when delivering pDNA encoding BMP-2 (126). These particles thus served as the basis for microRNA delivery in the research presented in this thesis.

1.9.Scaffolds for localised delivery of biomolecules in bone TE

The primary role of three-dimensional (3D) scaffolds in TE is to act as templates for cell attachment and tissue repair; however increasingly they are being used to locally deliver biomolecules in order to enhance their therapeutic potential while limiting the exposure of off-target tissues to these biomolecules, thus reducing safety concerns (147, 281, 290). To work effectively, scaffolds must be able to retain the biomolecule while providing sufficient exposure to infiltrating cells (328). Reciprocally, the incorporation of biomolecules must not negatively

affect the mechanical and structural features of the construct or deter cell retention and attachment to the scaffold (329). Another important consideration in scaffold design is to control the spatiotemporal sustained release of biomolecules in order to achieve a pharmacokinetic profile able to promote tissue repair (330-332). To meet these basic requirements different strategies have been explored using a wide range of scaffold types and biomolecule cargos.

1.9.1.Growth factor delivery from scaffolds and controlled release strategies

Currently, in bone repair, two products based on directly incorporating GFs onto collagen sponges have progressed to a commercial stage, which are the INFUSE® Bone Graft Kit, delivering BMP-2, and Osigraft™, delivering BMP-7. Although both have been granted FDA approval, a number of problems surfaced following their market launch, resulting from the uncontrolled GF release profile (146). Significant research is thus ongoing on strategies to improve control over the pharmacokinetic delivery profile using methods to sufficiently retain the GF such as attachment or physical inclusion methods (333, 334). Attachment methods physico-chemically immobilise GFs onto the scaffold surface (30), while physical inclusion methods involve the previous incorporation of the GFs in microparticulate polymer systems that protect the GF from degradation (335). For example, methods to control the release of GFs include loading of VEGF encapsulated within chitosan onto PLGA scaffolds (336) and incorporation of VEGF encapsulated in alginate and BMP-2 in PLGA microparticles into collagen-based scaffolds (337, 338).

1.9.2.Gene & RNAi-activated scaffolds

A critical consideration when applying gene & RNAi therapy relates to the need for efficiently sustained therapeutic effect in a localised manner (339). While the delivery vectors described in Section 1.8 may improve the process of cellular uptake of nucleic acids, their rapid clearance from the target site *in vivo* often results in excessively short therapeutic timeframes (340). Thus, combination of these vectors with 3D scaffolds may provide extended timeframes of localised delivery (61, 195, 341). The scaffold acts as a depot for the nucleic acid complexes with their respective vectors, and then infiltrating cells establish

contact with the nucleic acids deposited along the structure of the scaffolds and internalise them to become transfected. The idea of scaffold-based gene delivery emerged in the late 1990s, coining the term ‘gene-activated matrix’ (GAM) (195). In this seminal work collagen-based scaffolds delivering β-galactosidase pDNA significantly promoted new bone formation (195, 342). Scaffold-based nucleic acid delivery approaches can be classified as *in vivo* – ‘cell-free’- or *ex vivo* -‘cell-mediated’-. *In vivo* transfection consists of the direct application of the nucleic acid containing scaffold to the defect site (343, 344), and this approach has recently attracted interest for gene therapy. On the other hand, *ex vivo* transfection exposes the cells to the nucleic acid treatment prior to loading onto the scaffold. Although it requires *in vitro* culture before implantation in the defect site, being more laborious and cumbersome from a clinical application perspective (345), the small number of studies on scaffold-mediated RNAi therapy published to date have typically focused on this approach (58, 340).

Some examples of scaffold-mediated pDNA delivery for bone repair include the delivery of VEGF naked pDNA from collagen-CaP scaffolds (290) and the CaP-based delivery of BMP-2 pDNA from collagen scaffolds (85, 291). Of particular interest for this thesis, the use of coll-nHA scaffolds as GAMs for the incorporation of BMP-2 pDNA, VEGF pDNA and EphrinB4 pDNA has demonstrated successful osteogenesis and bone repair in recent work from our laboratory (126, 127, 346). The research presented in this thesis builds on this work and uses coll-nHA scaffolds for miRNA delivery. With regard to scaffold-mediated miRNA delivery, a small number of studies to-date have demonstrated the application of cell-mediated (58, 297, 299, 347, 348) and ‘cell-free’ or *in vivo* strategies (349, 350). Among the cell-mediated strategies, baculovirus and lentivirus transduction of stem cells with pre-miR-148b and miR-31 inhibitors significantly improved bone healing *in vivo* (297, 299). Alternatively, ‘cell-free’ approaches have used direct entrapment or surface immobilisation technologies. Direct entrapment appeared particularly suited for in situ-forming materials such as PEG-based hydrogels or electrospun nanofibres delivering naked miRNAs (349, 350). However, bolus release effects were observed with these approaches and additional incorporation of non-viral

vectors was proposed to improve pharmacokinetics of cargo delivery (309). In line with this, immobilisation approaches involve the prior step of miRNA complexation with polymers. An example by Wu *et al.* immobilised miRNA-Lipofectamine® 2000 complexes onto a microporous titanium oxide surface (351). As a central rationale for this thesis, it is speculated that 'cell-free' 3D platforms for miRNA delivery incorporating nHA within the in-house developed coll-nHA scaffold holds essential advantages from the biomaterial standpoint.

1.9.3.Combinatorial delivery of biomolecules from bone tissue-engineered scaffolds

Combinatorial delivery of biomolecules from bone tissue-engineered scaffolds represents a promising approach to recapitulate the natural tissue repair process (165, 352). This was initially approached using delivery of GFs (183, 353, 354) including delivery of GFs capable of promoting both angiogenesis and osteogenesis (165, 353, 355). The combinatorial approach has progressed more recently to the delivery of multiple genes (127, 288, 356). Within the *ex vivo* transfection approaches documented, delivery of VEGF plus BMP-2 pDNA to MSCs either by baculovirus or adenovirus transduction successfully improved bone formation (355, 357). Examples of 'cell-free' *in vivo* transfection approaches include adenoviral-based BMP-7 plus PDGF and VEGF plus BMP-2 pDNA delivery from collagen-chitosan scaffolds (289, 358). In the area of non-viral *in vivo* transfection, CaP cement scaffolds incorporating nanomicelles with activin receptor-like kinase 6 plus Runx2 pDNA (292) as well as recent work from our laboratory on coll-nHA VEGF plus BMP-2 GAMs (127) represent significant contributions to the field. In particular this in-house work underlined the importance of vector choice, with nHA-based delivery surpassing the outcome of PEI-based delivery. However, minimal research has been conducted on combinatorial approaches to scaffold-mediated RNAi and miRNA delivery with only one study on combined miRNA delivery from 3D scaffolds reported to date (58). In this study, Mariner *et al.* adopted an *ex vivo* approach where hMSCs nucleofected with miR-148b mimic plus antagomiR-489 were then incorporated on PEG-based hydrogel scaffolds (58). No published study delivering miRNA combinations has focused on simultaneous angiogenesis and osteogenesis yet. With this in mind, the research presented in Chapter 5 of this

thesis focused on combinatorial miRNA delivery to simultaneously promote an angiogenic and osteogenic response in MSCs.

1.10.Project aims and objectives

The overall goal of the research presented in this thesis was to determine the potential of using nano-sized hydroxyapatite particles (nHA) to act as non-viral vectors for the delivery of a series of miRNAs to human (h)MSCs and to determine the miRNA therapeutic combination leading to optimal osteogenesis and angiogenesis before ultimately producing miRNA-activated scaffolds capable of mediating enhanced osteogenesis by hMSCs.
The specific aims of this PhD project were thus to:

- Investigate the potential of in-house synthesised nHA particles as non-viral vectors for miRNA delivery using synthetic reporter miRNAs and determine the delivery profile and the optimal miRNA concentration for this system (Chapter 2)
- Assess the pro-osteogenic therapeutic efficacy of nHA-based delivery of (i) antagomiR-133a, (ii) antagomiR-16 and (iii) miR-210 mimic and establish the optimal candidate for incorporation in a miRNA-activated scaffold (Chapter 3)
- Assess the potential of coll-nHA scaffolds as miRNA delivery platforms to manipulate hMSC gene expression by incorporating reporter miRNAs (Chapter 4)
- Apply the miRNA-activated coll-nHA scaffold system to therapeutically enhance osteogenesis by incorporating the optimal therapeutic candidate earlier established, namely antagomiR-133a (Chapter 4)
- Investigate the pro-angiogenic therapeutic efficacy of nHA-based delivery of the miR-210 mimic to enhance the pro-angiogenic capabilities of hMSCs through the direct targeting of the EphrinA3 gene (Chapter 5)
- Assess the potential of combinatorial delivery of the miR-210 mimic with antagomiR-133a or antagomiR-16 to simultaneously enhance the angiogenesis and osteogenesis capabilities of hMSCs (Chapter 5)

Chapter 2. Investigation of nanohydroxyapatite particles as non-viral vectors for microRNA delivery to human mesenchymal stem cells

Research presented in this chapter has been included in the following peer-reviewed publication:
Castaño, IM et al., A Novel Collagen-Nanohydroxyapatite microRNA-activated Scaffold for Tissue Engineering Applications Capable of Efficient Delivery of both miR-mimics and antagomiRs to Human Mesenchymal Stem Cells. J Control Release 2015; 200: 42-51.

2.1.Introduction

A variety of biomolecules including proteins, GFs and pDNA have been explored in recent years to potentiate the body's own healing ability to repair tissue voids as part of advanced TE strategies. Recently, overexpression or inhibition of miRNAs is gaining attention in TE approaches, since delivering miR-mimics or antagomiRs respectively may enable the required modulation of protein expression to improve tissue regeneration. However, effective delivery of miRNAs remains the greatest challenge to unleashing their vast potential. Transient delivery of miR-mimics and antagomiRs into cells has been approached by using viral or non-viral vectors formerly applied to pDNA delivery. Although pDNA and miRNAs share several physicochemical properties, due to their negatively charged phosphodiester backbone, susceptibility to nucleases and poor intracellular cytosolic delivery, the chain size is critically smaller in miRNAs resulting in low charge density, in addition to having a short and rigid structure (326, 339). Taken together, this points to a necessity of tailoring efficient vectors for the successful delivery of miRNAs, which may not necessarily translate from successful DNA delivery (359).

Significant research efforts have focussed on using viruses belonging to the adenovirus and lentivirus families which are highly efficient at delivering miRNA-related molecules including both miR-mimics and antagomiRs; however their

clinical applicability is limited by the threat of adverse immune responses in patients and the risk of insertional mutagenesis following viral integration (57). Current developments in non-viral miRNA delivery technologies include nucleofection as well as the use of nanoscale complexes with Lipofectamine® 2000 (310), PEG (307) or PEI (308). Although these compounds exhibit efficient delivery yields, evidence of significant cell damage derived from their use remains a considerable drawback in terms of clinical application. Thus, research efforts are focussed on developing an ideal non-viral vector which would ensure maximum efficacy of delivery but without significant cytotoxicity concerns (315).

CaPs are a promising alternative non-viral vector as although their efficacy of delivery is typically lower than that of the aforementioned lipids and synthetic polymers, advantages include low toxicity, biodegradability and ease of use (126). CaP complexes with nucleic acids form precipitates at the cell surface and undergo endocytosis partially dependent on clathrin and dynamin (283, 360, 361). In spite of the advantageous high biocompatibility of CaPs, the growth in size of different phases of CaP crystals is associated with limited reproducibility in terms of efficiency of delivery, meaning a drawback for the application of these systems (318, 323). To overcome this limitation, different strategies have been undertaken with limited success so far (326), including customisation with synthetic or lipidic polymers. Some examples of modified CaP particles for siRNA delivery reported in the literature include incorporation of PEG added either directly in the particle synthesis process (324) or combined with calcium chelators or the nucleic acid cargo (325). Alongside this approach, CaP particle coating with conjugates of chitosan and 3,4-dihydroxyphenylalanine (dopa) as well as hyaluronic acid and dopa have also been investigated in the literature (326, 327).

In this study, we focused on the application nHA particles as novel non-viral miRNA delivery vectors. HA is a crystalline ceramic found predominantly in the bone extracellular matrix and thus is of particular interest for bone repair applications; a Darvan®-aided wet precipitation synthesis technique was previously developed in our group to overcome reproducibility limitations associated with HA crystal growth and therefore improve the applicability of this

material for bone repair (124). This methodology generates non-aggregating nanosize particles in a simple, low-cost manner by combining $CaCl_2$, Na_3PO_4 and NaOH solutions with low concentrations of Darvan® as a dispersant. Moreover, these nHA particles have been used to safely achieve higher transfection efficiency for pDNA delivery to hMSCs compared to a commercial CaP transfection kit (126). Therefore, the research presented in this chapter aimed to demonstrate for the first time that the combination of nHA particles with miRNAs can be tailored to result in an efficient non-viral system for miRNA delivery to BM-derived hMSCs, a cell type commonly utilized for TE strategies due to their multilineage differentiation capacity and accessible sourcing (362).

2.2.Hypothesis & aims of the study

The underlying hypothesis of this study was that these in house-synthesised nHA particles could act as non-viral vectors for miRNA delivery to hMSCs. Thus, the overall aim of this study was to determine the miRNA delivery profile for nHA particles, by utilising scrambled (scr) miR-mimic and antagomiR sequences, which act as controls and encompass sequences with non-existent targets in mammalian cells. A secondary aim was to determine the concentration of miRNAs most suitable for progression of the research presented in the following chapters of this thesis. The specific aims of this chapter involved:

- Determination of size and surface charge (zeta potential) of nHA particles loaded with miRNAs, (termed *nanomiRs* hereafter)
- Assessment of nanomiR morphology using transmission electron microscopy
- Analysis of hMSC cytotoxicity following nanomiR treatment
- Analysis of uptake efficiency using fluorescently tagged scrambled miRNAs
- Assessment of silencing capability of nanomiR-mimic delivery using a commercially available functionality reporter miR-mimic which targets GAPDH, expressed by hMSCs at a basal level

- Assessment of silencing capability of nanoantagomiR delivery with a commercially available functionality reporter antagomiR which targets miR-16, expressed by hMSCs at a basal level

2.3.Materials & Methods

2.3.1.nanohydroxyapatite (nHA) - miRNA (nanomiR) system

nHA particles were synthesised following a protocol established in our laboratory (124). Briefly, a solution of 12 mM phosphate, containing 0.017 % Darvan® 821A (RT Vandervilt, Norwalk, CT), was added to an equal volume of a 20 mM calcium chloride (Fisher Scientific, Ireland) solution and filtered through a 0.2 µm filter. The nanomiR transfection mix consisted of 150 µl of the nHA solution added to a miRIDIAN mimic or antagomiR (Dharmacon, ThermoScientific, Germany) solution prepared at final concentrations of either 10 or 20 nM and combined with 0.25 M $CaCl_2$, as adapted from the in-house method for pDNA delivery (126).

2.3.2.NanomiR physicochemical characterisation

In order to characterise the physicochemical properties of complexes formed by a delivery vector and the agent delivered, in this case miRNAs, size and surface charge were studied. Hydrodynamic size and surface charge was determined using dynamic light scattering (DLS; ZetaSizer 3000 HS, Malvern instruments, UK). DLS measures the time dependent fluctuations in the scattering intensity to determine the size of the particles in the form of the hydrodynamic diameter (DH), for which the particle sample must be contained in an aqueous solution to resemble the size adopted in the presence of physiological fluids. The surface charge of the particles determines their stability in dispersion. The zeta potential, which is the electrical potential at the hydrodynamic plane of shear of the particles, is the indicative parameter of surface charge of particles in suspension. Freshly prepared blank nHA particles or nanomiR samples were diluted 10 times in low UV absorbance ultra-pure water (Sigma Aldrich, Ireland). The solution was then transferred to a fine quality glass cuvette designed for

zeta potential and size analysis (Particular Sciences 74 Ltd., Ireland). The particle size and zeta potential of three samples was analysed. Measurements were performed at 25°C with the 100 mW laser set at an angle of 90° to the sample. The sample was allowed to equilibrate prior to five readings being taken. The mean particle size, the standard deviation and the polydispersity of the sample were determined using the systems data analysis functions based on cumulants analysis.

To analyse particle morphology, transmission electron microscopy (TEM) was used. In TEM, nanoscale high resolution images are obtained from the interaction of the electron beam with the sample. Before examination, 1 droplet of freshly prepared nHA or nanomiR samples were deposited onto rapid setting epoxy resin coated aluminium grids and allowed to precipitate while air drying. Imaging was carried out at 200 kV using a Jeol 2100 TEM (Jeol, UK).

2.3.3.Cell culture

Human mesenchymal stem cells (hMSCs) were derived from iliac crest bone marrow aspirates obtained from healthy human volunteers with informed consent at the Regenerative Medicine Institute, the National University of Ireland, Galway. All procedures were performed with ethical consent from the Clinical Research Ethical Committee at University College Hospital, Galway. hMSCs were isolated using standard protocols and stringent analysis of cell phenotype (363).

Cells were expanded in culture by direct plating (364), using hMSC growth medium consisting of low-glucose DMEM (Sigma-Aldrich, Ireland) supplemented with 10 % foetal bovine serum (FBS) plus 1 % penicillin/ streptomycin (Sigma-Aldrich, Ireland), and maintained at 37°C, 5 % CO_2 and 90 % humidity. Subsequently, cells were passaged using 0.25 % trypsin/EDTA at 5-7 day intervals and expanded until sufficient cell numbers were obtained at passage 5 for experimentation. Cells were then plated at a density of 5×10^4 cells per well in 6 well plates 24 hours before adding the control, nanomiR-mimic or nanoantagomiR treatments at final concentrations indicated in Section 2.3.1.

2.3.4.Cell viability after nanomiR treatment

Cell viability was studied to monitor potential cytotoxic effects derived from the nanomiR treatment of hMSCs, for which nHA particles were loaded with scrambled (scr) miR mimic/antagomiR, which act as controls and encompass cel-miR-67 sequences with non-existent targets in mammalian cells. The Quant-iT PicoGreen dsDNA kit (BioSciences, Ireland) was utilised according to the manufacturer's protocol to study cell number at days 3 and 7 post-treatment. Briefly, 100 µl of the PicoGreen reagent solution was added to samples containing the 0.2 M carbonate 1 % TritonX (Fisher, Ireland) cell lysate buffer and fluorescence was read at 538 nm using a VarioSkan Flash plate reader (ThermoScientific, Germany) and SkanIt RE for VarioSkan software. Complimentary cell redox metabolic activity was assessed with the colorimetric-based MTS assay CellTiter 96® AQueous One Solution (Promega, Ireland) following manufacturer's instructions. Briefly, 20 µl of the Celltiter 96® reagent per 100 µl of culture medium was added to each well and incubated for 3 h at 37°C, before absorbance was measured at 490 nm using the aforementioned VarioSkan Flash plate reader. The following equation was applied to calculate cell viability (%):

Equation 2.1

$$\text{cell viability } \% = abs_{[\text{treatment group}]} / abs_{[\text{untreated cells control}]} \times 100$$

2.3.5.Microscopy evaluation to assess nanomiR uptake efficiency in hMSCs

Dy547-miRIDIAN scr miRNA molecules (Dharmacon) incorporate a red fluorescent tag and so serve as tools for monitoring the uptake process by fluorescence emission at 547 nm. nHA particles were loaded with 10 and 20 nM doses of Dy547-tagged scr miR-mimic/antagomiR miRIDIAN molecules and added to hMSC monolayer culture in order to study the uptake of nanomiR complexes in the cells. Live cells were examined for nanomiR fluorescence at 3 and 7 days after treatment. To do so, fluorescence and phase contrast microscopy was performed using a Sony-Lennox Optika 4083.CL5 microscope digital system coupled to Optika Vision Pro software (Lennox, Ireland).

To achieve more detailed observation of the internalised nanomiRs, staining with Alexa488 Phalloidin (Invitrogen, UK) and counterstaining with diamidino-2-phenylindole (DAPI) was performed at 3 and 7 days after treatment. Cells were cultured on microscopy coverslips pre-coated with 0.001 % poly-L-lysine, fixed in 4 % para-formaldehyde (PFA), permeabilised with 0.1 % Triton-X100, blocked in 1 % bovine serum albumin (BSA) in phosphate buffered saline (PBS), stained and mounted onto glass coverslips using Ibidi® mounting medium (Ibidi GmbH, Ireland). Digital imaging was performed using the Olympus IX51-AnalySIS imaging system (Olympus Scientific Solutions Americas, UK).

2.3.6.Flow cytometry quantification of nanomiR uptake efficiency in hMSCs

Flow cytometry analysis was carried out to quantify the percentage of cells internalising the Dy547-labelled nanomiR complexes at 24 h, 3 days and 7 days after treatment. For flow cytometry sample preparation, cells were detached from cell culture wells using 0.25 % trypsin/EDTA, following which they were fixed in 5 % formalin for 15 minutes and centrifuged at 500 xg for 5 minutes. Samples were then resuspended in 200µl of PBS and analysed for red fluorescence emission using a BD FACS Canto II and BD FACS Diva software (BD Biosciences, UK). Percentage of uptake efficiency was calculated as the percentage population displaying high fluorescence intensity (over median), after substracting nHA alone treatment values from those of the Dy547-tagged nanomiRs.

2.3.7.Functionality assessment of nanomiR treated hMSCs using quantitative Real Time Polymerase Chain Reaction (qRT-PCR)

miRNA bioactivity after nHA-mediated delivery to hMSCs was verified by measuring the silencing functionality of reporter miRNA molecules by qRT-PCR. For this purpose, prior to addition to the monolayer culture, nHA particles were loaded with either the miRIDIAN positive controls (Dharmacon, ThermoScientific, Germany), which are designed to silence targets expressed at a basal level in healthy cells, or with their scrambled counterparts as

reference controls. The miR-mimic utilised is designed to target the mRNA of the housekeeping glyceraldehyde phosphate dehydrogenase (GAPDH), involved in the normal glucose metabolism of cells, and the selected antagomiR targets the tumour suppressor miR-16, basally expressed in non-tumorigenic cells (365).

Total RNA extraction including miRNA:
Total RNA extraction was performed adding 500 µl QIAzol lysis buffer (Qiagen, UK) directly onto the cell culture plates, then cell lysates were extracted using cell scrapers (Sarstedt, Ireland) and transferred into microcentrifuge tubes. This was followed by an ultracentrifugation step at 4°C and 8000 g for 15 min in the presence of 100 µl chloroform. The resulting aqueous phase was processed using the miRNeasy Mini purification kit (Qiagen, UK) according to manufacturer's instructions. RNA quality and concentration was determined using a Nanodrop 2000 (Thermo Scientific, UK) spectrophotometer.

Messenger (m)RNA Reverse Transcription and Polymerase Chain Reaction:
The Quantitect Reverse Transcription kit (Qiagen, UK) was used to perform mRNA reverse transcription (RT) reactions (20 µl) on 200 ng of total RNA. Real-time PCR reactions (15 µl) were carried out on an Eppendorf Realplex4 EpgradientS Mastercycler (Eppendorf, Germany) using the Quantitect SYBR Green PCR master mix (Roche, Ireland). The following validated pre-designed human Quantitect Primer Assays (Qiagen, UK) were applied for the measurement of GAPDH and 18S levels: Hs_GAPDH_1_SG and HS_RRN18S_1_SG. Consequently, the relative expression of GAPDH mRNA was calculated normalising to the level of the housekeeping 18S ribosomal RNA, and using the $2^{(-\Delta\Delta Ct)}$ method.

MiRNA Reverse Transcription and Polymerase Chain Reaction:
To assess miR-16 levels, the hsa-miR-16 Taqman® MicroRNA assay, the probe-specific Taqman® Micro RNA kit and Taqman® Universal PCR Master Mix were used (all from BioSciences, Ireland). Stem-loop miRNA RT reactions (15 µl) were carried out on 100 ng of total RNA using an Eppendorf Personal Mastercycler (Eppendorf, UK) and miR-PCR assays (10 µl) were performed using the aforementioned PCR system. Consequently, the relative expression

of miR-16 was calculated normalising to the level of the housekeeping 18S ribosomal RNA, and using the $2^{(-\Delta\Delta Ct)}$ method.

2.3.8.Statistical analysis

Experiments were performed in triplicate, unless otherwise specified within figure captions, and are representative of a minimum of three independent repetitions using two cell donors. Data analysis was performed using the SigmaPlot 11.0 software package. Results were presented as the mean + standard deviation and subjected to a two-way analysis of variance (ANOVA) plus a Tukey *post-hoc* test. $p<0.05$ and $p<0.001$ were considered significant differences.

2.4.Results

2.4.1.NanomiR complexes adopt multiparticulate formations and posses a negative surface charge

nHA particles utilised in this work were combined with a relatively low dose of 20 nM miRNA which was selected after reviewing the miRNA dosing range reported in the literature (220). DLS characterisation of the nanomiR complexes demonstrated an average hydrodynamic size of the particles within the 300 - 400 nm range (Figure 2.1a) with no statistical differences between groups: blank nHA particles were 301.5 nm, miR-mimic loaded nHA particles were 329.5 (± 24.7) nm, and antagomiR loaded nHA particles were 398.33 (± 79.6) nm. Zeta potential remained within the range of - 5 mV to - 10 mV with no statistical differences between groups, and was highest in the nanomiR-mimic group (-9.9 ± 5.3 mV, Figure 2.1b). Although not statistically significant, the observed changes indicated the existence of an electrostatic interaction between miRNAs and nHA particles. To further observe this interaction, TEM analysis was carried out. The topographic images of the precipitate complexes obtained in this study showed the formation of multiparticulate structures in varying shapes for both scr nanomiR-mimic and nanoantagomiR complexes (Figure 2.2b-c), in comparison to the rod-shaped conformation that the nHA particles adopted in the absence of miRNAs (Figure 2.2a).

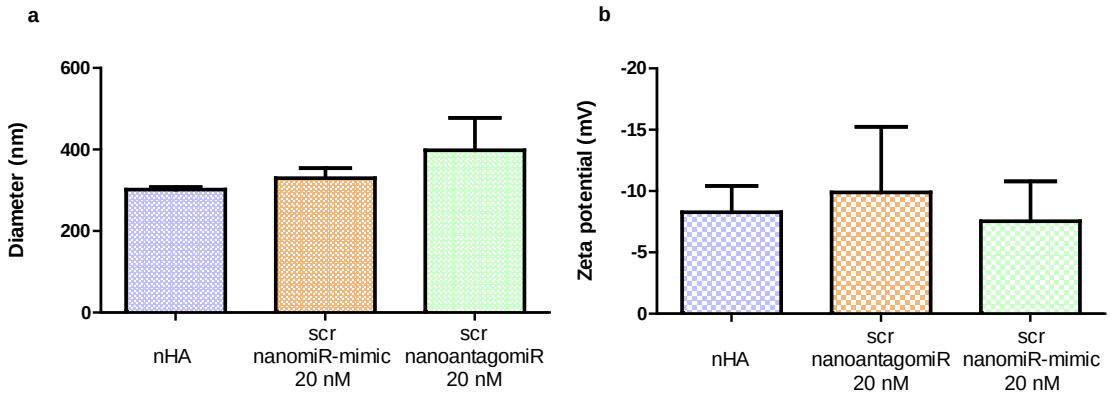

Figure 2.1 Physical characterisation of nanomiR complexes. nHA particles were loaded with a final concentration of 20 nM of scrambled (scr) miR-mimic or antagomiR. **a)** Size determination presented as particle diameter (nm) showed nanomiR complexes in the range of 300 to 400 nm. **b)** Surface charge analysis presented as zeta potential (mV) demonstrated a nanomiR surface charge of -7 to -10 mV. Mean + standard deviation, n = 3, no statistical significance.

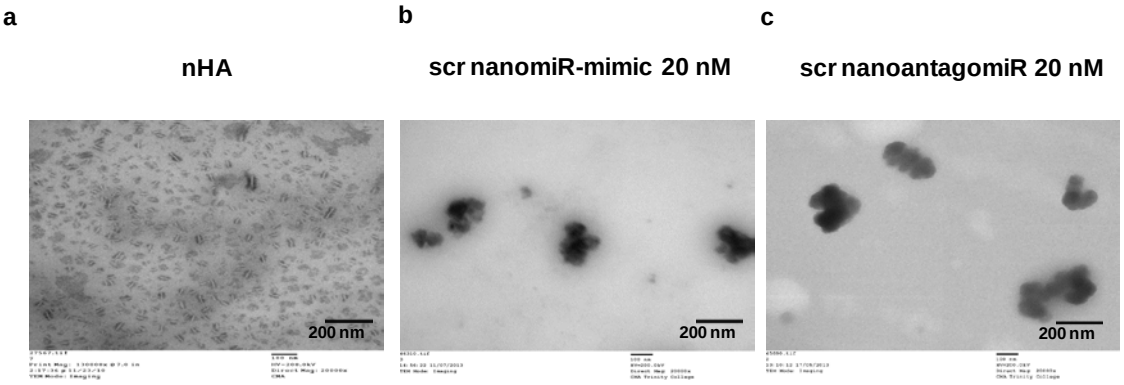

Figure 2.2 TEM analysis of nanomiR complexes. a) Blank nHA particles adopted rod-shape conformations while **b)** scr nanomiR-mimic and **c)** scr nanoantagomiR were arranged in bead-branched multiparticulate formations. Scale bar = 200 nm.

2.4.2.Cell viability was maintained after nanomiR treatment

The cell viability study demonstrated that there was no nanomiR treatment-derived cytotoxic effects at the doses tested (Figure 2.3). Cell number remained unaffected at day 3 after treatment although a reduction in cell metabolic activity was observed in the scr nanomiR-mimic 20 nM group. Nevertheless, the cells were capable of normal metabolic activity and even significantly increased proliferation at the later timepoint. Considering that after a longer period in culture no detrimental effects were observed, it is proposed that nanomiR

complexes at the studied concentrations did not result in a cytotoxic effect on hMSCs.

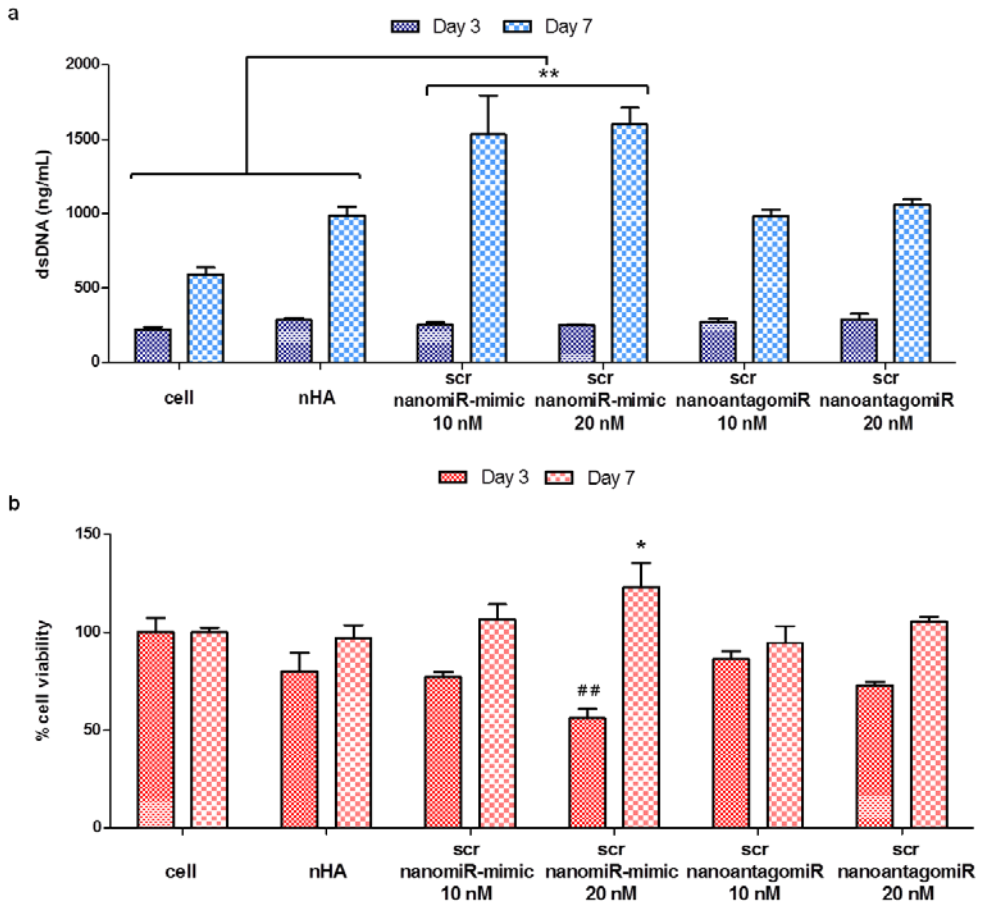

Figure 2.3 Cytotoxicity of scr nanomiR-mimic & nanoantagomiR in hMSCs. a) dsDNA quantification indicated that viable cell number was maintained (scr nanoantagomiR) or significantly increased (scr nanomiR-mimic) compared with control groups at day 7 post-treatment, demonstrating no treatment associated cytotoxic effects. Mean + standard deviation, n = 3, ** = p<0.001. **b)** Cell viability assessment by MTS assay. Mean + standard deviation, n = 3, ## = p<0.001 vs. cell at day 3, * = p<0.05 vs. cell at day 7.

2.4.3.NanomiR uptake in hMSC monolayer was highly efficient

In order for the nanomiR system to be effective, the first requirement is that the complexes are taken up by the cells. From the fluorescence microscopy images, the presence of Dy547 nanomiR deposits were noted, and phase contrast images captured for the respective fields were collated in merged images to serve as references for intra- or extracellular location of the complexes, since Dy547 nanomiR is inherently fluorescent (Figure 2.4b). Additionally, the phase contrast images showed no morphological changes

between groups at all timepoints and cells proliferated normally over the culture period, indicating no adverse effects with any treatment.

Further assessment of Dy547 nanomiR internalisation using complementary labelling of the actin cytoskeleton with phalloidin (green) and nuclei with DAPI (blue) confirmed the ability of nHA particles to deliver miRNAs intracellularly (Figure 2.5). Cell nuclei and actin cytoskeleton labelling allowed the detection of Dy547 nanomiRs in points of the cell cytoplasm as well as in the proximity of, or superimposed to, the nucleus. Qualitatively, it was noted that Dy547 nanomiR-mimic displayed co-localisation with cell nuclei at day 3 and a more cytoplasmic distribution at the later timepoint of day 7, while in the Dy547 nanoantagomiR treatment group, internalisation was more evident in the proximity of the cell nuclei at both timepoints.

Flow cytometry was used to quantify uptake efficiency at three timepoints: day 1, 3 and 7 (Figure 2.6). Uptake kinetics proved different for both types of molecules: Dy547 nanomiR-mimic at the 20 nM dose showed a cyclical uptake firstly peaking at day 1, then decreasing at day 3 and yielding maximum internalisation efficiency (17.4± 5.6 %) at day 7, while no uptake of 10 nM Dy547 nanomiR-mimic could be detected at the timepoints assessed. Furthermore, an initially sustained uptake profile with a 10 % reduction at the last timepoint was determined for both the 10 and 20 nM dose of Dy547 nanoantagomiRs. Specifically, 33.5 ± 1.5 % and 39.6 ± 4.7 % uptake efficiency values were quantified respectively for the 10 and 20 nM Dy547 nanoantagomiR doses by day 3, with significantly higher percentages over the complete time course in comparison to Dy547 nanomiR-mimics.

In summary, this study showed that the fluorescently labelled nanomiR complexes (indicated by the arrows) were internalised in hMSCs localising mostly in the proximity of the nucleus as well as depositing outside the cells, and achieved different uptake efficiencies reaching maximum levels close to 20 % for the 20 nM nanomiR-mimic at day 7 and 40 % for the 20 nM nanoantagomiR at day 3 post-treatment.

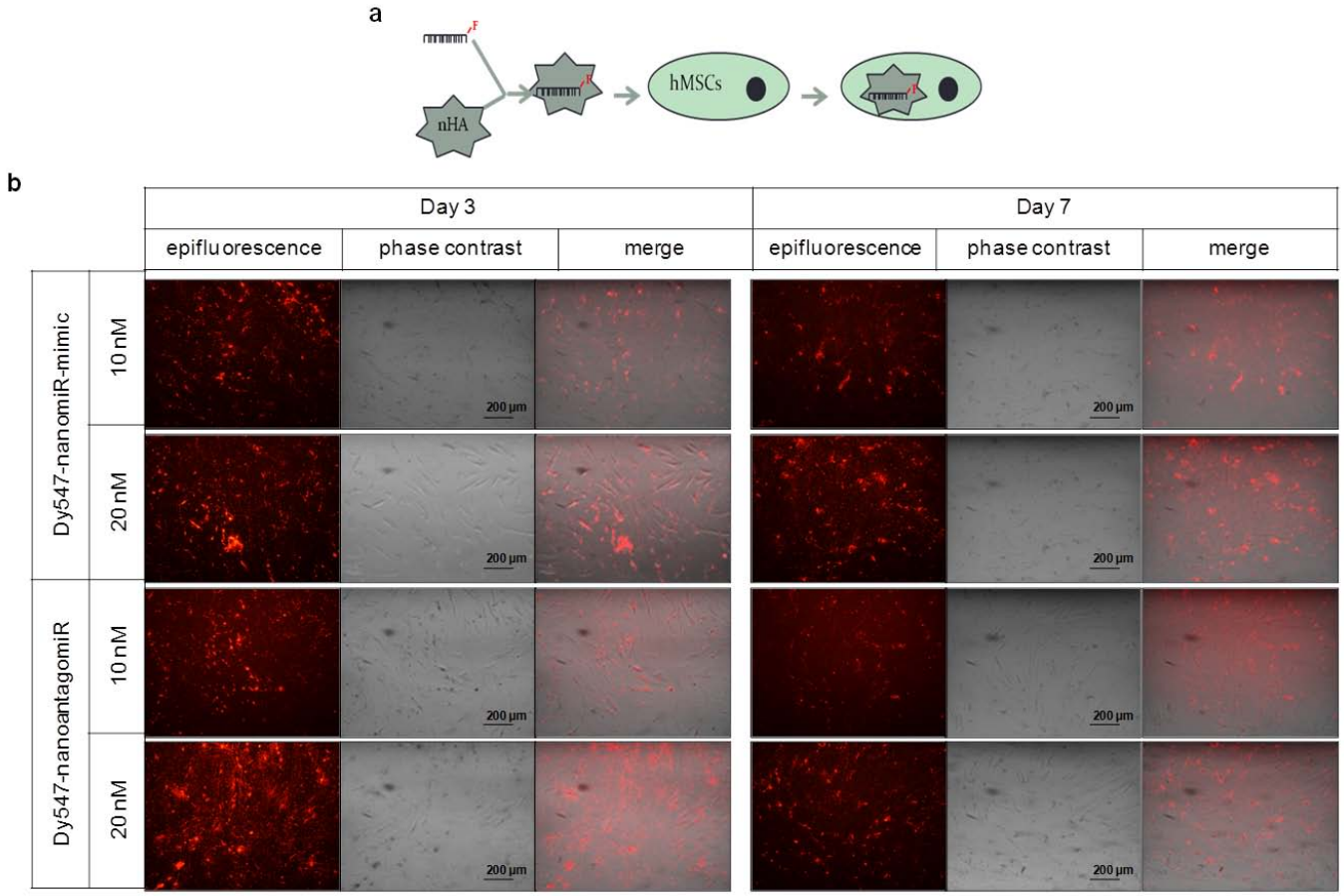

Figure 2.4 Live cell imaging of hMSCs after treatment with red fluorescently labelled (Dy547) scr nanomiR-mimic *&* nanoantagomiR. a) Schematic of the procedure to assess uptake efficiency. **b)** Composite depicting representative epifluorescence, phase contrast and merged images of hMSCs treated with 10 & 20 nM doses at two of the timepoints studied. NanomiR deposits can be observed both internally and extracellularly, while hMSCs displayed a normal fibroblastic-like morphology and increase in cell confluence indicated normal proliferative cell capacity over time. Scale bar = 200 µm, n = 3.

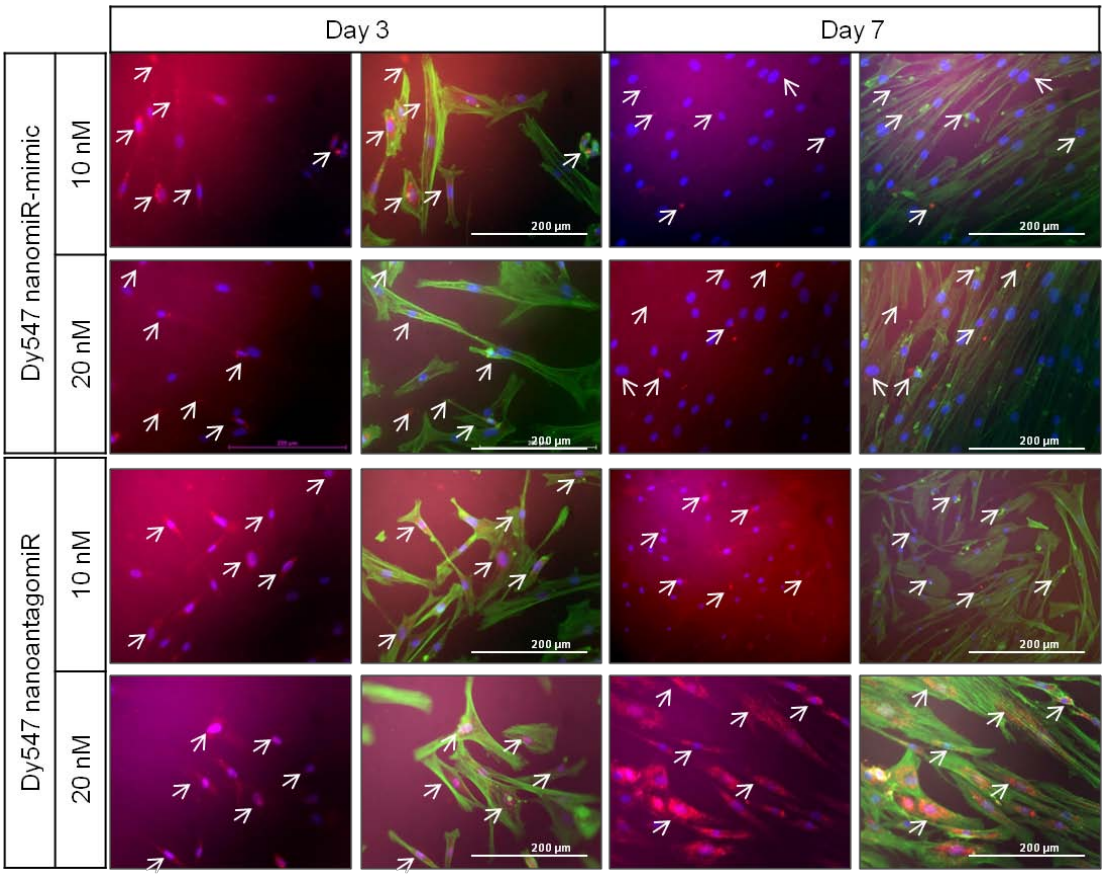

Figure 2.5 Assessment of nanomiR internalisation in hMSC. Composite images depicting representative fluorescence images of Dy547 nanomiRs (red) plus cell nuclei labelled with DAPI (blue) and merged images with cell cytoskeleton staining using Alexa488-Phalloidin (green). Arrows refer to nanomiR localisation, observed intracellularly in points of the cell cytoplasm and more predominantly in the area around the nucleus, but also localised extracellularly. Scale bar = 200 µm, n = 3.

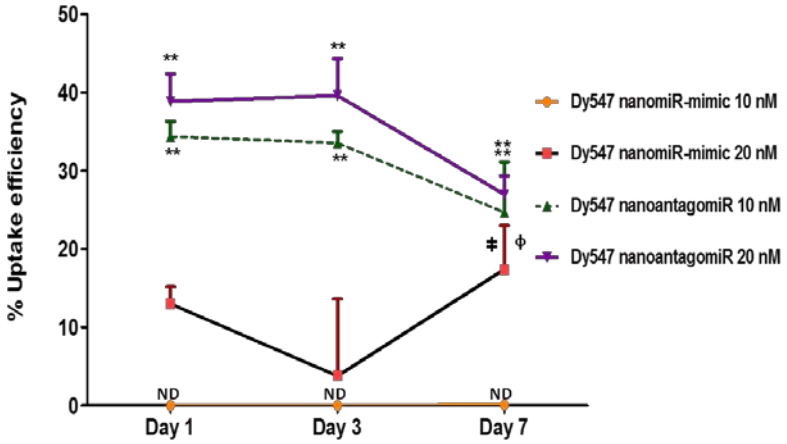

Figure 2.6 Quantification of nanomiR uptake efficiency in hMSCs. NanomiR-mimic and nanoantagomiR achieved different uptake efficiencies and kinetics at the doses and timepoints tested. Mean + standard deviation, n = 3. ** = $p<0.001$, ϕ = non-significant compared to day 7 nanoantagomiR 10 nM, ǂ = $p<0.05$ compared to day 7 nanoantagomiR 20 nM. ND= not detectable.

2.4.4.Reporter nanomiRs caused highly functional interference after nHA-based delivery

qRT-PCR analysis performed on samples 1, 3 and 7 days post-treatment with the 10 and 20 nM doses of the miRIDIAN positive controls of transfection, which are research tools designed to silence targets expressed at a basal level in healthy cells, demonstrated a high interfering activity of the reporter nanomiRs towards their respective targets.

The reporter nanomiR-mimic silenced GAPDH expression significantly to an average of 0.07 ± 0.02 fold of the relative expression level with both doses of 10 and 20 nM, indicating over 90 % functionality of the nHA-delivered miR-mimic once cellular internalisation occurred (Figure 2.7). Similarly, miR-16 expression decreased significantly upon treatment with the 10 and 20nM doses of reporter nanoantagomiR, to an average of 0.01 ± 0.01 fold of the relative expression level. This effect was maintained over 7 days for the lower dose, indicating ~99 % functionality of the nHA-delivered antagomiR after internalisation, although at the latter timepoint of 7 days a reduction to 30 % interfering functionality (0.7 ± 0.65 fold change) was detected for the 20 nM dose; this matched the trend of temporal reduction in uptake which was quantified previously (Figure 2.8).

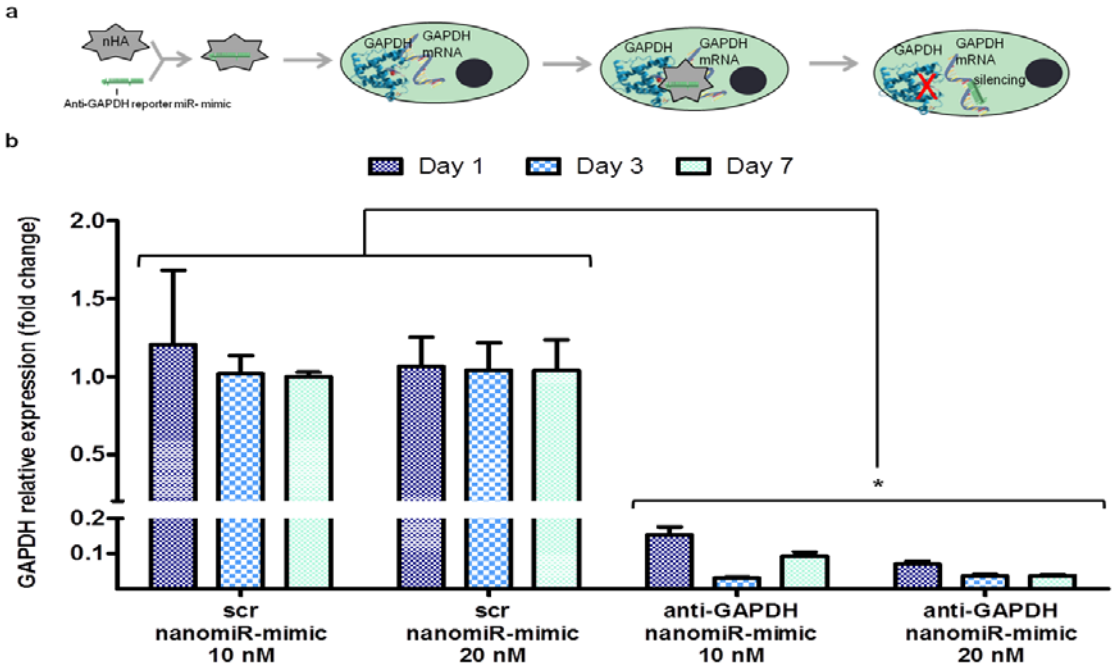

Figure 2.7 Functionality of reporter nanomiR-mimic. a) Schematic of the treatment carried out for nanomiR-mimic functionality tests. **b)** qRT-PCR analysis showed that treatment with reporter nanomiR-mimic significantly decreased GAPDH expression. Scr nanomiR-mimic was introduced as a reference control. Relative expression was normalised to 18S and calculated using the $2^{(-\Delta\Delta Ct)}$ method. Mean + standard deviation, n = 4, * = $p<0.05$.

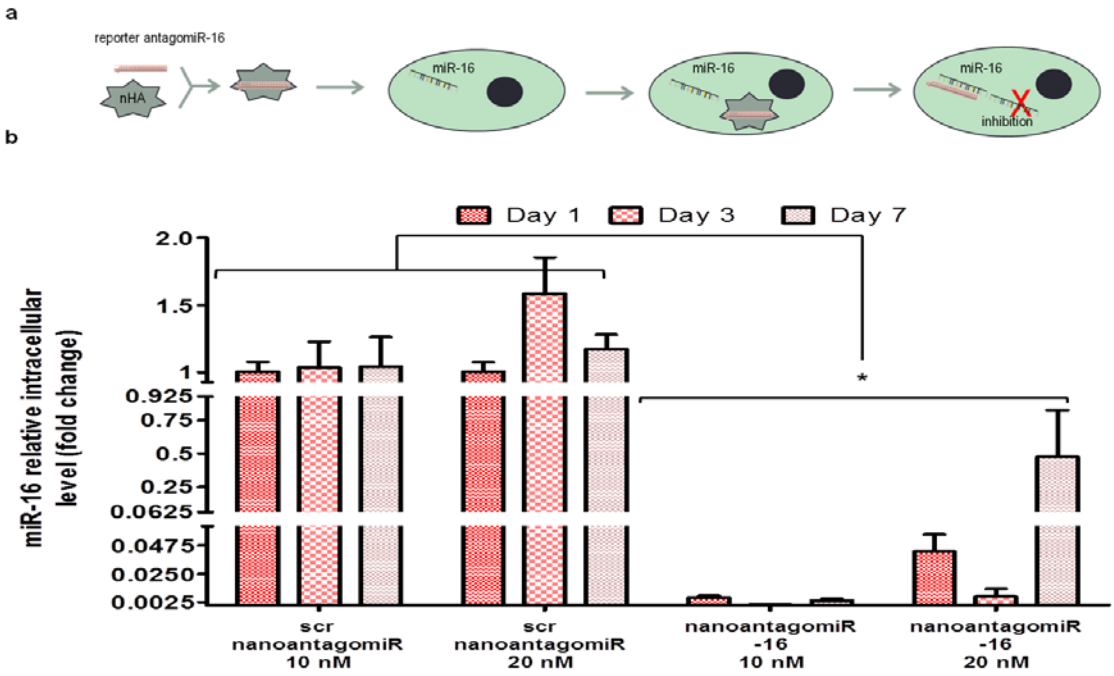

Figure 2.8 Functionality of reporter nanoantagomiR. a) Schematic of the treatment carried out for nanoantagomiR functionality tests. **b)** qRT-PCR analysis showed that treatment with reporter nanoantagomiR-16 significantly decreased miR-16 levels. Scr nanoantagomiR was introduced as a reference control. Relative expression was normalised to 18S and calculated using the $2^{(-\Delta\Delta Ct)}$ method. Mean + standard deviation, n = 4, * = $p<0.05$.

2.5.Discussion

Recently in the field of TE, a small number of explorations into incorporating RNAi therapeutics, such as siRNAs and miRNAs, in non-viral delivery systems have been performed. Notably, commercial vectors with recognised limitations have been applied for these few studies and miRNA delivery systems using nHA particles have not been reported previously in the literature. The aim of this study was to assess the potential of using in house-synthesised nHA particles to act as non-viral vectors for miRNA delivery to hMSCs, a particularly difficult cell type to transfect effectively. The data presented here showed that nHA particles combined with miR-mimics and antagomiRs, forming complexes we term *nanomiRs*, resulted in high cellular uptake in monolayer hMSCs with limited cytotoxicity at a 20 nM dose. Furthermore, single administration of reporter nanomiRs translated into high silencing functionality, to a level comparable to viral and lipid-based carriers for this cell type (219). Taken together, the results indicated that nHA particles are potentially efficient non-viral vectors for miRNA delivery, thus demonstrating the potential of using these natural-based nanoparticles to unleash the vast potential of miRNAs for therapeutic applications in TE and regenerative medicine.

It was determined that nanomiRs formed negatively charged complexes in the 300 - 400 nm range, which was consistent with the nHA-pDNA complexes which previously demonstrated successful transfection of hMSCs (124, 126). Several implications, including safety, release kinetics and cellular internalisation, have been described as dependant on particle size and surface charge properties (318). Classically, it is estimated that cellular internalisation requires positively charged particles of less than 200 nm (366). However, evidence of successful internalisation of miRNA-PEI or miRNA-chitosan complexes greater than 500 nm in size (256), as well as of negatively charged siRNA lipoplexes (367) has been noted, which support the potential of nanomiRs for effective miRNA delivery. Of note from the current study, small size variations were found between blank nHA particles and nanomiRs, with distinctive trends in size and charge variation found between miR-mimics and antagomiRs. The nHA dose previously optimised for pDNA delivery was

combined with the low miRNA doses of 10 and 20 nM in a cost effective low miRNA to nHA ratio; however, this ratio can conceal physicochemical differences between blank and miRNA loaded nHA particles. Taken together, both trends in size and charge variation found between miR-mimics and antagomiRs may be explained by the higher molecular weight of the latter, which results from the lipidic modifications in the phosphate groups of the backbone chain (83). In summary, the structural analysis demonstrated the ability of nHA particles to complex with both miR-mimics and antagomiRs, forming nanomiRs, meaning a successful translation of the ability of the nHA particles to form complexes with DNA to miRNA. Ultimately, bearing in mind the overall aim of this project, which was centred on the successful incorporation of nanomiRs within a 3D scaffold depot to target infiltrating cells, the physicochemical features of nanomiRs were deemed fit-for-purpose.

As a rule of thumb, safety of miRNA delivery methods is influenced by the dose of miRNA used, together with the amount and nature of the vector applied. In this study, no evidence of permanent nHA- or miRNA-derived cytotoxicity was found by observation of cell morphology over the culture period or by the quantitative data analysis. It is known that high miRNA doses may affect cell viability or metabolism, and dose reduction is desired to prevent side effects such as deregulation of the RNAi pathway and more specifically RISC overloading; when RISC is overloaded with exogenous miRNA, endogenous miRNA compete with them to carry out their RNAi functions, resulting in off-target effects (224). For example, doses ranging from 25 to 100 nM miRNA have been tested in studies assessing the role of various miRNAs in bone repair (237, 242, 243, 284, 368, 369). Interestingly, in this work, even lower doses of miR-mimics and antagomiRs were delivered to hMSCs, posing an advantage of the system in this regard. With regards the role of the vector in relation to safety and cytotoxicity, CaP-based delivery of nucleic acid is renowned for its excellent biocompatibility and enhanced cell proliferation (370). Although other researchers have reported a reduction in metabolic activity at early timepoints of culture (322, 371), this is in opposition to the elevated cytotoxic effects over the time course of cell culture of vectors like Lipofectamine® 2000 and RNAiMax® (280, 367, 372), which indicate

irreversible cell viability impairment. The transient reduction in metabolic activity associated with the use of CaPs at early timepoints correlated with high internalisation of calcium ions occurring immediately after treatment until the initial medium change (322, 371). This is consistent with the effect observed in this study, for which the time of initial medium change was three days after treatment: although a 14 % reduction in cell metabolic activity was observed at day 3 in the scr nanomiR-mimic 20 nM group, cell number remained unaffected across all groups. Since the cells were capable of normal metabolic activity and even significantly increased proliferation at the later timepoint, it is suggested that the transient metabolic decrease reflects a process of re-equilibration to *in vitro* culture and calcium internalisation that is surpassed after continued culture without permanent negative effects on cell viability, which is contrary to the issues with Lipofectamine® 2000 and RNAiMax®. Taken together, these results demonstrated that nanomiR treatment at the studied concentrations did not have a permanent detrimental effect on hMSC viability.

Analysis of intracellular localisation of nanomiRs demonstrated that complexes were found inside the cells in all treatment groups and at all timepoints with the presence of nanomiR complexes in proximity to the nucleus also noted. Despite the fact that the mature synthetic miRNA molecules introduced in the cells would be expected to bind to the RISC complex in the cytoplasm, localisation in areas in proximity to the nucleus was overall more prominent than cytoplasmic distribution. Interestingly, the amount of Dy547 nanoantagomiR complexes observed was notably higher than that of the Dy547 nanomiR-mimic treatment. Peri-nuclear localisation analysed qualitatively was more prominent across timepoints for the nanoantagomiRs, in contrast with that evidenced only at the early timepoint of 3 days for the nanomiR-mimic, revealing differences between the two types of molecules for the cellular internalisation process.

The different uptake kinetics for miR-mimics and antagomiRs were again evidenced by flow cytometry quantification, and consistent with the differences in size and charge between the two types of complexes, the bigger and more lipophilic nanoantagomiR complexes were internalised in a more rapid manner. This kinetic behaviour may be beneficial from the perspective of manipulation of

cellular miRNA levels with a temporal control in a combined system with a miR-mimic and an antagomiR targeted at processes occurring at different stages. Although a sensitivity limitation of flow cytometry to assay miRNA uptake from nanomiR-treated hMSCs might be implied from the presented data for the 10 nM dose, it is important to note that such a limitation may be influenced by the excess ratio of nHA particles at the lower miRNA dose in comparison with the 20 nM dose. Even though flow cytometry is a well-established technique for the purpose of uptake quantification of nucleic acid delivery, it is proposed that the detection limit for small RNA molecules tagged with fluorescent dyes may differ from that of transgene fluorescence emission assessed for pDNA delivery. Furthermore, the mismatch between this quantitative parameter and effective interference functionality has recently been noted for the case of miRNAs as opposed to siRNAs, and thus complementary assessment of silencing capacity by PCR is deemed crucial (219). In the current study however, the uptake efficiencies determined for nanomiR-mimic (20 nM) and nanoantagomiRs (10 and 20 nM) were higher than the 12 % previously reported for nHA-mediated delivery of pDNA (126), a system which successfully led to a subsequent improvement in tissue repair *in vivo* (127). This indicates that nanomiR delivery may have enhanced potential for the prospective application of therapeutic miRNAs. In summary, the combination of qualitative and quantitative assessment together confirmed the ability of the nHA particles to deliver both nanomiR-mimics and nanoantagomiRs to hMSCs, which from a therapeutic perspective, points to a wide spectrum of application possibilities for the tailoring of both types of RNAi.

Consequently, nanomiR treatment of hMSCs demonstrated greater than 90 % silencing functionality with a single dose, and this effect was generally maintained along all timepoints, as opposed to the different kinetics seen in the flow cytometry quantification of nanomiR uptake. Nevertheless, the 20 nM dose of the nanoantagomiR showed a reduction in silencing activity at day 7, therefore matching the reduction in uptake efficiency quantified by flow cytometry at this timepoint. Importantly, nanomiR-mimic at the 10 nM dose caused silencing levels similar to those of the 20 nM dose, despite the fact that uptake was undetected by flow cytometry experiments. Subsequently based on

these results, and considering the choice of doses in the available literature together with the risk of under-dosing resulting in negligible effects, the single 20 nM dose was selected as the lead candidate for progression of the research presented in the following chapters of this thesis.

Critically, the level of silencing functionality achieved with nanomiRs was comparable with the level described for viral and lipid-based vectors for delivery of siRNAs and shRNAs in different cell lines, but much higher than these type of systems for miRNA delivery to stem cells (219). A more relevant comparison of the silencing efficiency of nanomiRs presented in this chapter is perhaps versus CaP-based siRNA delivery systems reported to-date, (even though these have mainly been developed targeting different tumour-model cell lines, generally regarded as easier to transfect than stem cells). Luciferase siRNA complexes with CaP particles coated with Polyanion-modified PEG (at 100 nM doses) achieved 60 % efficiency in silencing luciferase expression in Huh-7 transfected cells, but this efficiency dropped to approx. 8 % when a 20 nM dose was administered (324). Lipid-CaP particles (LCP) were shown to exhibit a maximum of 70 % silencing of the H460 cell line with a dose that corresponded to approximately 16.6 µM at merely 24h post treatment (323). Although the effect of delivering lower siRNA doses *in vitro* using this system were not presented, a 50 % silencing effect was determined in their *in vivo* xenograft mouse model using the same cell line 24h after systemic intravenous (iv) administration of the siRNA-LCP complexes. Following this, the same research group developed an improved formulation involving an asymmetric lipid bilayer coating of CaP that yielded 90 % luciferase silencing functionality after 24 h *in vitro* when combined with 100 nM siRNA. However, once again, a 20 nM dose was associated with just 10 % silencing (373). Interestingly, the chelated PEG CaP complexes introduced by Giger *et al.* (325) were capable of significantly reducing Bcl-2 expression using and doses of 10 and 30 nM siRNA, which is closer to the results found in this chapter. Their work demonstrated 60 - 80 % silencing functionality for the respective doses after 48 h of treatment using PC-3 & J744.2 cell lines, which corresponded to 75 % silencing in protein levels assessed after 72 h. Lee *et al*. (326, 327) also produced dopa-conjugated CaP siRNA complexes that rendered silencing efficiency levels of approximately 50

% using a luciferase or GFP silencing approach respectively for HTC-29 LUC or MDA-MB-435-GFP cell lines, a result that was replicated with their *in vivo* xenograft model using the same cell line (326). In summary, the nanomiR delivery system developed within this chapter was able to outperform the silencing efficiency of the few CaP-based siRNA delivery systems reported to date, encouraging further experimentation to implement the nHA-based miRNA delivery system in a number of therapeutic applications not merely limited to the TE field.

2.6.Conclusion

The research presented in this chapter has demonstrated the potential of in house-synthesised nHA particles to act as non-viral vectors for miR-mimic and antagomiR delivery to hMSCs and to subsequently manipulate post-transcriptional gene regulation in a highly efficient and minimally cytotoxic manner, with single administration of low miRNA doses rendering very pronounced silencing activities. Specifically, nHA particles were able to complex with both miR-mimics and antagomiRs resulting in ~18 - 40 % uptake efficiency in hMSCs with different temporal patterns and silencing functionality to a level comparable to viral and lipid-based vectors. Furthermore, this study utilised low miRNA doses as compared with the literature and we determined that a 20 nM dose was optimal to continue the proposed work of the project. Ultimately, the results demonstrated the enormous potential of the nHA particles to act as miRNA delivery vectors. Following development of this system, we next investigated its application to (i) deliver pro-osteogenic miRNAs to hMSCs and (ii) incorporate the system into a collagen-nHA scaffold, as well as to (iii) deliver pro-angiogenic miRNAs to hMSCs, all of which is presented in the following chapters.

Chapter 3. Nanohydroxyapatite-based delivery of osteogenesis-related miRNAs to enhance hMSC osteogenic differentiation

Research presented in this chapter has been included in the following peer-reviewed publication:
Castaño, IM et al., Next generation bone grafting: Non-Viral Inhibition of MiR-133a Using Collagen-Nanohydroxyapatite microRNA-activated Scaffolds Rapidly Enhances Osteogenesis by Human Mesenchymal Stem Cells. *Manuscript submitted.*

3.1.Introduction

nHA particles are chemically similar to the inorganic component of bones and hold osteogenic potential beneficial for bone repair applications (109, 318, 374). Having characterised the efficient nHA-based delivery of reporter miRNAs in Chapter 2, this study applied the same system to bone repair. In order to do so the focus was placed on the incorporation of therapeutic miRNAs to enhance and/or accelerate hMSC osteogenesis. As outlined in Chapter 1, MSCs have significant potential for bone repair applications. Osteodifferentiation is regulated by complex fine-tuned mechanisms involving the activation of master transcription factors of osteogenesis including Runx2 (21). In addition to the protein-based control of osteogenesis, recent research efforts have unravelled the role of several miRNAs in regulating osteodifferentiation either positively or negatively (Figure 3.1; (220, 221, 234-240, 242, 244, 368, 375-378)). Strategies for manipulating miRNA levels have recently been proposed for the treatment of bone defects and bone-related diseases such as osteoporosis and osteoarthritis (220, 221). Recent research efforts carried out by several groups have collectively identified a selection of miRNAs as potential osteo-therapeutics; however, many of these miRNAs have direct targets that only play a secondary role in the osteogenesis pathway (379). In this study, three candidate miRNAs were selected for incorporation into the nanomiR system to investigate their resulting effect on hMSC osteodifferentiation in monolayer culture.

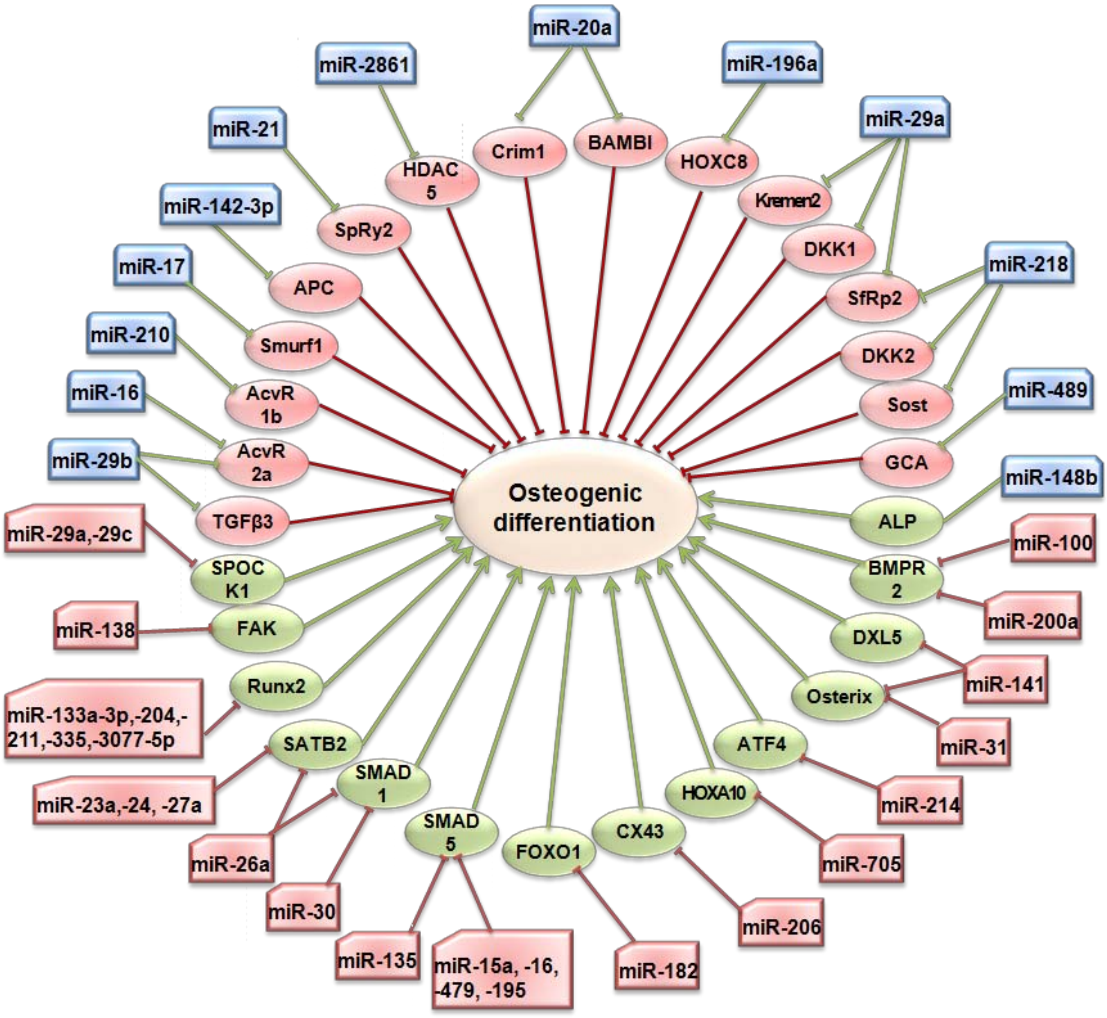

Figure 3.1 Panel of miRNAs influencing osteogenic differentiation and their reported targets (experimentally validated). Inner circle: red ovals accompanied by red brake symbols (⊣) indicate proteins with inhibitory roles in osteogenesis, green ovals accompanied by green arrows (→) indicate proteins which display an activator role in osteogenesis. Outer circle: miRNAs represented in blue are positive regulators of osteogenesis and miRNAs depicted in red are negative regulators of the process.

Firstly downregulation of miR-133a was pursued as it has been identified as a negative regulator of the master transcription factor of osteogenesis, Runx2 (242). Hence, the direct relationship between miR-133a levels and Runx2 expression provides a possibility to target a central activator of osteogenesis. It was hypothesised that exogenous inhibition of miR-133a levels in hMSCs with antagomiR treatment would increase Runx2 levels in these cells and enhance their osteogenic potential (Figure 3.2a).

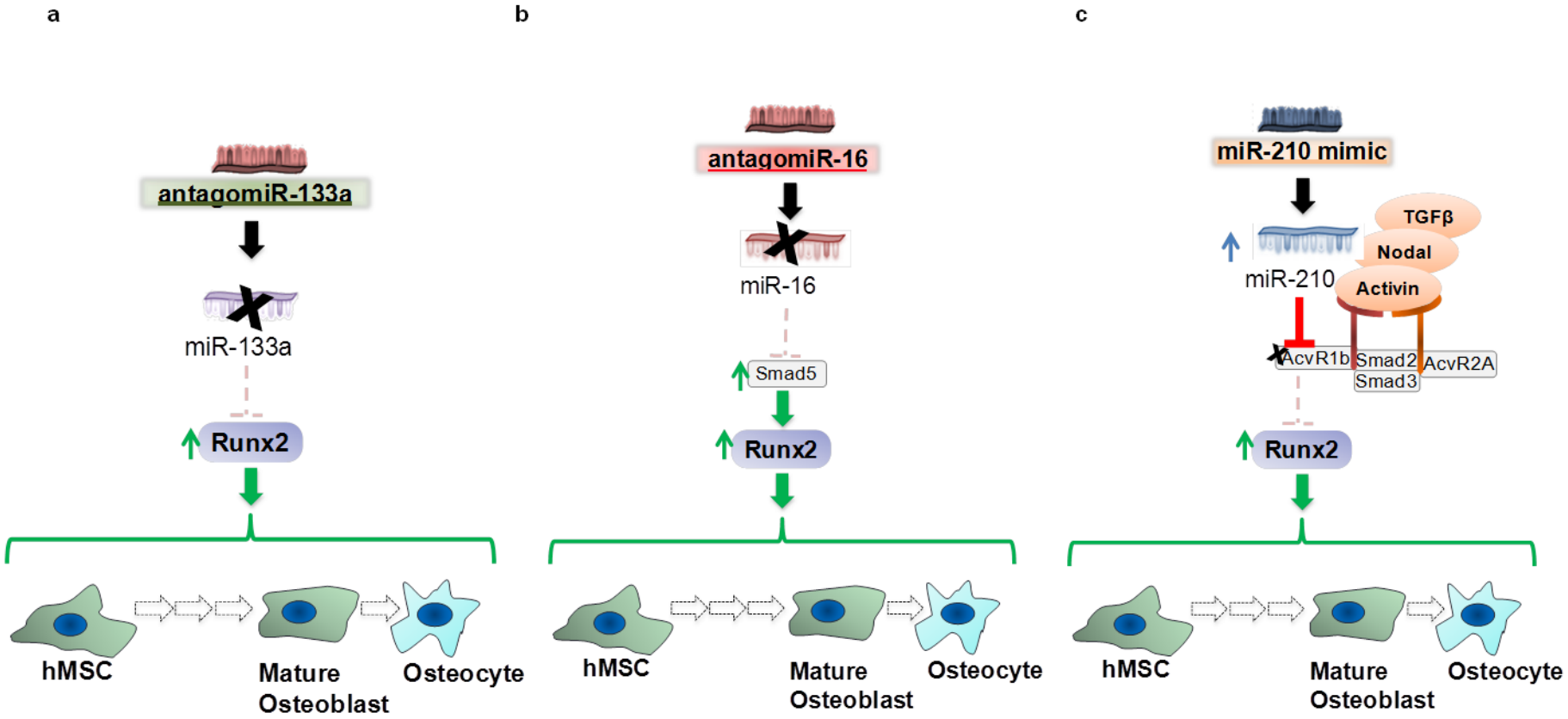

Figure 3.2 Schematic of molecular processes leading to enhanced osteogenesis following the manipulation of each of the miRNAs selected for this study. a) antagomiR-133a treatment, **b)** antagomiR-16 treatment, **c)** miR-210 mimic treatment. Black arrows indicate exogenous delivery, green arrows indicate activation or enhancement, brake symbols (⊣, red) represent inhibition, x symbols (black) depict decreased activity, discontinuous brake shapes symbolise abrogated silencing signal.

The second candidate for this work was miR-16. Many anti-tumoral approaches have sought to increase miR-16 to induce cancer cell apoptosis (380), while decreasing miR-16 has the therapeutic potential to promote cell survival. Currently, there is no defined role for miR-16 in osteogenesis but Eguchi *et al.* pointed at a potential marker role for miR-16 in maintaining stemness and deterring osteocyte maturation in human and murine MSC osteogenesis (239). Previously, Selbach *et al.* carried out proteome-wide analysis of manipulation of miR-16, alongside four other miRNAs belonging to highly conserved miRNA families, in HeLa cells (381). In that study, evidence of direct interaction between miR-16 and Smad5, an intermediate activator of BMP signalling in osteogenesis, was reported through proteomic analyses. More recently, all members of the miR-15 family, including miR-16 and miR-195, which encompasses a near-identical sequence to miR-16, were associated to multiple target genes involved in BMP signalling in mouse bone cells using quantitative PCR (382). Therefore, it can be proposed that treatment with antagomiR-16 may enhance SMAD5 levels and thus trigger MSC commitment towards the osteoblastic or osteocytic lineage (Figure 3.2b).

Lastly, miR-210 was selected due to its positive secondary role in osteogenesis, which has been described to occur by targeting activin receptor 1b (AcvR1b) in a study performed in BMP-4 induced differentiation of mouse BM-derived stromal ST2 cells (236). Little is known about the direct AcvR1b-mediated inhibition of osteogenesis; AcvR1b is involved in activin signalling as part of the TGFβ pathway, ultimately leading to Runx2 inhibition. Moreover, Mizuno *et al.* confirmed the inhibitory role of AcvR1b in osteogenesis by demonstrating the osteogenic phenotype following chemical inhibition of AcvR1b (236). Considering this, exogenous treatment with mature miR-210 mimics might be applied to further reduce AcvR1b and subsequently enhance hMSC osteogenesis (Figure 3.2c). Additionally miR-210 may indirectly benefit osteogenesis through the promotion of angiogenesis. miR-210 has been implicated as a positive regulator of angiogenesis (383), and increased angiogenesis has the potential to enhance osteogenesis, as reviewed in Chapter 1, thus this bi-modal function of miR-210 may lead to a robust beneficial effect on bone formation.

3.2.Hypothesis & aims of the study

The underlying hypothesis of this study was that efficient delivery of these three individual miRNAs might lead to enhanced hMSC osteogenesis. The overall aim of this study was thus to assess the pro-osteogenic therapeutic efficacy of nHA-based delivery of the following miRNAs: (i) nanoantagomiR-133a, (ii) nanoantagomiR-16 and (iii) nanomiR-210 mimic with a view to establishing the optimal osteo-therapeutic candidate for delivery in a 3D scaffold-based system in Chapter 4.

The following specific tasks were carried out in order to analyse the pro-osteogenic therapeutic efficacy of each of the nanomiR treatments selected:

- Identification of additional predicted and validated targets of interest that support the role of each miRNA in osteogenesis using bioinformatic tools
- Determination of efficient nHA-based miRNA delivery by confirmation of specific miRNA intracellular level manipulation
- Analysis of functional nHA-based miRNA delivery by confirmation of (i) increased mRNA levels of direct targets following nanoantagomiRs treatment or (ii) decreased mRNA levels of direct targets following nanomiR-mimic treatment
- Assessment of the efficacy of the miRNA treatment in influencing hMSC osteogenesis by osteogenic gene marker analysis, ALP bioactivity assays and mineral deposition examination

3.3.Materials & Methods

3.3.1.Bioinformatic analysis

Bioinformatic analysis provides detailed information about the features of putative and experimentally validated interactions of a given miRNA entry, which may further relate to a suggested function for such miRNA. To gather further knowledge regarding the function in osteogenesis of the three miRNAs studied in this chapter, online tools were explored in terms of (i) identification of putative messenger RNA targets implicated in osteogenesis and (ii)

identification of validated targets for which the miRNA interaction was assessed in the context of a cellular function different to osteogenesis. A subsequent analysis was carried out to assess (iii) homology in the interaction of miRNAs and their relevant direct targets across human, rat and mouse species, as well as (iv) the types of miRNA::mRNA target interaction taking place and (v) occupancy of nearby seed region by other neighbour miRNAs. All of these features were explored by searching the following peer-consulted databases available online: Targetscan (382), microRNA.org (384), miRTarBase (385).

3.3.2.Cell culture and treatment with nanomiR system

hMSCs were cultured in complete DMEM medium as described in Section 2.3.3 until sufficient cell numbers were obtained at passage number 4 for experimentation. 24 hours in advance of the nanomiR treatment, cells were plated at a density of 3 x 10^4 cells per well in 6 well plates. At the time of administering the control (blank nHA particles) or nanomiR treatments, nanomiR complexes were prepared with the antagomiR-133a, antagomiR-16 and miR-210 mimics as well as with scrambled (scr) antagomiR and scr miR-mimic (all from Dharmacon) at a final dose of 20 nM following the procedure detailed in Section 2.3.1. Immediately after the addition of the treatments, hMSCs were cultured in complete osteogenic medium, which consisted of standard growth medium supplemented with 50 µg/ml ascorbic acid-2-phosphate, 10 nM β–glycerophosphate and 100 nM dexamethasone and was administered to cells every 3/4 days until the experiment endpoint at day 14. Additionally, untreated cells were kept either in standard or osteogenic complete growth medium for the duration of the assay as a control for inherent hMSC osteogenesis.

3.3.3.Assessment of effective genetic manipulation following nanomiR treatment using qRT-PCR

qRT-PCR analysis was carried out to determine (i) miRNA intracellular levels as well as mRNA relative expression level of (ii) direct miRNA targets and (iii) the osteogenesis marker osteocalcin (OCN, also represented as BGLAP) after transient transfection using the nanomiR method. The hsa-miR-133a, hsa-miR-16 and hsa-miR-210 Taqman® MicroRNA assays as well as the following

validated pre-designed human Quantitect Primer Assays (Qiagen, UK) were applied: Hs_Runx2_1_SG, Hs_BGLAP_1_SG, Hs_SMAD5_va.1_SG, Hs_AcvR2a_1_SG and Hs_AcvR1b_va.1_SG. The scr nanoantagomiR group was set as the reference for the calculation of relative expression levels for the experiments with antagomiR treatments, while the scr nanomiR-mimic was set as the reference for the calculation of relative expression levels for the experiments with miR-210 mimic. Technique and calculations were carried out as described previously in Section 2.3.7.

3.3.4. Assessment of alkaline phosphatase (ALP) activity as a biofunctional marker of osteogenesis

ALP activity is a specific marker of biofunctional osteogenesis. In order to assess ALP activity in hMSCs 10 days post-treatment the SensoLyte® pNPP Alkaline Phosphatase Assay Kit (Cambridge Bioscience) was used under manufacturer's instructions. Absorbance of the colour product generated was read at 405 nm using a Varioskan Flash plate reader (ThermoScientific) and SkanIt ® for Varioskan software. The Quant-iT PicoGreen dsDNA kit (Invitrogen) assay was performed as previously described in Section 2.3.4 to normalise levels of ALP activity quantifed.

3.3.5. Mineral deposition assessment as end-stage marker of osteogenesis

Histological analysis:

Presence of calcium deposits in the extracellular matrix is regarded as an endpoint biofunctional parameter of osteogenesis. In order to visualise calcium deposits at 10 days after treatment samples were stained directly on culture-plates with 2 % Alizarin red, which stains calcium red. Briefly, samples were fixed using 10 % formalin and subjected to alizarin red staining for 5 min, following which excess staining was removed rinsing with distilled water. Microscopic imaging was carried out using an inverted microscope coupled to the LASV4.5 digital imaging system (Leica, Germany).

Mineral deposition quantification:

To provide quantitative data the Calcium Liquicolor kit (Stanbio Laboratories) was used under manufacturer's instructions at days 10 and 14 post-treatment.

Briefly, 1 ml of 0.5 M HCl was added to samples and maintained in agitation at 4°C overnight, then 100 µl of the substrate plus reagent mix (1:1) solution was added to 10 µl of the samples and absorbance of the colour product generated was read at 595 nm using a Varioskan Flash plate reader (ThermoScientific) and SkanIt® for Varioskan software. The Quant-iT PicoGreen dsDNA kit (Invitrogen) assay was performed at the corresponding timepoints as previously described in Section 2.3.4 to normalise levels of calcium quantifed.

3.3.6.Statistical analysis

Experiments were performed in triplicate, unless otherwise specified within figure captions, and are representative of a minimum of three independent repetitions using two cell donors. Results were analysed as described previously in Section 2.3.8 using two-way ANOVA plus Tukey *post-hoc* test for analysis of several time points and one-way ANOVA plus Tukey *post-hoc* test for data assessed at a singular time point. $p<0.05$ was considered significant and $p<0.001$ highly significant.

3.4.Results

The effect of the three individual nanomiR treatments on hMSC osteogenesis is presented herein in three separate sections focussing on nanoantagomiR-133a, nanoantagomiR-16 and lastly nanomiR-210 mimic treatments.

3.4.1.The effect of nanoantagomiR-133a treatment on hMSC osteogenesis

3.4.1.1.Bioinformatic analysis supports a negative role of miR-133a in osteogenesis

Bioinformatic tools provided the identification of 648 predicted hit interactions between potential mRNA targets and miR-133a in human species, seven of which were of interest for osteogenesis (Figure 3.3a). These target hits were then compared to the database of validated targets, miRTarBase. Fewer than 10 % of the total predicted targets have been experimentally validated, but interestingly the screening identified Runx2, collagen type 1α1 (COL1A1),

IGFR1, and Bcl2L as validated targets. Although Runx2 is key for orchestrating osteogenesis, COL1A1 and IGFR1 also play a positive role in the process, which further supports the inhibitory role of miR-133a in this process and hence reinforces the hypothesised potential of antagomiR-133a to promote osteogenesis in hMSCs. Key targets for this study have only been validated in mouse cells. Since we aimed to target these pathways in human cells, homology of the miRNA::target interaction across human, rat and mouse species was also studied (Figure 3.3b). The interaction type and score (context percentile) was maintained across the three species. However, additional parameters assessed in this analysis indicated the possibility of more robust interactions in the case of mouse and rat species compared to in human: firstly, additional seed regions were found in both mouse and rat; second and more importantly, the amount of miRNAs predicted to interact in the areas neighbouring the seed region was higher in human, denoting a possible reduced functionality for the miR-133a::Runx2 interaction in human.

a

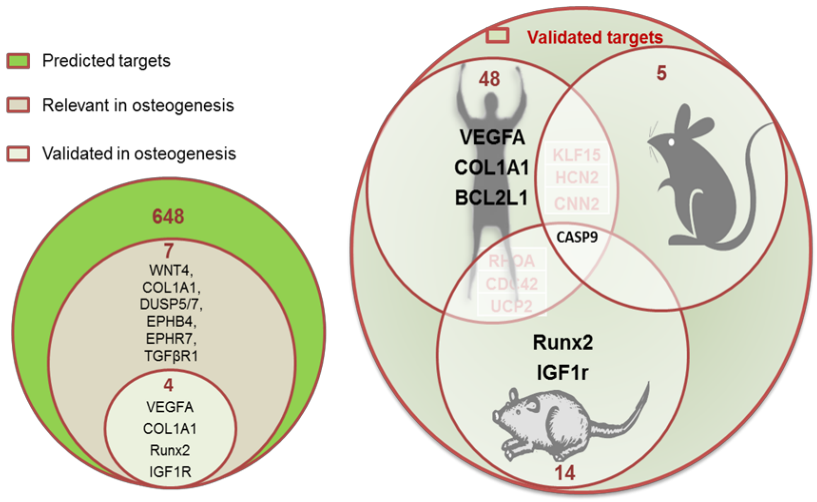

b

miR-133a::Runx2	Position of 3′ UTR	Predicted pairing of target (top) and miRNA (bottom)	Seed match	Context score percentile	Neighbouring interactions Other miRNAa with study target		
					Total sites	No. miRNAs	Role in osteog.
Human (hsa)	2763-9	5′ ...GAUUUGUGAUUUCAAGACCAAAG 3′ GUCGACCAACUUCCCCUGGUUU	7mer-1A	17	6	13	miR-148
Mouse (mmu)	2796-802	5′ ...GAUUUGUGGUUUUAA--GACCAAAG 3′ GUCGACCAACUUCCCCUGGUUU	7mer-1A	21	4	10	miR-148
Rat (rno)	2782-8	5′ ...GAUUUGUGGUUUUAA--GACCAAAG 3′ GUCGACCAACUUCCCCUGGUUU	7mer-1A	19	5	10	miR-148

Figure 3.3 Bioinformatic exploration of miR-133a. a) Putative or predicted (left circle) vs. validated (right circle) targets related to osteogenesis across human, mouse and rat for miR-133a. Overlapping sections of internal circles indicate that validation has been reported in both species. **b)** miRNA::target interaction for miR-133a and Runx2 across human (hsa), mouse (mmu) and rat (rno)species.

3.4.1.2.Effective manipulation of intracellular miR-133a levels in hMSC was achieved using nHA-based delivery

The temporal pattern of endogenous miR-133a expression during osteogenesis has not been previously assessed in hMSCs. Here, we found that hMSC miR-133a expression continuously increased in the standard (no osteogenic supplementation) medium group over the course of 14 days, whereas hMSCs in the osteogenic medium group showed a peak at day 3 but reduced levels at the later timepoints of days 7 and 14, pointing to a link between suppression of endogenous miR133a and the progression of *in vitro* osteogenesis (Figure 3.4).

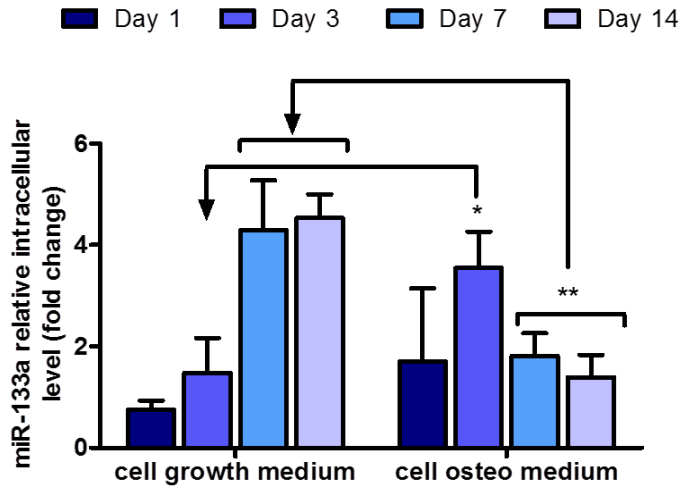

Figure 3.4 miR-133a levels during standard vs osteogenic monolayer culture. Comparison with cells cultured in standard (std) growth medium over the course of 14 days demonstrated a natural decrease in miR-133a at later time points in osteogenic culture. Cell std medium was set as the reference control group and relative expression was normalised to that of 18S and calculated using the $2^{(-\Delta\Delta Ct)}$ method. Mean + standard deviation, n = 4, * = $p<0.05$, ** = $p<0.001$.

Interestingly, following nHA-based delivery of antagomiR-133a, a sustained miR-133a downregulation was obtained with a functionality level over 80 %, while miR-133a was slightly increased from 3 to 7 days in the blank nHA particles group (Figure 3.5). Moreover, the effect of independent treatments with nanoantagomiR-16 or nanomiR-210 mimic on intracellular levels of miR-133a was explored to assess specific miRNA manipulation 7 days after treatment of hMSCs (Figure 3.6). This data showed that treatment with nanoantagomiR-16 or nanomiR-210 mimic did not alter miR-133a levels. In summary, this assessment indicated firstly that intracellular miR-133a levels endogenously decrease during hMSCs osteogenesis *in vitro* and secondly this can be

significantly potentiated at earlier timepoints using nanoantagomiR-133a treatment.

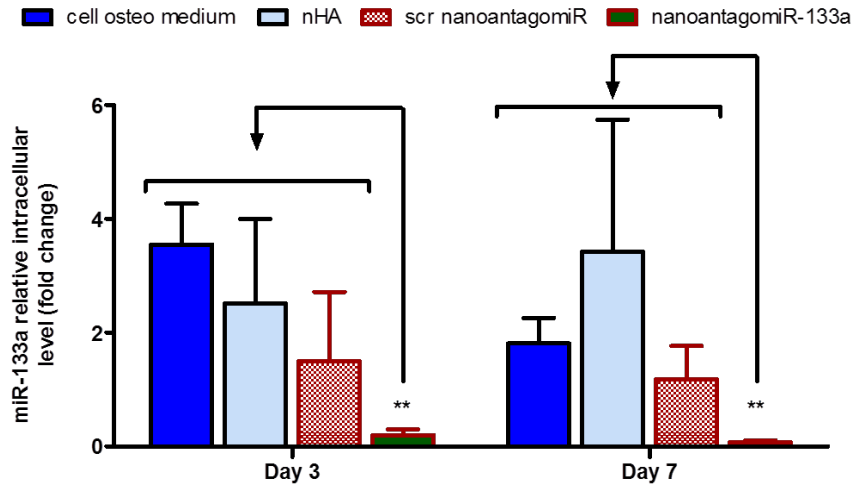

Figure 3.5 qRT-PCR analysis of miR-133a manipulation in hMSCs using nHA-based delivery. NanoantagomiR-133a demonstrated a maintained suppression of miR-133a intracellular levels from day 3. Scr nanoantagomiR was set as the reference control group and relative expression was normalised to that of 18S and calculated using the $2^{(-\Delta\Delta Ct)}$ method. Mean + standard deviation, n = 4, ** = p<0.001.

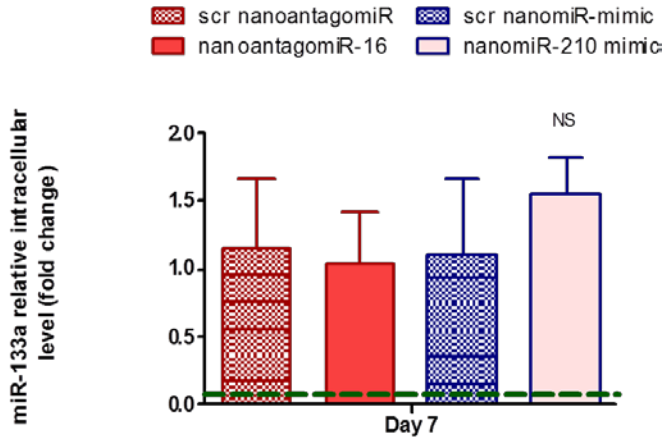

Figure 3.6 qRT-PCR analysis of specificity in miR-133a manipulation demonstrating non-manipulation of miR-133a following nanoantagomiR-16 or nanomiR-210 mimic treatment. NanoantagomiR-16 or nanomiR-210 mimic treatment did not significantly modify intracellular miR-133a level. Scr nanoantagomiR was set as the reference control group for nanoantagomiR-16 and scr nanomiR-mimic was set as the reference control group for nanomiR-210 mimic. Relative expression was normalised to that of 18S and calculated using the $2^{(-\Delta\Delta Ct)}$ method. Dashed green line indicates level determined for nanoantagomiR-133a treatment as a reference for comparison. Mean + standard deviation, n = 4, NS = not significant variation.

3.4.1.3.NanoantagomiR-133a treatment enhanced hMSC osteogenic gene expression

Runx2 and OCN gene levels are often analysed as the main indicators of the initiation and progression of osteogenesis in hMSCs (386). Here, these two osteogenic gene markers were analysed at day 7 to evaluate the effect of nanoantagomiR-133a treatment on its downstream direct target as well as the osteogenic response achieved as a consequence of the treatment. Runx2 expression was increased 8.9 (± 2.97) fold with a single dose of the treatment (Figure 3.7a) while a 14.23 (± 3.2) fold increase was found when OCN levels were analysed (Figure 3.7b). In summary, this assessment indicated that nanoantagomiR-133a treatment was capable of enhancing levels of Runx2 and OCN, both crucial indicators for osteogenic differentiation in hMSCs.

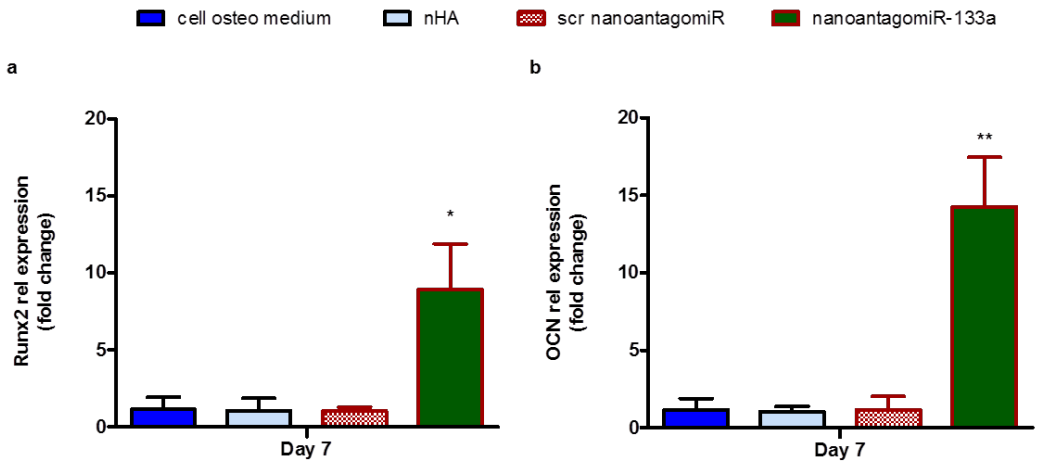

Figure 3.7 qRT-PCR analysis of the effect of nanoantagomiR-133a treatment on hMSC osteogenic gene expression. **a)** Runx2 and **b)** OCN were increased at 7 days after nanoantagomiR-133a treatment. Scr nanoantagomiR was set as the reference control group and relative expression was normalised to that of 18S and calculated using the $2^{(-\Delta\Delta Ct)}$ method. Mean + standard deviation, n = 4, * = $p<0.05$, ** = $p<0.001$.

3.4.1.4.ALP activity was increased in nanoantagomiR-133a treated hMSCs

ALP is an important marker of functional bioactivity during osteogenesis which also has previously been shown to be upregulated in hMSCs as a result of antagomiR-133a treatment (235). Bioactivity quantification normalised to dsDNA content, as a surrogate measure of cell number, showed nanoantagomiR-133a resulted in 17.37 and 13.23 fold higher levels of ALP than untreated cells and nHA groups respectively (Figure 3.8). These were also 1.87 fold higher than scr nanoantagomiR group, which unexpectedly increased ALP activity over untreated cells. In summary, this result indicated that nanoantagomiR-133a treatment was able to trigger enhanced functional osteogenesis in hMSCs.

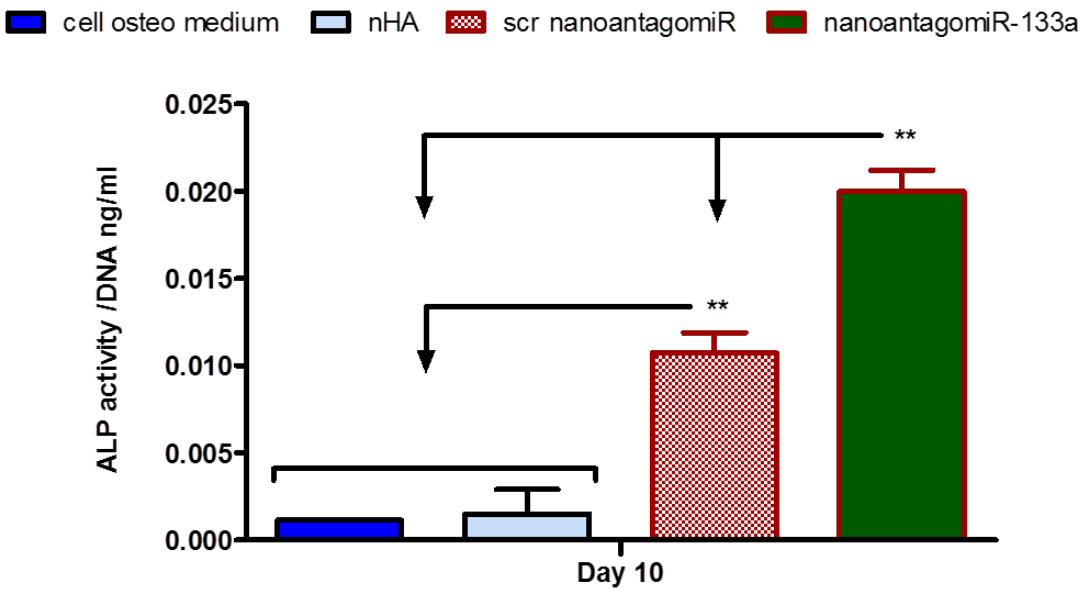

Figure 3.8 Analysis of ALP activity in nanoantagomiR-133a treated hMSCs. Quantification of ALP normalised to dsDNA content demonstrated significantly increased ALP activity levels in nanoantagomiR-133a over scr nanoantagomiR as well as of these two groups compared to cells alone and blank nHA 10 days after treatment. Mean + standard deviation, n = 3, ** = $p<0.001$.

3.4.1.5.Mineral deposition was enhanced in nanoantagomiR-133a treated hMSCs

To further assess functional osteogenesis, calcium deposition in the ECM was studied. Histological analysis showed enhanced calcium deposits at day 10 with nanoantagomiR-133a (Figure 3.9a). Subsequently, significantly enhanced calcium deposition, normalised to cell number, was observed for cells treated with nanoantagomiR-133a (Figure 3.9b). As early as day 10, calcium deposition was increased 4.67 fold over untreated cells (cells osteo medium). Moreover this effect was continued at 14 days, when nanoantagomiR-133a treatment enhanced calcium deposition 2.55 fold over untreated cells. In summary, this data indicated a potent ability of nanoantagomiR-133a to rapidly exert a significant mineralisation response.

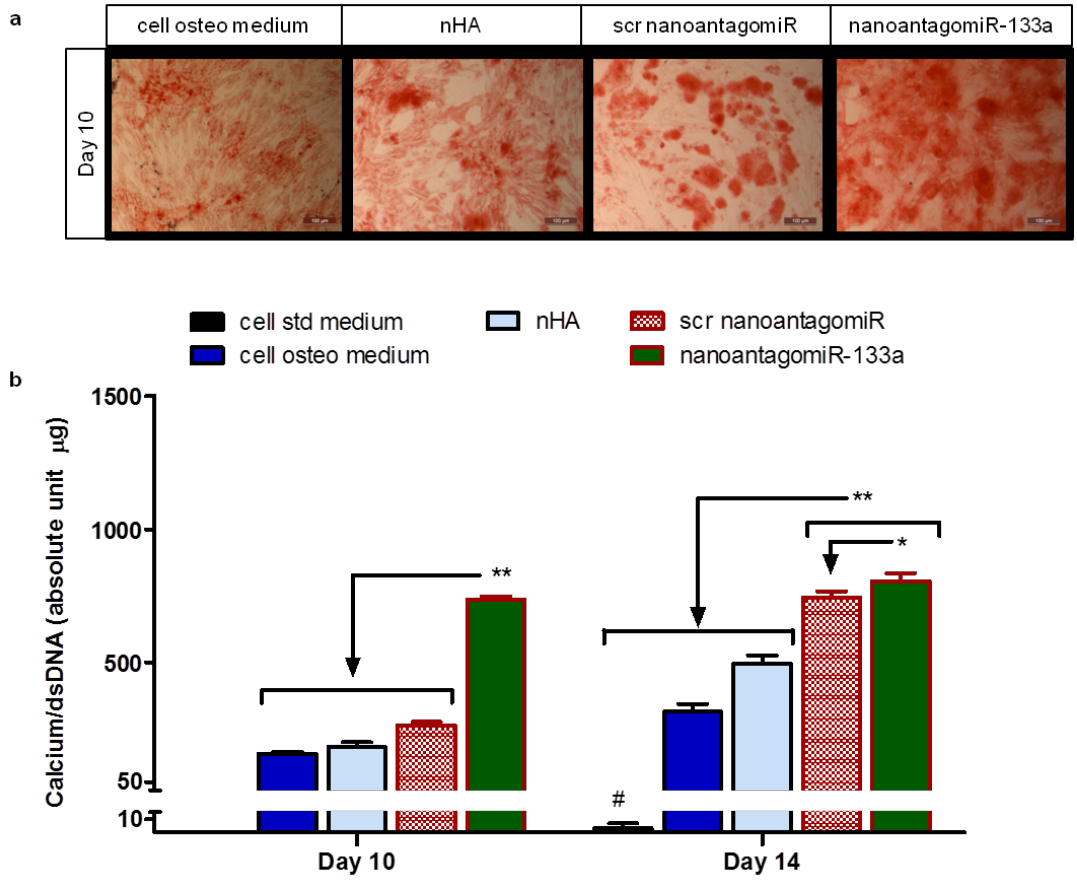

Figure 3.9 Analysis of calcium deposition in nanoantagomiR-133a treated hMSCs. a) Alizarin red staining showed calcium deposits at 10 days after treatment, scale bar= 200 µm. **b)** Calcium normalised to dsDNA content confirmed an increase in calcium deposition by day 10 after treatment with nanoantagomiR-133a in osteogenic culture and maintained increased calcium levels compared to the control groups after 14 days. Mean + standard deviation, n = 3, * = $p<0.05$, ** = $p<0.001$, # = $p<0.001$ against all other groups.

3.4.2.The effect of nanoantagomiR-16 treatment on hMSC osteogenesis

3.4.2.1.Bioinformatic analysis supports a negative role of miR-16 in osteogenesis

Bioinformatic tools provided the identification of 1273 predicted hit interactions between potential mRNA targets and miR-16 in human species, nine of which were of interest for osteogenesis (Figure 3.10a). These target hits were then compared to the database of validated targets, miRTarBase. More than 90 % of the total predicted targets have been experimentally validated. Interestingly in addition to Smad5, the screening identified seven targets of interest for osteogenesis as validated in human, including and COL4A2 and IGF2R, which also play a positive role in the osteogenesis, as well as AcvR2a, which was analysed in further detail as it is familiarly related to AcvR1b, the miR-210 target of focus to this study. Overall these additional targets further support the inhibitory role of miR-16 in this process and hence reinforce the hypothesised potential of antagomiR-16 to promote osteogenesis in hMSCs.

Bioinformatic tools were then searched to document further details of the miR-16::AcvR2a and miR-16::Smad5 interactions in terms of homology across human, rat and mouse (Figure 3.10b). Firstly for AcvR2a the 7mer-m8 binding type, together with context percentile score and remaining parameters tested were maintained across species. In relation to Smad5, a double number of binding sites was predicted for the interaction in mouse, and rat context percentile scores were lower than those of both human and mice. Taken together, this data confirmed the promising potential of miR-16 to exert multiple functions related with osteogenesis which is predicted to hold a robust homology across the three species of interest of this study.

a

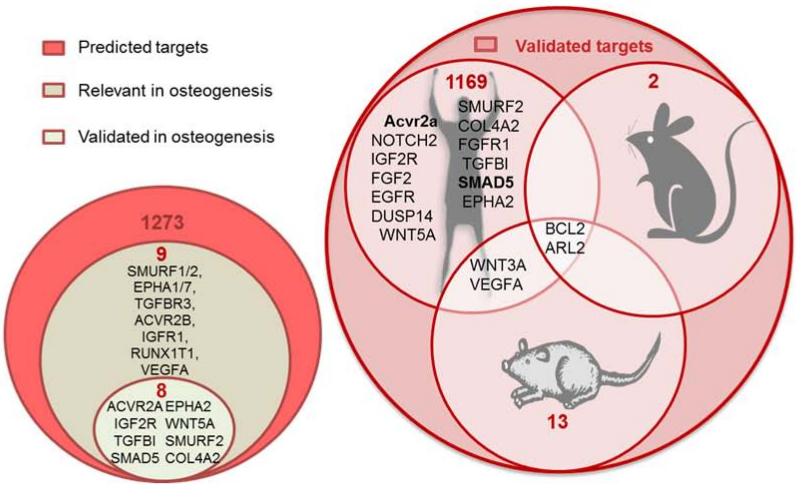

b

		Position of 3′ UTR	Predicted pairing of target (top) and miRNA (bottom)	Seed match	Context score percentile	Neighbouring interactions Other miRNAa with study target		
						Total sites	No. miRNAs	Role in osteog.
miR-16::AcvR2A	Human (hsa)	502-8	5′ ...UGUGAAUGUUUAGUGUGCUGCUG. 3′ GCGGUUAUAAAUGC-ACGACGAU	7mer-m8	68	2	9	miR-15 family members
	Mouse (mmu)	499-505	5′ ...UGUGAAUGUGUAGUGUGCUGCUG 3′ GCGGUUAUAAAUGCACGACGAU	7mer-m8	56	2	9	miR-15 family members
	Rat (rno)	483-9	5′ ...UGUGAAUGUGUAGUGUGCUGCUG. 3′ GCGGUUAUAAAUGCACGACGAU	7mer-m8	58	2	9	miR-15 family members
miR-16::Smad5	Human (hsa)	788-94	5′ ...UUGUUCAACUAUGUU--UGCUGCUU 3′ GCGGUUAUAAAUGCACGACGAU	7mer-m8	76	2	9	miR-15 family members
		5053-9	5′ ...GCUGCACUGUAGGUCUGCUGCUU 3′ GCGGUUAUAAAUGCACGACGAU	7mer-m8	79	2	9	
	Mouse (mmu)	715-21	5′ ...UUGUUCAGCAUUGUU-UGCUGCUU 3′ GCGGUUAUAAAUGCACGACGAU	7mer-m8	73	4	9	miR-15 family members
		910-16	5′ ...GACAGCUGUGAGCUGUGCUGCUU. 3′ GCGGUUAUAAAUGCACGACGAU	7mer-m8	30	4	9	
		4003-9	5′ ...UCUGUGUAUGGGUUCUGCUGCUG 3′ GCGGUUAUAAAUGC-ACGACGAU	7mer-m8	67	4	9	
		4006-12	5′ ...GUGUAUGGGUUCUGCUGCUGCUU 3′ GCGGUUAUAAAUGCACGACGAU	7mer-m8	61	4	9	
	Rat (rno)	710-6	5′ ...UUGUUCAGCUUCGUCUGCUGCUU 3′ GCGGUUAUAAAUGCACGACGAU	7mer-m8	24	2	9	miR-15 family members
		3888-94	5′ ...UACCGUUGGCUGAGCUGCUGCUU 3′ GCGGUUAUAAAUGCACGACGAU	7mer-m8	21	2	9	

Figure 3.10 Bioinformatic exploration of miR-16. a) Predicted (left circle) vs. validated (right circle) targets related to osteogenesis across human, mouse and rat for miR-16. Overlapping sections of internal circles indicate that validation has been reported in both species. **b)** miRNA::target interaction for (i) miR-16 and AcvR2a and (ii) miR-16 and Smad5 across hsa, mmu and rno species.

3.4.2.2.Effective manipulation of intracellular miR-16 level in hMSC was achieved using nHA-based delivery

When miR-16 intracellular levels were monitored during hMSC osteogenic culture, these remained generally unaffected in the untreated cells, only subjected to culture in osteogenic medium (cells osteo medium). In comparison to this, manipulation of miR-16 levels with nanoantagomiR-16 treatment proved highly efficient, yielding higher than 90 % reduction at both timepoints, in accordance with the data presented in Chapter 2 (Figure 3.11).

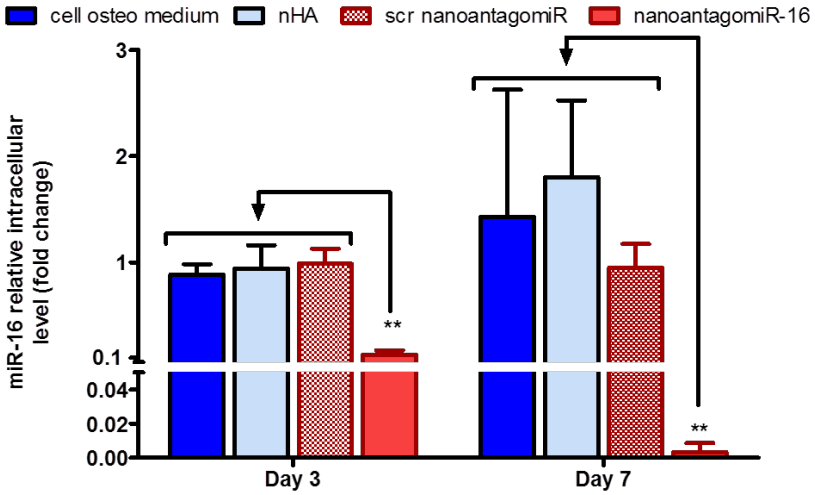

Figure 3.11 qRT-PCR analysis of miR-16 manipulation in hMSCs using nHA-based delivery. miR-16 intracellular levels demonstrated a maintained suppression with nanoantagomiR-16 up to 7 days after treatment. Scr nanoantagomiR was set as the reference control group and relative expression was normalised to that of 18S and calculated using the $2^{(-\Delta\Delta Ct)}$ method. Mean + standard deviation, n = 4, ** = p<0.001.

Next, the assessment of specific miRNA manipulation was carried out analysing the effect of independent treatments with nanoantagomiR-133a or nanomiR-210 mimic (Figure 3.12). This data showed that treatment with nanoantagomiR-133a did not vary miR-16 levels, although a significant increase was found in the nanomiR-210 mimic group, which again may be indicative of a yet unknown interaction between these two miRNAs. In summary, this data confirmed remarkable miR-16 inhibition using nHA-based delivery of antagomiR-16 in hMSCs osteogenic culture.

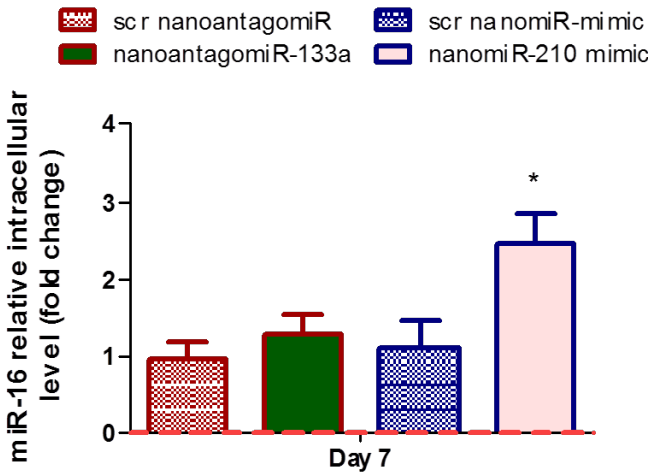

Figure 3.12 qRT-PCR analysis of specific miR-16 manipulation demonstrating non-manipulation of miR-16 following nanoantagomiR-133a treatment. NanoantagomiR-133a treatment did not modify intracellular miR-16 levels in opposition with nanomiR-210 mimic. Scr nanoantagomiR was set as the reference control group for nanoantagomiR-133a and scr nanmiR-mimic was set as the reference control group for nanomiR-210 mimic. Relative expression was normalised to that of 18S and calculated using the $2^{(-\Delta\Delta Ct)}$ method. Dashed red line indicates level determined for nanoantagomiR-16 treatment as a reference for comparison. Mean + standard deviation, n = 4, * = $p<0.05$.

3.4.2.3.NanoantagomiR-16 treatment enhanced hMSC osteogenic gene expression

To evaluate the effect of nanoantagomiR-16 treatment in hMSC osteogenic gene expression, the direct targets AcvR2a and Smad5, alongside the osteogenesis markers Runx2 and OCN were analysed at day 7 (Figure 3.13). As a consequence of the efficient inhibition of miR-16 with nanoantagomiR-16 treatment, messenger RNA levels of AcvR2a and Smad5 were increased to 10.92 (± 1.12) fold and 2.54 (± 0.55) fold respectively. Subsequently, Runx2 and OCN expression were increased to 6.29 (± 2.3) fold and 8.19 (± 1.96) fold respectively with the nanoantagomiR-16 treatment. In line with the hypothesised negative role of miR-16 in osteogenesis, this data supported that inhibition of miR-16 can have a positive outcome in hMSC osteogenesis at the gene level.

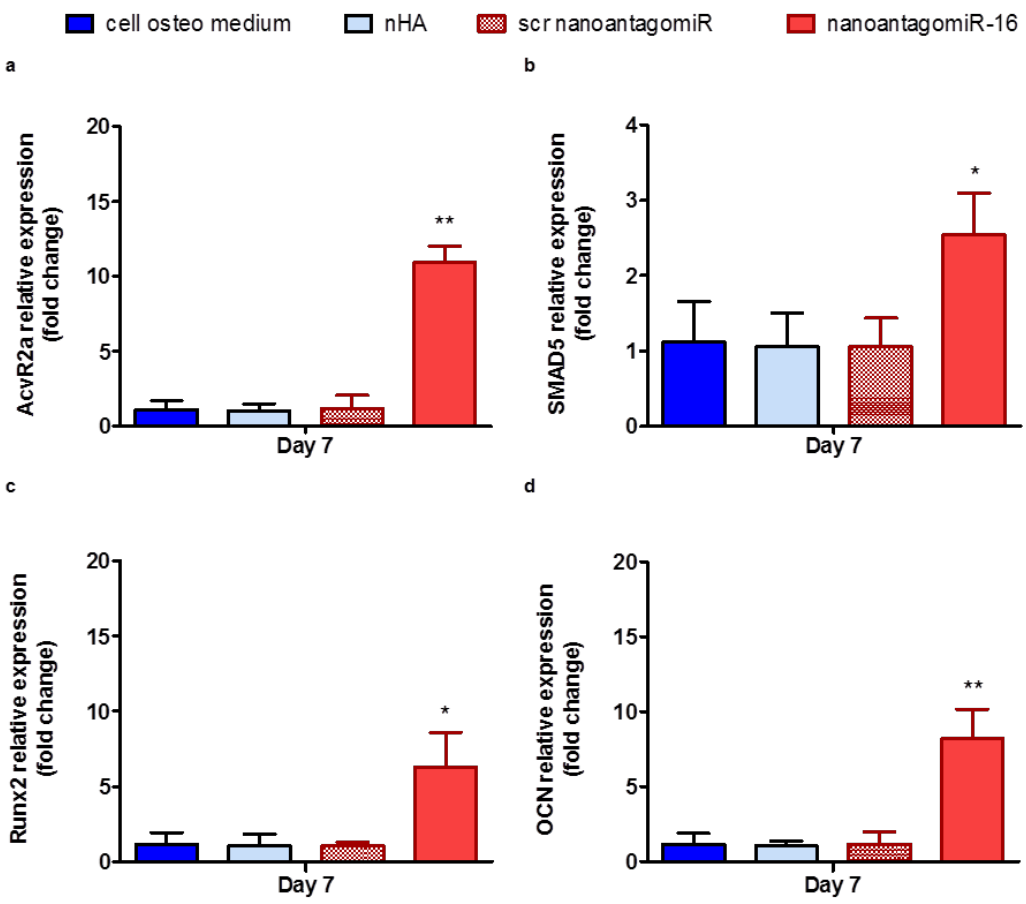

Figure 3.13 qRT-PCR analysis of the effect of nanoantagomiR-16 treatment on hMSC osteogenic gene expression. **a)** AcvR2a, **b**) Smad5, **c)** Runx2 and **d)** OCN were increased after 7 days. Scr nanoantagomiR was set as the reference control group and relative expression was normalised to that of 18S and calculated using the $2^{(-\Delta\Delta Ct)}$ method. Mean + standard deviation, n = 4, * = p<0.05, ** = p<0.001.

3.4.2.4.ALP activity was increased in nanoantagomiR-16 treated compared to untreated hMSCs

As part of the assessment of biofunctional osteogenic response, quantification of ALP activity showed that nanoantagomiR-16 treatment resulted in 11.32 and 8.62 fold higher levels than untreated cells and nHA groups respectively (Figure 3.14). These were also 1.22 fold higher than the scr nanoantagomiR group, which surprisingly enhanced ALP activity over untreated cells. In summary, this result reported a limited ability of nanoantagomiR-16 treatment to enhance functional osteogenesis in hMSCs at the timepoint assessed.

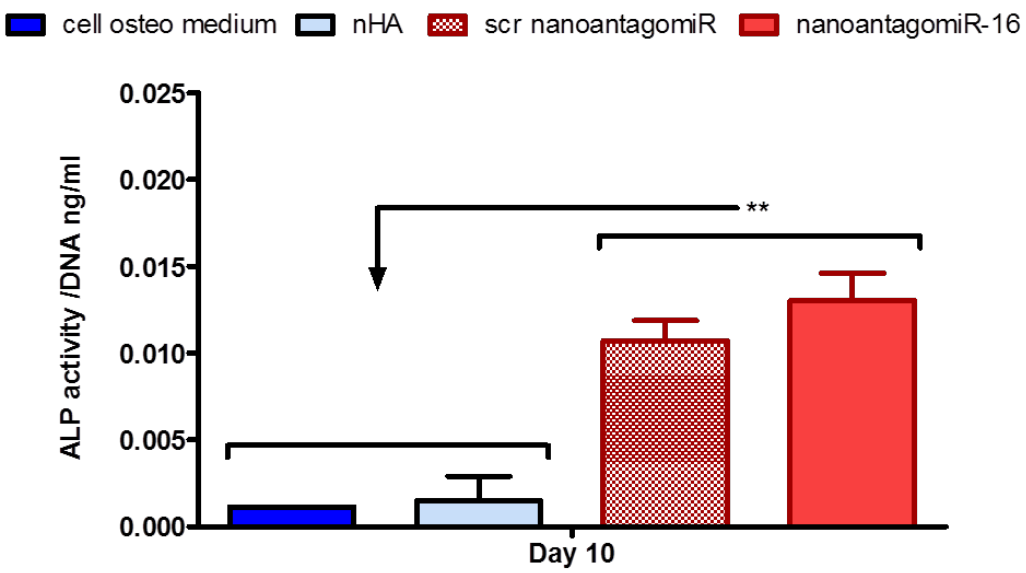

Figure 3.14 Analysis of ALP activity in nanoantagomiR-16 treated hMSCs. Quantification of ALP normalised to dsDNA content demonstrated increased ALP activity levels in both scr and -16 nanoantagomiR groups compared to untreated cells and blank nHA 10 days after treatment. Mean + standard deviation, n = 3, ** = p<0.001.

3.4.2.5.Mineral deposition was enhanced in nanoantagomiR-16 treated hMSCs

As an indication of osteo-induction, enhanced extracellular calcium deposits were observed at day 10 in the cells treated with nanoantagomiR-16 using alizarin red staining (Figure 3.15a). Correspondingly, quantification of calcium deposition levels at day 10 post-seeding revealed a significant enhancement in the nanoantagomiR-16 treatment group to 3.59 fold over untreated cells and this effect was maintained until day 14, achieving a 3.53 fold increase over untreated cells (Figure 3.15b). Taken together, this assessment indicated that nanoantagomiR-16 treatment holds potential to maintain an enhanced calcium mineralisation response from the early time point of day 10 onwards.

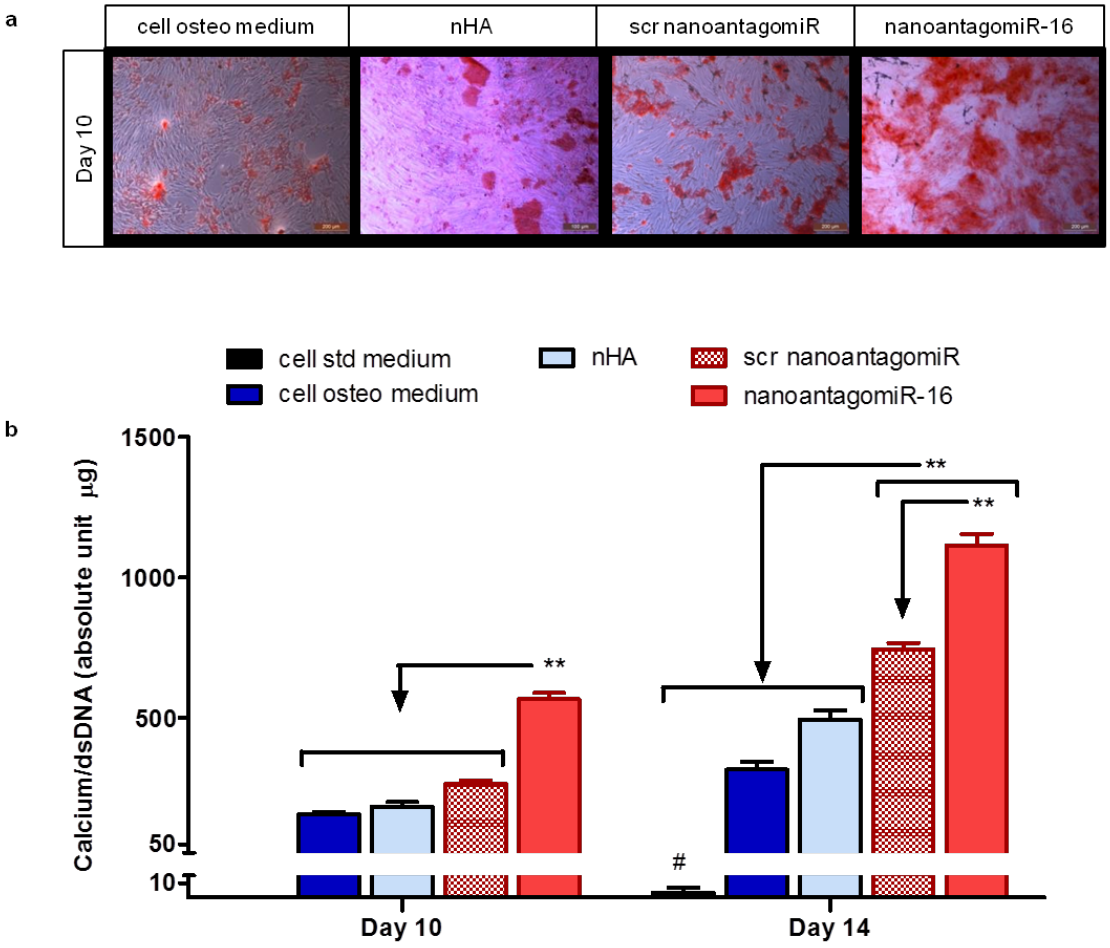

Figure 3.15 Analysis of calcium deposition in nanoantagomiR-16 treated hMSCs. a) Alizarin red staining showed calcium deposits at 10 and 14 day, scale bar= 200 µm. **b)** Calcium normalised to dsDNA content confirmed an increase in calcium deposition by day 10 after treatment with nanoantagomiR-16 in osteogenic culture and maintained increased calcium levels compared to the control groups after 14 days. Mean + standard deviation, n = 3, ** = $p<0.001$, # = $p<0.001$ against all other groups.

3.4.3.The effect of nanomiR-210 mimic treatment on hMSC osteogenesis

3.4.3.1.Bioinformatic analysis supports a bi-modal role of miR-210 in osteogenesis

Bioinformatic tools provided the identification of 586 putative targets predicted for miR-210 in human species, out of which approximately 10 % have been experimentally validated (Figure 3.16a). Although osteogenesis-related molecules such as BMP-6, Smad4 and IGF-2 were shortlisted from the predictions hit-list, none of these were found in the validated targets reported. Interestingly, entries of two angiogenesis related factors, namely hypoxia inducible factor 3α (HIF3A) and EphrinA3 (EFNA3), are validated targets for this miRNA, and this process is the focus of further work presented in Chapter 5. In summary, the direct interaction between miR-210 and the negative factor for osteogenesis AcvR1b has been validated experimentally in both human and mouse, which further supports the hypothesis that increased miR-210 levels will enhance hMSC osteogenesis.

With regards the homology of the miR-210::AcvR1b interaction across human, rat and mouse species (Figure 3.16b), the interaction type was maintained across the three species although additional binding sites were found in both human and rat as compared to mouse sequences, and these additional regions reported higher context percentile score, pointing to a more potent scope of their interaction. On the other hand, both human and rat sequences of the mRNA target site are susceptible of interaction with more neighbouring miRNAs than in mouse species, but these are not currently described as osteogenesis regulators, reinforcing a notable potency of the miR-210::AcvR1b interaction across the three species studied.

a

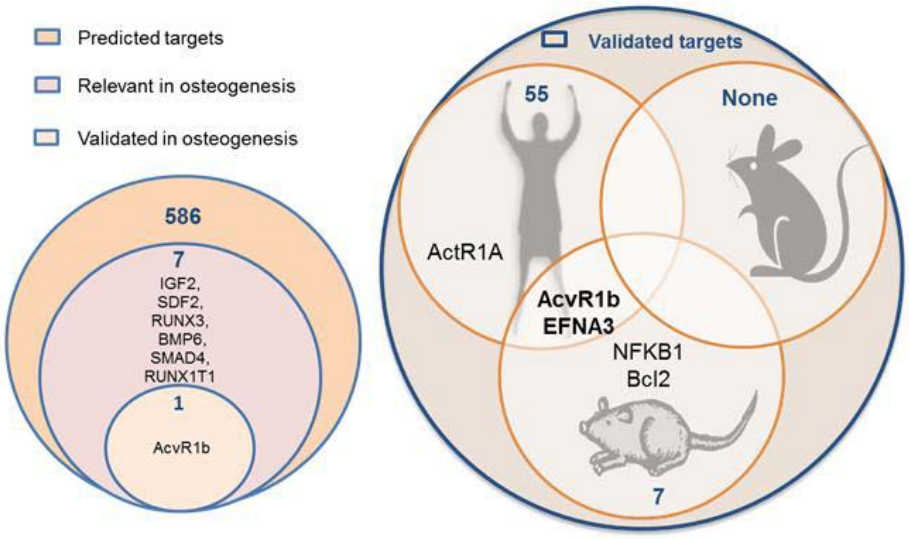

b

miR-210::AcvR1b	Position of 3′ UTR	Predicted pairing of target (top) and miRNA (bottom)	Seed match	Context score percentile	Neighbouring interactions Other miRNAa with study target		
					Total sites	No. miRNAs	Role in osteog.
Human (hsa)	42-48	5′ ...CUGGCAGCGAGAACUACGCACAG... 3′ AGUCGGCGACAGUGUGCGUGUC	7mer-m8	66	2	6	No
	1602-09	5′ ...AAAUUAUCCAAUUGAACGCACAU. 3′ AGUCGGCGACAGUGUGCGUGUC	7mer-m8	31	2	2	No
Mouse (mmu)	1563-9	5′ ...AAAUUCCAGACUCAAACGCACAU 3′ AGUCGGCGACAGUGUGCGUGUC	7mer-m8	40	3	4	No
Rat (rno)	137-43	5′ ...GACAGAGCCUGGGAGACGCACAC.. 3′ AGUCGGCGACAGUGUGCGUGUC	7mer-m8	56	4	10	No
	1542-8	5′ ...AAAUUGUAGACUCAGACGCACAU 3′ AGUCGGCGACAGUGUGCGUGUC	7mer-m8	20	4	5	No

Figure 3.16 Bioinformatic exploration of miR-210. a) Predicted (left circle) vs. validated (right circle) targets related to osteogenesis across human, mouse and rat for miR-210. Overlapping sections of internal circles indicate that validation has been reported in both species. **b)** miRNA::target interaction for (i) miR-210 and AcvR1b across hsa, mmu and rno species.

3.4.3.2.Effective manipulation of intracellular miR-210 level in hMSC was achieved using nHA-based delivery

When miR-210 intracellular levels were monitored during hMSC osteogenic culture, these remained generally unaffected in the untreated cells, only subjected to culture in osteogenic medium (cell osteo medium). In comparison to this, nanomiR-210 mimic treatment prominently increased miR-210 levels (Figure 3.17), while treatment with the remaining nanoantagomiR-133a and 16 did not affect miR-210 levels in hMSCs (Figure 3.18). In summary, the efficient delivery of miR-210 mimic using nHA particles was confirmed by this data.

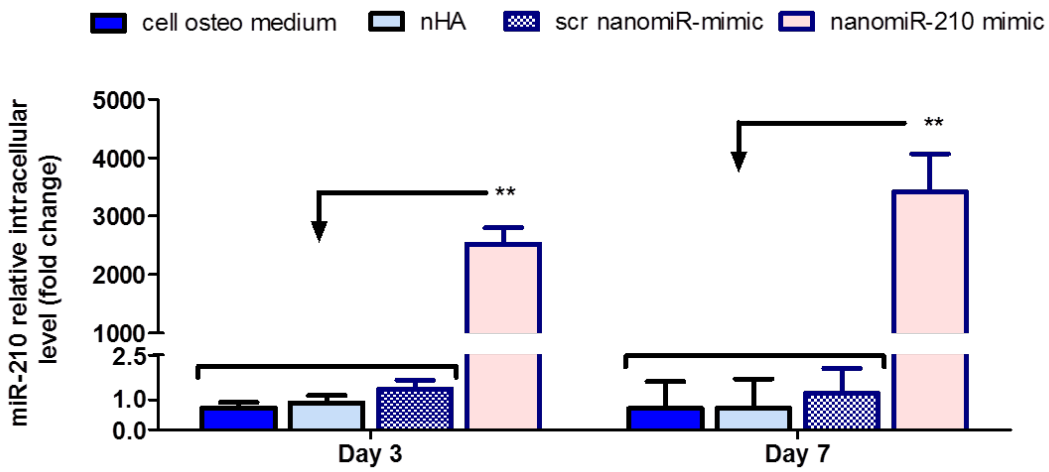

Figure 3.17 qRT-PCR analysis of miR-210 manipulation in hMSCs using nHA-based delivery. miR-210 mimic treatment demonstrated a maintained increase of miR-210 intracellular levels from day 3. Scr nanomiR-mimic was set as the reference control group and relative expression was normalised to that of 18S and calculated using the $2^{(-\Delta\Delta Ct)}$ method. Mean + standard deviation, n = 4, ** = p<0.001.

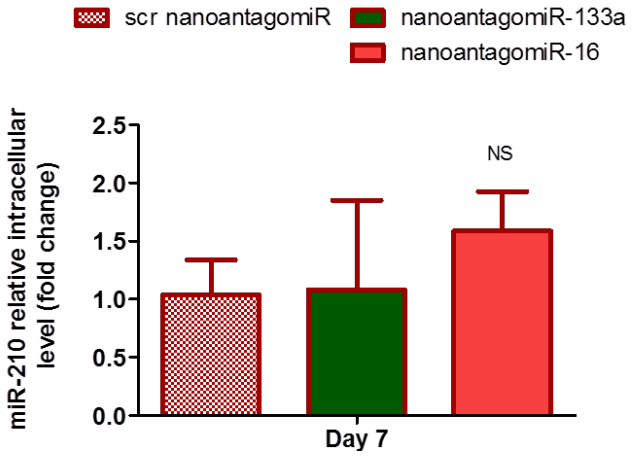

Figure 3.18 qRT-PCR analysis of specificity in miR-210 manipulation demonstrating non-manipulation of miR-210 following nanoantgomiR-133a or -16 treatment. NanoantagomiR-133a and -16 did not significantly affect miR-210 intracellular levels day 7. As a reference for comparison with nanomiR-210 mimic treatment, all groups presented in this figure fall within the range of the bottom section of Figure 3.18. Scr nanoantagomiR was set as the reference control group for both nanoantagomiR-133a and nanoantagomiR-16. Relative expression was normalised to that of 18S and calculated using the $2^{(-\Delta\Delta Ct)}$ method Mean + standard deviation, n = 4, NS = not significant variation.

3.4.3.3.NanomiR-210 mimic treatment did not enhance hMSC osteogenic gene expression

To evaluate the effect of nanomiR-210 mimic treatment on hMSC osteogenic gene expression, the direct target AcvR1b, as well as the osteogenesis markers Runx2 and OCN were analysed at day 7. NanomiR-210 mimic treatment resulted in an effective silencing effect of AcvR1b to 0.24 (± 0.14) fold (Figure 3.19a). Following this however, Runx2 levels remained unaffected (1.00 ± 0.20 fold expression, Figure 3.19b), and nanomiR-210 mimic had a negative effect on OCN, which was reduced to 0.27 (± 0.016) fold (Figure 3.19c). In summary this data indicated that successful manipulation of miR-210 levels did not correlate with enhanced hMSCs osteogenesis at the gene level.

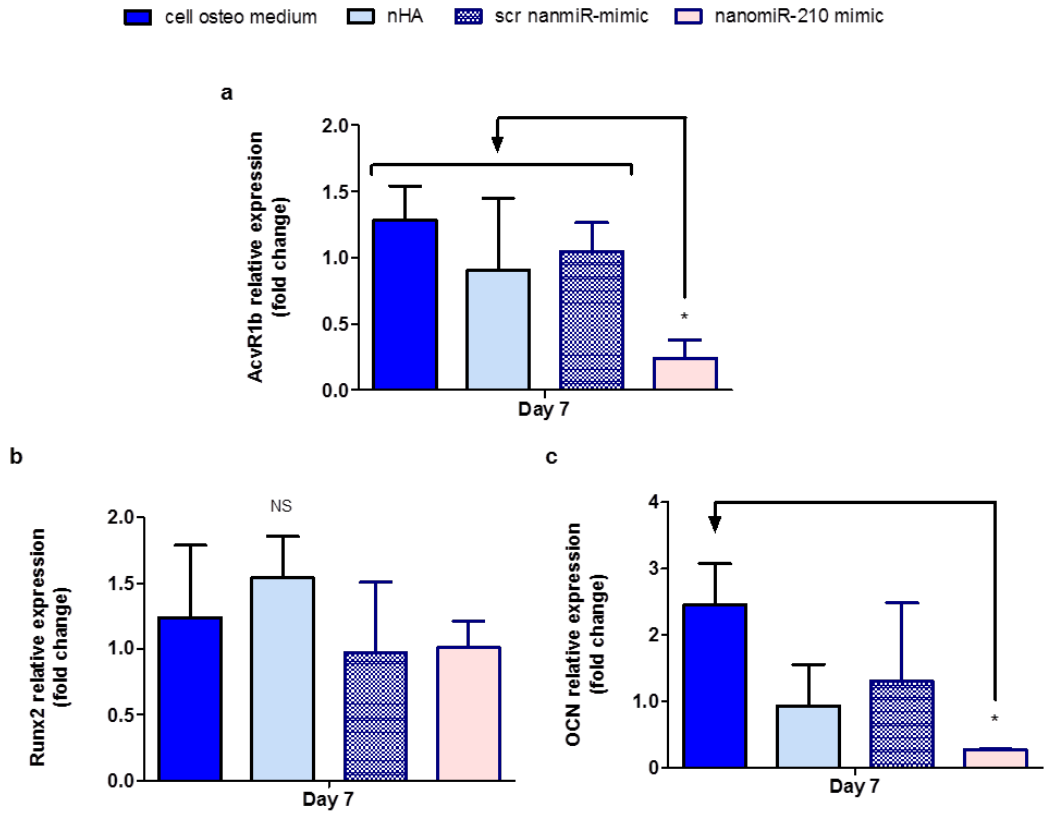

Figure 3.19 qRT-PCR analysis of the effect of nanomiR-210 treatment on hMSC osteogenic gene expression. **a)** A decrease in AcvR1b expression was found for the nanomiR-210 mimic group while **b)** Runx2 expression was unaffected and **c)** OCN relative level was also decreased. Scr nanomiR-mimic was set as the reference control group and relative expression was normalised to that of 18S and calculated using the $2^{(-\Delta\Delta Ct)}$ method. Mean + standard deviation, n = 4, NS = not significant variation, * = $p<0.05$.

3.4.3.4.ALP activity was enhanced in nanomiR-210 mimic treated compared to untreated hMSCs

As part of the assessment of biofunctional osteogenic response, quantification of ALP activity showed that nanomiR-210 mimic treatment increased ALP activity to 12.4 and 9.44 fold higher levels than untreated cells and nHA groups respectively, although this corresponded to 0.88 fold of the levels determined for scr nanomiR-mimic (Figure 3.20), which had promoted a surprising increase in ALP activity. Hence this result indicated a restricted ability of nanomiR-210 mimic treatment to trigger enhanced functional osteogenesis in hMSCs.

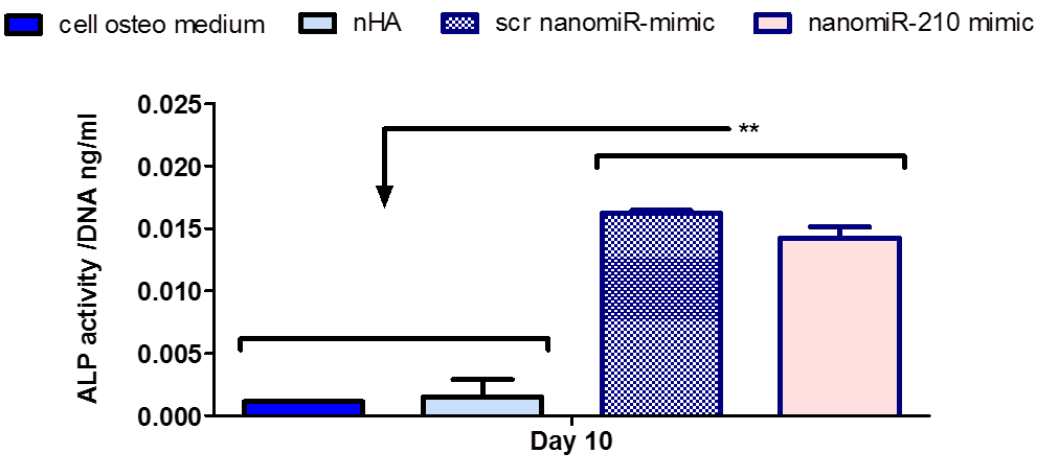

Figure 3.20 Analysis of ALP activity in nanomiR-210 mimic treated hMSCs. Quantification of ALP normalised to dsDNA content demonstrated increase ALP activity levels in both scr and -210 nanomiR-mimic groups compared to untreated cells and blank nHA at 10 days after treatment. Mean + standard deviation, n = 3, ** = $p<0.001$.

3.4.3.5.Mineral deposition was enhanced in nanomiR-210 treated compared to untreated hMSCs at the early timepoint of 10 days

Enhanced calcium deposition at day 10 was observed in the cells treated with nanomiR-210 mimic (Figure 3.21), indicating a positive effect of the treatment on osteogenesis. Alizarin red staining confirmed the presence of extracellular calcium deposits at this time point across all groups, with a higher amount of small deposits found in the nanomiR-210 mimic group (Figure 3.21a). Quantification of calcium deposition corroborated this observation, showing a 3.37 fold increase over untreated cells, although the scr nanomiR-mimic

treatment also produced a marked increase in quantified calcium deposits. Subsequently, at day 14 calcium deposition levels remained enhanced in the nanomiR-210 mimic treatment group by 1.64 fold in comparison to untreated cells, however this effect was approximately at the same level than the nHA alone group (516.39 ± 16.59 and 494.84 ± 31.91 respectively), and was highest for the scr nanomiR-mimic group at this timepoint (Figure 3.21b). This assessment indicated that increasing miR-210 levels promoted an early enhancement of calcium deposition, although this response was not robust enough to maintain enhanced functional osteogenesis at later timepoints.

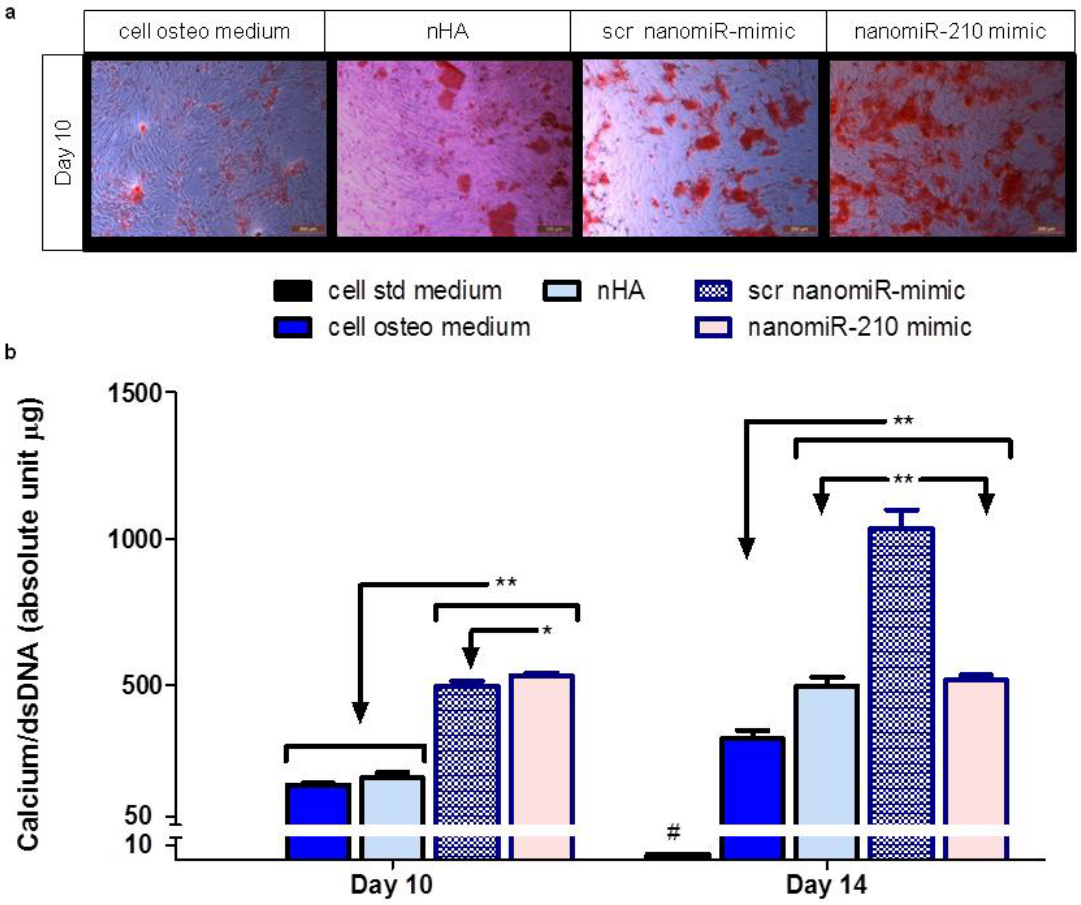

Figure 3.21 Analysis of calcium deposition in nanomiR-210 mimic treated hMSCs. a) Alizarin red staining showed calcium deposits visibly increased with nanomiR-210 mimic at day10, scale bar= 200 µm. **b)** Calcium was increased by day 10 after nanomiR-210 mimic and scr nanomiR-mimic treatment, which was maintained in comparison to untreated cells and blank particles at day 14, but the effect of nanomiR-210 mimic treatment did not surpass that of scr nanomiR-mimic by this later timepoint. Mean + standard deviation, n = 3, * = $p<0.05$, ** = $p<0.001$, # = compared to all other groups in that graph.

3.5.Discussion

The emerging interest in the use of miRNAs as osteo-therapeutics has led to the application of viral or lipid based delivery of miRNA to osteoprogenitors and stem cells. However, non-viral and non-lipid based delivery of potential candidates to hMSCs is an approach understudied in the bone TE field. To our knowledge, this is the first study to test the therapeutic ability of antagomiR-133a, antagomiR-16 and miR-210 mimic to enhance hMSC osteogenesis, with the additional novelty of using the nHA-based delivery system, as opposed to viral-based or commercially available lipid-based vectors. The results showed significant increases in Runx2 and OCN expression with nanoantagomiR-133a and, to a lesser extent, with nanoantagomiR-16. NanoantagomiR-133a treatment also resulted in the most promising enhancement of ALP activity in comparison with the two other nanomiR treatments assessed. Finally, calcium deposition was increased at both 10 and 14 days with the nanoantagomiR-133a and -16 groups, while nanomiR-210 mimic only had a positive effect at the early time point of 10 days. Taken together, the results from this study demonstrated that nHA-based delivery of these three miRNAs enhances hMSC osteogenesis albeit to different levels. Ultimately, the greatest osteogenic response of hMSCs was seen with nanoantagomiR-133a treatment.

The bioinformatic exploration reported the direct interaction of both miR-133a and miR-16 with additional positive mediators of osteogenesis, amongst which COL1A1 and COL4A2 were found respectively. This data further supported the negative role of these two miRNAs in osteogenesis. The bioinformatic exploration also predicted a direct interaction between miR-210 and positive mediators of osteogenesis, such as BMP-6 and Smad4. Although these interactions have not been experimentally validated yet, this data potentially implied miR-210 as a negative regulator of osteogenesis, in opposition with the positive role described in the literature (236).

Intracellular miRNA level manipulation was deemed successful for each of the nanomiR treatments studied. Initially, this study showed for the first time an endogenous downregulation in miR-133a levels during hMSC osteogenesis, which was in accordance with previous observations in C2C12 mouse

myoblasts and primary mouse vascular smooth muscle cells (242, 387). More importantly, nanoantagomiR-133a treatment reduced intracellular miR-133a levels to less than 0.2 fold of the scrambled (scr) nanoantagomiR control group which indicated a further enhanced effect over the endogenous miR-133a downregulation in untreated cells observed in this study. NanoantagomiR-16 also maintained silencing effects reducing miR-16 levels to less than 0.1 fold over 7 days, confirming the ability of the nanomiR system to achieve over 90 % silencing functionality. Moreover, nanoantagomiR-16 treatment did not affect intracellular miR-133a levels and vice versa, which was interpreted as an indication of specific manipulation of miRNA levels. This further supported the lack of RISC deregulation suggested by the results presented earlier in Chapter 2 using nanoantagomiR at the 20 nM dose. On the other hand, assessment of intracellular miR-210 following nanomiR-210 mimic treatment demonstrated a very prominent increase to levels that can be considered supra-physiological (388). Taken together, these results confirmed the capability of nHA-based delivery to successfully manipulate miRNA levels in hMSC monolayer osteogenic culture.

Subsequently, robust manipulation of all the direct gene targets selected for each nanomiR treatment was demonstrated at the mRNA level. Namely nanoantagomiR-133a enhanced Runx2 levels, nanoantagomiR-16 increased AcvR2a and Smad5 levels and nanomiR-210 mimic decreased AcvR1b expression. Although the effect of miR-133a mimic on Runx2 mRNA levels has been assessed previously by Li *et al*. (242), who showed results consistent with our study, this is the first time that the interaction between miR-16 and AcvR2a or Smad5, as well as the interaction between miR-210 and Acvr1b, has been assessed at the mRNA level. Up to 84 % of the changes in protein levels induced by miRNA regulation in mammalian species have been reported as attributable to changes in mRNA expression (389, 390). Hence, when miRNA manipulation induces detectable alterations at the mRNA level this can be interpreted as of high biological relevance. In this study, the beneficial role of each nanomiR treatment was supported by the efficient regulation of mRNA levels of the direct targets assessed.

Additionally in this study, nanoantagomiR-133a and nanoantagomiR-16 markedly increased Runx2 and OCN mRNA after 7 days in culture, however, nanomiR-210 mimic did not increase Runx2 or OCN. Several reports have tested the mRNA levels of Runx2 and OCN to evaluate the osteogenic response of bone progenitor cells, including MSCs, as part of assessing the role of several miRNAs in relation to osteogenesis (234, 237, 238, 386). Although the cell type, miRNA delivery method and miRNA dose utilised across these studies is heterogenous (Table 3.1), the range of changes reported for these genes by PCR is generally less than three-fold. The biological response to effective miRNA manipulation ranges from a fine-tuning to a phenotype switching response (391). Specifically, the fine-tuning response is associated with mild amplitude gene expression changes, i.e. less than three-fold, while higher amplitude changes, such as those observed in this chapter, better correlate with a phenotype-switching role (391). This fact highlights the promising implications of the marked increase determined for both Runx2 and OCN in this chapter, which was of a higher order for nanoantagomiR-133a treatment, but also promising for nanoantagomiR-16. With regards to the observations following nanomiR-210 mimic treatment, these differ from the work published by Mizuno *et al.* using different experimental conditions to those of this study: 100 nM miR-210 mimic (Ambion) was administered to the mouse NRG cell line using Lipofectamine® which resulted in a 1.3 fold increase in OCN mRNA expression compared to the control miRNA treatment (236). In summary, both nanoantagomiR-133a and -16 treatments appeared valuable as a pro-osteogenic therapeutic for hMSCs but a less encouraging response was seen with the nanomiR-210 mimic.

Table 3.1 Different experimental conditions across reports elucidating the implication of several miRNAs in osteogenesis.

miRNA	miRNA dose	Delivery method	Cell type	Reference
miR-29b	50-100 nM	Oligofectamine®	MC3T3, rat fetal calvaria OB	Li, Z. (234)
miR-2861	n/d	Lipofectamine®	ST2, mouse OB	Li, H. (238)
miR-196a	Pre-miRNAs n/a	Lentivirus	hASC	Kim, YJ. (237)
miR-218	Pre-miRNAs n/a 50nM	Lentivirus Oligofectamine®	MC3T3,mMSC	Hassan, MQ. (386)

Subsequently, ALP activity was increased in all nanomiR treatment groups compared to untreated cells in osteogenic medium, being highest in nanoantagomiR-133a but also significant versus the nanoantagomiR scr group for nanoantagomiR-16. Changes in ALP activity induced by manipulation of miRNA levels have been assessed in a comprehensive study by Schoolmeesters *et al*. (235). In that study inhibition of miR-133a was tested alongside a range of selected miRNAs, and resulted in a two-fold increase in ALP activity over untreated cells. From the perspective of this project, the detection of 17-fold increase in ALP activity in the nanoantagomiR-133a group suggested an encouraging beneficial effect for bone TE applications. In parallel, the 11-fold increase in ALP activity obtained with nanoantagomiR-16, also posed this treatment group as worthy of consideration. Meanwhile, consistent with the Runx2 and OCN gene expression results, the nanomiR-210 mimic did not display a positive effect, which was in opposition with the previous report by Mizuno *et al*. (236). In summary, this data indicate a standout capacity of miR-133a and miR-16 inhibition, in comparison to miR-210 enhancement, to functionally enhance osteogenesis in hMSCs.

Lastly, a significant increase in calcium deposition with both nanoantagomiR-133a and -16 was detected at each of the timepoints assessed, whereas nanomiR-210 mimic only increased calcium deposition at the earlier timepoint of

day 10. Calcium deposition in the ECM during osteogenic culture is regarded as definite functional marker of osteogenesis at the standard endpoint of 14 days in two-dimensional (2D) assays (226, 237, 238, 240, 348, 368, 369, 375, 382, 387). Of relevance, this is the first time that calcium deposition has been quantified following treatment with inhibitors of miR-133a or miR-16 as well as with miR-210 mimics. Other RNAi strategies to enhance osteogenesis have also been reported to increase calcium deposition when combining different delivery vectors, dosage regimes and cell types. As an example of other non-viral delivery approaches, a 2-fold increase in calcium quantification was reported after 14 days of osteogenic culture in both hMSC transfected with Chordin siRNA using lipoplexes (226) and human adipose-derived stem cells (hASCs) treated with 40 nM miR-148b mimic (348). Another study reported treatment of hASCs with baculoviruses separately encoding a range of miRNAs, namely miR-26a, miR-29b, miR-148b and miR-196a, demonstrating relevantly enhanced calcium within an approximate range of 3 to 6.8 fold over the miR-negative control group (299) after 14 days in osteogenic culture. Comparatively, the data presented in this chapter enhanced calcium deposition in a pronounced manner after just 10 days, to levels ranging from 3.37 to 4.67 fold increase over untreated cells, which effectively surpassed those reported for the non-viral vectors, even with a single application of the low dose of 20 nM, and sat within the range determined for the baculovirus system. Moreover, the range quantified for both antagomiR treatments at the endpoint of 14 days, from 2.55 to 3.53 fold increase over untreated cells, was still superior than that reported for the other non-viral vectors at this timepoint, highlighting the beneficial application of the nHA-based delivery. In summary, this data demonstrated the relevant ability of the three nanomiR treatments to rapidly increase mineral deposition at an early timepoint while the two nanoantagomiRs maintained this effect until the endpoint of analysis.

The presented data demonstrated that nanoantagomiR-133a treatment displayed a superior effect on hMSC osteogenesis than nanoantagomiR-16 and nanomiR-210 mimic, consistent with our knowledge that the key transcription factor of osteogenesis, Runx2, is a direct target for interaction with miR-133a. The application of antagomiR-16 as an osteo-therapeutic showed promising

results and served as foundation experimental evidence to implicate this miRNA in hMSC osteogenesis. Finally, the ability of nanomiR-210 mimic treatment to enhance hMSC osteogenesis was limited in comparison with the two other treatments, however its application warrants further investigation in relation to additional targets implicated in survival and angiogenesis and this will be explored in Chapter 5 of this thesis.

One surprising result from this study was that negative control miRIDIAN miRNAs, here scrambled (scr), in both the miR-mimic and antagomiR formulations, produced unspecific variations in ALP activity and calcium deposition. These commercially available controls encompass a cel-miR-67 based sequence and are anticipated to not possess targets in mammalian species, meaning that they function as a random nucleotide sequence that does not generate biological responses. However, surprisingly, a similar effect to that observed in this study was obtained when the scr molecules were delivered to the hMSC osteogenic culture using Lipofectamine® (data not shown). Consistent with this, previous studies have shown that ALP activity was affected by the treatment with a scr pre-miR (238) and a scr miR-mimic (237). Moreover, scr miRIDIAN controls utilised here were titrated by Schoolmeesters *et al.* to eliminate their effect on ALP activity (235). Further explanation for this effect is that BLAST analysis reported 20 - 30 % homology in approximately 100 hits of protein-coding sequences within human genome (392). As miRNA and non-coding research is a rapidly evolving field, it is expected that the challenging design of scr sequences to be used as controls may be improved in the coming years, providing improved negative control molecules for experimentation. Nevertheless, the effect of the scr sequences was surpassed by all the nanomiR treatments in varying degrees of significance, and the specificity of this effect can be related back to the adequate modification of mRNA levels of the direct targets assessed.

3.6.Conclusion

Taken together, the results of this study demonstrated that efficient nHA-based delivery of three individual miRNAs - antagomiR-133a, antagomiR-16 and miR-210 mimic - led to enhanced hMSC mediated osteogenesis. Firstly, the role of the three miRNAs in osteogenesis was supported by the bioinformatic analysis and successful miRNA intracellular level manipulation was confirmed for all three treatments. Next, promising enhancement of Runx2 and OCN gene levels was found following nanoantagomiR-133a and nanoantagomiR-16 treatment, but not with miR-210 mimic. ALP activity was also most enhanced with nanoantagomiR-133a indicating biofunctionally increased osteogenesis. Finally, calcium deposition was increased at both 10 and 14 days with the nanoantagomiR-133a and -16 groups, while nanomiR-210 mimic only had a positive effect at the early timepoint of 10 days. In summary, nanoantagomiR-133a emerged as the optimal osteo-therapeutic from this study. Hence, the incorporation of this therapeutic in a 3D carrier to form a next generation miRNA-activated scaffold capable of enhancing hMSC osteogenesis was the focus of the research presented in Chapter 4.

Chapter 4. Incorporation of nanomiRs into a collagen-nanohydroxyapatite scaffold

Research presented in this chapter has been included in the following peer-reviewed publications:
Castaño, IM et al., A Novel Collagen-Nanohydroxyapatite microRNA-activated Scaffold for Tissue Engineering Applications Capable of Efficient Delivery of both miR-mimics and antagomiRs to Human Mesenchymal Stem Cells. J Control Release 2015; 200: 42-51.
Castaño, IM et al., Next generation bone grafting: Non-Viral Inhibition of MiR-133a Using Collagen-Nanohydroxyapatite microRNA-activated Scaffolds Rapidly Enhances Osteogenesis by Human Mesenchymal Stem Cells. *Manuscript submitted.*

4.1.Introduction

A critical consideration when applying miRNAs to tissue repair, and particularly in bone repair, relates to the need for efficient delivery systems to trigger the desired therapeutic effect for a specified time period within a local environment, which involves the combined application of a delivery vector and a 3D scaffold (339). Vectors, typically nanoparticles, mediate uptake processes as well as provide protection from nucleases and may improve the lifetime of the cargo, but rapid *in vivo* clearance of nanoparticles from target locations, owing to their small size, limits their local effects to occur over short time periods (340). Since incorporation of nanoparticles in clinically-translatable 3D scaffolds provides the extended time frames of localised delivery needed in many TE applications, the application of 3D scaffolds as delivery systems holds great promise to fully realise the therapeutic potential of miRNAs for TE applications (61, 195, 341). Composite scaffolds produced from combinations of natural polymers and CaP ceramics have received significant attention in the field of bone TE (124), and the use of coll-nHA scaffolds as GAMs for pDNA delivery, with optimised architecture, pore structure and mechanical strength due to the introduction of the nHA phase, has produced encouraging results for bone TE in recent studies

within our laboratory (126, 127). Thus, using nHA particles to deliver osteogenic miRNAs within this 3D coll-nHA platform is the focus of the current study.

Recently, 3D PLGA and polyglycerol sebacate scaffolds incorporating viruses belonging to the baculovirus and lentivirus families have showed promising functional delivery of pre-miRs and miR-inhibitors to ASCs of human and rat origin respectively: in both cases achieving a noteworthy effect in the repair of bone defects *in vivo* (297, 299). However, clinical applicability of viral-based miRNA delivery methods is still limited by the threat of adverse immune responses in patients and the risk of insertional mutagenesis (57). Alternatively, non-viral, commercial lipid-based delivery vectors have recently been incorporated in 3D platforms such as titanium-based platforms, gelatin nanofibers, PEG-gelatin hydrogels and PCL porous scaffolds to enhance miRNA-mediated osteogenesis in rat, mouse and human BM-MSCs respectively (297, 299, 347-349, 393). Although lipid vectors are renowned as highly efficient for nucleic acid delivery, cell membrane damage associated with their detergent effect has been referred to as a limiting factor for their clinical application (313). As mentioned previously in Section 2.1 and Section 3.1 of this thesis, the nHA particles developed in our laboratory were shown previously to be highly biocompatible vectors for pDNA delivery to MSCs (319) and encompass both advantageous osteoinductive and osteoconductive properties for bone repair specifically. While the reported work collectively represents remarkable steps towards the realisation of miR-based bone TE, it is speculated that the coll-nHA porous scaffold developed previously in our laboratory holds essential advantages from the biomaterial standpoint, which combined with the beneficial aspects of nHA particles as non-viral, non-lipid vectors may significantly advance the field of miRNA-based bone TE.

Having characterised the efficient delivery of reporter miRNAs as nanomiR complexes with the nHA particles in Chapter 2, and observed the encouraging ability of nanoantagomiR-133a to enhance osteogenesis through directly targeting the key transcription factor of osteogenesis Runx2 in Chapter 3, the incorporation of reporter nanomiRs and subsequently nanoantagomiR-133a as a therapeutic in the coll-nHA scaffolds is explored here. Hence, the coll-nHA

scaffolds were assessed for their ability to act as efficient reservoirs for nHA-miRNA delivery and ultimately to serve as therapeutic platforms with enhanced potential for bone repair.

4.2.Hypothesis & aims of the study

The hypothesis for this study was that nanomiR incorporation into coll-nHA scaffolds may serve a two-fold purpose: (i) to provide a localised miRNA delivery system for a range of TE applications and (ii) by incorporating nanoantagomiR-133a into the scaffold, to act as a therapeutic to increase the regenerative potential of the coll-nHA scaffolds providing a next generation bone graft substitute. The study presented in this chapter thus aimed to assess the potential of coll-nHA scaffolds to serve as miRNA delivery platforms to manipulate hMSC gene expression and apply this system to therapeutically enhance osteogenesis.

The specific aims of Chapter 4 were to:

- Assess morphology of miRNA-activated scaffolds using SEM
- Analyse hMSC viability after 3D culture within miRNA-activated scaffolds
- Study hMSC uptake of fluorescently tagged miRNAs within the miRNA-activated scaffolds
- Assess silencing functionality of the delivery system following 3D culture of hMSCs within scaffolds activated with reporter miR-mimics and antagomiRs
- Assess the potential of nanoantagomiR-133a delivery from miRNA-activated scaffolds to decrease miR-133a levels and subsequently increase expression of the direct target and key transcription factor of osteogenesis, Runx2
- Analyse the effect of nanoantagomiR-133a delivery from miRNA-activated scaffolds to manipulate the expression of osteogenic markers in hMSCs as well as to stimulate mineral matrix deposition

4.3.Materials & methods

4.3.1.miRNA-activated scaffold fabrication

Coll-nHA scaffolds were manufactured according to the lyophilisation technique developed in the laboratory for a 1:1 ratio of collagen versus nHA weight content (91, 94, 97, 138). Coll-nHA scaffolds prepared following this procedure posses a compressive modulus of 1.5 kPa and a porosity of approx. 99.5 % (97, 125). This technique involved the following sequential steps:

Slurry preparation and lyophilisation:
Coll-nHA slurries were prepared by adding 1.8 g of collagen (Integra Life Sciences, USA) to 330 ml of 0.05 M glacial acetic acid (AcOH, Sigma Aldrich, Ireland) and blending at 15,000 rpm for 90 min using an overhead blender maintained at 4°C (Ultra Turrax T18 Overhead Blended, IKA Works Inc., USA). Subsequently, nHA particles with an equivalent weight of 1.8 g were fabricated following the Darvan®-aided precipitation technique described in Section 2.3.1. Darvan® was used at 0.2 % concentration (v/v) and a centrifugation step (1 h, 10000 rpm) was carried out, following which nHA particles were re-suspended in distilled water (30 ml). The nHA particle suspension was sonicated at a frequency of 40 KHz and 70 % amplitude in continuous mode during 2 min using a SLPt Sonifier® ultrasonic cell disruptor (Branson Process Equipment & Supply Inc. Ohio, US), then incorporated into the collagen slurry by directly adding the suspension onto the coll-AcOH mix over a 30 min period while continuing blending to a final time of 2.5 h (125). Coll-nHA slurries were de-gassed using a Leybold D16B double stage oil-sealed rotary vane vacuum pump (Biopharma, UK) and freeze-dried at a final freezing temperature of -40°C during a 35 h cycle program using a VirTis Genesis 25 EL freeze-dryer (Biopharma, UK).

Scaffold sterilisation and cross-linking:
Coll-nHA scaffolds obtained from the lyophilisation process where subjected to dehydrothermal treatment at 105°C during 24 h using a Vacucell vacuum oven (MMM Medcenter Einrichtungen GmbH, Germany). Scaffolds were then cut into cylindrical discs (8 mm x 4 mm) using circular biopsy punches, and chemically

cross-linked for 2 h with a solution of 14 mM 1-(3-Dimethylaminopropyl)-3-ethylcarbodiimide hydrochloride (EDAC, Sigma Aldrich) and 5.5 mM N-hydroxysuccinimide (NHS, Sigma Aldrich) to both sterilize and structurally reinforce the scaffold structure (65).

Scaffold activation with nanomiRs:
The following nanomiR complexes were prepared as described earlier in Section 2.3.1. at a final concentration of 20 nM of the following miRIDIAN miRNA molecules (Dharmacon): (i) scr nanomiR-mimic and scr nanoantagomiR, as target-lacking groups, utilised in morphological analysis and hMSC viability studies, as well as reference negative controls for functionality experiments and the scr nanoantagomiR as a negative control for osteogenesis experiments; (ii) scr Dy547-nanomiR-mimic and scr Dy547-nanoantagomiR to monitor miRNA uptake from the scaffolds, (iii) anti-GAPDH nanomiR-mimic and nanoantagomiR-16 as functionality reporters and (iv) nanoantagomiR-133a as an osteo-therapeutic. Freshly prepared nanomiR mix (75 µL) was soak-loaded onto coll-nHA scaffolds on each side, with an intermediate incubation time of 15 min.

4.3.2.miRNA-activated scaffold physical characterisation

The microstructure of the miRNA-activated coll-nHA scaffolds was examined using SEM as this technique allows for the examination of specimens with a thickness in the mm range. EDAC-NHS cross-linked coll-nHA scaffold discs without any soak-loaded nHA particles or scrambled (scr) nanomiRs were used as a reference to compare structural features after loading the nanoparticles. A second group of coll-nHA scaffolds were soak-loaded with blank nHA particles, not containing miRNAs, to control for nanomiR complex formation. Subsequently, coll-nHA scaffolds were soak-loaded with the scr nanomiR-mimics or nanoantagomiRs. All scaffold groups were then prepared by alcohol dehydration and critical point drying, fixed to an adhesive carbon stub, and then sputter coated with palladium/gold using a Polaron Sputter Coater (Quorum Tech., UK). Imaging was carried out using a Tescan MIRA XMU SEM (Tescan, UK) operated at 5 kV in secondary electron mode.

4.3.3.Cell culture

hMSCs were cultured in complete DMEM medium as described in Section 2.3.3 until a sufficient cell number was obtained at passage number 5-6 for experimentation. A total of 3 x 10^5 cells were seeded per scaffold, by drop-wise addition onto each side of the surface, with a 15-min incubation step after addition of nanomiRs, as adapted from the procedure of hMSC culture on coll-nHA GAMs used in the laboratory (126).

4.3.4.Cell viability after culture within miRNA-activated scaffolds

Cell viability was studied to monitor potential cytotoxic effects derived from the 3D culture of hMSCs in miRNA-activated scaffolds, for which nHA particles were loaded with scr miR mimic/antagomiR, which act as controls and encompass sequences with non-existent targets in mammalian cells. In order to determine the number of viable cells present across the different groups, dsDNA content per scaffold was analysed after 3 and 7 days in 3D culture using the Quant-iT PicoGreen dsDNA kit (Invitrogen) as described in Section 2.3.4.

4.3.5.Cellular uptake of fluorescently labelled nanomiRs on miRNA-activated scaffolds

To monitor nanomiR uptake on miRNA-activated scaffolds, hMSCs were cultured on coll-nHA scaffolds previously loaded with fluorescent Dy547 nanomiR mimic/antagomiR complexes (emission at 547 nm, red). Live cells were fluorescently labelled with calcein-AM (emission at 517 nm, green; BioSciences) following manufacturer's instructions prior to microscopy. Imaging was carried out using a Leica microscope coupled to the LAS V3.6 software imaging system (Leica, Ireland) and Image J software was utilised to generate the merged images. Effective uptake of miR-mimics or antagomiRs was shown by colocalisation (orange) in areas corresponding to intracellular spaces.

4.3.6.miRNA-activated scaffold functionality assessment by qRT-PCR

qRT-PCR was carried out to test the functionality of miRNA-activated scaffolds using the methodology and materials described in Section 2.3.7. The levels of

GAPDH messenger RNA and miR-16 were determined to assess the silencing ability of the reporter nanomiR-mimic and nanoantagomiR groups respectively.

4.3.7.Analysis of the osteo-therapeutic potential of nanoantagomiR-133a-activated scaffolds

Osteogenic cell culture:
hMSCs were obtained, expanded in culture and seeded drop-wise onto scaffolds as described in Section 4.3.3, following which they were cultured in complete osteogenic medium consisting of standard growth medium supplemented with 50 µg/ml ascorbic acid-2-phosphate, 10 nM β-glycerophosphate and 100 nM dexamethasone. A control osteodifferentiation group consisting of hMSCs seeded on coll-nHA scaffolds was maintained in standard complete medium, meaning that no osteo-supplements were added. Media was replaced every 3/4 days for the duration of the assay.

Assessment of effective miRNA and genetic manipulation using qRT-PCR:
qRT-PCR analysis was used to determine (i) miRNA intracellular levels of miR-133a as well as mRNA relative expression level of (ii) the direct miR-133a target, Runx2, and (iii) the osteogenesis markers OCN, ALP and EphrinB4 (EPHB4) using the methodology described in Section 2.3.7. The hsa-miR-133a Taqman® MicroRNA assays as well as the following validated pre-designed human Quantitect Primer Assays (Qiagen, UK) were applied: Hs_Runx2_1_SG, Hs_BGLAP_1_SG and Hs_ALPL_1_SG, Hs_EPHB4_1_SG. The scr nanoantagomiR group was set as the reference for the calculation of relative expression levels.

Osteocalcin immunofluorescence staining:
Scaffolds were removed from culture and fixed using 10 % formalin for 30 min, then dehydrated using an automatic tissue processor (ASP300, Leica Microsystems Nussloch GmbH, Germany) prior to paraffin wax embedding. Sections (8 µm) were cut using a rotary microtome (Microsystems GmbH, Germany) and sections were mounted on L-polysine coated glass slides (Thermo Scientific). Samples were then deparaffinised with xylene and rehydrated in descending grades of alcohol (100 % to 70 %). Subsequently, sections were permeabilised in 1 % Triton X100 solution. Blocking in 5 % horse

serum (HS) was followed by incubation in a 1:50 dilution of rabbit polyclonal IgG anti-osteocalcin primary antibody with subsequent 1:200 dilution of FITC-labelled goat anti-rabbit IgG secondary antibody (both from Santa Cruz Inc.) and mounting with Fluoroshield medium containing DAPI (Invitrogen). Digital imaging was carried out using a microscope system (Eclipse 90i plus DS Ri1, Nikon, Japan) coupled to NIS Elements software.

Mineral deposition quantification as end-stage marker of osteogenesis:
As a quantitative measure of osteogenesis a Stanbio Calcium Liquicolor kit (Stanbio Laboratories) was used following manufacturer's instructions for calcium quantification. Briefly, scaffolds were removed from culture and placed in 1ml of 0.5 M HCl and left to shake overnight at 4°C. Calcium content quantified for blank coll-nHA scaffolds (non cell-seeded) was subtracted from the content determined for all cell-seeded groups. Absorbance of the colour product was read using a Varioskan Flash plate reader (ThermoScientific). Complementarily, the dsDNA Quant-iT PicoGreen kit (BioSciences) was used following manufacturer's instructions using the Varioskan system as before.

Histological assessment of calcium deposition:
Serial sections prepared as described in the above section were prepared for histological analysis and rehydrated prior to staining with 2 % Alizarin red (Sigma-Aldrich, Ireland) as it stains calcium deposits red. Sections were then dehydrated and DPX mountant was used to attach cover slips to the slides. Digital imaging was carried out using a microscope system (Eclipse 90i plus DS Ri1, Nikon) coupled to NIS Elements software.

4.3.8.Statistical analysis

Experiments were performed in triplicate, unless otherwise specified within figure captions, and are representative of a minimum of three independent repetitions using two cell donors. Results were analysed as described in Section 2.3.7 using two-way analysis of variance (ANOVA) plus a Tukey *post-hoc* test to assess several timepoints and one-way ANOVA plus Tukey *post-hoc* test for the data tested at one timepoint only. $p<0.05$ and $p<0.001$ were considered significant.

4.4.Results

4.4.1.miRNA-activated scaffolds maintained an interconnected porous structure while retaining nanomiR complexes

The topographic images obtained by SEM demonstrated the capability of the coll-nHA scaffolds to be functionalised for miRNA delivery (Figure 4.1) Pore size, in the 100 μm range, and interconnectivity of the pores within the 3D structure was maintained in all scaffolds assessed (Figure 4.1a-d). This is important to enable cell infiltration inside the 3D structure, therefore matching a key requirement for bone TE. Higher magnification images showed the retention of the soak-loaded blank nHA particles and nanomiRs along the collagen fibres (Figure 4.1e-h). At the highest magnification, single particles present in the composites showed differences among the groups (Figure 4. i-l). Rod-shaped blank nHA particles were uniformly distributed along the surface of the scaffold structure (Figure 4.1j). Correspondingly, nanomiR-mimics (Figure 4.1k) and nanoantagomiRs (Figure 4.1l) showed a similar organisation to that observed in Chapter 2 by TEM (Figure 2.2b-c) forming branched multiparticulate structures, and populations of small rod particles were also detected in the nanomiR-loaded scaffolds. Overall, SEM observation demonstrated that nanomiR complexes can be effectively retained within the highly porous structure of the coll-nHA scaffolds.

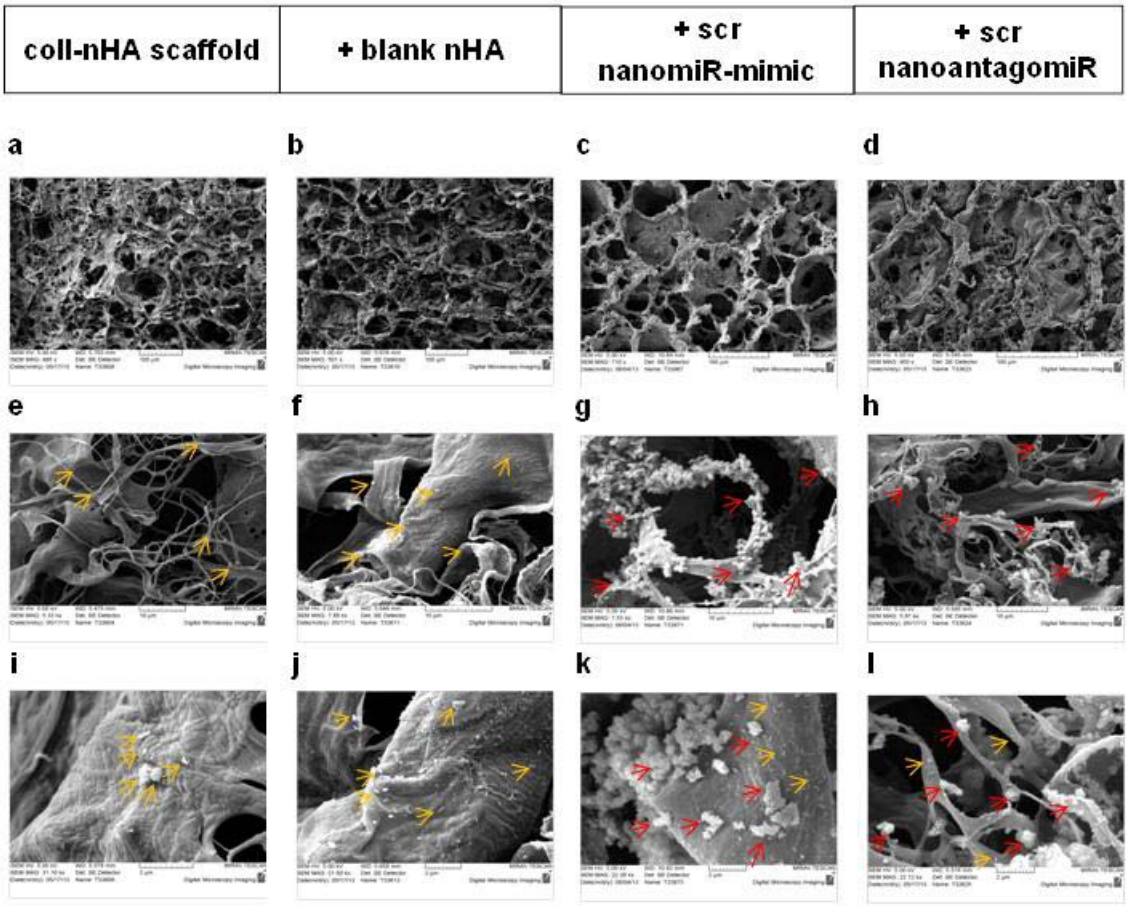

Figure 4.1 SEM analysis of nanomiR loaded coll-nHA scaffolds. a-d) Microstructural examination of nanomiR-loaded coll-nHA scaffolds showed the arrangement of the collagen fibres in an interconnected highly porous distribution, with pore size mantained in the range of 100 µm. Scale bar = 100 µm. **e-h)** blank nHA particles and nanomiR complexes were deposited and retained on the collagen fibres. Scale bar = 10 µm. **i-l)** Rod-shaped blank nHA particles and multiparticulate nanomiR complexes were detected at higher magnification. Scale bar = 2 µm. Arrows indicate deposits of nHA particles (yellow) and nanomiR complexes (red).

4.4.2.miRNA-activated scaffolds support nanomiR uptake without impairing cell viability of hMSCs

The *in vitro* assessment of uptake and cell viability demonstrated that red fluorescence was absent in cell-seeded but non-miRNA activated scaffolds, indicating that auto-fluorescence in this range of wavelength generated from the coll-nHA scaffold itself or the hMSCs was negligible (Figure 4. 2a). On the other hand, deposition of Dy547-labelled nanomiRs (red) could be detected throughout the structure of miRNA-activated scaffolds (Figure 4. 2b). Labelling live cells with fluorescent calcein-AM allowed the detection of Dy547 nanomiRs

intracellularly, with the detection of yellow and orange areas resulting from the green plus red co-localisation (Figure 4. 2c). This data indicated effective nanomiR uptake and maintenance of hMSC viability on the scaffolds, corroborating the ability of nHA particles to deliver miRNAs to hMSCs within the 3D platforms.

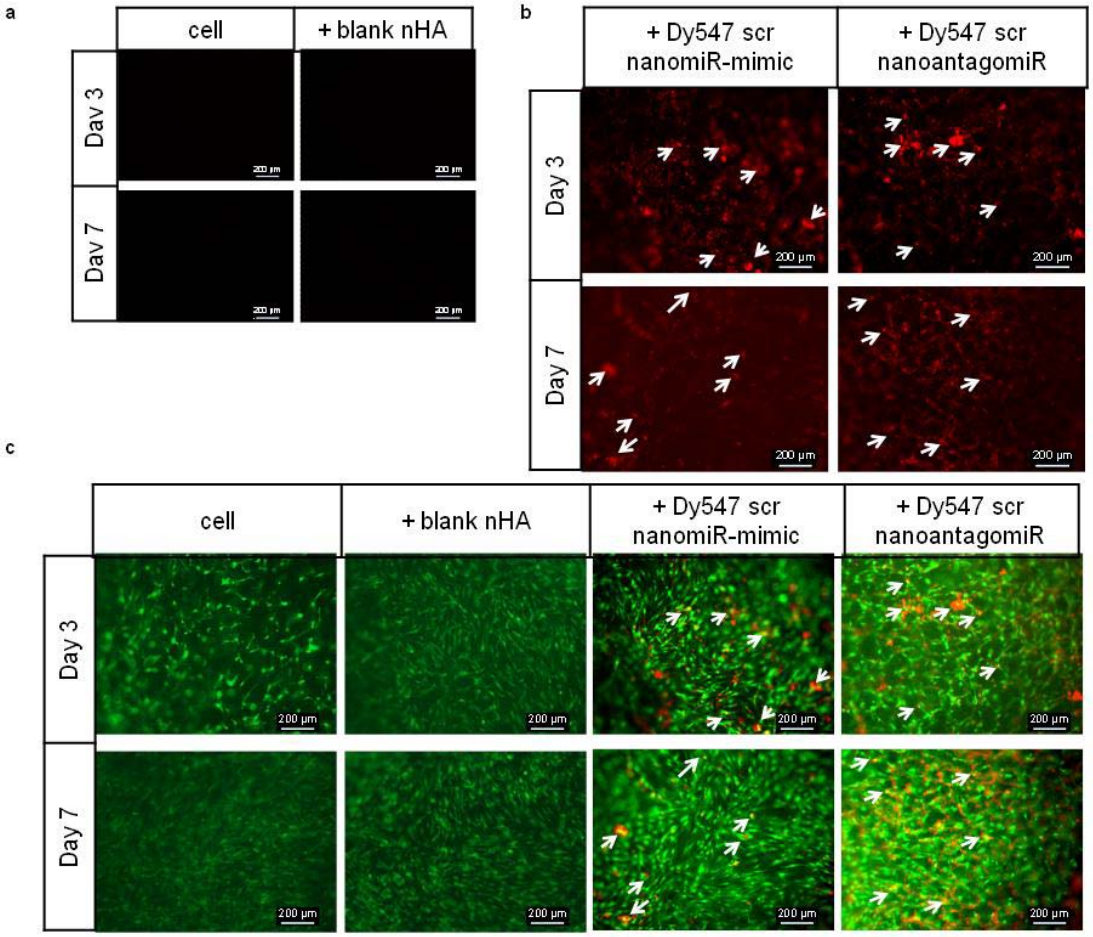

Figure 4.2 Assessment of hMSC nanomiR internalisation & cell viability on nanomiR loaded coll-nHA scaffolds. a) Red fluorescence background was controlled for in the nanomiR-free groups and **b)** Dy547-labelled scrambled (scr) nanomiR-mimic or nanoantagomiR (red) were detected within the cell-seeded scaffolds. **c)** Merged images of live cells fluorescently labelled with calcein-AM (green) and corresponding images of Dy547-labelled scr nanomiR-mimic or nanoantagomiR. Red fluorescence was observed colocalising within cells (yellow). Arrows in **b)** and **c)** indicate points of nanomiR internalisation. Scale bar = 200 µm, n = 3.

Similar to the analysis carried out in Chapter 2, dsDNA quantification was carried out to estimate cell viability after culture within the miRNA-activated scaffolds. dsDNA content was not significantly different among the groups,

indicating no impairment of hMSC viability after culture on the miRNA-activated scaffolds (Figure 4.3).

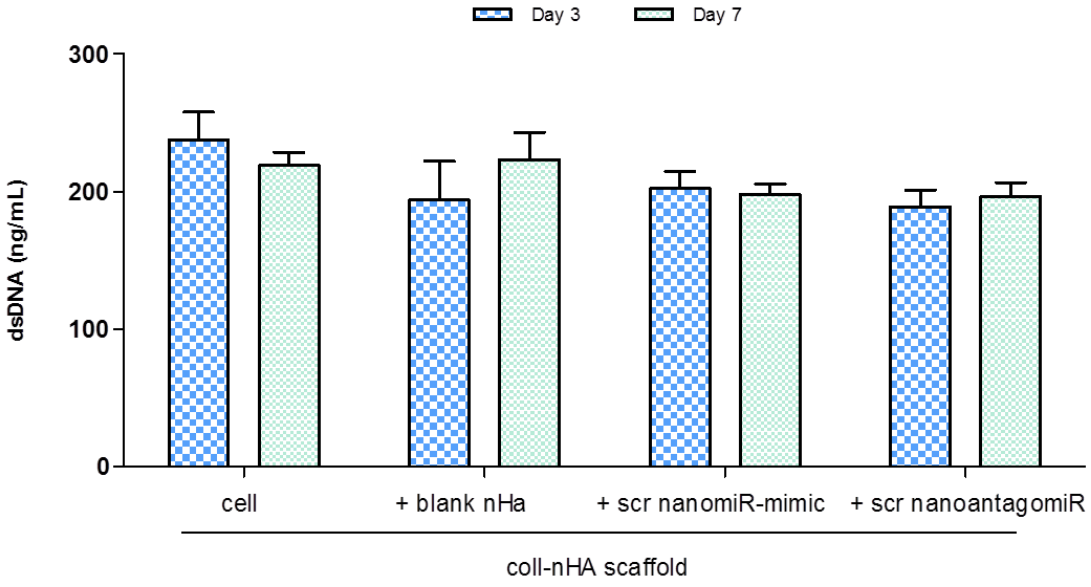

Figure 4.3 Assessement of hMSC cytotoxicity within nanomiR loaded coll-nHA scaffolds. dsDNA quantification indicated that viable cell number was maintained across all groups, therefore showing no treatment associated cytotoxic effects. Mean + standard deviation, n = 3, no statistical difference.

4.4.3.NanomiRs maintained significant functional interference after incorporation into coll-nHA scaffolds

The approach used to test the interfering functionality of nanomiRs in Chapter 2 was adapted to the culture of hMSCs within the 3D miRNA-activated scaffolds. A significant 20 % interference in GAPDH expression for the nanomiR-mimic was obtained, with relative levels decreasing to 0.80 ± 0.20 fold, an effect which was maintained over the 7 day period after cell seeding (Figure 4.4). Subsequently, to assess whether the 3D environment of the miRNA-activated scaffolds results in progressive and extended functionality, GAPDH interference levels were analysed at a later timepoint of 14 days after hMSC seeding on the anti-GAPDH nanomiR-mimic activated scaffolds. Extended culture on these bioactive platforms to 14 days showed a reduction in GAPDH relative levels to 0.45 ± 0.28 fold, which indicated that interfering functionality was improved to 55 % at this time and confirmed that localised delivery of miRNAs using the coll-

nHA scaffolds serves to achieve progressive and extended functional time frames.

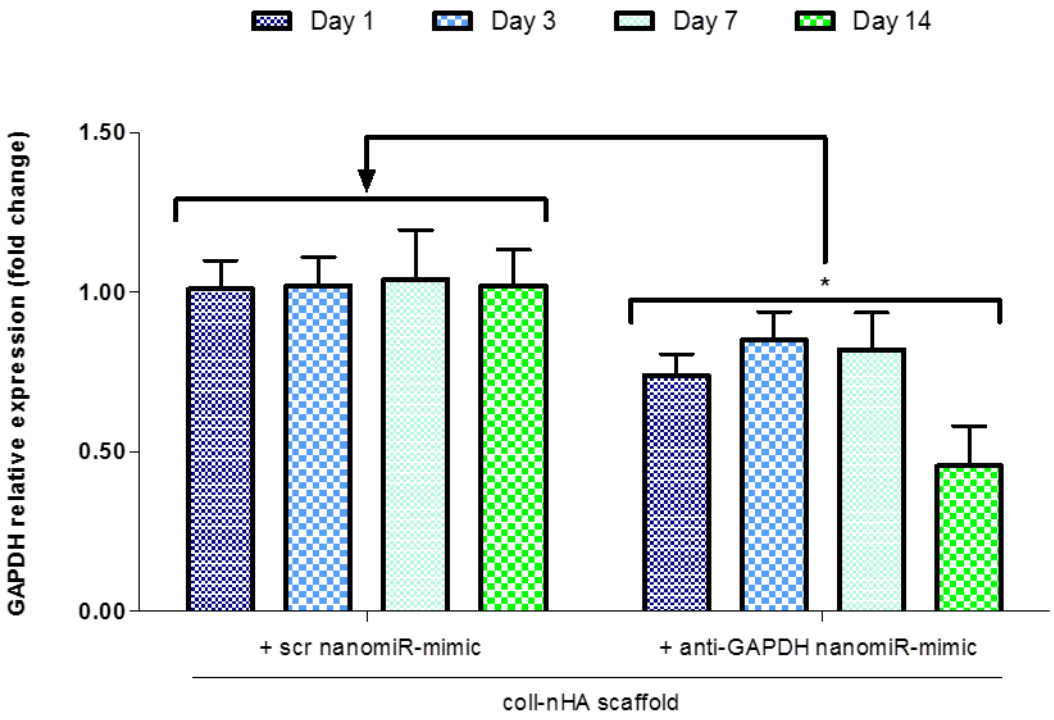

Figure 4.4 Silencing functionality of reporter anti-GAPDH nanomiR-mimic on coll-nHA scaffolds. qRT-PCR analysis revealed a significant decrease in GAPDH expression against the reference control, scr nanomiR-mimic, which improved to 55 % silencing with the extended culture at 14 days. Expression levels were normalised to those of 18S and calculated using the $2^{(-\Delta\Delta Ct)}$ method. Mean + standard deviation, n = 5, * = $p<0.05$.

Equally, the nanoantagomiR-16 activated scaffold decreased miR-16 expression significantly to relative levels of 0.12 ± 0.08 fold over the 7 day period, representing an interfering functionality of 88 % for the nHA-delivered antagomiRs incorporated in the coll-nHA scaffolds (Figure 4.5). Consequently, this data showed that the nanomiR complexes within the 3D structure of the coll-nHA scaffolds conserved significant bioactivity and can therefore these scaffolds serve as an effective platform for miRNA delivery.

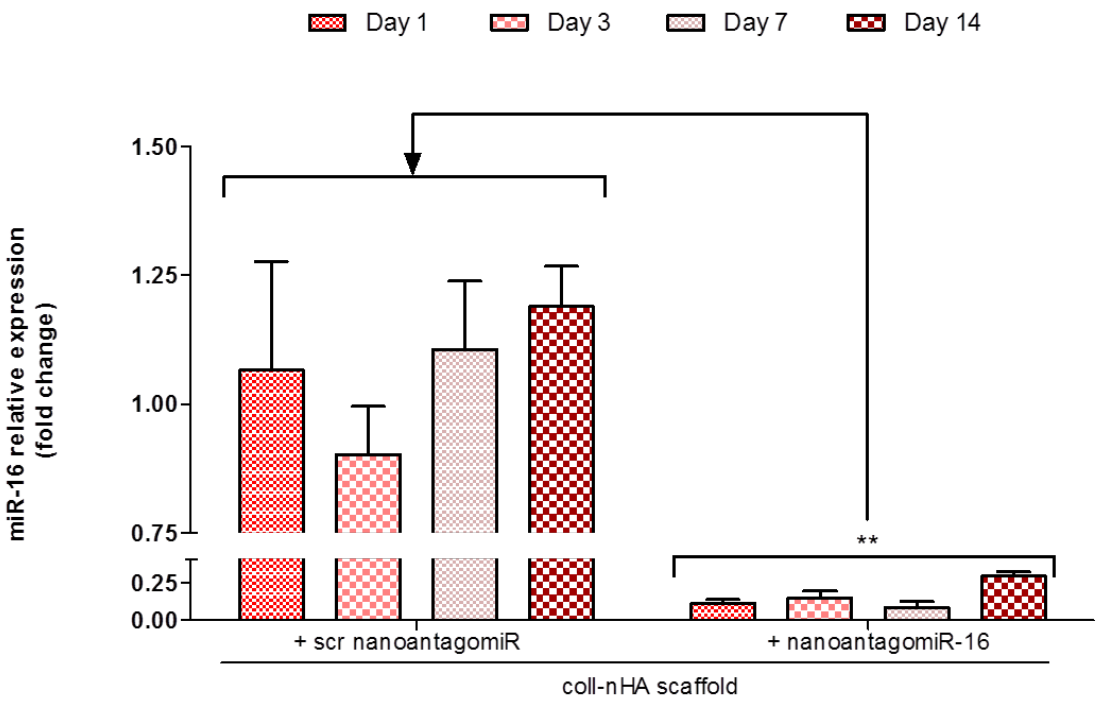

Figure 4.5 Silencing functionality of reporter nanoantagomiR-16 on coll-nHA scaffolds. Stem-loop qRT-PCR analysis showed that nanoantagomiR-16 treatment significantly decreased miR-16 expression with respect to scr nanoantagomiR, which was introduced as the negative control. Relative expression levels were normalised to those of 18S and calculated using the $2^{(-\Delta\Delta Ct)}$ method. Mean + standard deviation, n = 5, ** = $p<0.001$.

4.4.4.NanoantagomiR-133a activated scaffolds effectively decreased miR-133a intracellular levels and enhanced osteogenic gene expression

Following demonstration of efficient delivery of scrambled (scr) and reporter nanomiRs to hMSCs cultured on the coll-nHA scaffolds, the possibility of applying this system for therapeutic miRNA-mediated osteogenesis was explored. For this purpose, the candidate treatment selected from the results presented in Chapter 3, that is nanoantagomiR-133a, was introduced into the scaffolds. The nanoantagomiR-133a activated scaffolds significantly decreased the amount of miR-133a available in hMSCs to 0.49 ± 0.14 fold that of the reference group (scr) after 3 days (Figure 4.6). Furthermore, at the later time point of 7 days, miR-133a levels were further decreased within the nanoantagomiR-133a activated scaffolds (0.22 ± 0.05 fold vs reference group) while nHA markedly increased miR-133a at this timepoint (5.12 ± 2.66), resembling the effect observed at this same timepoint in the monolayer studies

presented in Chapter 3. This decrease in miR-133a was able to trigger a 2.74 ± 1.97 fold increase in the mRNA levels of the direct target of miR-133a, Runx2, at the initial timepoint assessed (Figure 4.7a), which serves as a hallmark for the initiation of the osteodifferentiation process. In addition, the mid stage markers of osteogenesis ALP, OCN and EPHB4 were upregulated 1.3, 1.5 and 2 fold respectively after 7 days (Figure 4.7b-d), which, very encouragingly, was significant relative to the levels detected for the cell osteo medium only group. This data confirmed the ability of coll-nHA scaffolds to mediate a substantially competent manipulation of post-transcriptional gene regulation in hMSC 3D culture.

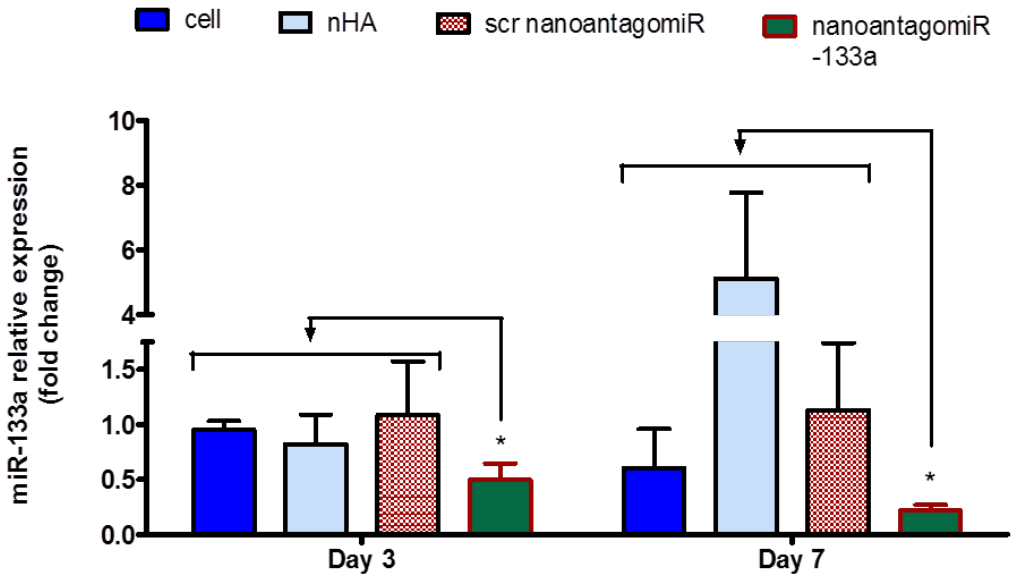

Figure 4.6 qRT-PCR analysis of miR-133a intracellular levels in hMSC osteogenic culture on miRNA-activated coll-nHA scaffolds. miR-133a was significantly decreased for the hMSCs cultured on the nanoantagomiR-133a activated scaffolds in comparison with the scr nanoantagomiR scaffolds over a time course of 7 days, demonstrating a high silencing functionality of the non-viral based 3D delivery system. Scr nanoantagomiR was set as the reference control group and relative expression was normalised to that of 18S and calculated using the $2^{(-\Delta\Delta Ct)}$ method. Mean + standard deviation, n = 5, * = $p<0.05$.

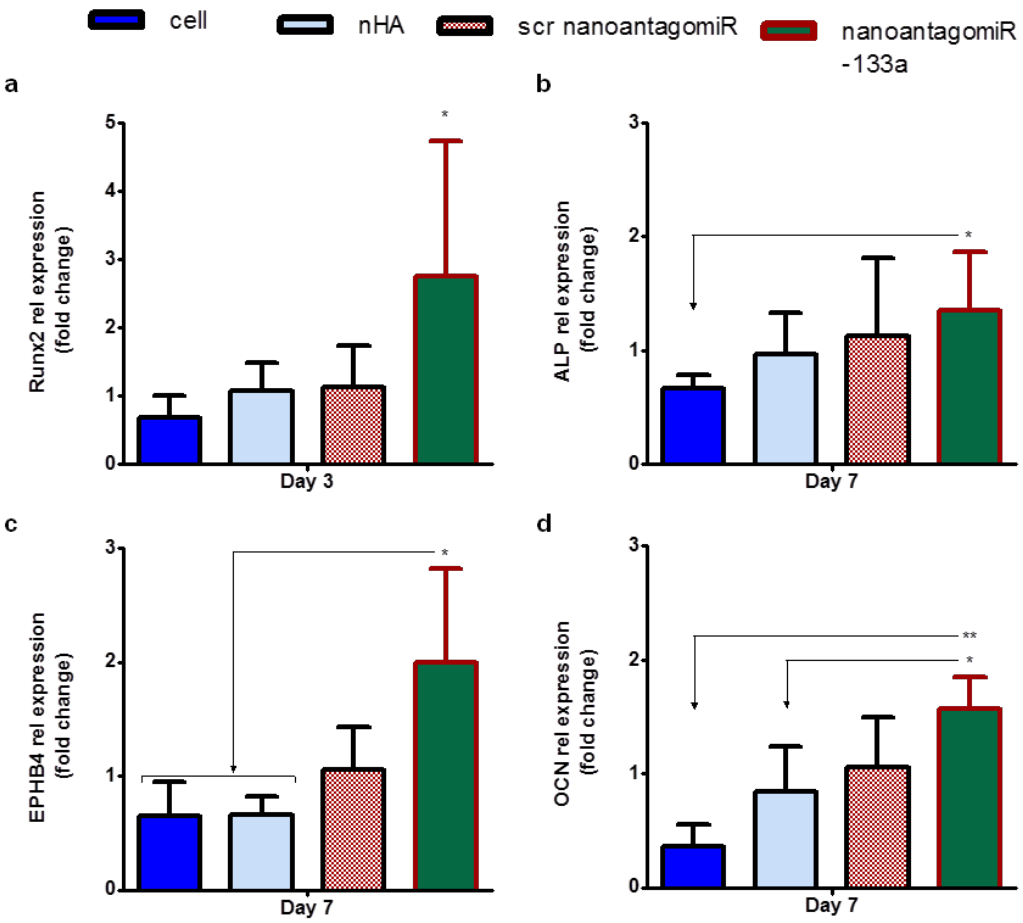

Figure 4.7 qRT-PCR analysis of the effect of nanoantagomiR-133a activated scaffolds on hMSC osteogenic gene expression. a) Runx2 mRNA expression was upregulated in the nanoantagomiR-133a activated scaffolds group after 3 days, while **b**) ALP, **c**) OCN and **d**) EPHB4 mRNA expression was upregulated in the nanoantagomiR-133a loaded scaffolds group after 7 days. Scr nanoantagomiR was set as the reference control group and relative expression was normalised to that of 18S and calculated using the $2^{(-\Delta\Delta Ct)}$ method. Mean + standard deviation, n = 4, * = $p<0.05$, ** = $p<0.001$.

4.4.5.NanoantagomiR-133a activated scaffolds enhanced osteocalcin protein levels

To further verify the osteogenic differentiation process, the presence of osteocalcin (OCN) at the protein level was assessed by immunofluorescence staining accompanied with DAPI labelling. At 14 days after hMSC seeding on the nanoantagomiR-133a activated scaffolds, OCN protein expression was qualitatively increased in comparison to the remaining groups, although cells cultured in coll-nHA scaffolds also presented higher OCN levels than the nHA-soak loaded coll-nHA scaffold and the scr nanoantagomiR activated scaffold

groups (Figure 4.8). At 28 days OCN expression had increased in the latter groups in comparison to their early timepoint levels, however the presence of OCN was visibly highest in the nanoantagomiR-133a activated scaffold group, confirming that nanoantagomiR-133a activated scaffolds resulted in increased osteogenic differentiation of hMSCs. In summary, this data correlated with the enhanced levels of OCN mRNA determined for nanoantagomiR-133a activated scaffolds in the gene analysis (Figure 4.7c) and collectively pointed to a robust enhancement of hMSC osteogenesis in 3D scaffold culture.

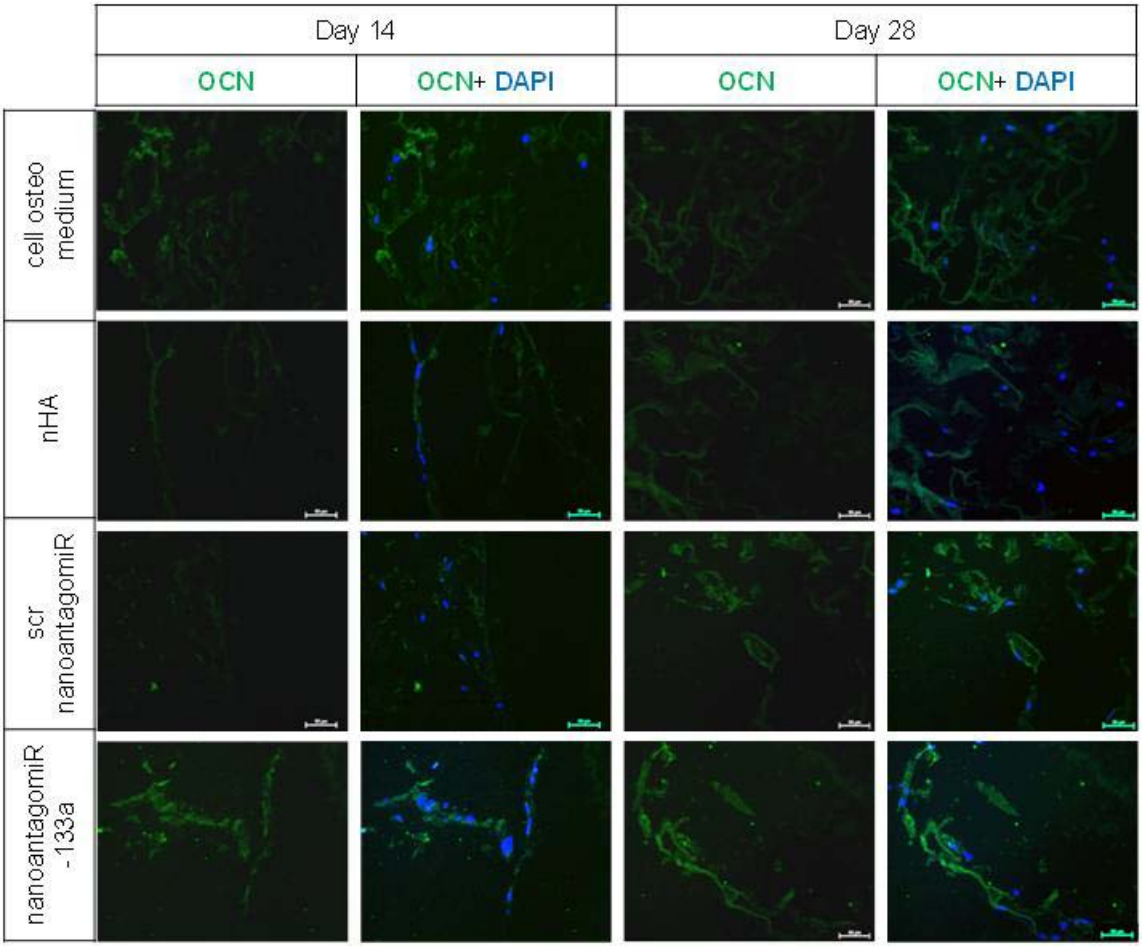

Figure 4.8 Effect of nanoantagomiR-133a activated scaffolds on OCN protein levels. OCN immunofluorescence staining (green) after 14 and 28 days in 3D osteogenic culture showed increased protein expression in the nanoantagomiR-133a activated scaffolds in comparison with the control treatment groups. Nuclei (blue) were stained with DAPI, Scale bar = 50 µm.

4.4.6.NanoantagomiR-133a activated scaffolds enhanced mineral matrix deposition

Mineral matrix deposition is regarded as an end-stage marker of functional osteogenesis. Similar to the assessment of mineral deposition carried out in Chapter 3, an early and a late timepoint of analysis, 14 and 28 days respectively, were evaluated to test for both an accelerated and a maintained increase in mineral matrix deposition. Consistent with the gene expression analysis, calcium deposition levels in nanoantagomiR-133a activated scaffolds were 78.4 % and 56.38 % higher than the untreated cells at day 14 and 28 respectively, while they were significantly increased in comparison to the nHA and scr nanoantagomiR groups at both time points tested (Figure 4.9), highlighting the ability of the antagomiR-133a activated scaffolds to rapidly trigger an enhanced functional osteogenesis and subsequently maintain it. Histological analysis using alizarin red staining depicted calcium deposition across all groups, which qualitatively increased from the earlier to the later timepoint; and importantly, more prominent, denser staining was found in the nanoantagomiR-133a treated group at both timepoints (Figure 4.10). In summary, this data pointed to the successful application of nanoantagomiR-133a for miRNA-mediated osteogenesis of hMSCs using the coll-nHA scaffolds as localised delivery platforms.

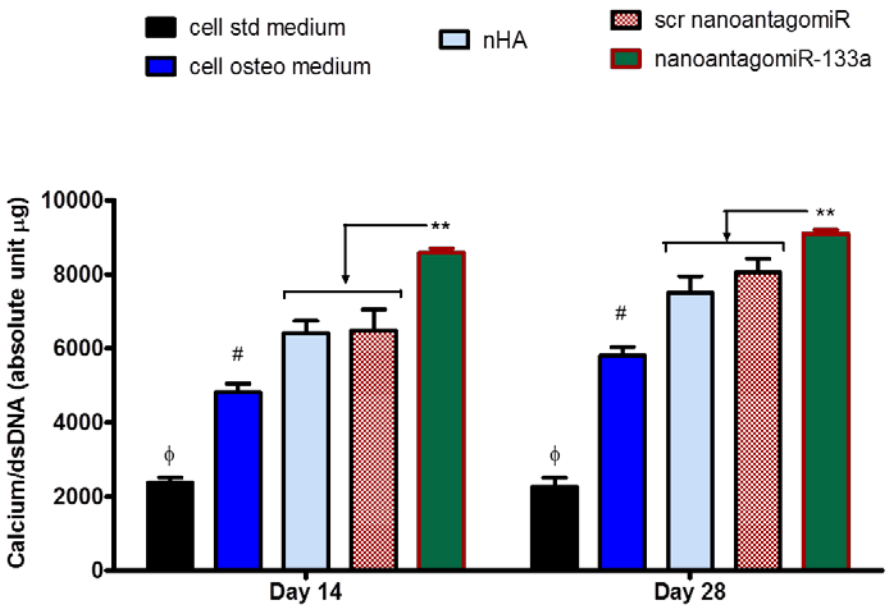

Figure 4.9 Effect of nanoantagomiR-133a activated scaffolds on hMSC mineral matrix deposition. Calcium normalised to dsDNA content confirmed an increase in calcium deposition by day 14 in nanoantagomiR-133a activated coll-nHA scaffolds and maintained increased calcium levels compared to the control groups after 28 days. Mean + standard deviation, n = 3,* * = $p<0.001$, ϕ = $p<0.001$ compared to all other groups, # = $p<0.001$ compared to nHA, scr nanoantagomiR and nanoantagomiR-133a activated scaffolds.

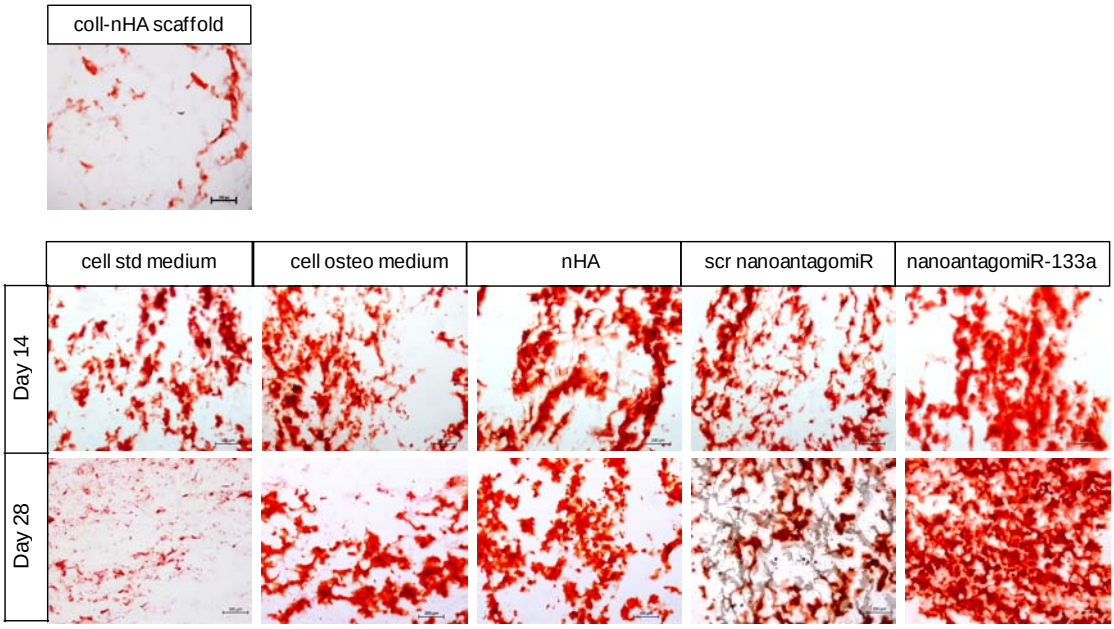

Figure 4.10 Alizarin red staining following 14 and 28 days of hMSC culture on nanoantagomiR-133a activated scaffolds. A prominently increased presence of calcium deposits was found within the nanoantagomiR-133a activated scaffolds at both timepoints. Non cell-seeded scaffolds were used as a control for the determination of basal calcium presence in the extracellular matrix. Scale bar = 50 µm.

4.5.Discussion

Incorporation of therapeutic miRNAs into 3D scaffold biomaterials is increasingly generating interest in the field of TE. This strategy offers the possibility to enhance the therapeutic potential of such scaffolds. The aim of this study was to assess the potential of bioactivating a coll-nHA scaffold, designed specifically for bone repair, to serve as miRNA delivery platforms to manipulate hMSC gene expression and apply this system to therapeutically enhance osteogenesis using antagomiR-133a. Taken together, the data presented here showcased the unprecedented development of the first non-viral, non-lipid scaffold technology to-date for the delivery of both miR-mimics and antagomiRs to hMSCs. When hMSCs were cultured on the miRNA-activated scaffolds, nanomiR internalisation and significant functional silencing with minimal cytotoxicity was observed. Ultimately, we demonstrated the therapeutic potential of the nanoantagomiR-133a activated coll-nHA scaffolds to rapidly enhance hMSC osteogenesis through targeting of the central transcription

factor of osteogenesis, Runx2, which ultimately resulted in the development of a highly innovative alternative to existing bone graft treatments, representing a promising new concept in bone TE.

SEM showed that pore size was consistently maintained following miRNA incorporation in the range of ~100 µm, which has been described as adequate for cell infiltration and migration throughout the structure (138). Particle deposition within the collagen fibres in the scaffolds did not result in pore occlusion, and indicated the binding of the mineral particles to the scaffold structure, possibly through electrostatic interactions. Because of the chemical nature of the nHA particles, hydrophobic or covalent-bond interaction types cannot be established with the available active groups that the collagen fibres present. Both the porosity and the particle retention mechanism ensured that the resultant scaffolds fulfil the necessary requirements to ensure cellular infiltration and nanoparticle exposure (340) that must be met in order for the bio-activated scaffold to be successful in simultaneously housing cells and locally delivering the therapeutic cargo. In summary, the SEM imaging indicated that nanomiR complexes can be effectively retained within the highly porous structure of the coll-nHA scaffolds, meaning that structurally, the miRNA-activated scaffolds hold potential to serve as depots for localised miRNA delivery.

The effective uptake of the nanomiR-mimic and nanoantagomiRs in hMSCs was demonstrated at both 3 and 7 days, as observed using fluorescence microscopy. As well as the nanomiR internalisation, the microscopic analysis of calcein-AM green labelled live cells indicated that cell viability was maintained across all groups. Additionally, the presence of nanomiR complexes in the 3D structure did not affect cell density. Noticeably, dsDNA content within each group did not differ between the two time points tested, reflecting a slower proliferation rate in 3D scaffold culture as compared to that seen in the monolayer experiments. This effect may relate to how cells adapt to the different extracellular microenvironment between 2D and 3D culture conditions. More specifically, cells attach to 3D scaffolds at a slower pace given that a larger surface area is available for cell contact (65, 280, 350), and this can result in delayed cell proliferation rates. Taken together, this data confirmed that

the deposition of nanomiR conjugates onto the scaffold did not hinder cell infiltration in the construct or intracellular uptake of the nanomiRs. Moreover, no cytotoxic effects arose from the 3D culture of hMSCs on the miRNA-activated scaffolds, indicating the safety and biocompatibility of this platform system.

Both functional reporter nanomiR-mimic and nanoantagomiR complexes incorporated in the coll-nHA scaffolds significantly and persistently maintained silencing of their respective targets GAPDH and miR-16 throughout the time period assessed. It has previously been proposed that transfection in a 3D scaffold environment relies on the migration of cells throughout the matrix and that the larger surface area reduces the relative exposure of cells to the transfection complexes at early timepoints, while extended culture periods allow for cells to further infiltrate within the 3D structure and be exposed to the cargo (394). The data presented in this chapter for the anti-GAPDH nanomiR-mimic activated scaffolds correlated with this observation and served to confirm the utility of 3D scaffold biomaterials as depots for functional delivery of miRNA-mimics for progressive and extended timeframes. The differences between groups found in this analysis can be explained by the more hydrophilic nature of the miR-mimics, which might establish stronger electrostatic interactions with the bioactive sites present on the collagen fibres of the scaffolds. Importantly, the silencing functionality detected for the nanomiR-mimic is within the range of the single report to-date where cells were added onto a functionalised scaffold (350), a result which is widely surpassed here with the nanoantagomiR-avtivated scaffold. In the previous study, a silencing range between 0.6 to 0.8 fold was achieved with miR-29b-mimic activated collagen-based scaffolds, which led to improvements in wound healing when tested *in vivo*. In contrast with our approach, the previous report involved the naked incorporation of the miR-mimic within the scaffold and targeted primary rat cardiac fibroblasts. Since hMSCs are regarded as more difficult to transfect that other cell types, including fibroblasts, it is proposed that the complexes of both miR-mimics and antagomiRs with the nHA particles are a key element for the relevant silencing efficiency demonstrated by the miRNA-activated scaffolds developed in this chapter.

Next, the therapeutic potential of manipulating miR-133a levels using the miRNA activated scaffold platform to enhance hMSC ostegenic differentiation was demonstrated for the first time. Only 8 studies have been published to date which have used miRNAs as osteo-therapeutics in 3D biomaterials in comparison with the panel of over 30 miRNAs described to be involved in osteogenesis (58, 297, 299, 347-349, 393, 395). It is important to note that the majority of miRNAs tested as osteo-therapeutics so far, with the exception of miR-31 (297, 395), directly target molecules which are part of secondary signalling pathways in many cases (393), meaning that their ability to drive the osteogenesis process on their own is limited. The innovative approach developed in this study resulted in miRNA-mediated manipulation of Runx2, the transcription factor regarded as the primary driver of the osteogenic pathway. The results presented showed a significant decrease in miR-133a intracellular levels and subsequently increased expression of Runx2 at the early timepoint of 3 days. This highlighted the capability of the coll-nHA scaffolds to functionally deliver the therapeutic nanoantagomiR-133a complexes with beneficial repercussions in modulating Runx2 levels. As a consequence of the increased Runx2 production, upregulated expression of a panel of osteogenic markers in hMSCs at the genetic level as well as enhanced presence of osteocalcin at the protein level at successive timepoints was demonstrated. Most importantly, the effective genetic manipulation of hMSCs on the nanoantagomiR-133a activated scaffolds subsequently translated into a rapidly and significantly enhanced calcium deposition on the scaffolds, which was maintained until the end timepoint of analysis. Calcium production is interpreted as hallmark of effectively enhanced osteogenic differentiation of hMSCs (226, 237, 238, 240, 348, 368, 369, 375, 382, 387), hence this result perhaps signifies the more significant outcome of the study presented in this chapter, where collectively this data pointed to a robust and coordinated enhancement in hMSC osteogenesis within the miR-activated scaffolds in comparison to the non-activated coll-nHA scaffolds.

A major advantage of the systems developed in this chapter relates to incorporating the nanomiR complexes in the 3D scaffolds in a cell-free manner and hence utilising the coll-nHA scaffolds as reservoirs for the localised delivery

of the miRNA complexes i.e. with a view to transfecting host cells when applied *in vivo*. This differs from the typical application of cell-mediated miRNA therapy in scaffolds shown in the literature (58, 297, 299, 347, 348, 395), where the scaffolds do not mediate the localised miRNA delivery to the cells, but the cells are instead seeded on the scaffolds after having internalised the miRNAs in advance of seeding. Our approach is a major breakthrough as it means that the miRNA activated scaffolds have the potential to exist as an 'off-the-shelf' platform which could be used for a variety of therapeutic applications depending on the specific miRNA chosen for delivery. While this system was developed with bone regeneration in mind, the functionalisation process described in this study may be applied to other scaffolds and to the incorporation of any miRNA with a role in tissue regeneration, therefore representing a promising approach for a wide variety of TE applications.

4.6.Conclusion

In summary, the research presented in this chapter demonstrated the significant potential of coll-nHA scaffolds to serve as the first non-viral, non-lipid localised miRNA delivery scaffold platforms developed in the field to-date. This platform was capable of efficient delivery of mature miRNA molecules and gene expression manipulation in human MSCs, a particularly difficult cell type to transfect effectively. The microstructure of the miRNA-activated scaffolds promoted effective cell infiltration, while efficient uptake and significant silencing functionality was demonstrated for both nanomiR-mimics and nanoantagomiRs. When antagomiR-133a was applied, this advanced system led to a successful reduction of miR-133a intracellular levels, achieved a subsequent increase in Runx2 in the MSCs and most importantly accelerated calcium deposition on the scaffolds - thus showing the therapeutic potential of the platform.

Angiogenesis in addition to osteogenesis plays a major role during the process of bone fracture repair. In Chapter 5 we investigated the application of this miRNA delivery system to deliver different miRNA combinations in order to achieve a simultaneous effect on both MSC-mediated angiogenesis and osteogenesis.

Chapter 5. Investigation of nanomiR-210 mimic as (i) a pro-angiogenic therapeutic and (ii) as a simultaneous pro-angiogenic and pro-osteogenic therapeutic as a part of a dual nanomiR formulation

5.1.Introduction

The beneficial application of nHA-based miRNA delivery for use in bone repair has been demonstrated in Chapters 3 & 4 of this thesis with the focus of enhancing hMSC osteogenesis. Importantly, angiogenesis also plays a pivotal role in bone repair (396, 397) and based on their biodegradability and biocompatibility, nHA particles are hypothesised to serve as potentially useful miRNA delivery vectors for applications beyond osteogenesis. Hence in this chapter the focus was placed on the nHA-based delivery of therapeutic miRNAs to enhance angiogenesis simultaneously to enhancing osteogenesis.

MSCs have potential to mediate angiogenesis via secretion of pro-angiogenic factors (378, 398), as well as acting as pericytes to provide support for the newly formed vascular networks (399). Additionally, it is known that VEGF plays a pivotal role during angiogenesis and stimulates vessel formation in bone defects, which has served as the rationale for its use in bone TE (144, 400, 401). While VEGF promotes endothelial cell migration, proliferation, survival and differentiation (146), it has also been implicated in the stimulation of bone repair through a number of mechanisms. These include (i) promoting bone turnover (152), (ii) stimulating the differentiation of osteoblasts (402, 403) and (iii) recruiting osteoprogenitor cells and MSCs to the defect site (404, 405), as well as (iv) promoting the survival and activity of bone-forming cells at the defect site (71, 406). Recent efforts have unravelled the role of several miRNAs in regulating angiogenesis either positively or negatively (Figure 5.1; (383, 407-412)), as well as their ability to further enhance MSC angiogenic capacity (347). Hence, strategies for manipulating miRNA levels have begun to be proposed to treat angiogenesis-related pathologies such as cardiovascular diseases (413), diabetes and diabetes induced retinopathy (414-416), as well as exacerbated vascularisation associated with several cancer types (417).

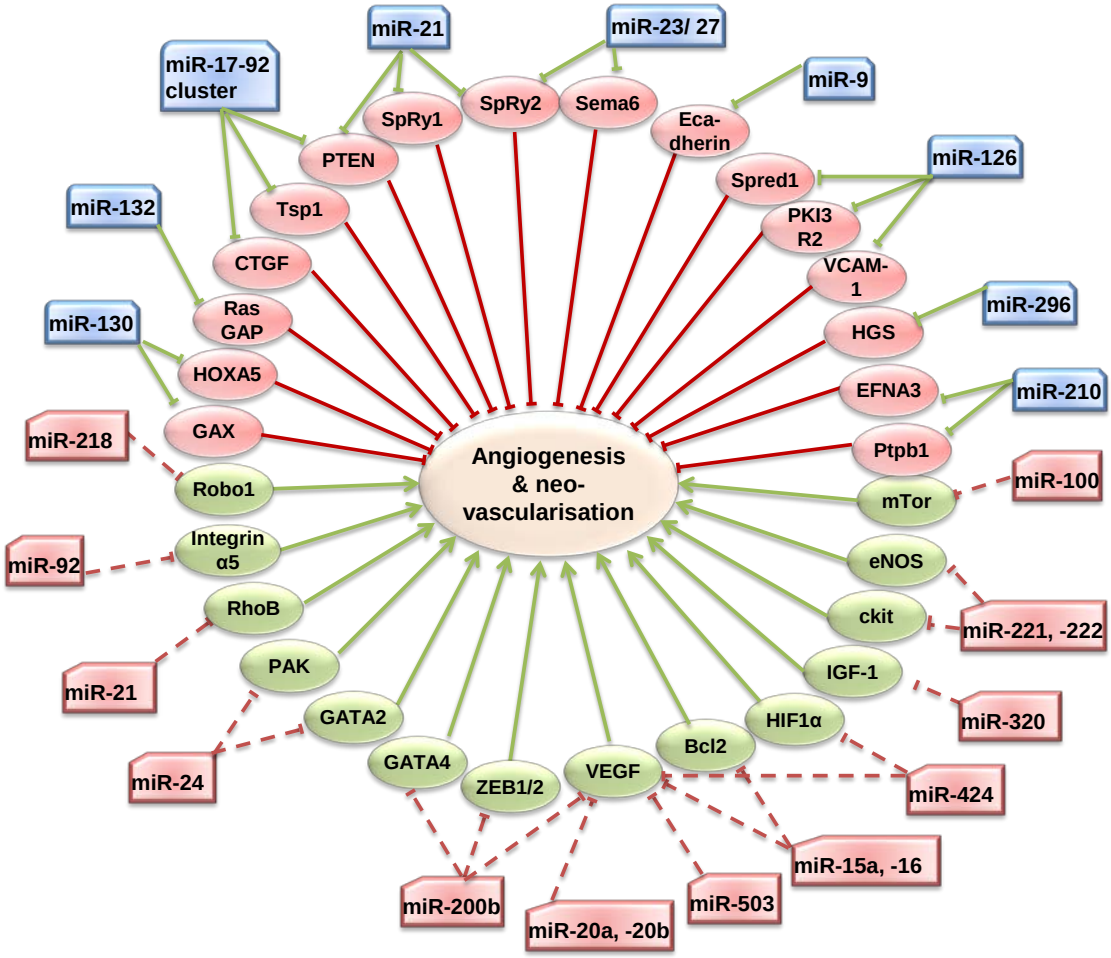

Figure 5.1 Panel of miRNAs influencing angiogenesis and neovascularisation and their reported targets (experimentally validated). Inner circle: red ovals accompanied by red brake symbols (⊣) indicate proteins with inhibitory role in angiogenesis, green ovals accompanied by green arrows (→) indicate proteins which display an activator role in angiogenesis. Outer circle: miRNAs represented in blue are positive regulators of angiogenesis and miRNAs depicted in red are negative regulators of the process (383, 407-412).

An exciting property towards the therapeutic application of miRNAs is the multi-faceted transcriptional control that they exert over entire gene cohorts (381). From a bone repair perspective, miRNAs simultaneously targeting osteogenic and angiogenic processes are of particular interest (347). This rationale was explored by Li *et al.* who harnessed the bi-functional potential of miR-26a to simultaneously enhance hMSC-mediated angiogenesis and osteogenesis *in vivo* (347). As described in Chapter 3, a bi-functional positive role for miR-210 in angiogenesis and osteogenesis is also established in different cell types. Specifically, it has been shown that up-regulation of miR-210 expression was induced by VEGF (418), which upregulated endothelial cell tubulogenesis,(an *in*

vitro marker for angiogenesis) by targeting EphrinA3 ligand (383). EphrinA3 belongs to the ephrin superfamily (419) and has been described to ultimately inhibit the initiation of the transcription program of pro-angiogenic genes (383). Additionally, miR-210 mimic accelerated angiogenesis *in vivo* in a pre-clinical model of anterior cruciate ligament injury (420). Collectively, this indicates the potential of miR-210 level manipulation as a promising strategy to control angiogenesis. While we demonstrated in Chapter 3 that miR-210 mimic delivery did not drive a robustly enhanced osteogenic response, in this study we aimed to assess the pro-angiogenic therapeutic potential of this miRNA in hMSCs and to determine whether it might have the potential to simultaneously direct angiogenesis and osteogenesis.

With this in mind, the exploration of a combinatorial miRNA therapy was further proposed in the second part of this chapter. This approach was inspired by a number of *in vitro* and *in vivo* studies targeting angiogenesis and osteogenesis simultaneously by combinatorial growth factor or gene delivery, all of which have reported synergistic effects on bone repair (127, 353, 354, 421, 422). Previous work carried out in our laboratory using combinatorial pDNA delivery of BMP-2 and VEGF comparatively assessed the in-house synthesised nHA particles and PEI as delivery vectors, where nHA-based GAMs outperformed the *in vivo* bone repair capacities of the PEI counterpart GAMs (127). Building on this concept, having successfully utilised nHA particles to deliver individual miRNAs to hMSCs directly from coll-nHA scaffolds, it was proposed in this chapter that this system might be a promising platform for combined delivery of multiple miRNA therapeutics.

Combinatorial miRNA delivery is a very new concept. Indeed the combination of a miRNA with another therapeutic, including pDNA or small chemical drugs has been recently reported (299, 423) and only two studies in the literature have approached dual miRNA delivery to promote osteogenesis *in vitro* (58, 235). These studies involved the assesment of osteo-therapeutic efficiency of antagomiR-27a, antagomiR-489 and miR-148b mimic in a monolayer and a 3D hydrogel scaffold respectively (58, 235). The study presented in this chapter thus focused on investigating the pro-angiogenic and pro-osteogenic

therapeutic potential of two nHA-miRNA combinations: miR-210 mimic plus antagomiR-133a and miR-210 mimic plus antagomiR-16.

5.2.Hypothesis & aims of the study

The underlying hypothesis of this study was that nanomiR-210 mimic treatment may enhance the pro-angiogenic capabilities of hMSCs and thus simultaneously enhance hMSC osteogenesis when administered in a dual nanomiR formulation. Hence this chapter aimed (i) to assess the effect of the nanomiR-210 mimic alone to influence the pro-angiogenic capabilities of hMSCs through the direct targeting of EphrinA3 and (ii) to explore the potential of a nanomiR-210/133a dual formulation or (iii) a nanomiR-210/16 dual formulation to simultaneously enhance the pro-angiogenic and osteogenic capabilities of hMSCs.

The specific aims of Chapter 5 were to:

- Assess the effective manipulation of miR-210 and its direct target EphrinA3 following nanomiR-210 mimic treatment
- Investigate VEGF secretion by hMSCs following nanomiR-210 mimic treatment
- Study the effect of pro-angiogenic factors secreted by hMSCs, following nanomiR-210 mimic treatment, to influence angiogenic and proliferation capabilities of endothelial cells
- Examine hMSC pro-angiogenic and osteogenic ability following treatment with a nanomiR-210/133a dual formulation
- Examine hMSC pro-angiogenic and osteogenic ability following treatment with a nanomiR-210/16 dual formulation

5.3.Materials & methods

5.3.1.Assessment of the pro-angiogenic effect of nanomiR-210 mimic treatment

5.3.1.1.hMSC cell culture and nanomiR-210 mimic treatment

hMSCs were cultured in complete DMEM medium as described in Section 2.3.3 until sufficient cell numbers were obtained at passage number 5-6 for experimentation. 24 hours in advance of the nanomiR treatment cells were plated at a density of 5 x 10^4 cells per well in 6 well plates. At the time of administering the control (blank nHA particles), scr or -210 nanomiR-mimic treatments, complexes were prepared at the 20 nM dose following the procedure detailed in Section 2.3.1.

5.3.1.2.Assessment of effective manipulation of miR-210 and its direct target EphrinA3 following nanomiR-210 mimic treatment

qRT-PCR analysis of miR-210 and EphrinA3 manipulation:
qRT-PCR analysis was carried out to determine the effective manipulation of miR-210 intracellular levels as well as mRNA relative expression level of the direct target EphrinA3 (EFNA3) after transient transfection with nanomiR-210 mimic. The hsa-miR-210 Taqman® MicroRNA assay as well as the validated pre-designed human Quantitect Primer Assay Hs_EFNA3_1_SG, (Qiagen, UK) were applied. The scr nanomiR-mimic group was set as the reference for the calculation of relative expression levels. Technique and calculations were carried out as described previously in Section 2.3.7.

EphrinA3 immunofluorescence staining and confocal imaging:
To further investigate the effect of miR-210 manipulation on its direct target EphrinA3 at the protein level, immunofluorescence staining followed by confocal microscopy imaging was carried out. To allow detailed observation of the presence of EphrinA3, hMSCs were seeded on tissue-culture ready plastic coverslips of 25 mm diameter (Sarstedt Inc., Ireland) within 6-well plates and subjected to treatment as described at the beginning of this section. At the timepoints of analysis, namely 7 and 10 days, medium was removed and samples rinsed with PBS, fixed in 10 % formalin and permeabilised in 1 %

Triton-X100 solution. Following blocking in 5 % horse serum (HS) samples were incubated in a 1:50 dilution of rabbit polyclonal IgG anti-EFNA3 primary antibody (Santa Cruz Inc.) and subsequently in a 1:200 dilution of Alexa488-labelled (green) goat anti-rabbit IgG secondary antibody (Invitrogen). Samples were then mounted on microscopy glass slides (Fisherbrand, UK) using Fluoroshield mounting medium (Invitrogen), which contains DAPI to stain cell nuclei (blue). To do so, coverslips were placed onto microscopy glass slides leaving the cell monolayer in the inside of the interacting surface between the two parts. As a final preparatory step, glass coverslips of 35 mm diameter (VWR International LLC.) were placed over the plastic coverslips and the final three-layered preparation was sealed using transparent nail polish.

Digital imaging was performed using an upright Carl Zeiss 710 confocal laser scanning microscope in sequential scanning mode and controlled by the Zen 2008 software. All images were captured using identical imaging parameters optimised according to the software. The increase in the signal to noise ratio produced by 4x averaging was used to ensure the punctate distribution of EFNA3 was not misinterpreted. Z stacks encompassing the whole cell were captured using a Plan-Apochromat 40x/1.4 Oil DIC M27 objective. FIJI (424) was used to generate the final images which are maximum image projections of the Z stacks.

5.3.1.3.Assessment of the effect of hMSC treatment with nanomiR-210 mimic on VEGF secretion

VEGF Quantikine plus Duo Set Development enzyme-linked immunosorbent assay (ELISA) Kit (R&D Systems) was used according to manufacturer's instructions to quantify levels of VEGF secreted into the medium by hMSCs in culture or subjected to nanomiR-210 mimic treatment. Absorbance of the coupled enzymatic reaction of biotin-streptavidin-HRP (horseradish peroxidase) was read at 450 nm and background corrected at 570 nm using a Varioskan Flash plate reader (ThermoScientific) and SkanIt ® for Varioskan software.

5.3.1.4.Assessment of the effect of nanomiR-210 mimic treatment on endothelial cell behaviour

Since nanomiR-210 mimic treatment of hMSC was anticipated to enhance the secretion of angiogenesis-related growth factors, the ability of these soluble factors to influence endothelial cell behaviour was tested. In order to do so, conditioned media (CM) was collected from hMSCs treated with the control or nanomiR-210 mimic groups after 7 days in culture and stored at -20°C until analysis, when it was sterile filtered and diluted in a 1:1 ratio with standard endothelial growth medium with the VEGF supplement removed.

Human umbilical vein endothelial cell (HUVEC) culture:

To assess the pro-angiogenic effect of nanomiR-210 mimic treatment HUVECs were employed as a model endothelial cell. HUVECs (Lonza, Wokingham, Ltd.) were cultured in EndoGRO^{TM}-2 (EGM-2) medium (Merck Millipore Ltd.) containing 2 % FBS, 5 % L-Glutamine, ascorbic acid 0.05 µg/ml, hydrocortisone hemisuccinate 1 ng/ml, heparin sulfate 0.375 u, IGF-1 0.015 ng/ml, epidermal growth factor (EGF), basic FGF and VEGF 0.005 ng/ml (EndoGRO™-VEGF Supplement Kit, Merck Millipore Ltd.). HUVECs were maintained in an incubator at standard culture conditions. Media was replaced every 3 days and cells were passaged upon reaching 80-90 % confluency.

HUVEC Matrigel^{TM} assay:

In order to assess the ability of VEGF released by hMSCs in response to nanomiR-210 treatment to enhance angiogenesis, a Matrigel™ assay was carried out. Matrigel™ is a basement membrane matrix commonly used to observe angiogenesis *in vitro* as it allows the formation of an interconnected tubular network (tubulogenesis) by endothelial-like cells (363, 425, 426). Prior to commencement of the assay, all pipette tips and 48-well plates were placed at 4°C overnight, and Matrigel™ was allowed to thaw on ice at 4°C. Matrigel™ (120 µl per well) was allowed to set for 30 min in standard culture conditions. Subsequently, HUVECs were plated in triplicate onto the Matrigel™ matrix at a seeding density of 3 x 10^5 per well. HUVECs were cultured in 1ml of the different CM, with a control group cultured in 100 % EGM-2 medium with no VEGF. The wells were imaged under a 10x objective at 5 random locations in each well at 24h post seeding using a Leica DMIL inverted microscope coupled to the LASV4.5 digital imaging system (Leica, Germany). The length of tubule

network formation (µm) and number of tubules formed by endothelial cells was measured in response to the various culture conditions and used as a surrogate marker of angiogenesis.

HUVEC proliferation assay:
In order to further investigate the pro-angiogenic functionality of nanomiR-210 treatment, its potential to act as a mitogen for endothelial cell proliferation was investigated. Endothelial cells display a proliferative response when subjected to the effect of pro-angiogenic factors, including VEGF and angiopoietin1 (427). As such, HUVECs were plated at a seeding density of 2 x 10^4 cells/well in 12-well plates, cultured in the appropriate CM groups (as above) and harvested for dsDNA quantification after 3 days of culture. dsDNA quantification was performed using the dsDNA Quant-iT PicoGreen dsDNA kit (BioSciences, Ireland) as described in Section 2.3.4.

5.3.2.Analysis of the simultaneous pro-angiogenic and pro-osteogenic effect of miR-210 mimic delivery as part of a dual nanomiR treatment

5.3.2.1.hMSC cell culture

hMSCs were cultured in complete DMEM medium as described in Section 2.3.3 until sufficient cell numbers were obtained at passage number 4-5 for experimentation. 24 hours in advance of the nanomiR treatment cells were plated at a density of 5 x 10^4 cells per well in 6 well plates. Immediately after the addition of the treatments, hMSCs were cultured in complete osteogenic medium as described in Section 3.3.2.

5.3.2.2.NanomiR-dual system

The preparation of nanomiR complexes was modified to explore the dual delivery of miR-mimics and antagomiRs (Figure 5.2). nHA particles (150 µl) were synthesised following the method described in Section 2.3.1 and added to a miRNA solution containing 0.25 M $CaCl_2$. The miRNA solution was prepared at the final concentration of 20 nM, in which the effective dose of both miR-mimic and antagomiR components was respectively 10 nM, that is, effectively

half than that of the single nanomiR-mimics or nanoantagomiRs assessed in Chapters 3 and 4 of this thesis.

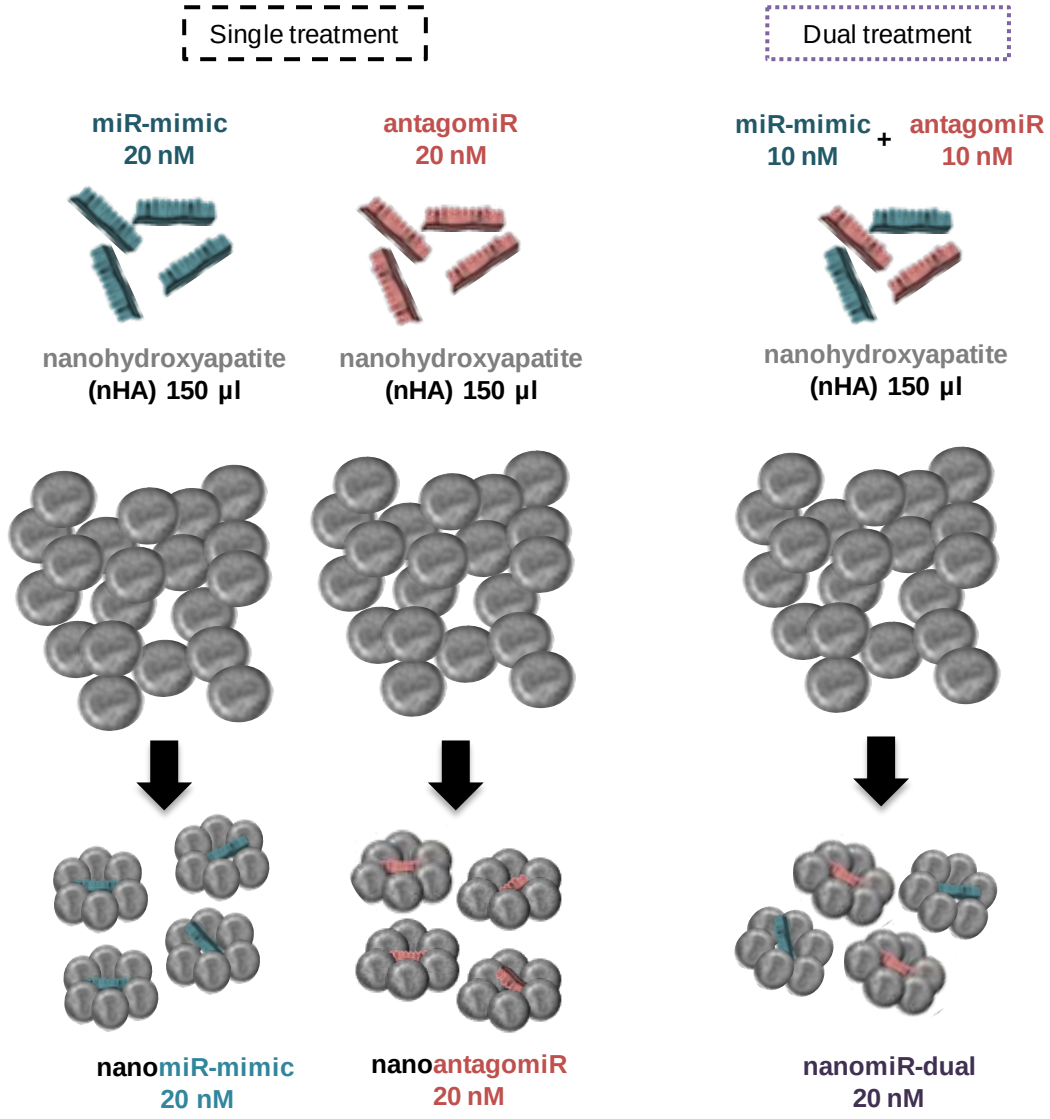

Figure 5.2 Schematic of the miRNA dosage regime differences between single and dual nanomiR formulation. While a final miRNA concentration is set at 20 nM in all groups, the effective dose of each therapeutic in the dual formulation is half that of the same molecule in the single nanomiR group. Colour coding: Addition of miR-mimic, blue, plus antagomiR, red, make result in purple to represent the nanomiR-dual groups from here onwards.

This procedure was applied to generate the control and treatment groups detailed in Table 5.1. In this study single scr nanomiR-mimic and nanomiR-210 mimic (used at 20 nM respectively) were administered to hMSCs additionally to serve as a comparative reference.

Table 5.1 Composition of the nanomiR-dual formulations tested in this chapter.

Group	Tested as	miR-mimic 10 nM (miRIDIAN)	antagomiR 10 nM (miRIDIAN)
scr nanomiR-dual	target lacking, negative control	nc#1 available from supplier, sequence based on *cel-miR-67*	nc#1 available from supplier, sequence based on *cel-miR-67*
nanomiR-210/133a dual	treatment (i)	sequence based on *hsa-miR-210*	sequence based on *hsa-miR-133a*
nanomiR-210/16 dual	treatment (ii)	sequence based on *hsa-miR-210*	sequence based on *hsa-miR-16*

5.3.2.3.Assessment of effective manipulation of miR-210 and its direct targets EFNA3 and AcvR1b using qRT-PCR analysis

qRT-PCR analysis was carried out to determine the compare manipulation of miR-210 intracellular levels as well as mRNA relative expression level of the direct targets EFNA3, involved in angiogenesis, and AcvR1b, involved in osteogenesis, after transient transfection with nanomiR-210 mimic single treatment or nanomiR-dual formulations. The hsa-miR-210 Taqman® MicroRNA assay as well as the validated pre-designed human Quantitect Primer Assays Hs_EFNA3_1_SG and Hs_ACVR1B_va.1_SG (Qiagen, UK) were applied. The scr nanomiR-dual group was set as the reference for the calculation of relative expression levels. Technique and calculations were carried out as described previously in Section 2.3.7.

5.3.2.4.Investigation of the effect of hMSC treatment with nanomiR-dual on VEGF secretion using ELISA

VEGF Quantikine plus Duo Set Development ELISA Kit (R&D Systems) was used as described earlier in section 5.3.1. to quantify levels of VEGF secreted into the medium by hMSC osteogenic culture when subjected to transient transfection with nanomiR-210 mimic single treatment or nanomiR-dual formulations. Briefly, absorbance of the coupled enzymatic reaction was read at 450 nm and background corrected at 570 nm.

5.3.2.5.Analysis of the effect of nanomiR-dual treatment on endothelial cell behaviour

Transient transfection of hMSCs with nanomiR-210 mimic single treatment or nanomiR-dual formulations was anticipated to enhance the secretion of a panel of angiogenesis-related growth factors by hMSCs during their osteogenic differentiation. In parallel with the methodology applied to asses this objective in the first part of this study (Section 5.3.1.4), the ability of these soluble factors to influence HUVEC behaviour was tested in terms of tubulogenesis (Matrigel ^{TM}) and proliferation assays. In order to do so, CM collected from hMSCs osteogenic culture at 3 and 7 days was pooled together and banked at -20°C until commencement of the assays described below, when it was thawed, sterile filtered and used undiluted.

HUVECs culture, Matrigel^{TM} and proliferation assays were carried out as described in Section 5.3.1.4. Briefly, complete EGM-2 medium (Merck Millipore Ltd., Ireland) was replaced every 3 days in culture and cells were passaged upon reaching 80 - 90 % confluency. For the Matrigel^{TM} assay all materials were pre-chilled O/N and 120 µl Matrigel™ per well (~1 cm^2) were seeded with 3 x 10^5 HUVECs and cultured in 1ml of the different CM, with a control group cultured in 100 % EGM-2 medium void of VEGF. Following imaging at 4h post seeding, quantification of total tubule number and total tubule length (µm) per micrograph section (10x) was carried out using Image J software. For the proliferation assay, 3 x 10^4 cells/well were seeded in 12-well plates, cultured in the appropriate CM groups and harvested for dsDNA quantification after 3 days of culture.

5.3.2.6.Analysis of the effect of nanomiR-dual treatment on hMSC osteogenic gene expression using qRT-PCR

qRT-PCR analysis was carried out as indicated above to determine relative mRNA expression level of the osteogenic markers Runx2 and OCN after transient transfection with nanomiR-dual formulations. The validated pre-designed human Quantitect Primer Assays Hs_RUNX2_1_SG and Hs_BGLAP_1_SG (Qiagen, UK) were applied.

5.3.2.7.Mineral deposition assessment as end-stage marker of osteogenesis

In order to visualise calcium deposits at 14 days after transient transfection with nanomiR-dual formulations, samples were stained directly on culture-plates with

2 % Alizarin red as previously described in Section 3.3.5. Macroscopic imaging was carried out using a personal digital camera. To provide quantitative data the Calcium Liquicolor kit (Stanbio Laboratories) was used under manufacturer's instructions at 10 and 14 days post-treatment as previously described in Section 3.3.5.

5.3.3.Statistical analysis

Experiments were performed in triplicate, unless otherwise specified within figure captions, and are representative of a minimum of three independent repetitions using two cell donors. Data analysis was performed using the SigmaPlot 11.0 software package. Results were presented as the mean + standard deviation and subjected to a two-way analysis of variance (ANOVA) plus a Tukey *post-hoc* for analysis of several time points and one-way ANOVA plus Tukey *post-hoc* test for data assessed at a singular time point.. $p<0.05$ and $p<0.001$ were considered significant differences.

5.4.Results

5.4.1.Pro-angiogenic effect of nanomiR-210 mimic treatment

5.4.1.1.Effective manipulation of miR-210 but not its direct target EphrinA3 was achieved following nanomiR-210 mimic treatment

The effective manipulation of miR-210 levels following nanomiR-210 mimic treatment of hMSCs was assessed as the first step to analyse the effect of this treatment in angiogenesis. Similarly to the observation from Chapter 3, intracellular level of miR-210 was prominently increased in the nanomiR-210 mimic group after 3 days compared to all other groups, and this was further enhanced at 7 days in culture, which was quantified as greater than 6000 fold change (6155.59 ± 452.75) (Figure 5.3a). Interestingly, both cell and nHA groups contained higher miR-210 levels than the scr nanomiR-mimic group at day 3, while by 7 days miR-210 levels were maintained at the relative level baseline for the three control groups. Overall this data pointed at an efficient delivery of miR-210 mimic using the nHA-based delivery.

The levels of the miR-210 direct target involved in angiogenesis, EphrinA3 (EFNA3), were decreased in both untreated cells and nanomiR-210 mimic groups to approximately 0.3 fold as compared with scr nanomiR-mimic control at 3 days, while nHA particles alone induced an increase to 1.6 fold (Figure 5.3b). At the later timepoint of 7 days, the untreated cell group displayed the lowest levels of EphrinA3 at 0.2 fold versus the scr nanomiR-mimic control, but nHA and nanomR-210 mimic also presented decreased levels of this gene. In contrast to the effect hypothesised, nanomiR-210 mimic treatment did not silence EFNA3 levels below those of untreated cells. Altogether this data indicated a negligible silencing effect over EFNA3 following the efficient miR-210 mimic delivery using nHA particles.

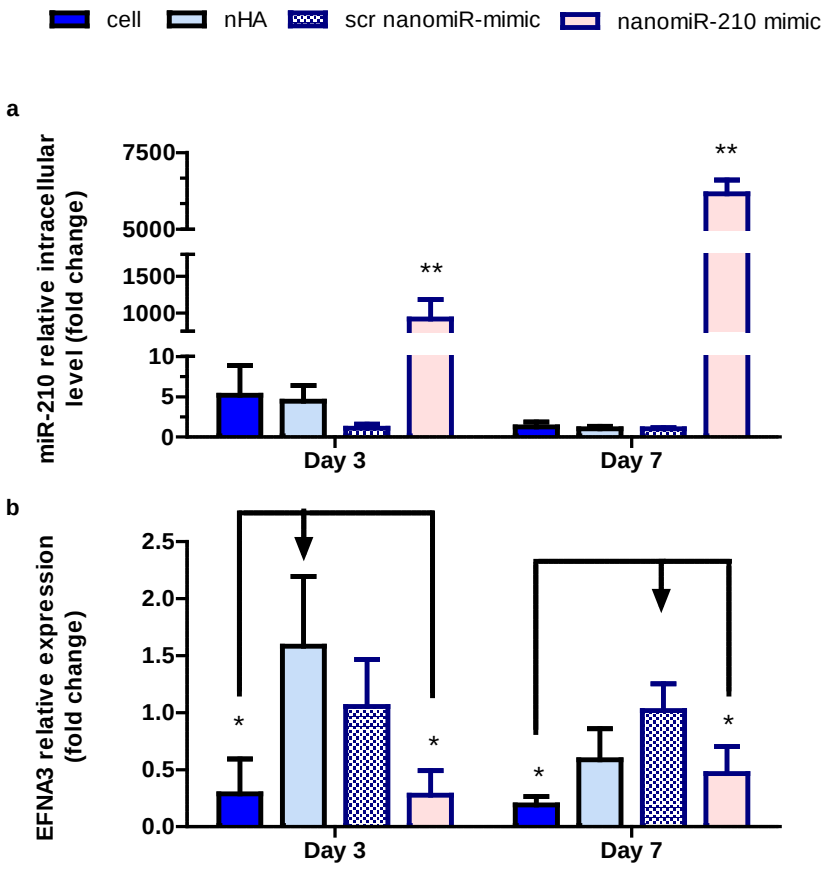

Figure 5.3 Analysis of hMSC genetic manipulation of miR-210 & EFNA3 levels following nanomiR-210 mimic treatment. a) NanomiR-210 mimic treatment successfully increased miR-210 levels intracellularly at 3 and 7 days after treatment. **b)** EFNA3 expression was significantly reduced for the cell and miR-210 mimic groups in comparison with the scr group at the 7 day timepoint. Scr nanomiR-mimic was set as the reference control group and relative expression was normalised to that of 18S and calculated using the $2^{(-\Delta\Delta Ct)}$ method. Mean + standard deviation, n = 3, * = $p<0.05$, ** = $p<0.001$.

To further characterise the biological effect of nanomiR-210 mimic on the protein levels of the direct target EphrinA3, immunofluorescence staining was carried out. A higher presence of EphrinA3 was quantified in the untreated cells and nHA groups after both 7 and 10 days in culture; however nanomiR-210 mimic did not reduce the EphrinA3 protein levels in comparison with the scr nanomiR-mimic group, which was more pronounced at the 10 day timepoint (Figure 5.4). This data again pointed to negligible biological effect following the efficient miR-210 mimic delivery using nHA particles.

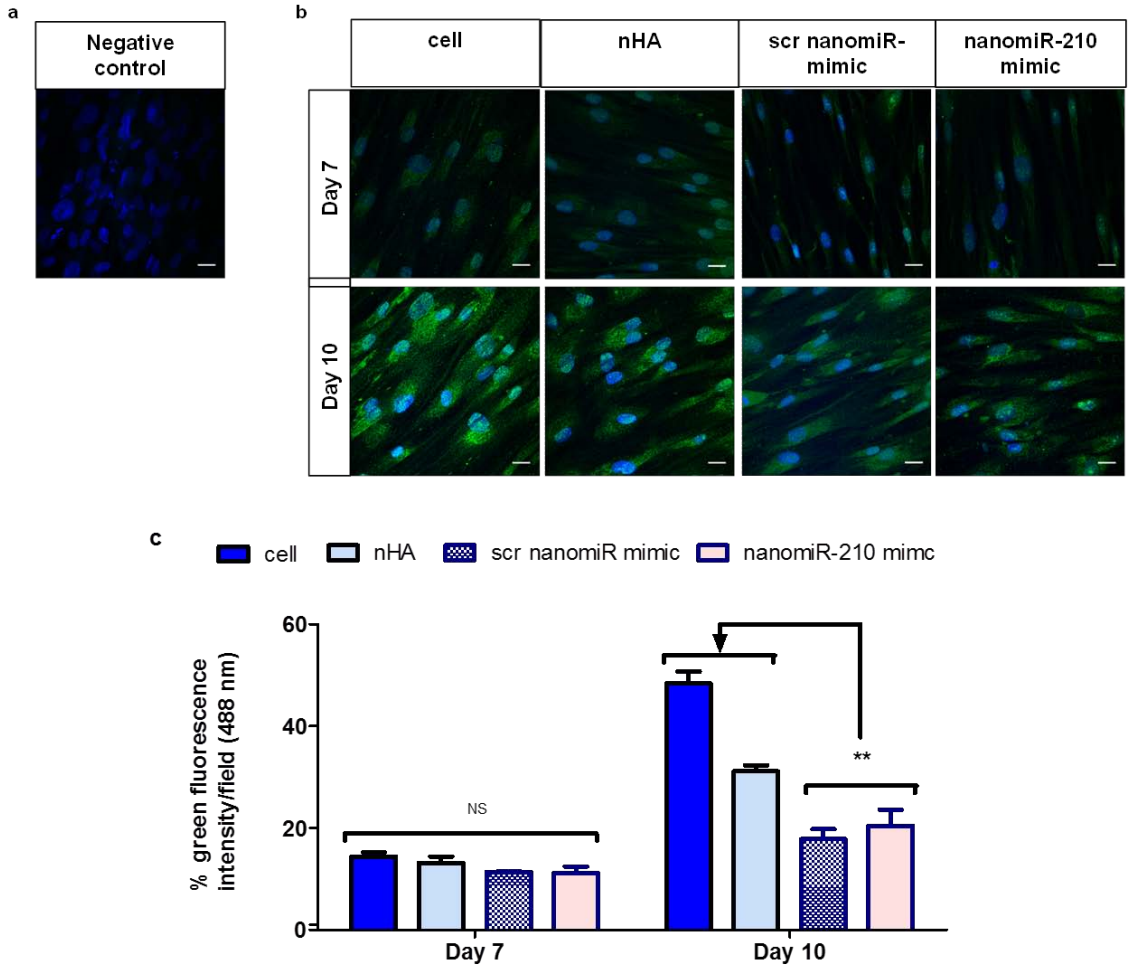

Figure 5.4 Assessment of EphrinA3 protein expression following nanomiR-210 mimic treatment. Composite depicting representative confocal microscopy images of **a)** DAPI labelling (blue, nuclei) of the negative control of EphrinA3 staining (no primary antibody) and **b)** EphrinA3 immunofluorescence staining (green) merged with DAPI labelling (blue, nuclei) at 7 and 10 days after nanomiR treatment. Scale bar = 20 µm, n = 3. **c)** Quantification of green fluorescence (%) indicated that nanomiR-210 mimic treatment did not reduce EphrinA3 protein levels when compared with the scr nanomiR-mimic group. Mean + standard deviation, n = 3, ** = $p<0.001$, NS = not significant.

5.4.1.2.VEGF secretion was enhanced in nanomiR-210 mimic treated compared to untreated hMSCs

VEGF is the main secreted growth factor that promotes angiogenesis, and miR-210 levels have been shown to increase following VEGF supplementation, supporting a pro-angiogenic activity of miR-210 (383). Based on this, VEGF secretion in nanomiR-210 mimic treated hMSCs was evaluated. The ELISA data indicated non-significant changes in the levels of VEGF secretion at day 3, within the range of 1000 to 2000 pg/ml (Figure 5.5). After 7 days VEGF secretion was significantly enhanced in both scr nanomiR-mimic and nanomiR-210 mimic groups, the latter to a higher magnitude of ~ 4200 pg/ml, corresponding to a 77 % increase over that of untreated cells. Taken together this result indicated that nanomiR-210 mimic was able to enhance the secretion of VEGF by hMSC after 7 days in comparison to untreated cells.

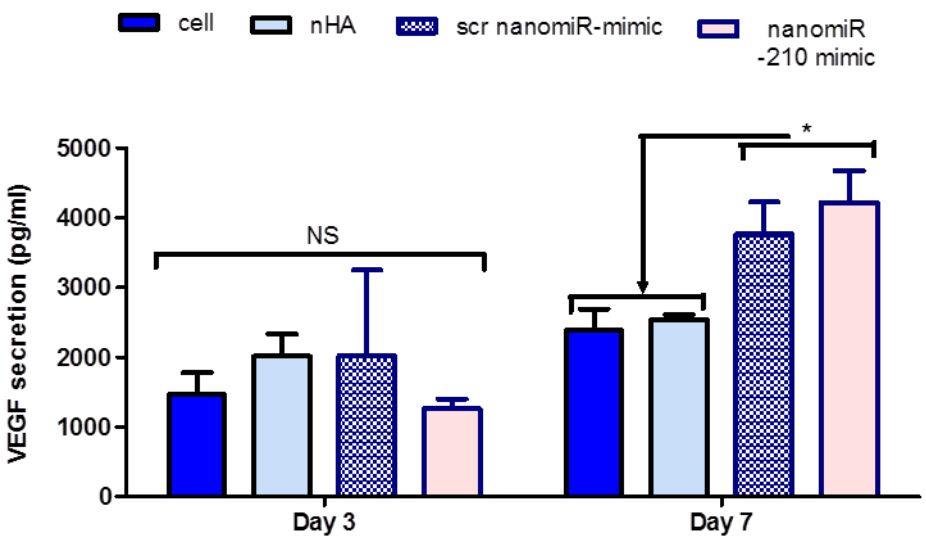

Figure 5.5 Analysis of the effect of nanomiR-210 mimic treatment on VEGF secretion by hMSCs. ELISA assays indicated that both scr nanomiR-mimic and nanomiR-210 mimic treatment enhanced VEGF protein secretion at 7 days in standard culture conditions. Mean + standard deviation, n = 3, * = $p<0.05$, NS = not significant variation.

5.4.1.3.NanomiR-210 mimic treated MSCs had limited influence on endothelial cell behaviour

The increased VEGF secretion determined for the nanomiR-210 mimic treatment in the previous section was anticipated to be accompanied by the secretion of additional soluble pro-angiogenic factors. To further examine the biological response of endothelial cells (HUVEC) to these soluble factors, conditioned media from the different treatment groups was applied firstly in a Matrigel™ tubulogenesis assay. Quantification of tubule formation at 24h showed that longer tubules were formed in the untreated cell group in comparison with the nanomiR-210 mimic group (Figure 5.6a). This indicated that the pro-angiogenic factors secreted upon hMSC treatment with nanomiR-210 mimic were unable to enhance tubule formation by HUVECs, compared to untreated cells. Secondly, the HUVEC proliferation assay showed a trend towards higher proliferation in the nanomiR-210 mimic CM group after 3 days in culture (Figure 5.6b). This pointed to an enhanced presence of soluble pro-proliferation factors in nanomiR-210 mimic conditioned medium. Taken together, this data demonstrated some capability, albeit modest, of nanomiR-210 mimic treatment to induce a pro-angiogenic effect on hMSCs when compared to untreated cells.

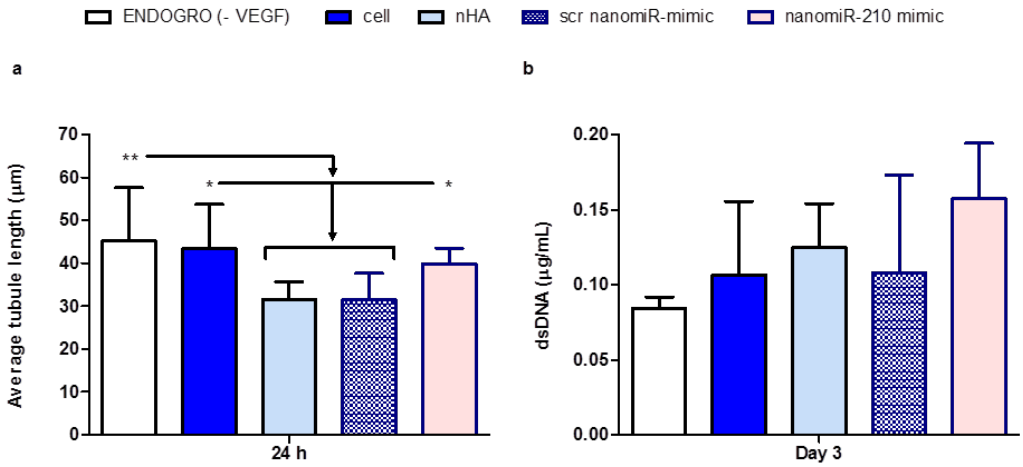

Figure 5.6 Analysis of the capability of nanomiR-210 mimic treated hMSC conditioned medium (CM) to influence endothelial cell behaviour. a) Quantification of HUVEC tubule formation in Matrigel™. When average tubule length was assessed, longer tubules were detected in the positive control, cell and nanomiR-210 mimic groups in comparison to nHA and scr groups after 24 h. Mean + std deviation, n = 15, * = $p<0.05$, ** = $p<0.001$. **b)** A trend towards higher HUVEC proliferation was determined in the nanomiR-210 mimic group after 3 days. Mean + standard deviation, n = 3, non-significant differences.

5.4.2.Simultaneous pro-angiogenic and pro-osteogenic effect of miR-210 mimic delivery as part of a dual combination with antagomiR-133a

The results above and in Chapter 3 showed the limited capability of miR-210 mimic to separately induce a therapeutic pro-osteogenic and pro-angiogenic effects. We next hypothesised that a nanomiR-210/133a dual formulation may induce a simultaneous pro-angiogenic and pro-osteogenic effect beneficial for bone repair.

5.4.2.1.Effective manipulation of miR-210 following nanomiR-210/133a dual treatment did not lead to silencing of EFNA3 and AcvR1b

Intracellular miR-210 level was prominently increased following both nanomiR-210 mimic and nanomiR-210/133a dual treatment after 3 days in osteogenic culture (Figure 5.7a). Interestingly, the nanomiR-210/133a dual formulation, containing only 10 nM of miR-210 mimic, increased intracellular levels 8×10^3 fold over the control scr group, an effect which was 3.18 times higher than that achieved with the single miR-210 mimic administered at the 20 nM dose. Taken together, this data confirmed the efficient delivery of miR-210 mimic using nHA particles in both the single and the dual nanomiR formulations.

Subsequently, the simultaneous effect of miR-210 manipulation on angiogenesis and osteogenesis, through the direct targeting of EFNA3 and AcvR1b respectively, was demonstrated after 3 days in osteogenic culture (Figure 5.7b-c). NanomiR-210 mimic successfully silenced EFNA3 to 0.5 ± 0.32 fold (Figure 5.7b), below that of untreated hMSCs (0.93 ± 0.5 fold). Additionally, this treatment silenced AcvR1b levels to 0.21 ± 0.05 fold (Figure 5.7c), consistent with previous observations in Chapter 3. Surprisingly, the nanomiR-210/133a dual formulation did not correlate with improved silencing of either EFNA3 or AcvR1b compared with the single miR-210 mimic administration, demonstrating unmodified levels of EFNA3 expression (1.1 ± 0.07 fold), and increased expression of AcvR1b (1.37 ± 0.24 fold). Taken together, this data indicated a complex relationship between the effective delivery of miR-210 mimic achieved with the nanomiR-210/133a dual and negligible silencing of the direct miR-210 targets.

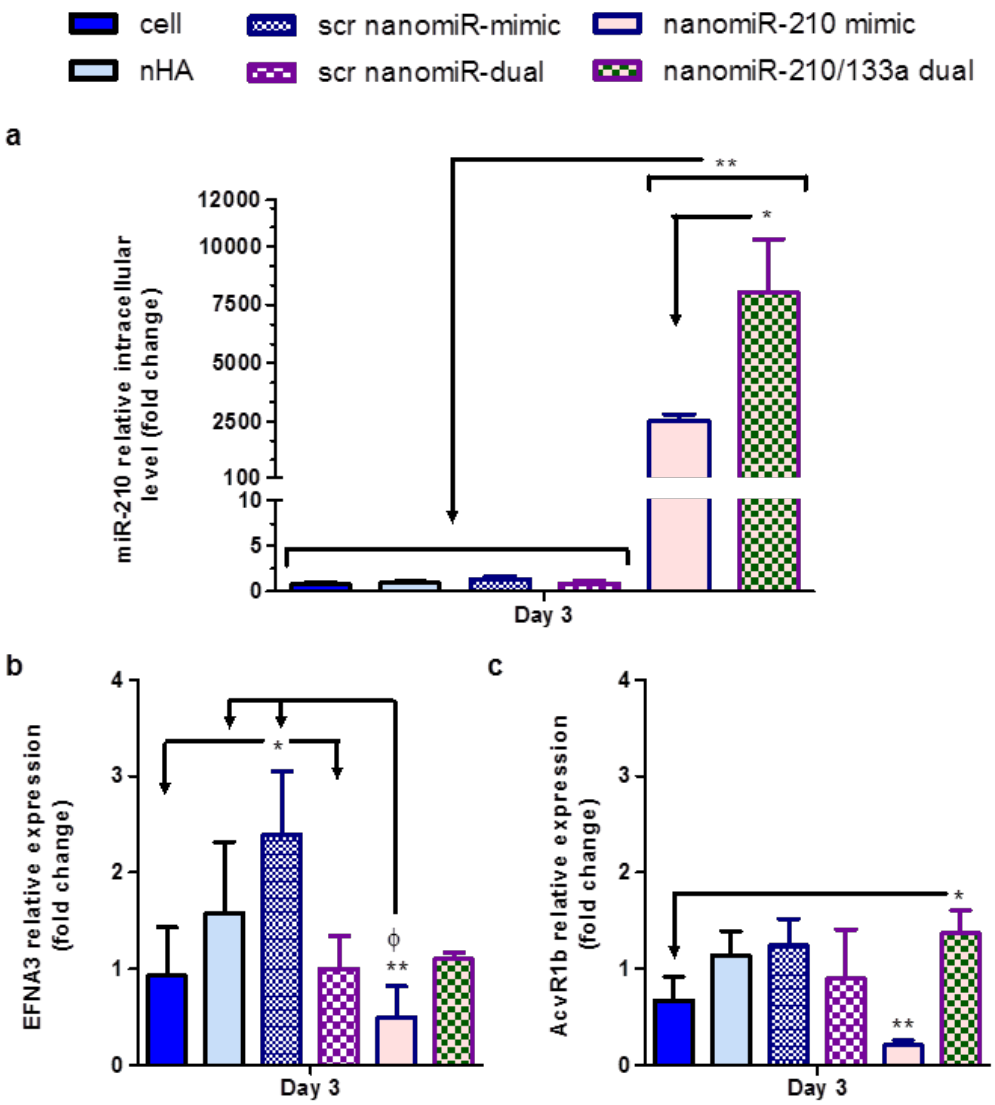

Figure 5.7 Comparative analysis of effectivity in miR-210, EFNA3 & AcvR1b manipulation following treatment with nanomiR-210 mimic & nanomiR-210/133a dual. a) Both groups containing miR-210 mimic successfully increased miR-210 intracellularly. **b)** EFNA3 expression was silenced with nanomiR-210 mimic after 3 days. **c)** A marked decrease in AcvR1b expression was found at the same time point in osteogenic culture for the nanomiR-210 mimic group, while nanomiR-210/133a dual increased AcvR1b when compared to untreated cells. Scr nanomiR-dual was set as the reference control group and relative expression was normalised to that of 18S and calculated using the $2^{(-\Delta\Delta Ct)}$ method. Mean + standard deviation, n = 4, NS = not significant variation, * = $p<0.05$, ** = $p<0.001$, ϕ= $p<0.05$ compared to nHA treatment.

5.4.2.2.VEGF secretion was enhanced in both nanomiR-210 mimic & nanomiR-210/133a dual treated hMSCs

VEGF secretion was increased in both nanomiR-210 mimic and nanomiR-210/133a dual treated hMSCs (1334.85 ± 148.22 pg/ml and 1391.4 ± 172.35 pg/ml respectively) compared to all other groups after 3 days in osteogenic culture (Figure 5.8). At the later timepoint of 7 days, a single administration of 20 nM miR-210 mimic produced lower VEGF than its counterpart scr group, to a level that was not significantly increased over that of untreated cells. Conversely, VEGF secretion was highest in the nanomiR-210/133a dual group, which corresponded to a 47.4 % increase over VEGF secreted by untreated cells and 42.77 % higher than the counterpart scr nanomiR dual group at the same timepoint. Taken together, this result indicated that nanomiR-210/133a dual was able to further potentiate the effect of miR-210 mimic on VEGF secretion at the later timepoint assessed in hMSC osteogenic culture.

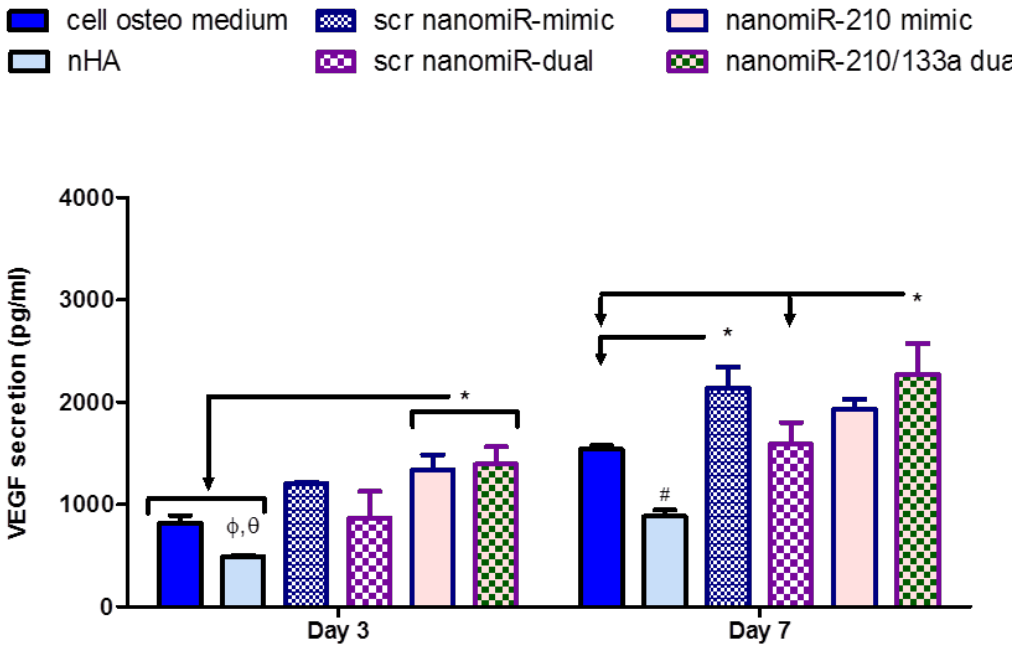

Figure 5.8 Comparative analysis of the effect of nanomiR-210 mimic & nanomiR-210/133a dual treatment on VEGF secretion by hMSCs. NanomiR-210 mimic & 210/133a dual groups enhanced VEGF protein secretion over untreated cells 3 days after treatment. At the later time point of 7 days the nanomiR-210/133a dual group achieved higher levels in comparison to all other groups. Mean + standard deviation, n = 3, * = $p<0.05$, ϕ = $p<0.05$ compared to cell osteo medium, Θ = $p<0.001$ compared to nanomiR-210 mimic and nanomiR-210/133a dual, # = $p<0.001$ vs all other groups.

5.4.2.3.NanomiR-210/133a dual treatment did not enhance osteogenic gene expression

Runx2 and OCN were analysed after 7 days in osteogenic culture as the main indicators of the initiation and progression of osteogenesis in hMSCs. Runx2 levels remained unaffected (0.89 ± 0.20 fold) with nanomiR-210/133a dual treatment, in a similar level to that determined for nanomiR-210 mimic previously in Chapter 3 (Figure 5.9a). OCN expression was also unaffected in the nanomiR-210/133a dual group, although this level was greater than that previously determined for nanomiR-210 mimic (Figure 5.9b). In summary this data indicated that nanomiR-210/133a dual treatment did not correlate with enhanced hMSC osteogenesis at the gene level.

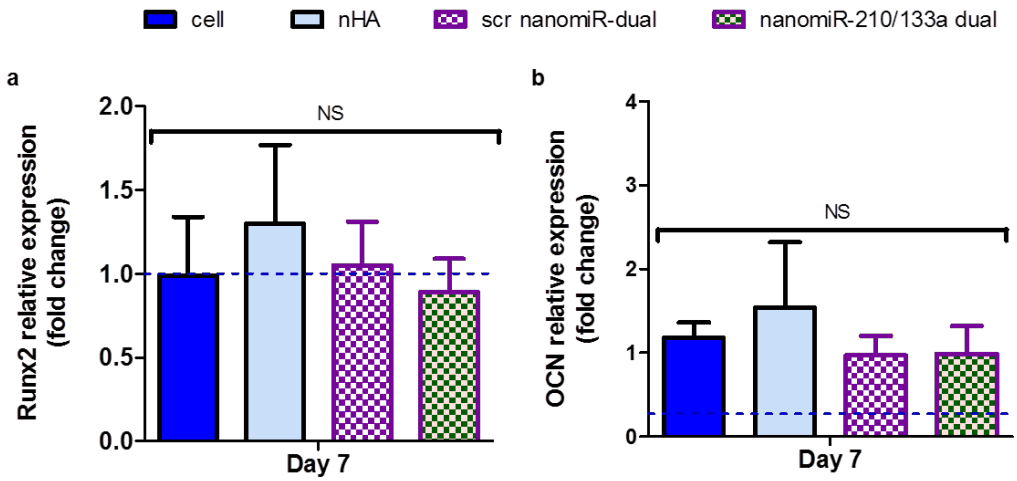

Figure 5.9 qRT-PCR analysis of the effect of nanomiR-210/133a dual treatment on hMSC osteogenic gene expression markers. a) Runx2 expression was unmodified in the nanomiR-210/133a dual treatment by 7 days. **b)** No significant changes were detected in OCN relative expression level 7 days after treatment but all groups were above the level previously determined OCN relative level for nanomiR-210 mimic. Dashed blue line represents corresponding expression level determined for nanomiR-210 mimic previously in Chapter 3. Scr nanomiR-dual was set as the reference control group and relative expression was normalised to that of 18S and calculated using the $2^{(-\Delta\Delta Ct)}$ method. Mean + standard deviation, n = 4, NS = not significant variation**.**

5.4.2.4.Mineral deposition was not enhanced in nanomiR-210/133a dual treated hMSCs

Calcium deposition quantification indicated that the scr nanomiR-dual group enhanced calcium deposition to the same level than the nanomiR-210/133a dual treatment (Figure 5.10a), at both day 10 and day 14, which was also maintained to the levels previously determined for nanomiR-210 mimic. Additionally, alizarin red staining indicated higher presence of extracellular calcium deposits at 14 days in both the scr and nanomiR-210/133a dual groups in comparison with the untreated cells (Figure 5.10b). In summary, while some increases over untreated cells were seen, this assessment indicated that nanomiR-210/133a dual was not able to further enhance the effect of the miR-210 mimic on calcium deposition.

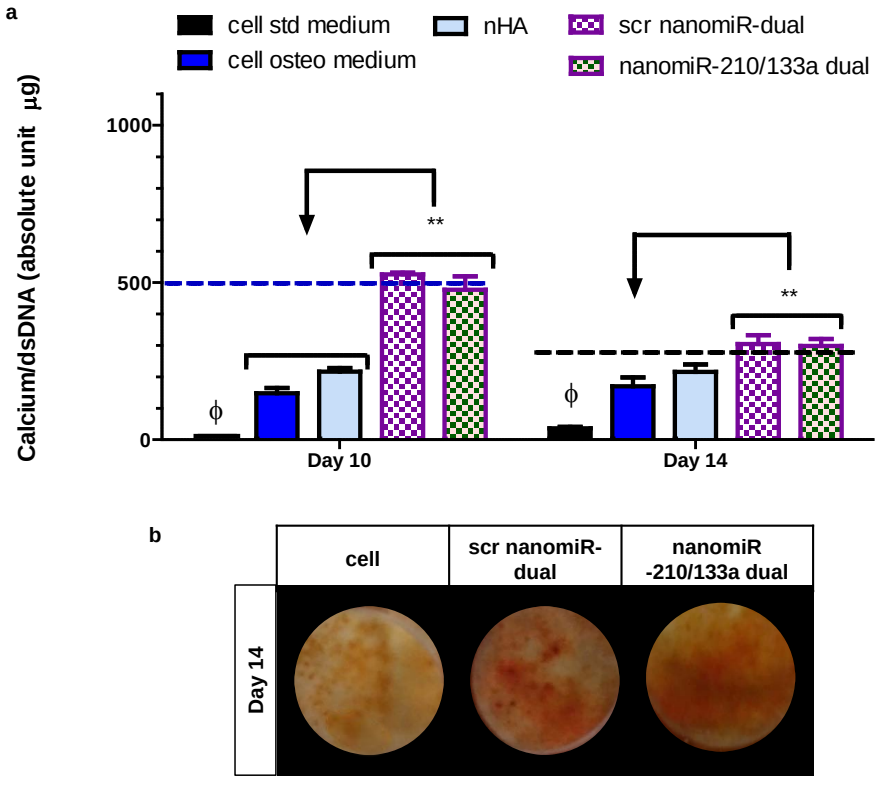

Figure 5.10 Effect of nanomiR-210/133a dual treatment on hMSC calcium matrix deposition. **a)** Calcium quantification normalised to dsDNA content showed that nanomiR-210/133a dual treatment did not enhance calcium deposition after 10 or 14 days in osteogenic culture. Dashed blue and black lines (day 10 and 14 respectively) represent corresponding fold increase of nanomiR-210 mimic over untreated cells determined previously in Chapter 3. Mean + standard deviation, n = 3, ** = $p<0.001$, ϕ = $p<0.01$ compared to all other groups. **b)** Macroscopic images of alizarin red staining indicated increased calcium deposition in both the scr and nanomiR-210/133a dual groups after 14 days in osteogenic culture.

5.4.3.Simultaneous pro-angiogenic and pro-osteogenic effect of miR-210 mimic delivery as part of a dual nanomiR treatment in combination with antagomiR-16

For the last part of this study, it was hypothesised that a dual formulation combining miR-210 mimic with antagomiR-16, that also robustly enhanced osteogenesis in Chapter 3 and additionally directly interacts with targets of the same family as miR-210, could potentiate the therapeutic effect of miR-210 mimic as well as inducing a simultaneous pro-angiogenic and pro-osteogenic effect, which would be highly beneficial for bone tissue repair.

5.4.3.1.Effective manipulation of miR-210 and its direct targets EFNA3 and AcvR1b was achieved with nanomiR-210/16 dual treatment

Intracellular miR-210 levels were prominently increased following both nanomiR-210 mimic and nanomiR-210/16 dual treatment after 3 days in osteogenic culture (Figure 5.11a). Interestingly, the opposite pattern to that observed in Section 5.4.2.1 was found between the two miR-210 mimic containing groups: the nanomiR-210/16 dual formulation, containing only 10 nM of miR-210 mimic, lead to intracellular levels increased to 3×10^2 fold over the control scr group, an effect which was 8.5 times lower than that achieved with the single miR-210 mimic administered at the 20 nM dose. This data confirmed the efficient delivery of miR-210 mimic in both the single treatment and the nanomiR-210/16 dual formulation.

Subsequently, the simultaneous effect of miR-210 manipulation over angiogenesis and osteogenesis, through the direct targeting of EFNA3 and AcvR1b respectively, was demonstrated after 3 days in osteogenic culture (Figure 5.11b-c). Here, the successful 50 % silencing of nanomiR-210 mimic over EFNA3 was further improved to 0.15 ± 0.14 fold with the nanomiR-210/16 dual formulation (Figure 5.11b), in contrast to the observations for the nanomiR-210/133a dual system (Figure 5.7b). Additionally, AcvR1b silencing was also seen with the nanomiR-210/16 dual formulation (0.32 ± 0.11 fold; figure 5.12c). These data showed an improved manipulation of the direct target involved in angiogenesis with less pronounced increase in miR-210 intracellular levels, indicating that a more relevant genetic manipulation may be achieved through

moderately altering miRNA levels with the nanomiR-210/16 dual formulation. Taken together, this data indicated the effective delivery of nanomiR-210/16 dual and the functional silencing of the direct miR-210 targets.

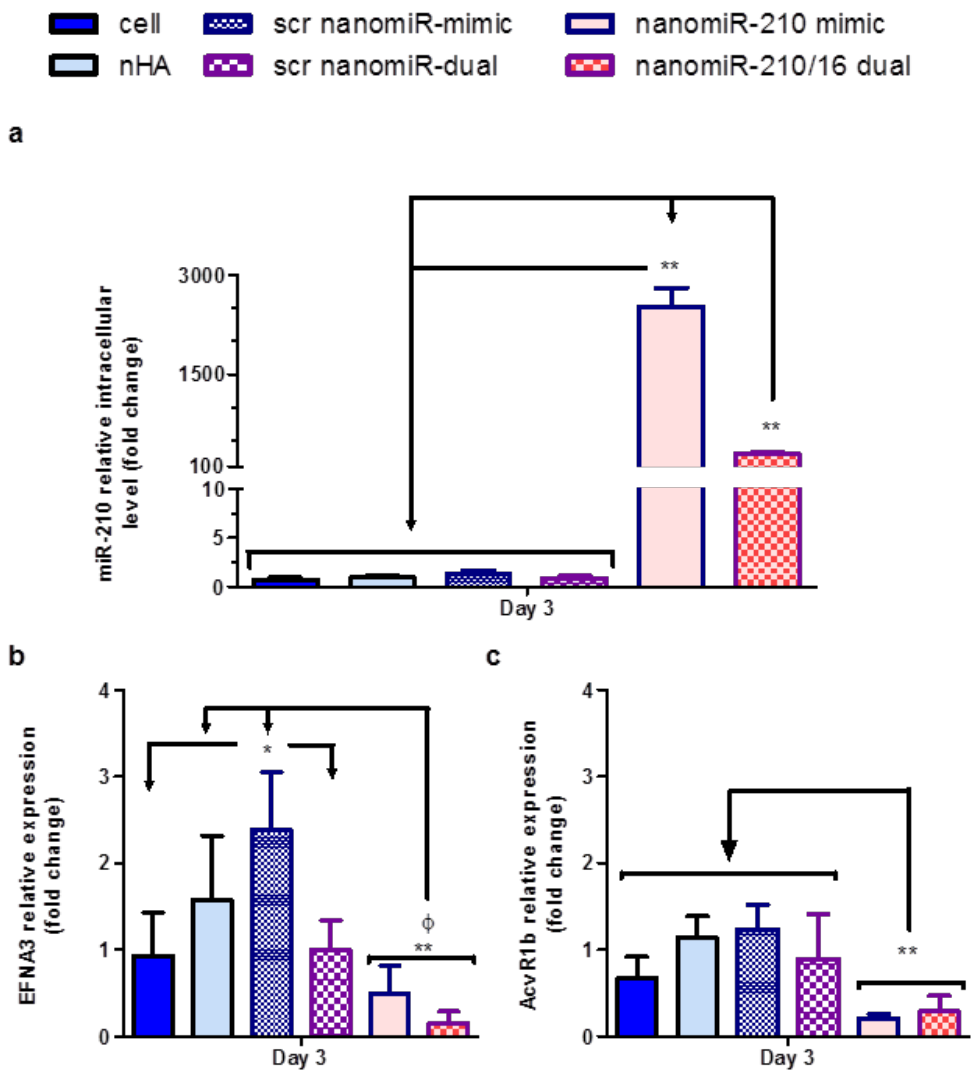

Figure 5.11 Comparative analysis of effectivity in miR-210, EFNA3 & AcvR1b manipulation following treatment with nanomiR-210 mimic & nanomiR-210/16 dual. a) miR-210 analysis confirmed that all groups containing miR-210 mimic successfully increased miR-210 intracellularly. **b)** The effect of nanomiR-210 mimic silencing EFNA3 expression was further promoted with the nanomiR-210/16 dual group at the same time point. **c)** A marked decrease in AcvR1b expression was found after 3 days in ostoegenic culture for the nanomiR-210 mimic and nanomiR-210/16 dual groups. Scr nanomiR-dual was set as the reference control group and relative expression was normalised to that of 18S and calculated using the $2^{(-\Delta\Delta Ct)}$ method. Mean + standard deviation, n = 4, * = p<0.05, ** = p<0.001, ϕ = p<0.05 compared to nHA treatment.

5.4.3.2.VEGF secretion was enhanced in nanomiR-210/16 dual treated hMSCs

NanomiR-210 mimic increased VEGF secretion by hMSCs compared to all other control groups after 3 days in osteogenic culture, but this effect was significantly augmented in nanomiR-210/16 dual treated hMSCs (Figure 5.12). While the nanomiR-210 mimic did not increase VEGF over untreated cells at the later timepoint of 7 days, nanomiR-210/16 dual treatment markedly increased VEGF secretion over all other groups, corresponding to an 84.3 % increase over VEGF secreted by untreated cells and 78.5 % higher than the counterpart scr group. Taken together, this result indicated that nanomiR-210/16 dual was able to significantly enhance the effect of the miR-210 mimic on VEGF secretion at both timepoints assessed in hMSC osteogenic culture.

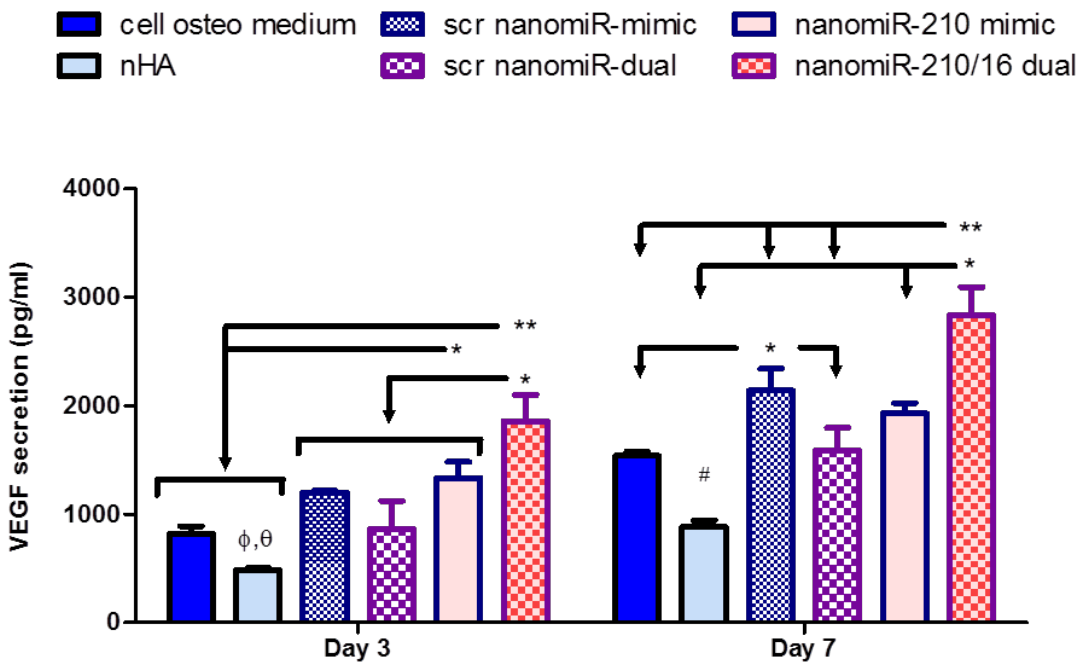

Figure 5.12 Comparative analysis of the effect of nanomiR-210 mimic & nanomiR-210/16 dual treatment on VEGF secretion by hMSCs. NanomiR treatment enhanced VEGF protein secretion over untreated cells with highest levels for the nanomiR-210/16 dual group at both 3 and 7 days after treatment. Mean + standard deviation, n = 3, * = $p<0.05$, ** = $p<0.001$, ϕ = $p<0.05$ compared to cell osteo medium, θ = $p<0.001$ compared to nanomiR-210 mimic, # = $p<0.001$ vs all other groups.

5.4.3.3.The capacity of hMSCs to influence HUVEC behaviour was enhanced following treatment with nanomiR-210/16 dual

To further examine the biological response of HUVECs to the increased VEGF secretion determined above, conditioned media (CM) from the different treatment groups was applied in a Matrigel™ tubulogenesis assay and a proliferation assay. Firstly, the Matrigel™ assay indicated an enhanced tubulogenic capability of HUVECs maintained in the nanomiR-210/16 dual CM group, in comparison to all other types of CM (Figure 5.13 a-c). The quantification of this assay at 4 h showed that tubule length was significantly increased in the nanomiR-210/16 dual CM group, being the highest group immediately after the positive control (complete endothelial medium - ENDOGRO - lacking VEGF) (Figure 5.14a). Secondly, the HUVEC proliferation assay showed a trend towards higher proliferation in the nHA and nanomiR-210/16 dual CM groups compared to the remaining CM groups after 3 days in culture (Figure 5.14b). Taken together, this data demonstrated an improved capability of nanomiR-210/16 dual formulation over nanomiR-210 mimic alone to induce a pro-angiogenic effect on hMSCs when compared to untreated cells.

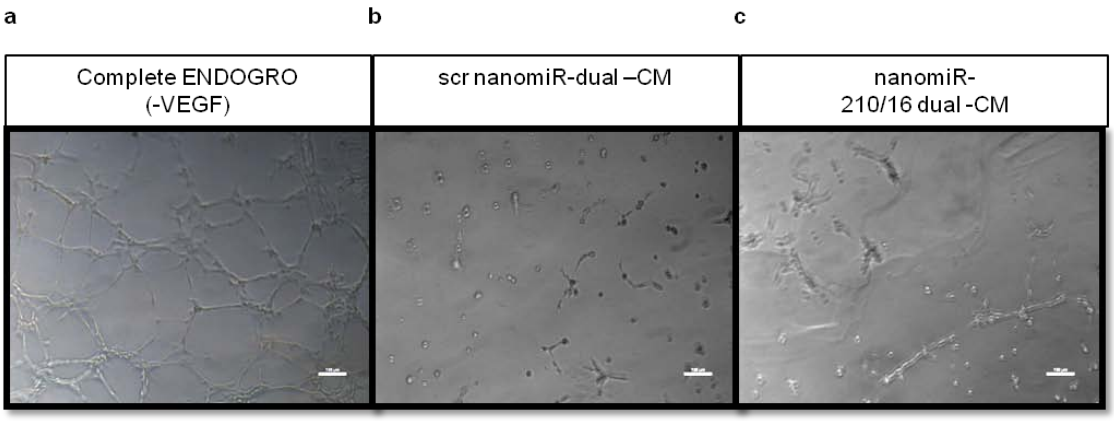

Figure 5.13 Analysis of the capability of nanomiR-210/16 dual treated hMSC conditioned medium (CM) to influence HUVEC tubulogenesis. a-c) Representative bright field images of HUVECs after 4 h in Matrigel™ assay. n = 15, scale bar = 100 µm. **a)** A complex and interconnected network of tubules was observed in the positive control group (complete ENDOGRO - VEGF). **b)** scr nanomiR-dual CM representing the relegated tubule-forming capacity of negative control groups and **c)** nanomiR-210/16 dual group demonstrating an increased length in the tubules formed in comparison to the negative control group.

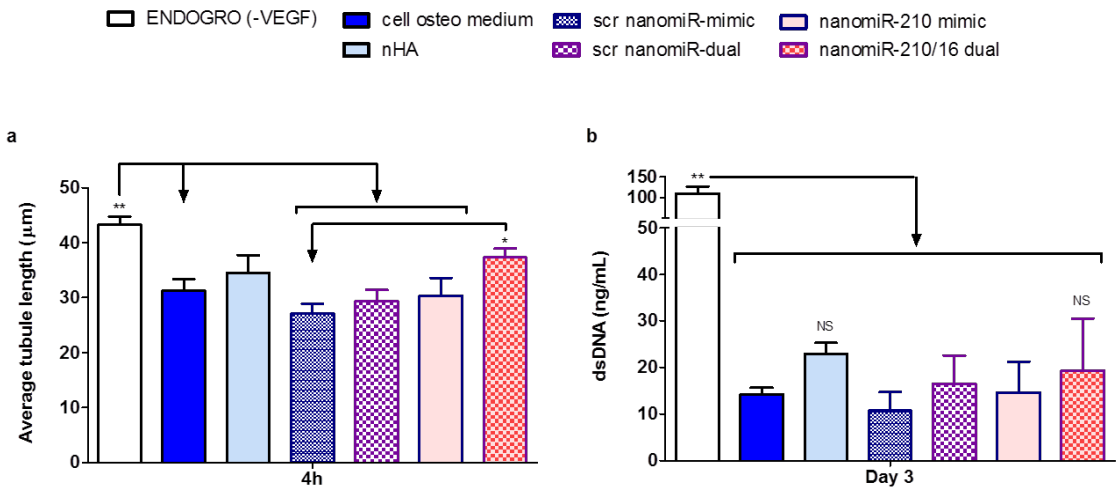

Figure 5.14 Analysis of the capability of nanomiR-210/16 dual treated hMSC conditioned medium (CM) to influence HUVEC behaviour. a) Quantification of HUVEC tubule formation after 4 h in Matrigel™. Longer tubules were detected in the positive control and nanomiR-210/16 dual groups, followed by nHA. Mean + std deviation, n= 15, *=p<0.05,**=p<0.001. **b)** HUVEC proliferation in nanomiR-hMSC CM: A trend towards higher proliferation was determined in the nanomiR-210 mimic group vs scr nanomiR-mimic and in the nanomiR-210/16 dual vs scr nanomiR-dual after 3 days. Mean + standard deviation, n = 3, ** = p<0.001, NS=not significant variation.

5.4.3.4.NanomiR-210/16 dual treatment did not enhance osteogenic gene expression

Runx2 and OCN were analysed after 7 days in osteogenic culture. The levels determined for both Runx2 and OCN following nanomiR-210/16 dual treatment (Figure 5.15) exceeded those previously determined for nanomiR-210 mimic on its own (Chapter 3). However, in comparison to the control groups of this study, the effect of nanomiR-210/16 dual on Runx2 level was deemed non-significant and OCN expression remained unaffected. In summary this data indicated that nanomiR-210/16 dual treatment did not correlate with enhanced hMSCs osteogenesis at the gene level.

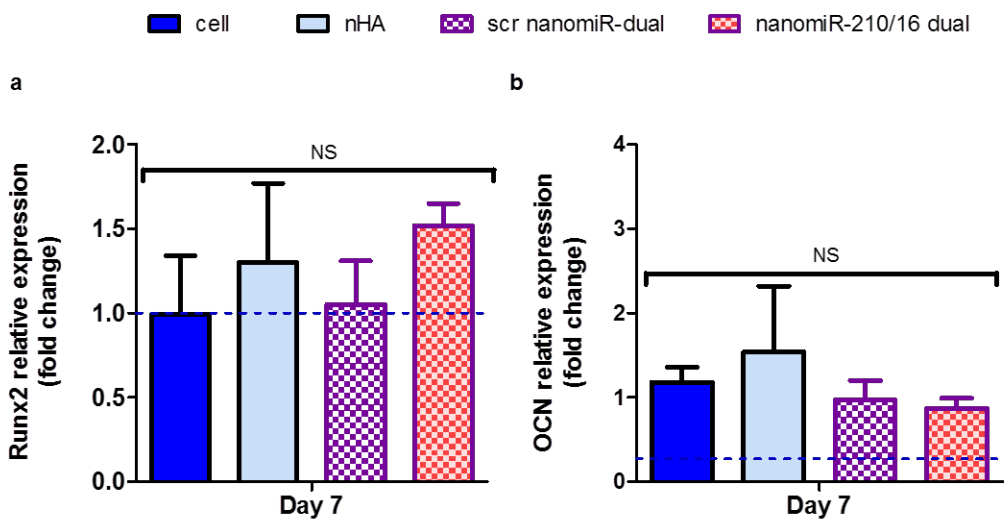

Figure 5.15 Comparative qRT-PCR analysis of the effect of nanomiR-210 mimic & nanomiR-210/16 dual treatment on hMSC osteogenic gene expression. Non-significant changes in **a)** Runx2 expression and **b)** OCN relative expression were found 7 days after nanomiR-210/16 dual treatment. Dashed blue line represents corresponding expression level determined for nanomiR-210 mimic previously in Chapter 3. Scr nanomiR-dual was set as the reference control group and relative expression was normalised to that of 18S and calculated using the $2^{(-\Delta\Delta Ct)}$ method. Mean + standard deviation, n = 4, NS = not significant variation, * = $p<0.05$.

5.4.3.5.Mineral deposition was enhanced in nanomiR-210/16 dual treated hMSCs

The nanomiR-210/16 dual group demonstrated the greatest calcium deposition levels in comparison to all other groups at both 10 and 14 days (Figure 5.16a). This result largely surpassed the calcium deposition levels previously determined for nanomiR-210 mimic, corresponding to a 1.96 fold increase at the earlier timepoint and a 2.65 fold increase at the later timepoint. Additionally, alizarin red staining confirmed the presence of calcium deposits in the nanomiR-210/16 dual group after 14 days (Figure 5.16b). In summary, this assessment indicated that nanomiR-210/16 dual was able to further potentiate the effect of miR-210 mimic on calcium deposition.

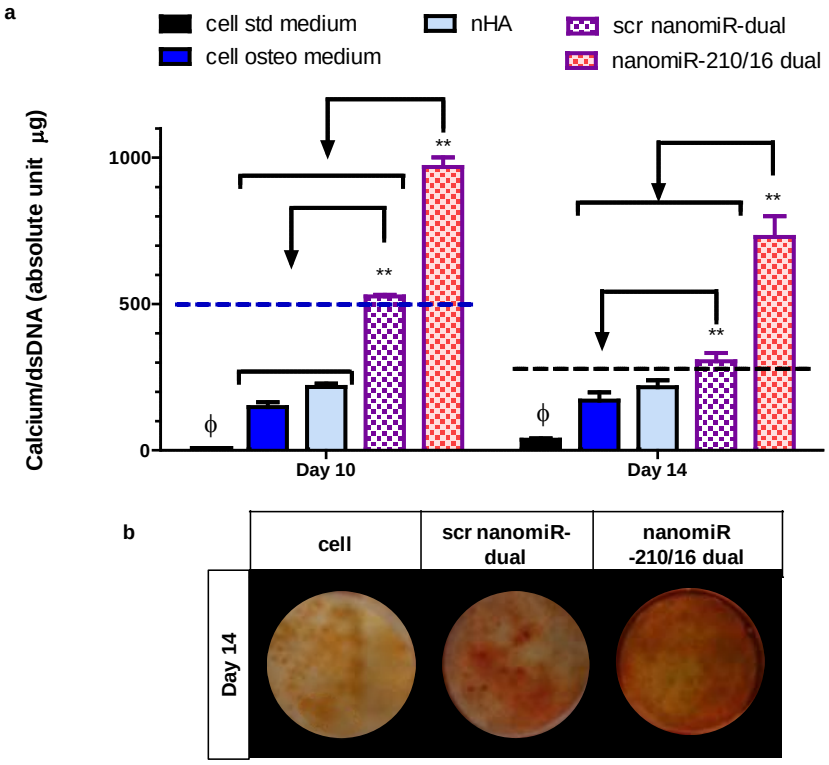

Figure 5.16 Effect of nanomiR-210/16 dual treatment on hMSC calcium matrix deposition. **a)** Calcium quantification normalised to dsDNA content showed highest levels of calcium deposition in the nanomiR-210/16 dual group at both 10 and 14 days in osteogenic culture. Dashed blue and black lines (day 10 and 14 respectively) represent corresponding fold increase of nanomiR-210 mimic over untreated cells determined previously in Chapter 3. Mean + standard deviation, n = 3, ** = $p<0.001$, ϕ = $p<0.001$ in comparison to all other groups. **b)** Macroscopic images of alizarin red staining indicated increased calcium deposition in the nanomiR-210/16 dual group.

5.5.Discussion

The application of miRNA therapeutics simultaneously targeting angiogenesis and osteogenesis might be an attractive avenue for future bone repair strategies. This chapter aimed firstly to investigate the pro-angiogenic therapeutic potential of nanomiR-210 mimic and subsequently the capacity of a combinatorial miRNA therapy approach, namely nanomiR-210/133a dual and nanomiR-210/16 dual formulations, to simultaneously enhance the pro-angiogenic and osteogenic capabilities of hMSCs. The data presented here showed that nanomiR-210 mimic treatment resulted in effective manipulation of miR-210, albeit with no silencing effects on EphrinA3 compared to untreated cells and limited pro-angiogenic effect in terms of VEGF secretion or endothelial

cell response. Subsequently, while nanomiR-210/133a dual treatment of hMSCs did not result in a robust simultaneous pro-angiogenic and osteogenic effect, the nanomiR-210/16 dual treatment proved beneficial in this regard; this was demonstrated by the effective genetic manipulation of miR-210 and its direct targets, significantly increased VEGF secretion and calcium deposition, as well as enhanced endothelial cell tubulogenic potential compared to untreated cells. Taken together, the results showcased the promise of using nHA-based delivery of multiple miRNAs as a prospective therapy use in TE.

Initially, the effective manipulation of miR-210 levels following nanomiR-210 mimic treatment of hMSCs was demonstrated, although this effect did not result in functional EphrinA3 silencing in comparison to untreated cells. miR-210 induction of EphrinA3 silencing has been demonstrated in two different cell types, namely HUVECs and U2OS cells, using a 40 nM miRNA dose delivered by a commercial lipid-based vector (383). While it was hypothesised that this effect of miR-210 could be extended to the MSCs, the data presented in this chapter did not support this hypothesis. This might be explained by the findings of relatively low endogenous expression of EphrinA3 in the untreated hMSCs along the culture period, which evidenced a putative limitation of the strategy based on reducing expression of this target.

The nanomiR-210 mimic treatment did however enhance secretion of VEGF by hMSCs. VEGF-induced angiogenesis has been reported to stimulate increases in miR-210 levels (383, 418), however, the increase of VEGF as a consequence of enhanced miR-210 levels *in vitro* has not been reported previously. This study thus provided evidence for the first time that miR-210 level manipulation can beneficially impact VEGF secretion by hMSCs, therefore showing potential in angiogenesis-mediated bone TE strategies (151). Interestingly however, the endothelial cells showed a limited tubulogenesis capacity in response to conditioned medium from the treated hMSCs in comparison to untreated cells although a trend towards higher proliferation was observed. Importantly, the influence of miR-210 on angiogenesis has been strongly associated as a response to hypoxic (low oxygen) conditions *in vitro* (428, 429) and during osteonecrosis *in vivo* (430). This may suggest that in order to fully realise the pro-angiogenic effect of miR-210 mimic treatment on hMSCs, exploration of

experimental hypoxic conditions is worthy of future consideration. Taken together, this data indicated that nanomiR-210 mimic showed potential to enhance the secretion of VEGF by hMSCs after 7 days in culture, but overall this was not sufficient to influence endothelial cell behaviour.

The secondary focus of this chapter was the evaluation of a simultaneous pro-angiogenic and osteogenic response in hMSCs following combinatorial miRNA delivery. Although previous studies have not used a combinatorial miRNA delivery approach to simultaneously target angiogenesis and osteogenesis, superior bone repair has been reported with co-delivery of angiogenic and osteogenic growth factors (GFs) or plasmid DNA (145, 286, 292). We proposed that by combining miR-210 mimic with antagomiR-133a a simultaneous pro-angiogenic and pro-osteogenic effect could be obtained, which would be more potent than the single miR-210 mimic treatment. The ability of both nanomiR-210 mimic and nanomiR-210/133a dual groups to increase miR-210 intracellular level was demonstrated. However, while the nanomiR-210 mimic treatment achieved functional silencing of the direct angiogenesis and osteogenesis targets, EphrinA3 and AcvR1b respectively, no silencing was detected for the nanomiR-210/133a dual group. This may be due to a negative interaction between miR-210 and miR-133a, unrelated to base-pair complementarity between the two molecules (392), which may take place at a signalling level. Interestingly, the silencing of EphrinA3 following single nanomiR-210 mimic treatment in hMSC osteogenic culture was more effective than that observed in standard culture. It is proposed that the effective detection of this silencing effect can be related to an endogenous pattern of increased EphrinA3 expression in osteogenic culture in comparison with standard culture.

Further analysis indicated that nanoantagomiR-210/133a dual treatment did not result in a simultaneous pro-angiogenic and osteogenic effect. While VEGF was increased at both 3 and 7 days, osteogenic gene expression and calcium deposition were not enhanced. Altogether, this data indicated a complex and perhaps detrimental interaction when miR-210 mimic and antagomiR-133a were combined. This effect has also been noted for certain combinations of GFs and genes that separately are positive for angiogenesis, osteogenesis, or both processes. As an example, FGF-2 combinations with BMP-2 or VEGF have

reported detrimentral effects in MSC mediated osteogenesis and bone repair (174, 431). This is an indication of the complexity of possible cross-signalling responses between the components of the mix. Overall the data presented in this part of the study demonstrated an unfavourable effect of the miR-210 mimic plus antagomiR-133a combination as a therapy to enhance simultaneous angiogenesis and osteogenesis.

For the last part of this study, an alternative combinatorial miRNA delivery approach utilising antagomiR-16 in combination with miR-210 mimic was undertaken. Here, consideration was placed on the fact that some direct targets of the two miRNAs are familiarly-related molecules and part of associated pathways. Specifically, the pair of tyrosine-kinase receptors AcvR1b and AcvR2a are described to counter-balance TGFβ signalling (379). The data from this study demonstrated that the highly effective genetic manipulation of miR-210 levels and its direct targets EphrinA3 and AcvR1b could be improved with the nanomiR-210/16 dual treatment. The nanomiR-210/16 dual treated hMSCs displayed significantly increased VEGF secretion over all other groups. This result was supported by the detection of longer tubules formed by endothelial cells when subjected to nanomiR-210/16 dual conditioned medium. This is consistent with combinatorial GF or gene delivery approaches where increased angiogenesis and osteogenesis were observed when BMP-2 plus VEGF were dually delivered (127, 165, 355). Taken together, this data indicated that nanomiR-210/16 dual significantly enhanced the angiogenic capabilities of hMSCs in comparison to a single nanomiR-210 mimic treatment.

Furthermore, assessment of osteogenesis in this nanomiR-210/16 dual group revealed improved Runx2 and OCN gene expression in comparison with the levels previously determined for the nanomiR-210 mimic. Moreover, a greater enhancement in calcium deposition was demonstrated at both 10 and 14 days for this nanomiR-210/16 dual group, indicating that the dual treatment was able to further enhance functional osteogenesis in comparison with single miR-210 mimic delivery. Only two studies to-date have assessed combinatorial miRNA delivery (58, 235). From these studies a synergistic effect in ALP activity was demonstrated for the miR-148b mimic plus antagomiR-489 combination, although notably this dual treatment did not increase the calcium deposition

levels induced by the single miR-148b treatment. This outcome underlined that simultaneous delivery of various miRNAs is a complex task, although it holds promising potential as a therapeutic approach.

In summary, the successful results with the nanomiR-210/16 dual group highlighted the ability of the nHA particles to deliver pro-angiogenic miRNA therapeutics. This was an important addition to the previous success in delivering reporter and pro-osteogenic miRNA therapeutics presented in previous chapters of this thesis. Moreover, this observation is consistent with the benefits of nHA as the vector of choice in the GAMs developed in our laboratory to address combined angiogenesis and osteogenesis (127). Taken together, the data presented in this chapter showcased a highly beneficial interaction when miR-210 mimic and antagomiR-16 were combined, resulting in an exciting capability of this combinatorial nanomiR delivery approach to simultaneously enhance hMSC angiogenesis and osteogenesis.

5.6.Conclusion

While the results from this chapter demonstrated a limited therapeutic effect of hMSC treatment with either single nanomiR-210 mimic or a nanomiR-210/133a dual treatment, a promising simultaneous pro-angiogenic and pro-osteogenic response with a nanomiR-210/16 dual treatment was demonstrated. The nanomiR-210/16 dual formulation remarkably improved direct target silencing, enhanced endothelial cell tubulogenesis and increased calcium deposition at both 10 and 14 days. Overall, this study successfully presents nanomiR-210/16 dual treatment as the first combinatorial miRNA delivery approach to simultaneously target angiogenesis and osteogenesis. This represents a highly beneficial paradigm for bone repair applications. Moreover, this work underlines the possibility of extending nHA-based miRNA delivery to pathways beyond osteogenesis by tailoring the miRNA therapeutic incorporated in the complexes. As such, the work presented in this chapter presents enormous potential for alternative TE applications.

Chapter 6. Discussion

6.1.Overview

The field of tissue engineering (TE) focuses on creating new tissue for the therapeutic regeneration of defects within the human body (9). A substantial and unmet need for the development of tissue-engineered approaches to repair bone exists. Implantation of bone grafts harvested from a patient or donor remains the gold standard for bone repair, in spite of having documented failure rates as high as 30 % (26). With this in mind, bone TE research concentrates on developing 3D scaffolds capable of directing cells to lay down new bone (23) and is increasingly shifting towards the use of these scaffolds to act as carriers for therapeutic biomolecules. microRNAs (miRNAs) have recently emerged as highly promising therapeutics to direct bone repair; however, the development of a safe and efficient localised delivery system is required for successful clinical translation. Thus, the introduction of miRNA therapeutics within 3D scaffolds was the concept guiding the research presented in this thesis.

A series of collagen-based scaffolds have previously been developed in our laboratory, including a collagen-nanohydroxyapatite (coll-nHA) scaffold with optimised properties for bone repair (97). This scaffold has demonstrated potential as a depot for localised delivery of genes - in the form of plasmid DNA -, which are also known as gene-activated matrices (GAMs; (126, 127, 346, 394)). Moreover, in house-synthesised nHA particles and polyethylenimine (PEI) complexes were incorporated within these GAMs as non-viral plasmid DNA delivery vectors (126, 127). PEI is a popular non-viral vector due to its high transfection efficiency but has also been shown to be cytotoxic, while nHA particles are generally regarded as safe but less efficient for transfection. Hence it was of major relevance that the nHA-based GAMs demonstrated improved capacity to induce bone repair in comparison to PEI-based GAMs *in vivo* (127). In the context of producing superior bone graft substitutes, the overall goal of the research presented in this thesis was to establish the potential of using nHA to act as a non-viral vector for the delivery of a series of miRNAs to human

MSCs and to determine, from a panel of select candidates, the optimal miRNA therapeutic leading to enhanced osteogenesis and angiogenesis before ultimately producing miRNA-activated scaffolds capable of mediating enhanced osteogenesis by human MSCs.

Chapter 2 of this thesis focused on assessing the potential of these in house-synthesised nHA particles as non-viral vectors for miRNA delivery to human MSCs, a particularly difficult cell type to transfect effectively. The data presented here showed that nHA particles combined with both miR-mimics and antagomiRs, formed complexes (we term *nanomiRs*), which resulted in efficient delivery with limited cytotoxicity at a 20 nM dose. A single administration of our reporter nanomiR achieved high uptake efficiency and further translated into high silencing levels, comparable to viral and lipid-based vectors (219).

The aim of Chapter 3 was to determine the pro-osteogenic therapeutic efficacy of nHA-based delivery of antagomiR-133a, antagomiR-16 and a miR-210 mimic, targets with known osteogenic influence, and establish the optimal candidate for incorporation in a miRNA-activated scaffold. The results demonstrated that nHA-based delivery of these three miRNAs enhanced human MSC mediated osteogenesis, albeit to different levels. Ultimately, the nanoantagomiR-133a treatment showed the highest increases in Runx2 and OCN expression and ALP activity as well as rapidly enhancing calcium deposition as early as 10 days, sustaining this effect up to day 14.

Subsequently, Chapter 4 assessed the potential of the coll-nHA scaffolds as miRNA delivery platforms to manipulate human MSC gene expression and the application of this system to therapeutically enhance osteogenesis using antagomiR-133a. This work led to the development of the first non-viral, non-lipid scaffold technology to-date for the delivery of both miR-mimics and antagomiRs to human MSCs. When human MSCs were cultured on these scaffolds, nanomiR uptake and significant functional silencing with minimal cytotoxicity was observed. Ultimately, we demonstrated the therapeutic potential of the nanoantagomiR-133a activated coll-nHA scaffolds to effectively inhibit miR-133a resulting in upregulation of Runx2 expression and rapidly enhanced deposition of mineralised bone matrix. Taken together, Chapter 4

presents a highly promising concept in bone TE to effectively utilise miRNA therapeutics for enhanced osteogenesis.

An alternative approach was adopted in Chapter 5 which investigated the therapeutic efficacy of nHA-based delivery of the miR-210 mimic to enhance the pro-angiogenic capabilities of human MSCs. In addition, we assessed the potential of combinatorial delivery of the miR-210 mimic with antagomiR-133a or antagomiR-16 to simultaneously enhance the angiogenesis and osteogenesis capabilities of human MSCs. Overall, this study presents nanomiR-210/16 dual treatment as the first combinatorial miRNA delivery approach to simultaneously enhance angiogenesis and osteogenesis. This represents a highly beneficial paradigm for bone repair applications and also underlines the possibility of extending nHA-based miRNA delivery to pathways beyond osteogenesis by tailoring the miRNA therapeutic combinations incorporated in the system.

The following sections will summarise the key findings and implications from each individual chapter and review the possible future directions which have arisen from this research.

6.2.Chapter 2: Investigation of nanohydroxyapatite particles as non-viral vectors for microRNA delivery to human mesenchymal stem cells

Recently in the field of TE, incorporating RNA interference (RNAi) therapeutics, such as siRNAs and miRNAs, in non-viral delivery systems has gained significant interest (281). Notably, commercial vectors with recognised safety limitations have been applied for these few studies and miRNA delivery systems using nano-sized hydroxyapatite particles (nHA) have not been reported previously. The data presented in this study supported the hypothesis that in house-synthesised nHA particles can act as non-viral vectors for miRNA delivery to human MSCs, a particularly difficult cell type to transfect effectively (219). Taken together, the results presented in this chapter demonstrated the relevant potential of using these natural-based nanoparticles as delivery vectors to apply miRNA therapeutics to TE.

Initially in this study it was determined that nHA particles formed negatively charged complexes in the 300 nm range with both miR-mimics and antagomiRs, which was consistent with the nHA-pDNA complexes which previously demonstrated successful transfection of human MSCs (124, 126). Classically, it is estimated that cellular uptake requires positively charged particles of less than 200 nm (366). However, evidence of successful uptake of miRNA-PEI or miRNA-chitosan complexes greater than 500 nm in size (256), as well as of negatively charged siRNA lipoplexes (367) has been noted, which support the potential of our nHA particles for effective miRNA delivery. Given that the overall aim of this thesis was to successfully incorporate nanomiRs within a 3D scaffold, the physicochemical features of nanomiRs were deemed fit-for-purpose.

No evidence of permanent nHA- or miRNA-derived cytotoxicity was found. In relation to vector safety and cytotoxicity, CaP-based delivery of nucleic acids is known to minimise cytotoxicity, and even enhance cell proliferation (370). Although CaPs can transiently reduce metabolic activity (322, 371), consistent with the effect observed in this study, vectors like Lipofectamine® 2000 and RNAiMax® (280, 367, 372) have been associated with irreversibly impaired cell viability. Taken together, the results of this study demonstrated that nanomiR treatment did not have a permanent detrimental effect on human MSC viability. Analysis of uptake and intracellular localisation of nanomiRs demonstrated that complexes were found inside the cells in all treatment groups and at all timepoints. The amount of Dy547 nanoantagomiR complexes observed was notably higher than that of the Dy547 nanomiR-mimic treatment. Differences in the uptake kinetics of the two types of molecules were revealed, which we proposed might be beneficial for the combinatorial delivery of miR-mimics and antagomiRs that was pursued later, as presented in Chapter 5. Of note, the uptake efficiencies determined for nanomiRs were higher than those previously reported for nHA-mediated delivery of pDNA (12 %), which was shown to be successful for enhanced bone repair (126, 127). This prospect combined with the ability of single miRNAs to intercept entire gene cohorts indicates that nanomiR delivery may have enhanced therapeutic efficacy over nHA-pDNA delivery *in vivo*.

Having determined the high intracellular uptake of nanomiR complexes by human MSCs, greater than 90 % silencing functionality was demonstrated with a single dose of nanomiR treatment, which was generally maintained over time. Interestingly, this level of silencing was comparable with the level described for viral and lipid-based vectors for delivery of siRNAs and shRNAs in different cell lines, but much higher than for miRNA delivery to stem cells (219). NanomiR silencing functionality was also superior in comparison to CaP-based siRNA delivery systems targeting different tumour-model cell lines, which have reported a 8 -10 % range of silencing efficiency at 20 nM doses (324, 373) and 60 % silencing functionality for a 10 nM dose (325). In summary, the nanomiR delivery system developed in this chapter outperformed the silencing efficiency of a range of RNAi delivery vectors, pointing to a significant potential for therapeutic applications beyond the bone TE field. Consequently based on these results, the single 20 nM dose was selected as the optimal concentration for this system and brought forward for further application in the studies presented in the following chapters of this thesis.

6.3.Chapter 3: Nanohydroxyapatite-based delivery of osteogenesis-related miRNAs to enhance hMSC osteogenic differentiation

The emerging interest in the use of miRNAs as osteo-therapeutics has led to the application of viral or lipid-based miRNA delivery to osteoprogenitors and stem cells. However, minimal investigation into non-viral and non-lipid based delivery of potential miRNA candidates to human MSCs has been carried out in the TE field. Ours is the first study to test not only the therapeutic ability of antagomiR-133a, antagomiR-16 and miR-210 mimic to enhance human MSC osteogenesis but also to use a nHA-based delivery system. Taken together, the results from this study demonstrated that nHA-based delivery of each of these three miRNAs enhances human MSC osteogenesis albeit to different levels depending on which one was used. Ultimately, nanoantagomiR-133a induced the greatest osteogenic response of human MSCs and hence was established as the optimal therapeutic candidate for incorporation in a miRNA-activated scaffold.

Our exploration of bioinformatic databases revealed the direct interaction of both miR-133a and miR-16 with additional targets that are positive mediators of osteogenesis, further supporting the negative role of these two miRNAs in osteogenesis, while a bi-functional role of miR-210 in osteogenesis and angiogenesis was underlined by the bioinformatic analysis. Intracellular miRNA level manipulation was deemed successful for each of the nanomiR treatments studied. Specifically, nanoantagomiR-133a and nanoantagomiR-16 reduced intracellular levels of their target miRNAs to less than 0.2 and 0.1 fold respectively compared to the control group (scrambled nanomiR) over 7 days. Additionally, this study showed for the first time an endogenous downregulation in miR-133a levels during human MSC mediated osteogenesis, which was in accordance with previous observations in mice cells (242, 387). The nanomiR-210 mimic treatment also manipulated miR-210 levels effectively, as demonstrated by the prominent increase of intracellular miR-210, to levels that can be considered supra-physiological (388). Taken together, these results confirmed the capability of nHA-based delivery to successfully manipulate miRNA levels in human MSC osteogenic culture.

Subsequently, robust manipulation of all the direct gene targets selected for each nanomiR treatment was demonstrated at the mRNA level. This result supported the beneficial effect of each of these three nanomiR treatments. The highest increase in both Runx2 and OCN levels was seen with nanoantagomiR-133a treatment, followed by nanoantagomiR-16. Other studies in miRNA-induced osteogenesis have reported a range of changes for these genes generally less than three-fold. The pronounced changes observed in this chapter, markedly higher than previous reports, may indicate a phenotype switching effect (391) of relevant benefit as osteo-therapeutics. Following on from this finding, the nanoantagomiR-133a group demonstrated a 17-fold increase in ALP activity compared to untreated cells, followed by a 11-fold increase with nanoantagomiR-16, consistent with the Runx2 and OCN gene expression results. The nanomiR-210 mimic did not display a positive effect, which was in opposition with the previous report by Mizuno *et al*. using the mouse NRG cell line (236). miRNA-induced changes in ALP activity were also assessed in a study by Schoolmeesters *et al*. (235), where inhibition of miR-

133a resulted in a two-fold increase in ALP activity over untreated cells. In this project, the significantly enhanced ALP activity following nanoantagomiR-133a treatment denoted a standout capacity of this treatment group to increase osteogenesis, which is encouraging for its potential use in bone TE applications.

Most importantly from a therapeutic perspective, a significant increase in calcium deposition to levels ranging from 3.37 to 4.67 fold over untreated cells was detected, at the early timepoint of 10 days, across the three treatment groups assessed. At the endpoint of analysis, 14 days, both nanoantagomiR-133a and -16 treatments resulted in a 2.55 to 3.53 fold increase over untreated cells, whereas nanomiR-210 mimic did not maintain the effect detected at 10 days. Calcium deposition is regarded as an end-stage marker of osteogenesis (226, 237, 238, 240, 348, 368, 369, 375, 382, 387) and other non-viral RNAi delivery approaches have reported a 2-fold increase in calcium quantification (226, 348). Comparatively, the data presented in this chapter showed superior calcium deposition response using these three nanomiR treatments than previously assessed non-viral vectors, highlighting the beneficial application of the nHA-based delivery. Overall, nanoantagomiR-133a treatment displayed a superior effect on human MSC osteogenesis than nanoantagomiR-16 and nanomiR-210 mimic, and was selected for the work presented in Chapter 4. Additionally, the application of antagomiR-16 as an osteo-therapeutic, with results implicating this miRNA in human MSC osteogenesis for the first time, served as the basis for further investigation. Finally, although the ability of nanomiR-210 mimic treatment to enhance human MSC osteogenesis was comparatively limited, its application to additional targets implicated in angiogenesis warranted further study in Chapter 5.

6.4.Chapter 4: Incorporation of nanomiRs into a collagen-nano hydroxyapatite scaffold

The primary goal of this research thesis was to incorporate therapeutic miRNAs into our 3D scaffold biomaterials. The research presented in this chapter thus investigated the hypothesis that coll-nHA scaffolds might serve as effective

miRNA delivery platforms capable of manipulating human MSC gene expression in order to therapeutically enhance osteogenesis.

nanomiR complexes were shown to be effectively retained within the highly porous structure of the coll-nHA scaffolds and internalised in human MSCs, leading to significant manipulation of gene expression without affecting cell viability. Both functional reporter nanomiR-mimic and nanoantagomiR complexes significantly maintained silencing of their respective targets, GAPDH and miR-16, confirming the capability of coll-nHA scaffolds as depots for sustained miRNA delivery. This correlated with the observation that, due to the cell migration throughout the 3D scaffold, extended culture periods result in improved functionality outcomes (394). The silencing functionality detected for the nanomiR-mimic is within the range reported from a previous study for cells added onto a functionalised scaffold (350), a result which was widely surpassed with the nanoantagomiR-activated scaffold. These results are even more impressive when it is considered that human MSCs are regarded as particularly difficult to transfect.

Having established the significant potential of the coll-nHA scaffolds for delivery of reporter miRNAs, the osteo-therapeutic potential of incorporating antagomiR-133a levels was demonstrated for the first time. Only 8 studies have been published to date which have used miRNAs as osteo-therapeutics in 3D biomaterials. This is low considering that over 30 miRNAs have now been identified to play a role in osteogenesis (58, 297, 299, 347-349, 393, 395). These previous 3D studies have relied on commercially available transfection methods associated with cytotoxicity concerns (367) and none of them performed assessment of direct silencing functionality (58, 393). The innovative approach developed in this chapter showed a significant decrease in miR-133a intracellular levels, resulting in increases in Runx2 and consequently, a panel of osteogenic markers was upregulated at the gene level, which was accompanied by enhanced presence of osteocalcin protein within the ECM and most importantly, translated into rapidly enhanced calcium deposition on the scaffolds. Taken together, this data pointed to a robust and coordinated therapeutic enhancement in human MSC-mediated osteogenesis within the miR-activated scaffolds illustrating the therapeutic potential of the system.

A major advantage of this system relates to the fact that the nanomiR complexes are incorporated in the 3D scaffolds prior to cell seeding i.e. utilising the coll-nHA scaffolds as reservoirs for the localised delivery of the miRNA complexes with a view to transfecting host cells when applied *in vivo*. This approach differs from *ex vivo* 'cell-mediated' miRNA therapy systems that introduce miRNAs in the cells and then seed the transformed cells onto scaffolds (58, 297, 299, 347-349, 395), as it means that the miRNA activated scaffolds have the potential to exist as an 'off-the-shelf' platform. While this system was developed with bone regeneration in mind, the functionalisation process described in this study may be applied to other scaffolds and to the incorporation of any miRNA with a role in tissue regeneration, therefore representing a promising approach for a wide variety of TE applications. Considering the positive results reported to-date on the ongoing clinical trials of miR-122 inhibitor, *Miravirsen* – by Santaris Pharma -, for hepatitis C (277) and miR-34 mimic, *MRX-34* - by Mirna Therapeutics -, for liver cancer treatment (278), the clinical translation of the technology developed in this chapter has the potential to impact the market of tissue engineered musculoskeletal products.

6.5.Chapter 5: Investigation of nanomiR-210 mimic as (i) a pro-angiogenic therapeutic and (ii) as a simultaneous pro-angiogenic and pro-osteogenic therapeutic as a part of a dual nanomiR formulation

The final study presented in this thesis focussed on the application of miRNA therapeutics capable of simultaneously targeting angiogenesis and osteogenesis. We firstly investigated the pro-angiogenic therapeutic potential of nanomiR-210 mimic, showing effective manipulation of miR-210, albeit with limited pro-angiogenic effect in terms of endothelial cell response. Subsequently, exploration of two combinatorial miRNA approaches, namely nanomiR-210/133a dual and nanomiR-210/16 dual formulations, demonstrated that only the nanomiR-210/16 dual treatment was able to simultaneously enhance the pro-angiogenic and pro-osteogenic capabilities of human MSCs. Taken together, the results showcased the promise of using nHA-based delivery of multiple miRNAs as a prospective therapy in bone TE.

Initially, the effective manipulation of miR-210 levels following nanomiR-210 mimic treatment did not correspond with functional silencing of the direct target EphrinA3. While miR-210 induction of EphrinA3 silencing has been demonstrated in two different cell types (383), the data presented in this chapter did not support the hypothesis that this effect could be extended to the MSCs. However, this study showed for the first time that miR-210 level manipulation can enhance VEGF secretion by human MSCs although not to a sufficient level that it enhanced tubulogenesis and proliferation of endothelial cells (HUVECs). Notably, the influence of miR-210 on angiogenesis has been strongly associated with hypoxic (low oxygen) conditions (428-430), perhaps suggesting that to fully realise the pro-angiogenic potential of miR-210 mimic, hypoxic conditions might be required. Taken together, this data pointed to the differences in miRNA manipulation depending on cell type and indicated a limited therapeutic efficacy of nanomiR-210 mimic to enhance the pro-angiogenic capabilities of human MSCs through the direct targeting of the EphrinA3 gene.

The second part of this chapter evaluated the simultaneous pro-angiogenic and osteogenic response in human MSCs following combinatorial miRNA delivery of miR-210 mimic with antagomiR-133a. The efficient ability of nanomiR-210/133a dual to increase miR-210 intracellular level was demonstrated. However, no silencing of the direct angiogenesis and osteogenesis targets, EphrinA3 and AcvR1b respectively, or increased mineralisation was detected although increased VEGF levels were seen. Although combinatorial delivery of growth factors or genes has generally accounted for superior bone repair outcomes than delivery of the individual components (145, 286, 292), detrimental response seen for FGF-2 combinations with BMP-2 or VEGF (174, 431) illustrates that complex cross-talk may occur. Taken together, this data pointed to minimal potential of the combination of miR-210 mimic plus antagomiR-133a for bone repair.

Most interestingly, the final study showed that an improved therapeutic response could be achieved if the correct therapeutic combination was identified. In this study, an alternative combinatorial approach using the combination of antagomiR-16 plus miR-210 mimic was undertaken. Results

demonstrated the highly effective manipulation of miR-210 levels and the direct targets EphrinA3 and AcvR1b with this nanomiR-210/16 dual treatment. This combination significantly enhanced VEGF secretion by human MSCs, and longer tubules were formed by HUVECs in response demonstrating the potential of this combinatorial approach as a pro-angiogenic therapeutic. In addition, the osteogenesis assessment revealed increased calcium deposition at both 10 and 14 days indicating that nanomiR-210/16 dual combination was also able to enhance functional osteogenesis. To summarise, the results of this study highlighted the ability of nHA particles to deliver pro-angiogenic miRNA therapeutics, consistent with the benefits of nHA as the vector of choice in the delivery of pro-angiogenic and pro-osteogenic plasmid DNA within GAMs developed previously in our laboratory (127). Taken together, this data showcased an exciting capability of this combinatorial nanomiR delivery approach to simultaneously enhance the angiogenesis and osteogenesis capabilities of human MSCs.

6.6.Future Work

- This study demonstrated the potential of in-house synthesised nHA particles to deliver both miR-mimics and antagomiRs, quantifying uptake efficiency and silencing functionality utilising different molecules in each case. Further insight could be obtained on uptake and functionality of nanomiRs by using fluorescently-tagged silencing reporters or incorporating a fluorophore in the core of the nHA particles, in combination with *in situ* hybridisation techniques (219, 388).

- The considerable potential of antagomiR-133a, antagomiR-16 and miR-210 mimic as osteo-therapeutics was demonstrated *in vitro* by way of PCR analysis, ALP activity and calcium deposition, all hallmarks of osteogenesis which yielded conclusive data in this study. It would be interesting to carry out a high-throughput analysis such as the pSILAC-proteomic analysis (381), to evaluate in more detail the possible widespread effects on human MSC fate and metabolism resultant from manipulation of each of these miRNAs.

- Commercially available negative control miRNAs were shown to produce unspecific responses by human MSCs. Significant homology in human protein-coding genes can be determined for these sequences by BLAST analysis (392), which underlines the challenging design of these control sequences. It is expected that improvements in the coming years will generate advanced candidates which will more adequately serve as negative controls.

- Perhaps the most obvious follow on study from this research is to assess the systems developed *in vivo*. An investigation of the capability of the miRNA-activated scaffolds to mediate *in vivo* miRNA delivery, together with the induction of bone healing following application of the antagomiR-133a activated scaffolds would categorically identify the therapeutic potential of this system as a bone graft substitute. In order to do so, rat calvarial and/or femoral defect models could be assessed, which are widely accepted in bone research as preclinical models to monitor defect

healing in response to the bone graft substitute applied (432). This research is planned in the coming months in our laboratory.

- This work has laid the foundation for combinatorial miRNA delivery harnessing a simultaneous pro-angiogenic and pro-osteogenic effect. A more thorough investigation of downstream molecular mechanisms involved in the interaction of the miRNAs utilised in this combinatorial approach would be worth performing. In addition, and of clear relevance to this entire thesis, is that the optimal combinatorial group identified i.e. the miR-210-mimic plus antagomiR-16 dual group merits incorporation into the coll-nHA scaffolds and subsequent *in vivo* investigation in order to realise its full potential as an advanced bone graft substitute.

- For the purpose of this research, a localised delivery system for reporter miR-mimics and antagomiRs as well as the osteo-therapeutic antagomiR-133a was developed using the coll-nHA scaffolds. It would be of great interest to adapt these 3D platforms for a plethora of other tissue repair applications. For instance, the system could be applied to cartilage regeneration by delivering miR-140 mimic (433), and this could be combined with other scaffolds optimised for cartilage repair in our laboratory (66, 96). Neurogenesis and lung recovery are also areas where miRNA therapeutic candidates are starting to emerge, such as miR-106b and miR-375 (434, 435). Ongoing research in our laboratory is focussing on the optimisation of collagen-based scaffolds for the repair of both tissue types (unpublished data) and hence offers the possibility to design miRNA-activated scaffolds targeting both neural and lung repair.

- A further translation opportunity for the system developed in this thesis relates to RNAi-activated scaffolds attracting interest as advanced *in vitro* models for drug development (436) by offering a closer representation of the complex microenvironment found *in vivo*. Such approach is garnering efforts in the landscape of cancer research. The application of miRNA-activated scaffolds to the field of miRNA-related cancer research may thus generate significant interests in the near future.

6.7.Thesis Conclusions

- This study has demonstrated the potential of in-house synthesised nHA particles as non-viral vectors for delivery of both miR-mimics and antagomiRs to human MSCs in a highly efficient and minimally cytotoxic manner, with single administration of low miRNA doses rendering very pronounced silencing activities to a level comparable to viral and lipid-based vectors. Ultimately, a 20 nM dose was deemed optimal for this system.

- Efficient nHA-based delivery of antagomiR-133a, antagomiR-16 and miR-210 mimic led to enhanced osteogenesis by human MSCs. Comparative analysis revealed that nanoantagomiR-133a showed greatest potential as an osteo-therapeutic while both antagomiR-16 and the miR-210 mimic were deemed to warrant further investigation.

- This study has developed the first non-viral, non-lipid, ‘off-the shelf’ 3D system for microRNA delivery. The coll-nHA scaffolds demonstrated significant potential as delivery platforms to manipulate human MSC gene expression when incorporating both miR-mimics and antagomiRs. AntagomiR-133a activated scaffolds upregulated Runx2 and orchestrated accelerated calcium deposition thus showcasing the osteo-therapeutic potential of this innovative strategy.

- While the miR-210 mimic showed a limited pro-angiogenic therapeutic efficacy, the combinatorial delivery of the miR-210 mimic with antagomiR-16 demonstrated significant potential to simultaneously enhance the angiogenesis and osteogenesis capabilities of human MSCs. This combinatorial miRNA approach represents a highly beneficial paradigm for bone repair applications. Moreover, this work underlines the possibility of extending nHA-based miRNA delivery to pathways beyond osteogenesis by tailoring the miRNA therapeutic incorporated in the complexes.

Bibliography

1. Viola J, Lal B, Grad O, Hicks D. Emergence and Evolution of a Shared Concept [Report: EEC-9815425]. Cambridge, Massachusetts: The National Science Foundation WBA; 2003.
2. Langer R, Vacanti, J. Tissue engineering. Science. 1993;260(5110):920-6.
3. Haseltine WA. The Emergence of Regenerative Medicine: A New Field and a New Society. e-biomed: J. Regener. Med. 2001;2(4):17-23.
4. Sheyn D, Mizrahi O, Benjamin S, Gazit Z, Pelled G, Gazit D. Genetically modified cells in regenerative medicine and tissue engineering. Adv Drug Deliv Rev. 2010;62(7-8):683-98.
5. Tcherpakov M. Tissue Engineering and Regeneration: Technologies and Global Markets [Book]. 2012;.
6. Younger EM, Chapman MW. Morbidity at bone graft donor sites. J Orthop Trauma. 1989;3(3):192-5.
7. Gleeson JP, Plunkett NA, O'Brien FJ. Addition of hydroxyapatite improves stiffness, interconnectivity and osteogenic potential of a highly porous collagen-based scaffold for bone tissue regeneration. Eur. Cells Mater. 2010;20:218-30.
8. Quinlan E. Controlled Release of Bioactive Molecules from Collagen-Based Scaffolds for Bone Repair [Research Thesis]. Dublin: Royal College of Surgeons in Ireland; 2014.
9. Mikos AG, McIntire LV, Anderson JM, Babensee JE. Host response to tissue engineered devices. Adv Drug Deliv Rev. 1998;33(1-2):111-39.
10. Estrategies in TE. Online webpage [Accesed 30/7/15]; available from: http://www.centropede.com/UKSB2006/ePoster/images/background/TE_model_large.jpg.
11. Martini FH, Nath JL, Bartholomew EF. Fundamentals of Anatomy & Physiology [Book]. 9th Edition. San Francisco: P.E.I. Editorial; 2006.
12. McCalden RW, McGeough JA, Court-Brown CM. Age-related changes in the compressive strength of cancellous bone. The relative importance of

changes in density and trabecular architecture. J. Bone Jt. Surg., Am. Vol. 1997;79(3):421-7.

13. Winslow T. Cancer research glossary: bone marrow. NHI, National Cancer Institute; 2014. Online webpage [Accesed 30/7/15]; available from: http://www.cancer.gov/images/cdr/live/CDR755927-750.jpg

14. Parsian T. Bone Graft Substitutes. Part medical co. 2013-14. Online webpage [Accesed 30/7/15]; available from: http://www.partmedical.com/articles/medical-articles/spinal-column-a-brain/90-bone-graft-substitutes.html.

15. Aubin JE. Osteoprogenitor cell frequency in rat bone marrow stromal populations: role for heterotypic cell-cell interactions in osteoblast differentiation. J. Cell. Biochem. 1999;72(3):396-410.

16. Wang Y, Azais T, Robin M, Vallee A, Catania C, Legriel P, et al. The predominant role of collagen in the nucleation, growth, structure and orientation of bone apatite. Nat Mater. 2012;11(8):724-33.

17. Aarden EM, Burger EH, Nijweide PJ. Function of osteocytes in bone. J. Cell. Biochem. 1994;55(3):287-99.

18. Katagiri T, Takahashi N. Regulatory mechanisms of osteoblast and osteoclast differentiation. Oral Dis. 2002;8(3):147-59.

19. Shapiro F. Bone development and its relation to fracture repair. The role of mesenchymal osteoblasts and surface osteoblasts. Eur. Cells Mater. 2008;15:53-76.

20. Gerstenfeld LC, Barnes GL, Shea CM, Einhorn TA. Osteogenic differentiation is selectively promoted by morphogenetic signals from chondrocytes and synergized by a nutrient rich growth environment. Connect Tissue Res. 2003;44 Suppl 1:85-91.

21. Chen G, Deng C, Li YP. TGF-beta and BMP signaling in osteoblast differentiation and bone formation. Int. J. Biol. Sci.2012;8(2):272-88.

22. Yamaguchi A, Komori T, Suda T. Regulation of osteoblast differentiation mediated by bone morphogenetic proteins, hedgehogs, and Cbfa1. Endocr Rev. 2000;21(4):393-411.

23. Jeon EJ, Lee KY, Choi NS, Lee MH, Kim HN, Jin YH, et al. Bone morphogenetic protein-2 stimulates Runx2 acetylation. J. Biol. Chem. 2006;281(24):16502-11.

24. Stein GS, Lian JB. Molecular mechanisms mediating proliferation/differentiation interrelationships during progressive development of the osteoblast phenotype. Endocr Rev. 1993;14(4):424-42.
25. Kirker-Head CA. Potential applications and delivery strategies for bone morphogenetic proteins. Adv Drug Deliv Rev. 2000;43(1):65-92.
26. Gautschi OP, Frey SP, Zellweger R. Bone morphogenetic proteins in clinical applications. ANZ J Surg. 2007 Aug;77(8):626-31.
27. Jahangir AA, Nunley RM, Mehta S, Sharan A. Bone-graft substitutes in orthopaedic surgery. 2008;2(1)1-5.
28. Boccaccio A, Ballini A, Pappalettere C, Tullo D, Cantore S, Desiate A. Finite element method (FEM), mechanobiology and biomimetic scaffolds in bone tissue engineering. Int. J. Biol. Sci. [Review]. 2011;7(1):112-32.
29. Kurien T, Pearson RG, Scammel BE. Bone graft substitues currently available in orthopaedic practice. Bone Joint J. 2013;95(B):583-97.
30. Blackwood KA, Bock N, Dargaville TR, Ann Woodruff M. Scaffolds for Growth Factor Delivery as Applied to Bone Tissue Engineering. Int. J. Polym. Sci. 2012;2012:1-25.
31. Guilak F, Butler DL, Goldstein SA, Mooney D. Functional Tissue Engineering [Book]. New York: Springer Science & Business Media; 2006.
32. Sudo H, Kodama HA, Amagai Y, Yamamoto S, Kasai S. In vitro differentiation and calcification in a new clonal osteogenic cell line derived from newborn mouse calvaria. J. Cell Biol. 1983;96(1):191-8.
33. Otsuka E, Yamaguchi A, Hirose S, Hagiwara H. Characterization of osteoblastic differentiation of stromal cell line ST2 that is induced by ascorbic acid. Am. J. Physiol. 1999;277(1 Pt 1):C132-8.
34. Park HJ, Zhang Y, Georgescu SP, Johnson KL, Kong D, Galper JB. Human umbilical vein endothelial cells and human dermal microvascular endothelial cells offer new insights into the relationship between lipid metabolism and angiogenesis. Stem Cell Rev. 2006;2(2):93-102.
35. Armstrong L, Lako M, Buckley N, Lappin TR, Murphy MJ, Nolta JA, Pittenger M, et al. Editorial: Our top 10 developments in stem cell biology over the last 30 years. Stem Cells. 2012;30(1):2-9.
36. Chamberlain G, Fox J, Ashton B, Middleton J. Concise review: mesenchymal stem cells: their phenotype, differentiation capacity,

immunological features, and potential for homing. Stem Cells. 2007;25(11):2739-49.
37. Barry FP, Murphy JM. Mesenchymal stem cells: clinical applications and biological characterization. Int. J. Biochem Cell Biol. 2004;36(4):568-84.
38. clinicaltrials.gov [database on the Internet] [cited 16/07/2015]. Available from: http://www.clinicaltrials.gov/ct2/results?term=mesenchymal+stem+cell&Search=Search.
39. Caplan AI. Mesenchymal stem cells. J. Orthop. Res. 1991;9(5):641-50.
40. Prockop DJ. Marrow stromal cells as stem cells for nonhematopoietic tissues. Science. 1997;276(5309):71-4.
41. Fuchs JR, Hannouche D, Terada S, Zand S, Vacanti JP, Fauza DO. Cartilage engineering from ovine umbilical cord blood mesenchymal progenitor cells. Stem Cells. 2005;23(7):958-64.
42. Zuk PA, Zhu M, Mizuno H, Huang J, Futrell JW, Katz AJ, et al. Multilineage cells from human adipose tissue: implications for cell-based therapies. Tissue Eng. 2001;7(2):211-28.
43. Chim H, Schantz JT. Human circulating peripheral blood mononuclear cells for calvarial bone tissue engineering. Plast. Reconstr. Surg.2006;117(2):468-78.
44. De Coppi P, Bartsch G, Jr., Siddiqui MM, Xu T, Santos CC, Perin L, et al. Isolation of amniotic stem cell lines with potential for therapy. Nat Biotechnol. 2007;25(1):100-6.
45. Lee S, An S, Kang TH, Kim KH, Chang NH, Kang S, et al. Comparison of mesenchymal-like stem/progenitor cells derived from supernumerary teeth with stem cells from human exfoliated deciduous teeth. J. Regener. Med. 2011;6(6):689-99.
46. In 't Anker PS, Scherjon SA, Kleijburg-van der Keur C, de Groot-Swings GM, Claas FH, Fibbe WE, et al. Isolation of mesenchymal stem cells of fetal or maternal origin from human placenta. Stem Cells. 2004;22(7):1338-45.
47. Caplan AI, Correa D. The MSC: an injury drugstore. Cell Stem Cell. 2011;9(1):11-5.
48. Mooney DJ, Vandenburgh H. Cell delivery mechanisms for tissue repair. Cell Stem Cell. 2008;2(3):205-13.

49. Pittenger M. Sleuthing the source of regeneration by MSCs. Cell Stem Cell. 2009;5(1):8-10.
50. Meirelles Lda S, Fontes AM, Covas DT, Caplan AI. Mechanisms involved in the therapeutic properties of mesenchymal stem cells. Cytokine Growth Factor Rev. 2009 Oct-Dec;20(5-6):419-27.
51. Buhring HJ, Battula VL, Treml S, Schewe B, Kanz L, Vogel W. Novel markers for the prospective isolation of human MSC. Ann N Y Acad Sci. 2007;1106:262-71.
52. Pittenger MF, Mackay AM, Beck SC, Jaiswal RK, Douglas R, Mosca JD, et al. Multilineage potential of adult human mesenchymal stem cells. Science. 1999;284(5411):143-7.
53. English K, Barry FP, Mahon BP. Murine mesenchymal stem cells suppress dendritic cell migration, maturation and antigen presentation. Immunol Lett. 2008;115(1):50-8.
54. English K, French A, Wood KJ. Mesenchymal stromal cells: facilitators of successful transplantation? Cell Stem Cell. 2010;7(4):431-42.
55. Caplan AI, Dennis JE. Mesenchymal stem cells as trophic mediators. J. Cell. Biochem. 2006;98(5):1076-84.
56. Thompson EM, Matsiko A, Farrell E, Kelly DJ, O'Brien FJ. Recapitulating endochondral ossification: a promising route to in vivo bone regeneration. J Tissue Eng Regen Med. 2014;9(8):889-902.
57. Gordeladze JO, Reseland, J. E., Duroux-Richard, I., Apparailly, F. and Jorgensen, C. from stem cells to bone: phenotype acquisition, stabilization and tissue engineering in animal models. ILAR Journal. 2010;51(1):42-61.
58. Mariner PD, Johannesen E, Anseth KS. Manipulation of miRNA activity accelerates osteogenic differentiation of hMSCs in engineered 3D scaffolds. Tissue Eng Regen Med. 2011;6(4):314-24.
59. Lutolf MP, Hubbell JA. Synthetic biomaterials as instructive extracellular microenvironments for morphogenesis in tissue engineering. Nat. Biotechnol. 2005;23:47-55.
60. Scadden DT. The stem-cell niche as an entity of action. Nature. 2006;441(7097):1075-9.

61. O'Brien FJ, Harley BA, Waller MA, Yannas IV, Gibson LJ, Prendergast PJ. The effect of pore size on permeability and cell attachment in collagen scaffolds for tissue engineering. Technol Health Care. 2007;15(1):3-17.
62. Bucholz RW. Nonallograft osteoconductive bone graft substitutes. Clin Orthop Relat Res. 2002;(395):44-52.
63. Engler AJ, Sen S, Sweeney HL, Discher DE. Matrix elasticity directs stem cell lineage specification. Cell. 2006;126(4):677-89.
64. Karageorgiou V, Kaplan D. Porosity of 3D biomaterial scaffolds and osteogenesis. Biomaterials. 2005;26(27):5474-91.
65. Tierney CM, Haugh MG, Liedl J, Mulcahy F, Hayes B, O'Brien FJ. The effects of collagen concentration and crosslink density on the biological, structural and mechanical properties of collagen-GAG scaffolds for bone tissue engineering. J Mech Behav Biomed Mater. 2009;2(2):202-9.
66. Murphy CM, Matsiko A, Haugh MG, Gleeson JP, O'Brien FJ. Mesenchymal stem cell fate is regulated by the composition and mechanical properties of collagen-glycosaminoglycan scaffolds. J. Mech. Behav. Biomed Mater. 2012;11:53-62.
67. Yannas IV. Tissue and Organ Regeneration in Adults [Book]. Springer NM, editor. New York, 2001.
68. Stevens MM, George JH. Exploring and engineering the cell surface interface. Science. [Review]. 2005;310(5751):1135-8.
69. Pina S, Oliveira JM, Reis RL. Natural-based nanocomposites for bone tissue engineering and regenerative medicine: A Review. Adv. Mater. 2015;27:1143–69.
70. Lyons F, Partap S, O'Brien FJ. Part 1: scaffolds and surfaces. Technol Health Care. 2008;16(4):305-17.
71. Lee SH, Shin H. Matrices and scaffolds for delivery of bioactive molecules in bone and cartilage tissue engineering. Adv Drug Deliv Rev. 2007;59(4-5):339-59.
72. Taboas JM, Maddox RD, Krebsbach PH, Hollister SJ. Indirect solid free form fabrication of local and global porous, biomimetic and composite 3D polymer-ceramic scaffolds. Biomaterials. 2003;24(1):181-94.

73. Lin AS, Barrows TH, Cartmell SH, Guldberg RE. Microarchitectural and mechanical characterization of oriented porous polymer scaffolds. Biomaterials. 2003;24(3):481-9.
74. Gough JE, Downes S. Osteoblast cell death on methacrylate polymers involves apoptosis. J Biomed Mater Res. 2001;57(4):497-505.
75. Dawes E, Rushton N. The effects of lactic acid on PGE2 production by macrophages and human synovial fibroblasts: a possible explanation for problems associated with the degradation of poly(lactide) implants? Clin Mater. 1994;17(4):157-63.
76. Liao S, Wang W, Uo M, Ohkawa S, Akasaka T, Tamura K, et al. A three-layered nano-carbonated hydroxyapatite/collagen/PLGA composite membrane for guided tissue regeneration. Biomaterials. 2005 Dec;26(36):7564-71.
77. Cui K, Zhu Y, Hong Wang X, Ling Feng Q, Cui FZ. A Porous Scaffold from Bone-like Powder Loaded in a Collagen-Chitosan Matrix. Journal of Bioactive and Compatible Polymers 2004;19(January 2004):17-31.
78. Arpornmaeklong P, Suwatwirote N, Pripatnanont P, Oungbho K. Growth and differentiation of mouse osteoblasts on chitosan-collagen sponges. Int J Oral Maxillofac Surg. 2007;36(4):328-37.
79. Barrere F, Mahmood TA, de Groot K, van Blitterswijk CA. Advanced biomaterials for skeletal tissue regeneration: Instructive and smart functions. Mater. Sci. Eng., R. 2008;59(1-6):38.
80. Hubbell JA. Materials as morphogenetic guides in tissue engineering. Curr Opin Biotechnol. 2003;14(5):551-8.
81. Daamen WF, Veerkamp JH, van Hest JC, van Kuppevelt TH. Elastin as a biomaterial for tissue engineering. Biomaterials. 2007;28(30):4378-98.
82. Park S-N, Park J-C, Kim HO, Song MJ, Suh H. Characterization of porous collagen/hyaluronic acid scaffold modified by 1-ethyl-3-(3-dimethylaminopropyl)carbodiimide cross-linking. Biomaterials. 2002;23(4) 1205-12.
83. Dawson JI, Wahl DA, Lanham SA, Kanczler JM, Czernuszka JT, Oreffo ROC. Development of specific collagen scaffolds to support the osteogenic and chondrogenic differentiation of human bone marrow stromal cells. Biomaterials. 2008;29(21)3105-16.

84. Nazarov R, Jin H-J, Kaplan DL. Porous 3-D Scaffolds from Regenerated Silk Fibroin. Biomacromolecules. 2004;5(3):718-26.
85. Harley BAC, Gibson LJ. In vivo and in vitro applications of collagen-GAG scaffolds. Chem. Eng. J. (Loughborough, Engl.) 2008;137(1):102-21.
86. Garate A, Murua A, Orive G, Hernandez RM, Pedraz JL. Stem cells in alginate bioscaffolds. Ther. Delivery. 2012;3(6):761-74.
87. Benders KEM, van Weeren PR, Badylak SF, Saris DBF, Dhert WJA, Malda J. Extracellular matrix scaffolds for cartilage and bone regeneration. Trends Biotechnol. 2013;31(3):169-76.
88. Yannas IV, Lee E, Orgill DP, Skrabut EM, Murphy GF. Synthesis and characterization of a model extracellular matrix that induces partial regeneration of adult mammalian skin. P N A S. 1989;86(3):933-7.
89. Geiger M, Li RH, Friess W. Collagen sponges for bone regeneration with rhBMP-2. Adv Drug Deliv Rev. 2003;55(12):1613-29.
90. Lee CH, Singla A, Lee Y. Biomedical applications of collagen. Int. J. Pharm. 2001;221(1-2):1-22.
91. O'Brien FJ, Harley BA, Yannas IV, Gibson LJ. The effect of pore size on cell adhesion in collagen-GAG scaffolds. Biomaterials. 2005;26(4):433-41.
92. O'Brien FJ. Biomaterials & scaffolds for tissue engineering. Materials Today. 2011;14(3):88-95.
93. Wiesmann HP, Nazer N, Klatt C, Szuwart T, Meyer U. Bone tissue engineering by primary osteoblast-like cells in a monolayer system and 3-dimensional collagen gel. Int. J Oral Surg. 2003;61(12):1455-62.
94. O'Brien FJ, Harley BA, Yannas IV, Gibson L. Influence of freezing rate on pore structure in freeze-dried collagen-GAG scaffolds. Biomaterials. 2004;25(6):1077-86.
95. Al-Munajjed AA, Plunkett NA, Gleeson JP, Weber T, Jungreuthmayer C, Levingstone T, et al. Development of a biomimetic collagen-hydroxyapatite scaffold for bone tissue engineering using a SBF immersion technique. J Biomed Mater Res B Appl Biomater. 2009;90(2):584-91.
96. Matsiko A, Levingstone TJ, O'Brien FJ, Gleeson JP. Addition of hyaluronic acid improves cellular infiltration and promotes early-stage chondrogenesis in a collagen-based scaffold for cartilage tissue engineering. J Mech Behav Biomed Mater. 2012;11:41-52.

97. Cunniffe GM, Dickson GR, Partap S, Stanton KT, O'Brien FJ. Development and characterisation of a collagen nano-hydroxyapatite composite scaffold for bone tissue engineering. J. Mater. Sci.: Mater. Med. 2010;21(8):2293-8.
98. Khan Y, Yaszemski MJ, Mikos AG, Laurencin CT. Tissue engineering of bone: material and matrix considerations. J. Bone Jt. Surg., Am. Vol. 2008;90 Suppl 1:36-42.
99. Stevens MM. Biomaterials for bone tissue engineering. Mater. Today. 2008;11(5):18-25.
100. Hench LL. The story of Bioglass. J. Mater. Sci.: Mater. Med. 2006;17(11):967-78.
101. Finkemeier CG. Bone-grafting and bone-graft substitutes. The Journal of bone and joint surgery American volume. 2002 Mar;84-A(3):454-64.
102. Barralet JE, Grover L, Gaunt T, Wright AJ, Gibson IR. Preparation of macroporous calcium phosphate cement tissue engineering scaffold. Biomaterials. 2002;23(15):3063-72.
103. Weinand C, Pomerantseva I, Neville CM, Gupta R, Weinberg E, Madisch I, et al. Hydrogel-beta-TCP scaffolds and stem cells for tissue engineering bone. Bone. 2006;38(4):555-63.
104. Ribeiro CC, Barrias CC, Barbosa MA. Preparation and characterisation of calcium-phosphate porous microspheres with a uniform size for biomedical applications. J. Mater. Sci.: Mater. Med. 2006;17(5):455-63.
105. Porter AE, Patel N, Skepper JN, Best SM, Bonfield W. Effect of sintered silicate-substituted hydroxyapatite on remodelling processes at the bone-implant interface. Biomaterials. 2004;25(16):3303-14.
106. Porter NL, Pilliar RM, Grynpas MD. Fabrication of porous calcium polyphosphate implants by solid freeform fabrication: a study of processing parameters and in vitro degradation characteristics. J Biomed. Mater. Res. 2001;56(4):504-15.
107. Pilliar RM, Filiaggi MJ, Wells JD, Grynpas MD, Kandel RA. Porous calcium polyphosphate scaffolds for bone substitute applications -- in vitro characterization. Biomaterials. 2001;22(9):963-72.

108. Chu TM, Halloran JW, Hollister SJ, Feinberg SE. Hydroxyapatite implants with designed internal architecture. J. Mater. Sci.: Mater. Med. 2001;12(6):471-8.
109. Sadat-Shojai M, Khorasani M-T, Dinpanah-Khoshdargi E, Jamshidi A. Synthesis methods for nanosized hydroxyapatite with diverse structures. Acta Biomater. 2013;9(8):7591-621.
110. Náray-Szabó S. The structure of apatite (CaF)Ca4(PO4)3. Zeitschrift für Kristallographie – Cryst. Mater. 1930;75(1):387-98.
111. Mehmel M. Über die Struktur des Apatits. I. Zeit.Krist.- Cryst. Mater. 1930;75(1):323-31.
112. Pryor LS, Gage E, Langevin CJ, Herrera F, Breithaupt AD, Gordon CR, et al. Review of bone substitutes. Craniomaxillofacial trauma & reconstruction. 2009;2(3):151-60.
113. Habibovic P, Yuan H, van den Doel M, Sees TM, van Blitterswijk CA, de Groot K. Relevance of osteoinductive biomaterials in critical-sized orthotopic defect. J. Orthop. Res. 2006 May;24(5):867-76.
114. Blaker JJ, Gough JE, Maquet V, Notingher I, Boccaccini ARI. In vitro evaluation of novel bioactive composites based on Bioglass®-filled polylactide foams for bone tissue engineering scaffolds. J. Biomed. Mater. Res., Part A. 2003;67A(4):1401-11.
115. Marra KG, Szem JW, Kumta PN, DiMilla PA, Weiss LE. In vitro analysis of biodegradable polymer blend/hydroxyapatite composites for bone tissue engineering. J Biomed Mater Res. 1999;47(3):324-35.
116. Ma PX, Zhang R, Xiao G, Franceschi R. Engineering new bone tissue in vitro on highly porous poly(alpha-hydroxyl acids)/hydroxyapatite composite scaffolds. J Biomed Mater Res. 2001;54(2):284-93.
117. Ferraz MP, Monteiro FJ, Manuel CM. Hydroxyapatite nanoparticles: A review of preparation methodologies. J Appl Biomater Biomech. 2004;2(2):74-80.
118. Tran N, Webster TJ. Nanotechnology for bone materials. Wiley Interdiscip Rev Nanomed Nanobiotechnol. 2009;1(3):336-51.
119. Li P. Biomimetic nano-apatite coating capable of promoting bone ingrowth. Journal of biomedical materials research Part A. 2003;66(1):79-85.

120. Heo SJ, Kim SE, Wei J, Kim DH, Hyun YT, Yun HS, et al. In vitro and animal study of novel nano-hydroxyapatite/poly(epsilon-caprolactone) composite scaffolds fabricated by layer manufacturing process. Tissue Eng., Part A. 2009;15(5):977-89.
121. Wei G, Ma PX. Structure and properties of nano-hydroxyapatite/polymer composite scaffolds for bone tissue engineering. Biomaterials. 2004;25(19):4749-57.
122. Shi Z, Huang X, Cai Y, Tang R, Yang D. Size effect of hydroxyapatite nanoparticles on proliferation and apoptosis of osteoblast-like cells. Acta Biomater. 2009;5(1):338-45.
123. Kumta PN, Sfeir C, Lee DH, Olton D, Choi D. Nanostructured calcium phosphates for biomedical applications: novel synthesis and characterization. Acta Biomater. 2005;1(1):65-83.
124. Cunniffe GM, O'Brien FJ, Partap S, Levingstone TJ, Stanton KT, Dickson GR. The synthesis and characterization of nanophase hydroxyapatite using a novel dispersant-aided precipitation method. J. Biomed. Mater. Res., Part A. 2010;95(4):1142-9.
125. Cunniffe G. Development of a NanoHydroxyapatite-Collagen Composite Scaffold for Bone Tissue Engineering [Dissertation]. Belfast: Queen's University 2009.
126. Curtin CM, Cunniffe GM, Lyons FG, Bessho K, Dickson GR, Duffy GP, et al. Innovative Collagen Nano-Hydroxyapatite Scaffolds Offer a Highly Efficient Non-Viral Gene Delivery Platform for Stem Cell-Mediated Bone Formation. Adv Mater. 2012;24(6):749-54.
127. Curtin CM, Tierney EG, Duffy GP, O'Brien FJ. Combinatorial Gene Therapy Accelerates Bone Regeneration: Non-Viral Dual Delivery of VEGF and BMP2 in a Collagen-Nanohydroxyapatite Scaffold. Adv Healthc Mat. 2015;4(2):223-7.
128. Boccaccini AR, Notingher I, Maquet V, Jerome R. Bioresorbable and bioactive composite materials based on polylactide foams filled with and coated by Bioglass particles for tissue engineering applications. J. Mater. Sci.: Mater. Med. 2003;14(5):443-50.
129. Hutmacher DW. Scaffolds in tissue engineering bone and cartilage. Biomaterials. 2000;21(24):2529-43.

130. Thomson RC, Yaszemski MJ, Powers JM, Mikos AG. Hydroxyapatite fiber reinforced poly(alpha-hydroxy ester) foams for bone regeneration. Biomaterials. 1998;19(21):1935-43.
131. Kikuchi M, Itoh S, Ichinose S, Shinomiya K, Tanaka J. Self-organization mechanism in a bone-like hydroxyapatite/collagen nanocomposite synthesized in vitro and its biological reaction in vivo. Biomaterials. 2001;22(13):1705-11.
132. Boccaccini AR, Roelher JA, Hench LL, Maquet V, Jerome R. A Composites Approach to Tissue Engineering. 26th Annual Conference on Composites, Advanced Ceramics, Materials, and Structures in : B: Ceramic Engineering and Science Proceedings. 2008;23(4):805-16.
133. McManus AJ, Doremus RH, Siegel RW, Bizios R. Evaluation of cytocompatibility and bending modulus of nanoceramic/polymer composites. Journal of biomedical materials research Part A. 2005;72(1):98-106.
134. Kim HW, Knowles JC, Kim HE. Hydroxyapatite and gelatin composite foams processed via novel freeze-drying and crosslinking for use as temporary hard tissue scaffolds. Journal of biomedical materials research Part A. 2005;72(2):136-45.
135. Pek YS, Gao S, Arshad MS, Leck KJ, Ying JY. Porous collagen-apatite nanocomposite foams as bone regeneration scaffolds. Biomaterials. 2008;29(32):4300-5.
136. Wahl DA, Sachlos E, Liu C, Czernuszka JT. Controlling the processing of collagen-hydroxyapatite scaffolds for bone tissue engineering. Journal of materials science Materials in medicine. 2007;18(2):201-9.
137. Wahl DA, Czernuszka JT. Collagen-hydroxyapatite composites for hard tissue repair. European cells & materials. 2006;424(11):43-56.
138. Murphy CM, Haugh MG, O'Brien FJ. The effect of mean pore size on cell attachment, proliferation and migration in collagen-glycosaminoglycan scaffolds for bone tissue engineering. Biomaterials. 2010;31(3):461-6.
139. Haugh MG, Murphy CM, O'Brien FJ. Novel freeze-drying methods to produce a range of collagen-glycosaminoglycan scaffolds with tailored mean pore sizes. Tissue Eng Part C Methods. 2010;16(5):887-94.
140. Saito N, Okada T, Horiuchi H, Murakami N, Takahashi J, Nawata M, et al. Biodegradable Poly-d,l-Lactic Acid-Polyethylene Glycol Block Copolymers as

a BMP Delivery System for Inducing Bone. J. Bone Joint Surg Am. 2001; 83-A Suppl1 (Pt 2):S92-8.
141. Okubo Y, Bessho K, Fujimura K, Iizuka T, Miyatake S-i. In Vitro and in Vivo Studies of a Bone Morphogenetic Protein-2 Expressing Adenoviral Vector. J. Bone Joint Surg Am. 2001;83-A Suppl1 (Pt 2):S99-104.
142. Andersen MO, Nygaard JV, Burns JS, Raarup MK, Nyengaard JR, Bunger C, et al. siRNA nanoparticle functionalization of nanostructured scaffolds enables controlled multilineage differentiation of stem cells. Mol Ther. 2010;18(11):2018-27.
143. Cao H, Jiang X, Chai C, Chew SY. RNA interference by nanofiber-based siRNA delivery system. J Control Release. 2010;144:203-12.
144. Vo TN, Kasper FK, Mikos AG. Strategies for controlled delivery of growth factors and cells for bone regeneration. Adv Drug Deliv Rev. 2012;64(12):1292-309.
145. Chen FM, Zhang M, Wu ZF. Toward delivery of multiple growth factors in tissue engineering. Biomaterials. 2010;31(24):6279-308.
146. Tayalia P, Mooney DJ. Controlled growth factor delivery for tissue engineering. Adv Mater. 2009;21(32-33):3269-85.
147. Lee K, Silva EA, Mooney DJ. Growth factor delivery-based tissue engineering: general approaches and a review of recent developments. J R Soc Interface. 2011;8(55):153-70.
148. Lutolf MP, Gilbert PM, Blau HM. Designing materials to direct stem-cell fate. Nature. 2009;462(7272):433-41.
149. Huang Z, Ren PG, Ma T, Smith RL, Goodman SB. Modulating osteogenesis of mesenchymal stem cells by modifying growth factor availability. Cytokine. 2010;51(3):305-10.
150. McKay WF, Peckham SM, Badura JM. A comprehensive clinical review of recombinant human bone morphogenetic protein-2 (INFUSE Bone Graft). Int Orthop. 2007;31(6):729-34.
151. Geiger F, Bertram H, Berger I, Lorenz H, Wall O, Eckhardt C, et al. Vascular endothelial growth factor gene-activated matrix (VEGF165-GAM) enhances osteogenesis and angiogenesis in large segmental bone defects. J. Bone Jt. Surg., Am. Vol. 2005;20(11):2028-35.

152. Street J, Bao M, deGuzman L, Bunting S, Peale FV, Jr., Ferrara N, et al. Vascular endothelial growth factor stimulates bone repair by promoting angiogenesis and bone turnover. P N A S. 2002;99(15):9656-61.
153. Novosel EC, Kleinhans C, Kluger PJ. Vascularization is the key challenge in tissue engineering. Adv Drug Deliv Rev. 2011;63(4-5):300-11.
154. Murakami N, Saito N, Takahashi J, Ota H, Horiuchi H, Nawata M, et al. Repair of a proximal femoral bone defect in dogs using a porous surfaced prosthesis in combination with recombinant BMP-2 and a synthetic polymer carrier. Biomaterials. 2003;24(13):2153-9.
155. Tsurushima H, Marushima A, Suzuki K, Oyane A, Sogo Y, Nakamura K, et al. Enhanced bone formation using hydroxyapatite ceramic coated with fibroblast growth factor-2. Acta Biomater. 2010;6(7):2751-9.
156. Ripamonti U, Parak R, Petit JC. Induction of cementogenesis and periodontal ligament regeneration by recombinant human transforming growth factor-beta3 in Matrigel with rectus abdominis responding cells. J Periodontal Res. 2009;44(1):81-7.
157. Ripamonti U, Ramoshebi LN, Teare J, Renton L, Ferretti C. The induction of endochondral bone formation by transforming growth factor-beta(3): experimental studies in the non-human primate Papio ursinus. J Cell Mol Med. 2008;12(3):1029-48.
158. Teare JA, Ramoshebi LN, Ripamonti U. Periodontal tissue regeneration by recombinant human transforming growth factor-beta 3 in Papio ursinus. J Periodontal Res. 2008 Feb;43(1):1-8.
159. Herford AS, Lu M, Akin L, Cicciu M. Evaluation of a porcine matrix with and without platelet-derived growth factor for bone graft coverage in pigs. The International journal of oral & maxillofacial implants. 2012;27(6):1351-8.
160. Moore DC, Ehrlich MG, McAllister SC, Machan JT, Hart CE, Voigt C, et al. Recombinant human platelet-derived growth factor-BB augmentation of new-bone formation in a rat model of distraction osteogenesis. The Journal of bone and joint surgery American volume. 2009;91(8):1973-84.
161. Vahle JL, Zuehlke U, Schmidt A, Westmore M, Chen P, Sato M. Lack of bone neoplasms and persistence of bone efficacy in cynomolgus macaques after long-term treatment with teriparatide [rhPTH(1-34)]. J Bone Mineral Res. 2008;23(12):2033-9.

162. Arrighi I, Mark S, Alvisi M, von Rechenberg B, Hubbell JA, Schense JC. Bone healing induced by local delivery of an engineered parathyroid hormone prodrug. Biomaterials. 2009;30(9):1763-71.
163. Bostrom MP, Gamradt SC, Asnis P, Vickery BH, Hill E, Avnur Z, et al. Parathyroid hormone-related protein analog RS-66271 is an effective therapy for impaired bone healing in rabbits on corticosteroid therapy. Bone. 2000;26(5):437-42.
164. Trejo CG, Lozano D, Manzano M, Doadrio JC, Salinas AJ, Dapia S, et al. The osteoinductive properties of mesoporous silicate coated with osteostatin in a rabbit femur cavity defect model. Biomaterials. 2010;31(33):8564-73.
165. Gothard D, Smith EL, Kanczler JM, Rashidi H, Qutachi O, Henstock J, et al. Tissue engineered bone using select growth factors: A comprehensive review of animal studies and clinical translation studies in man. European cells & materials. 2014;28:166-207.
166. Epstein NE. Pros, cons, and costs of INFUSE in spinal surgery. Surg Neurol Int. 2011;2:10.
167. Urist MR. Bone: formation by autoinduction. Science. 1965 12;150(3698):893-9.
168. Chen D, Zhao M, Mundy GR. Bone morphogenetic proteins. Growth Factors. 2004;22(4):233-41.
169. Haidar ZS, Hamdy RC, Tabrizian M. Delivery of recombinant bone morphogenetic proteins for bone regeneration and repair. Part A: Current challenges in BMP delivery. Biotechnol Lett. 2009;31(12):1817-24.
170. Senger D, Galli SJ, Dvorak AM, Perruzzi CA, Harvey VS, Dvorak HF. Tumor cells secrete a vascular permeability factor that promotes accumulation of ascites fluid. Science. 1983;219(4587):983-5.
171. Olsson A-K, Dimberg A, Kreuger J, Claesson-Welsh L. VEGF receptor signalling — in control of vascular function. Nature Reviews Molecular Cell Biology. 2006;7(5):359-71.
172. Ferrara N, Gerber HP, LeCouter J. The biology of VEGF and its receptors. Nat Med. 2003;9(6):669-76.
173. Yang YQ, Tan YY, Wong R, Wenden A, Zhang LK, Rabie AB. The role of vascular endothelial growth factor in ossification. International journal of oral science. 2012;4(2):64-8.

174. Behr B, Sorkin M, Lehnhardt M, Renda A, Longaker MT, Quarto N. A comparative analysis of the osteogenic effects of BMP-2, FGF-2, and VEGFA in a calvarial defect model. Tissue Eng Part A. 2012;18(9-10):1079-86.
175. Ferrara N, Alitalo K. Clinical applications of angiogenic growth factors and their inhibitors. Nat Med. 1999;5(12):1359-64.
176. Ferrara N. VEGF and the quest for tumour angiogenesis factors. Nat Rev Cancer. 2002;2(10):795-803.
177. Kaigler D, Wang Z, Horger K, Mooney DJ, Krebsbach PH. VEGF scaffolds enhance angiogenesis and bone regeneration in irradiated osseous defects. Journal Bone Mineral Res. 2006;21(5):735-44.
178. Orive G, Hernandez RM, Rodriguez Gascon A, Dominguez-Gil A, Pedraz JL. Drug delivery in biotechnology: present and future. Curr Opin Biotechnol. 2003;14(6):659-64.
179. Takeda K. Delivery of magic bullets: on the still rocky road to gene therapy. Br J Pharmacol. 2009;157(2):151-2.
180. Yilgor P, Tuzlakoglu K, Reis RL, Hasirci N, Hasirci V. Incorporation of a sequential BMP-2/BMP-7 delivery system into chitosan-based scaffolds for bone tissue engineering. Biomaterials. 2009;30(21):3551-9.
181. Zhao Z, Zhao M, Xiao G, Franceschi RT. Gene transfer of the Runx2 transcription factor enhances osteogenic activity of bone marrow stromal cells in vitro and in vivo. Mol Ther. 2005;12(2):247-53.
182. Jaklenec A, Hinckfuss A, Bilgen B, Ciombor DM, Aaron R, Mathiowitz E. Sequential release of bioactive IGF-I and TGF-beta 1 from PLGA microsphere-based scaffolds. Biomaterials. 2008;29(10):1518-25.
183. De la Riva B, Sanchez E, Hernandez A, Reyes R, Tamimi F, Lopez-Cabarcos E, et al. Local controlled release of VEGF and PDGF from a combined brushite-chitosan system enhances bone regeneration. J Control Release. 2010;143(1):45-52.
184. Fischbach C, Mooney DJ. Polymers for pro- and anti-angiogenic therapy. Biomaterials. 2007;28(12):2069-76.
185. Chung YI, Kim SK, Lee YK, Park SJ, Cho KO, Yuk SH, et al. Efficient revascularization by VEGF administration via heparin-functionalized nanoparticle-fibrin complex. J Control Release. 2010;143(3):282-9.

186. Pang Y, Wang X, Ucuzian AA, Brey EM, Burgess WH, Jones KJ, et al. Local delivery of a collagen-binding FGF-1 chimera to smooth muscle cells in collagen scaffolds for vascular tissue engineering. Biomaterials. 2010 Feb;31(5):878-85.
187. Rives CB, des Rieux A, Zelivyanskaya M, Stock SR, Lowe WL, Jr., Shea LD. Layered PLG scaffolds for in vivo plasmid delivery. Biomaterials. 2009 Jan;30(3):394-401.
188. Cao L, Arany PR, Wang YS, Mooney DJ. Promoting angiogenesis via manipulation of VEGF responsiveness with notch signaling. Biomaterials. 2009 Sep;30(25):4085-93.
189. Sheridan C. Gene therapy finds its niche. Nat Biotechnol. 2011 Feb;29(2):121-8.
190. Rinn JL, Chang HY. Genome regulation by long noncoding RNAs. Annual review of biochemistry. 2012;81:145-66.
191. Pearson H. Genetics: What is a gene? Nature. 2006;441(7092):398-401.
192. Alberts B, Johnson A, Lewis J, Raff M, Roberts K, Walter P. Molecular Biology of the Cell [Book]. 4th edition. New York: Garland Science; 2002.
193. Haussecker D. Current issues of RNAi therapeutics delivery and development. J Control Release. 2014;195:49-54.
194. Griffiths A, Gelbart W, Miller J. Modern Genetics Analysis [Book]. Freeman WH, editor. New York,1999.
195. Bonadio J, Smiley E, Patil P, Goldstein S. Localized, direct plasmid gene delivery in vivo: prolonged therapy results in reproducible tissue regeneration. Nat Med. 1999;5(7):753-9.
196. Wozney JM, Rosen V. Bone morphogenetic protein and bone morphogenetic protein gene family in bone formation and repair. Clin Orthop Relat Res. 1998;(346):26-37.
197. Bernstein E, Caudy AA, Hammond SM, Hannon GJ. Role for a bidentate ribonuclease in the initiation step of RNA interference. Nature. 2001;409(6818):363-6.
198. Hamilton AJ, Baulcombe DC. A species of small antisense RNA in posttranscriptional gene silencing in plants. Science. 1999;286(5441):950-2.

199. Hammond SM, Bernstein E, Beach D, Hannon GJ. An RNA-directed nuclease mediates post-transcriptional gene silencing in Drosophila cells. Nature. 2000;404(6775):293-6.
200. Parrish S, Fleenor J, Xu S, Mello C, Fire A. Functional anatomy of a dsRNA trigger: differential requirement for the two trigger strands in RNA interference. Mol Cell. 2000;6(5):1077-87.
201. Zamore PD, Tuschl T, Sharp PA, Bartel DP. RNAi: double-stranded RNA directs the ATP-dependent cleavage of mRNA at 21 to 23 nucleotide intervals. Cell. 2000;101(1):25-33.
202. Grishok A, Pasquinelli AE, Conte D, Li N, Parrish S, Ha I, et al. Genes and mechanisms related to RNA interference regulate expression of the small temporal RNAs that control C. elegans developmental timing. Cell. 2001;106(1):23-34.
203. Ketting RF, Fischer SE, Bernstein E, Sijen T, Hannon GJ, Plasterk RH. Dicer functions in RNA interference and in synthesis of small RNA involved in developmental timing in C. elegans. Genes & development. 2001;15(20):2654-9.
204. Knight SW, Bass BL. A role for the RNase III enzyme DCR-1 in RNA interference and germ line development in Caenorhabditis elegans. Science. 2001;293(5538):2269-71.
205. Elbashir SM, Lendeckel W, Tuschl T. RNA interference is mediated by 21- and 22-nucleotide RNAs. Genes & development. 2001;15(2):188-200.
206. Elbashir SM, Martinez J, Patkaniowska A, Lendeckel W, Tuschl T. Functional anatomy of siRNAs for mediating efficient RNAi in Drosophila melanogaster embryo lysate. EMBO J. 2001;20(23):6877-88.
207. Nykanen A, Haley B, Zamore PD. ATP requirements and small interfering RNA structure in the RNA interference pathway. Cell. 2001;107(3):309-21.
208. Martinez J, Patkaniowska A, Urlaub H, Luhrmann R, Tuschl T. Single-stranded antisense siRNAs guide target RNA cleavage in RNAi. Cell. 2002;110(5):563-74.
209. Schwarz DS, Hutvagner G, Haley B, Zamore PD. Evidence that siRNAs function as guides, not primers, in the Drosophila and human RNAi pathways. Mol Cell. 2002;10(3):537-48.

210. Rao DD, Vorhies JS, Senzer N, Nemunaitis J. siRNA vs. shRNA: Similarities and differences. Adv Drug Deliv Rev. 2009;61(9):746-59.
211. Siolas D, Lerner C, Burchard J, Ge W, Linsley PS, Paddison PJ, et al. Synthetic shRNAs as potent RNAi triggers. Nat Biotechnol. 2005;23(2):227-31.
212. Ge Q, Ilves H, Dallas A, Kumar P, Shorenstein J, Kazakov SA, et al. Minimal-length short hairpin RNAs: the relationship of structure and RNAi activity. RNA. 2010;16(1):106-17.
213. Liu YP, Schopman NCT, Berkhout B. Dicer-independent processing of short hairpin RNAs. Nucleic Acids Res. 2013;41(6):3723-33.
214. Lytle JR, Yario TA, Steitz JA. Target mRNAs are repressed as efficiently by microRNA-binding sites in the 5′ UTR as in the 3′ UTR. PNAS. 2007;104(23):9667-72.
215. Bartel DP. MicroRNAs: genomics, biogenesis, mechanism, and function. Cell. 2004;116(2):281-97.
216. Carthew RW, Sontheimer EJ. Origins and Mechanisms of miRNAs and siRNAs. Cell. 2009;136(4):642-55.
217. Levy O, Ruvinov E, Reem T, Granot Y, Cohen S. Highly efficient osteogenic differentiation of human mesenchymal stem cells by eradication of STAT3 signaling. Int. J.Biochem Cell Biol. 2010;42(11):1823-30.
218. Beavers KR, Nelson CE, Duvall CL. MiRNA inhibition in tissue engineering and regenerative medicine. Adv Drug Deliv Rev. 2015;88:123-37.
219. Yau WW, Rujitanaroj PO, Lam L, Chew SY. Directing stem cell fate by controlled RNA interference. Biomaterials. 2012;33(9):2608-28.
220. Hu R, Li,H.,Liu, W., Yang, L., Tan, Y. and Luo, X. Targeting miRNAs in osteoblast differentiation and bone formation. Expert Opinion in Therapeutic Targets. 2010;14(10):1109-20.
221. Jensen ED, Gopalakrishnan R, Westendorf JJ. Regulation of gene expression in osteoblasts. Biofactors. 2010;36(1):25-32.
222. van Rooij E. The Art of MicroRNA Research. Circulation research. 2011;108(2):219-34.
223. van Rooij E, Purcell AL, Levin AA. Developing microRNA therapeutics. Circulation research. 2012;110(3):496-507.
224. Bader AG, Brown D, Winkler M. The promise of microRNA replacement therapy. Cancer research. 2010;70(18):7027-30.

225. Hribal ML, Nakae J, Kitamura T, Shutter JR, Accili D. Regulation of insulin-like growth factor-dependent myoblast differentiation by Foxo forkhead transcription factors. The Journal of cell biology. 2003;162(4):535-41.
226. Kwong FN, Richardson SM, Evans CH. Chordin knockdown enhances the osteogenic differentiation of human mesenchymal stem cells. Arthritis Res Ther. 2008;10(3):R65. doi: 10.1186/ar2436.
227. Liu YB, Kharode Y, Bodine PV, Yaworsky PJ, Robinson JA, Billiard J. LPA induces osteoblast differentiation through interplay of two receptors: LPA1 and LPA4. Journal of cellular biochemistry. 2010;109(4):794-800.
228. Kumar A, Salimath BP, Schieker M, Stark GB, Finkenzeller G. Inhibition of metastasis-associated gene 1 expression affects proliferation and osteogenic differentiation of immortalized human mesenchymal stem cells. Cell Prolif. 2011 ;44(2):128-38.
229. Martin SK, Fitter S, Bong LF, Drew JJ, Gronthos S, Shepherd PR, et al. NVP-BEZ235, a dual pan class I PI3 kinase and mTOR inhibitor, promotes osteogenic differentiation in human mesenchymal stromal cells. J. Bone Mineral Res. 2010;25(10):2126-37.
230. Tsai CC, Chen YJ, Yew TL, Chen LL, Wang JY, Chiu CH, et al. Hypoxia inhibits senescence and maintains mesenchymal stem cell properties through down-regulation of E2A-p21 by HIF-TWIST. Blood. 2011;117(2):459-69.
231. Miraoui H, Severe N, Vaudin P, Pages JC, Marie PJ. Molecular silencing of Twist1 enhances osteogenic differentiation of murine mesenchymal stem cells: implication of FGFR2 signaling. J. Cell Biochem. 2010;110(5):1147-54.
232. Tay YM, Tam WL, Ang YS, Gaughwin PM, Yang H, Wang W, et al. MicroRNA-134 modulates the differentiation of mouse embryonic stem cells, where it causes post-transcriptional attenuation of Nanog and LRH1. Stem Cells. 2008;26(1):17-29.
233. Tay Y, Zhang J, Thomson AM, Lim B, Rigoutsos I. MicroRNAs to Nanog, Oct4 and Sox2 coding regions modulate embryonic stem cell differentiation. Nature. 2008 Oct 23;455(7216):1124-8.
234. Li Z, Hassan MQ, Jafferji M, Aqeilan RI, Garzon R, Croce CM, et al. Biological functions of miR-29b contribute to positive regulation of osteoblast differentiation. The Journal of biological chemistry. 2009;284(23):15676-84.

235. Schoolmeesters A, Eklund T, Leake D, Vermeulen A, Smith Q, Force Aldred S, et al. Functional profiling reveals critical role for miRNA in differentiation of human mesenchymal stem cells. PloS one. 2009;4(5):e5605.
236. Mizuno Y, Tokuzawa Y, Ninomiya Y, Yagi K, Yatsuka-Kanesaki Y, Suda T, et al. miR-210 promotes osteoblastic differentiation through inhibition of AcvR1b. FEBS letters. 2009;583(13):2263-8.
237. Kim YJ, Bae SW, Yu SS, Bae YC, Jung JS. miR-196a regulates proliferation and osteogenic differentiation in mesenchymal stem cells derived from human adipose tissue. Journal of bone and mineral research : the official journal of the American Society for Bone and Mineral Research. 2009;24(5):816-25.
238. Li H, Xie H, Liu W, Hu R, Huang B, Tan YF, et al. A novel microRNA targeting HDAC5 regulates osteoblast differentiation in mice and contributes to primary osteoporosis in humans. The Journal of clinical investigation. 2009;119(12):3666-77.
239. Eguchi T, Watanabe K, Hara ES, Ono M, Kuboki T, Calderwood SK. OstemiR: a novel panel of microRNA biomarkers in osteoblastic and osteocytic differentiation from mesencymal stem cells. PloS one. 2013;8(3):e58796.
240. Baglìo SR, Devescovi V, Granchi D, Baldini N. MicroRNA expression profiling of human bone marrow mesenchymal stem cells during osteogenic differentiation reveals Osterix regulation by miR-31. Gene. 2013;527(1):321-31.
241. Zeng Y, Qu X, Li H, Huang S, Wang S, Xu Q, et al. MicroRNA-100 regulates osteogenic differentiation of human adipose-derived mesenchymal stem cells by targeting BMPR2. FEBS letters. 2012;586(16):2375-81.
242. Li Z, Hassan MQ, Volinia S, van Wijnen AJ, Stein JL, Croce CM, et al. A microRNA signature for a BMP2-induced osteoblast lineage commitment program. Proceedings of the National Academy of Sciences of the United States of America. 2008;105(37):13906-11.
243. Itoh T, Nozawa Y, Akao Y. MicroRNA-141 and -200a are involved in bone morphogenetic protein-2-induced mouse pre-osteoblast differentiation by targeting distal-less homeobox 5. J. Biol Chem. 2009;284(29):19272-9.
244. Grunhagen J, Ott CE. On microRNA-214 suppressing osteogenic differentiation of C2C12 myoblast cells by targeting Osterix. Bone. 2013;57(1):325-7.

245. Lagos-Quintana M, Rauhut R, Lendeckel W, Tuschl T. Identification of novel genes coding for small expressed RNAs. Science. 2001;294(5543):853-8.
246. Lau NC, Lim LP, Weinstein EG, Bartel DP. An abundant class of tiny RNAs with probable regulatory roles in Caenorhabditis elegans. Science. 2001;294(5543):858-62.
247. Lee RC, Ambros V. An extensive class of small RNAs in Caenorhabditis elegans. Science. 2001;294(5543):862-4.
248. Lee RC, Feinbaum RL, Ambros V. The C. elegans heterochronic gene lin-4 encodes small RNAs with antisense complementarity to lin-14. Cell. 1993;75(5):843-54.
249. Wightman B, Ha I, Ruvkun G. Posttranscriptional regulation of the heterochronic gene lin-14 by lin-4 mediates temporal pattern formation in C. elegans. Cell. 1993;75(5):855-62.
250. Reinhart BJ, Slack FJ, Basson M, Pasquinelli AE, Bettinger JC, Rougvie AE, et al. The 21-nucleotide let-7 RNA regulates developmental timing in Caenorhabditis elegans. Nature. 2000;403(6772):901-6.
251. Slack FJ, Basson M, Liu Z, Ambros V, Horvitz HR, Ruvkun G. The lin-41 RBCC gene acts in the C. elegans heterochronic pathway between the let-7 regulatory RNA and the LIN-29 transcription factor. Mol Cell. 2000;5(4):659-69.
252. Pasquinelli AE, Reinhart BJ, Slack F, Martindale MQ, Kuroda MI, Maller B, et al. Conservation of the sequence and temporal expression of let-7 heterochronic regulatory RNA. Nature. 2000;408(6808):86-9.
253. miRBase [database on the Internet]. Faculty of Life Sciences University of Manchester. [cited 25 July 2015]. Available from: http://www.mirbase.org/cgi-bin/mirna_summary.pl?org=hsa.
254. Friedman RC, Farh KK, Burge CB, Bartel DP. Most mammalian mRNAs are conserved targets of microRNAs. Genome Res. 2009;19(1):92-105.
255. McKiernan PJ, Greene CM. MicroRNA Dysregulation in Cystic Fibrosis. Mediators of inflammation. 2015;2015:529642. doi: 10.1155/2015/529642.
256. McKiernan P, Cunningham O, Greene C, Cryan S-A. Targeting miRNA-based medicines to cystic fibrosis airway epithelial cells using nanotechnology. Int. J. Nanomed. 2013;8:3907-15.
257. Greene CM, Gaughan KP. microRNAs in asthma: potential therapeutic targets. Curr Opin Pulm Med. 2013;19(1):66-72.

258. Oglesby IK, McElvaney NG, Greene CM. MicroRNAs in inflammatory lung disease--master regulators or target practice? Respir Res. 2010;11:148.
259. Lee Y, Jeon K, Lee JT, Kim S, Kim VN. MicroRNA maturation: stepwise processing and subcellular localization. EMBO J. 2002;21(17):4663-70.
260. Zeng Y, Cullen BR. Sequence requirements for micro RNA processing and function in human cells. RNA. 2003;9(1):112-23.
261. Basyuk E, Suavet F, Doglio A, Bordonne R, Bertrand E. Human let-7 stem-loop precursors harbor features of RNase III cleavage products. Nucleic acids research. 2003;31(22):6593-7.
262. Lee Y, Ahn C, Han J, Choi H, Kim J, Yim J, et al. The nuclear RNase III Drosha initiates microRNA processing. Nature. 2003 Sep 25;425(6956):415-9.
263. Yi R, Qin Y, Macara IG, Cullen BR. Exportin-5 mediates the nuclear export of pre-microRNAs and short hairpin RNAs. Genes & development. 2003;17(24):3011-6.
264. Lund E, Guttinger S, Calado A, Dahlberg JE, Kutay U. Nuclear export of microRNA precursors. Science. 2004;303(5654):95-8.
265. Hutvagner G, McLachlan J, Pasquinelli AE, Balint E, Tuschl T, Zamore PD. A cellular function for the RNA-interference enzyme Dicer in the maturation of the let-7 small temporal RNA. Science. 2001;293(5531):834-8.
266. Chen CZ, Li L, Lodish HF, Bartel DP. MicroRNAs modulate hematopoietic lineage differentiation. Science. 2004;303(5654):83-6.
267. Aravin AA, Lagos-Quintana M, Yalcin A, Zavolan M, Marks D, Snyder B, et al. The small RNA profile during Drosophila melanogaster development. Developmental cell. 2003;5(2):337-50.
268. Lim LP, Lau NC, Weinstein EG, Abdelhakim A, Yekta S, Rhoades MW, et al. The microRNAs of Caenorhabditis elegans. Genes & development. 2003;17(8):991-1008.
269. Khvorova A, Reynolds A, Jayasena SD. Functional siRNAs and miRNAs exhibit strand bias. Cell. 2003 Oct 17;115(2):209-16.
270. Schwarz DS, Hutvagner G, Du T, Xu Z, Aronin N, Zamore PD. Asymmetry in the assembly of the RNAi enzyme complex. Cell. 2003;115(2):199-208.

271. Mourelatos Z, Dostie J, Paushkin S, Sharma A, Charroux B, Abel L, et al. miRNPs: a novel class of ribonucleoproteins containing numerous microRNAs. Genes & development. 2002;16(6):720-8.
272. Zhang Y, Wang Z, Gemeinhart RA. Progress in microRNA delivery. J. Control Release. 2013;172(3):962-74.
273. Griffiths-Jones S, Grocock RJ, van Dongen S, Bateman A, Enright AJ. miRBase: microRNA sequences, targets and gene nomenclature. Nucleic acids research. 2006;34 (Database issue):D140-4.
274. Bernardo BC, Charchar FJ, Lin RCY, McMullen JR. A MicroRNA guide for clinicians and basic scientists: background and experimental techniques. Heart, Lung and Circulation. 2012;21(3):131-42.
275. Ebert MS, Sharp PA. MicroRNA sponges: progress and possibilities. RNA. 2010;16(11):2043-50.
276. Zhang S, Chen L, Jung EJ, Calin GA. Targeting microRNAs with small molecules: from dream to reality. Clin Pharmacol Ther. 2010;87(6):754-8.
277. Janssen HL, Kauppinen S, Hodges MR. HCV infection and miravirsen. N Engl J Med. 2013;369(9):878.
278. Multicenter Phase I Study of MRX34, MicroRNA miR-RX34 Liposome Injectable Suspension [database on the Internet]. U.S. National Institutes of Health. 2013 [cited October 30, 2013]. Available from: http://clinicaltrials.gov/show/NCT01829971.
279. United States Patent and Trademark Office [database on the Internet]. eGovernment. [cited 4th August 2015]. Available from: http://www.uspto.gov/.
280. Monaghan M, Pandit A. RNA interference therapy via functionalized scaffolds. Adv Drug Deliv Rev. 2011;63(4-5):197-208.
281. Chew SY. MicroRNAs in tissue engineering & regenerative medicine. Adv Drug Deliv Rev. 2015;88:1-2.
282. Villemejane J, Mir LM. Physical methods of nucleic acid transfer: general concepts and applications. Br J Pharmacol. 2009;157(2):207-19.
283. Ilina P, Hyvonen Z, Saura M, Sandvig K, Yliperttula M, Ruponen M. Genetic blockage of endocytic pathways reveals differences in the intracellular processing of non-viral gene delivery systems. J Control Release. 2012;163(3):385-95.

284. Midoux P, Pichon C, Yaouanc JJ, Jaffres PA. Chemical vectors for gene delivery: a current review on polymers, peptides and lipids containing histidine or imidazole as nucleic acids carrier. British Journal of Pharmacology. 2009;157(2):166-78.
285. Park J, Ries J, Gelse K, Kloss F, von der Mark K, Wiltfang J, et al. Bone regeneration in critical size defects by cell-mediated BMP-2 gene transfer: a comparison of adenoviral vectors and liposomes. Gene Ther. 2003 Jul;10(13):1089-98.
286. Zhao M, Zhao Z, Koh JT, Jin T, Franceschi RT. Combinatorial gene therapy for bone regeneration: cooperative interactions between adenovirus vectors expressing bone morphogenetic proteins 2, 4, and 7. J. Cell Biochem. 2005;95(1):1-16.
287. Betz OB, Betz VM, Nazarian A, Pilapil CG, Vrahas MS, Bouxsein ML, et al. Direct percutaneous gene delivery to enhance healing of segmental bone defects. J. Bone Jt. Surg., Am. Vol. 2006;88(2):355-65.
288. Koh JT, Zhao Z, Wang Z, Lewis IS, Krebsbach PH, Franceschi RT. Combinatorial gene therapy with BMP2/7 enhances cranial bone regeneration. J Dent Res. 2008;87(9):845-9.
289. Zhang Y, Shi B, Li C, Wang Y, Chen Y, Zhang W, et al. The synergetic bone-forming effects of combinations of growth factors expressed by adenovirus vectors on chitosan/collagen scaffolds. J Control Release. 2009;136(3):172-8.
290. Keeney M, van den Beucken JJ, van der Kraan PM, Jansen JA, Pandit A. The ability of a collagen/calcium phosphate scaffold to act as its own vector for gene delivery and to promote bone formation via transfection with VEGF(165). Biomaterials. 2010;31(10):2893-902.
291. Endo M, Kuroda S, Kondo H, Maruoka Y, Ohya K, Kasugai S. Bone regeneration by modified gene-activated matrix: effectiveness in segmental tibial defects in rats. Tissue Eng. 2006;12(3):489-97.
292. Itaka K, Ohba S, Miyata K, Kawaguchi H, Nakamura K, Takato T, et al. Bone regeneration by regulated in vivo gene transfer using biocompatible polyplex nanomicelles. Mol Ther. 2007;15(9):1655-62.
293. Pack DW, Hoffman AS, Pun S, Stayton PS. Design and development of polymers for gene delivery. Nat. Rev. Drug Discovery. 2005;4(7):581-93.

294. Liu YP, Berkhout B. miRNA cassettes in viral vectors: Problems and solutions. Biochimica et Biophysica Acta (BBA) - Gene Reg Mech. 2011;1809(11-12):732-45.
295. Xia H, Mao Q, Paulson HL, Davidson BL. siRNA-mediated gene silencing in vitro and in vivo. Nat Biotechnol. 2002;20(10):1006-10.
296. Boudreau RL, Martins I, Davidson BL, Davidson BL. Artificial microRNAs as siRNA shuttles: improved safety as compared to shRNAs in vitro and in vivo. Mol Ther. 2009;17(1):169-75.
297. Deng Y, Bi X, Zhou H, You Z, Wang Y, Gu P, et al. Repair of critical-sized bone defects with anti-miR-31-expressing bone marrow stromal stem cells and poly(glycerol sebacate) scaffolds. Eur Cell Mater. 2014;27:13-25.
298. Gao J, Yang T, Han J, Yan K, Qiu X, Zhou Y, et al. MicroRNA expression during osteogenic differentiation of human multipotent mesenchymal stromal cells from bone marrow. J Cellular Biochem. 2011;112(7):1844-56.
299. Liao Y-H, Chang Y-H, Sung L-Y, Li K-C, Yeh C-L, Yen T-C, et al. Osteogenic differentiation of adipose-derived stem cells and calvarial defect repair using baculovirus-mediated co-expression of BMP-2 and miR-148b. Biomaterials. 2014;35(18):4901-10.
300. Peng H, Usas A, Gearhart B, Young B, Olshanski A, Huard J. Development of a self-inactivating tet-on retroviral vector expressing bone morphogenetic protein 4 to achieve regulated bone formation. Mol Ther. 2004;9(6):885-94.
301. Hasharoni A, Zilberman Y, Turgeman G, Helm GA, Liebergall M, Gazit D. Murine spinal fusion induced by engineered mesenchymal stem cells that conditionally express bone morphogenetic protein-2. J Neurosurg Spine. 2005;3(1):47-52.
302. Check E. Gene Therapy: a tragic setback. Nature. 2002;420(6912):116-8.
303. Jo J, Tabata Y. Non-viral gene transfection technologies for genetic engineering of stem cells. Eur J Pharm Biopharm. 2008;68(1):90-104.
304. Santos JL, Pandita D, Rodrigues J, Pego AP, Granja PL, Tomas H. Non-viral gene delivery to mesenchymal stem cells: methods, strategies and application in bone tissue engineering and regeneration. Curr Gene Ther. 2011;11(1):46-57.

305. Lipchina I, Elkabetz Y, Hafner M, Sheridan R, Mihailovic A, Tuschl T, et al. Genome-wide identification of microRNA targets in human ES cells reveals a role for miR-302 in modulating BMP response. Genes & Development. 2011;25(20):2173-86.
306. Hamm A, Krott N, Breibach I, Blindt R, Bosserhoff AK. Efficient transfection method for primary cells. Tissue Eng. 2002;8(2):235-45.
307. Kim SH, Jeong JH, Lee SH, Kim SW, Park TG. Local and systemic delivery of VEGF siRNA using polyelectrolyte complex micelles for effective treatment of cancer. J Control Release. 2008;129(2):107-16.
308. Ibrahim AF, Weirauch U, Thomas M, Grunweller A, Hartmann RK, Aigner A. MicroRNA replacement therapy for miR-145 and miR-33a is efficacious in a model of colon carcinoma. Cancer Res. 2011;71(15):5214-24.
309. Peng B, Chen Y, Leong KW. MicroRNA delivery for regenerative medicine. Adv. Drug Deliv. Rev. 2015;88:108-22.
310. Nelson CE, Kim AJ, Adolph EJ, Gupta MK, Yu F, Hocking KM, et al. Tunable Delivery of siRNA from a Biodegradable Scaffold to Promote Angiogenesis In Vivo. Adv. Mater. 2014;26(4):607-14.
311. Kulkarni M, Greiser U, O'Brien T, Pandit A. Liposomal gene delivery mediated by tissue-engineered scaffolds. Trends Biotechnol. 2010;28(1):28-36.
312. Corsi K, Chellat F, Yahia L, Fernandes JC. Mesenchymal stem cells, MG63 and HEK293 transfection using chitosan-DNA nanoparticles. Biomaterials. 2003;24(7):1255-64.
313. Li J, Yu X, Wang Y, Yuan Y, Xiao H, Cheng D, et al. A reduction and pH dual-sensitive polymeric vector for long-circulating and tumor-targeted siRNA delivery. Adv. Mater. 2014;26(48):8217-24.
314. Tierney EG, Duffy GP, Cryan SA, Curtin CM, O'Brien FJ. Non-viral gene-activated matrices-next generation constructs for bone repair. Organogenesis. 2013;9(1):22-8.
315. Ghosh R, Singh LC, Shohet JM, Gunaratne PH. A gold nanoparticle platform for the delivery of functional microRNAs into cancer cells. Biomaterials. 2013;34(3):807-16.
316. Raftery R, O'Brien FJ, Cryan SA. Chitosan for gene delivery and orthopedic tissue engineering applications. Molecules. 2013;18(5):5611-47.

317. Graham FL, van der Eb AJ. A new technique for the assay of infectivity of human adenovirus 5 DNA. Virology. 1973;52(2):456-67.
318. Bose S, Tarafder S. Calcium phosphate ceramic systems in growth factor and drug delivery for bone tissue engineering: A review. Acta Biomater. 2012;8(4):1401-21.
319. Pedraza CE, Bassett DC, McKee MD, Nelea V, Gbureck U, Barralet JE. The importance of particle size and DNA condensation salt for calcium phosphate nanoparticle transfection. Biomaterials. 2008;29(23):3384-92.
320. Wu Q, Chen D, Zuscik MJ, O'Keefe RJ, Rosier RN. Overexpression of Smurf2 stimulates endochondral ossification through upregulation of beta-catenin. J Bone Mineral Res. 2008;23(4):552-63.
321. Andersen MO, Lichawska A, Arpanaei A, Rask Jensen SM, Kaur H, Oupicky D, et al. Surface functionalisation of PLGA nanoparticles for gene silencing. Biomaterials. 2010;31(21):5671-7.
322. Neumann S, Kovtun A, Dietzel ID, Epple M, Heumann R. The use of size-defined DNA-functionalized calcium phosphate nanoparticles to minimise intracellular calcium disturbance during transfection. Biomaterials. 2009;30(35):6794-802.
323. Li J, Chen YC, Tseng YC, Huang L. Biodegradable Calcium Phosphate Nanoparticle with Lipid Coating for Systemic siRNA Delivery. J Control Release. 2010;142(3):416-21.
324. Zhang M, Ishii A, Nishiyama N, Matsumoto S, Ishii T, Yamasaki Y, et al. PEGylated Calcium Phosphate Nanocomposites as Smart Environment-Sensitive Carriers for siRNA Delivery. Adv. Mater. 2009;21(34):3520-5.
325. Giger EV, Castagner B, Raikkonen J, Monkkonen J, Leroux JC. siRNA transfection with calcium phosphate nanoparticles stabilized with PEGylated chelators. Adv Healthc Mater. 2013;2(1):134-44.
326. Lee MS, Lee JE, Byun E, Kim NW, Lee K, Lee H, et al. Target-specific delivery of siRNA by stabilized calcium phosphate nanoparticles using dopa–hyaluronic acid conjugate. J Control Release. 2014;192:122-30.
327. Lee K, Oh MH, Lee MS, Nam YS, Park TG, Jeong JH. Stabilized calcium phosphate nano-aggregates using a dopa-chitosan conjugate for gene delivery. International journal of pharmaceutics. 2013;445(1-2):196-202.

328. Zhang L, Webster TJ. Nanotechnology and nanomaterials: Promises for improved tissue regeneration Nano Today. 2009;4:66-80.
329. Hedberg EL, Shih CK, Lemoine JJ, Timmer MD, Liebschner MA, Jansen JA, et al. In vitro degradation of porous poly(propylene fumarate)/poly(DL-lactic-co-glycolic acid) composite scaffolds. Biomaterials. 2005 Jun;26(16):3215-25.
330. Chen RR, Mooney DJ. Polymeric growth factor delivery strategies for tissue engineering. Pharm Res. 2003;20(8):1103-12.
331. Campbell PG, Miller ED, Fisher GW, Walker LM, Weiss LE. Engineered spatial patterns of FGF-2 immobilized on fibrin direct cell organization. Biomaterials. 2005;26(33):6762-70.
332. Wan AC, Ying JY. Nanomaterials for in situ cell delivery and tissue regeneration. Adv Drug Deliv Rev. 2010;62(7-8):731-40.
333. Kearney CJ, Mooney DJ. Macroscale delivery systems for molecular and cellular payloads. Nat Mater. 2013;12(11):1004-17.
334. Gainza G, Villullas S, Pedraz JL, Hernandez RM, Igartua M. Advances in drug delivery systems (DDSs) to release growth factors for wound healing and skin regeneration. Nanomedicine. 2015;11(6):1551-73.
335. Ulbrich K, Pechar M, Strohalm J, Subr V, Rihova B. Synthesis of biodegradable polymers for controlled drug release. Ann N Y Acad Sci. 1997;831:47-56.
336. des Rieux A, Ucakar B, Mupendwa BP, Colau D, Feron O, Carmeliet P, et al. 3D systems delivering VEGF to promote angiogenesis for tissue engineering. J Control Release. 2011;150(3):272-8.
337. Quinlan E, Lopez-Noriega A, Thompson EM, Hibbitts A, Cryan SA, O'Brien FJ. Controlled release of vascular endothelial growth factor from spray-dried alginate microparticles in collagen-hydroxyapatite scaffolds for promoting vascularization and bone repair. J Tissue Eng Regen Med. 2015; doi: 10.1002/term.2013. [Epub ahead of print].
338. Quinlan E, López-Noriega A, Thompson E, Kelly HM, Cryan SA, O'Brien FJ. Development of collagen–hydroxyapatite scaffolds incorporating PLGA and alginate microparticles for the controlled delivery of rhBMP-2 for bone tissue engineering. J Control Release. 2015;198:71-9.

339. Pan Y, Zhang Y, Jia T, Zhang K, Li J, Wang L. Development of a microRNA delivery system based on bacteriophage MS2 virus-like particles. The FEBS journal. 2012;279(7),1198-208.
340. Nguyen MK, Jeon O, Krebs MD, Schapira D, Alsberg E. Sustained localized presentation of RNA interfering molecules from in situ forming hydrogels to guide stem cell osteogenic differentiation. Biomaterials. 2014;35(24):6278-86.
341. Sriram M, Sainitya R, Kalyanaraman V, Dhivya S, Selvamurugan N. Biomaterials mediated microRNA delivery for bone tissue engineering. International Journal of Biological Macromolecules. 2015;74:404-12.
342. Fang J, Zhu YY, Smiley E, Bonadio J, Rouleau JP, Goldstein SA, et al. Stimulation of new bone formation by direct transfer of osteogenic plasmid genes. Proceedings of the National Academy of Sciences of the United States of America. 1996;93(12):5753-8.
343. Pelled G, Ben-Arav A, Hock C, Reynolds DG, Yazici C, Zilberman Y, et al. Direct gene therapy for bone regeneration: gene delivery, animal models, and outcome measures. Tissue Eng., Part B, Rev. 2010;16(1):13-20.
344. Kimelman-Bleich N, Pelled G, Zilberman Y, Kallai I, Mizrahi O, Tawackoli W, et al. Targeted gene-and-host progenitor cell therapy for nonunion bone fracture repair. Mol Ther. 2011;19(1):53-9.
345. Evans CH. Gene therapy for bone healing. Expert Rev. Mol. Med. 2010;12:e18.
346. Tierney EG, McSorley K, Hastings CL, Cryan SA, O'Brien T, Murphy MJ, et al. High levels of ephrinB2 over-expression increases the osteogenic differentiation of human mesenchymal stem cells and promotes enhanced cell mediated mineralisation in a polyethyleneimine-ephrinB2 gene-activated matrix. J Control Release. 2013;165(3):173-82.
347. Li Y, Fan L, Liu S, Liu W, Zhang H, Zhou T, et al. The promotion of bone regeneration through positive regulation of angiogenic-osteogenic coupling using microRNA-26a. Biomaterials. 2013;34(21):5048-58.
348. Qureshi AT, Monroe WT, Dasa V, Gimble JM, Hayes DJ. miR-148b eNanoparticle conjugates for light mediated osteogenesis of human adipose stromal/stem cells. Biomaterials. 2013;34(21)7799-810.

349. James EN, Delany AM, Nair LS. Post-transcriptional regulation in osteoblasts using localized delivery of miR-29a inhibitor from nanofibers to enhance extracellular matrix deposition. Acta Biomater. 2014;10(8):3571-80.
350. Monaghan M, Browne S, Schenke-Layland K, Pandit A. A collagen-based scaffold delivering exogenous microRNA-29b to modulate extracellular matrix remodelling. Mol Ther. 2014;22(4):786-96.
351. Wu K, Song W, Zhao L, Liu M, Yan J, Andersen MØ, et al. MicroRNA functionalized microporous titanium oxide surface by lyophilization with enhanced osteogenic activity. ACS Appl. Mater. Interf. 2013;5(7):2733-44.
352. Young S, Patel ZS, Kretlow JD, Murphy MB, Mountziaris PM, Baggett LS, et al. Dose effect of dual delivery of vascular endothelial growth factor and bone morphogenetic protein-2 on bone regeneration in a rat critical-size defect model. Tissue Engin., Part A. 2009;15(9):2347-62.
353. Kempen DH, Lu L, Heijink A, Hefferan TE, Creemers LB, Maran A, et al. Effect of local sequential VEGF and BMP-2 delivery on ectopic and orthotopic bone regeneration. Biomaterials. 2009;30(14):2816-25.
354. Patel ZS, Young S, Tabata Y, Jansen JA, Wong ME, Mikos AG. Dual delivery of an angiogenic and an osteogenic growth factor for bone regeneration in a critical size defect model. Bone. 2008;43(5):931-40.
355. Xiao C, Zhou H, Liu G, Zhang P, Fu Y, Gu P, et al. Bone marrow stromal cells with a combined expression of BMP-2 and VEGF-165 enhanced bone regeneration. Biomed Mater. 2011;6(1):015013.
356. Franceschi RT. Biological approaches to bone regeneration by gene therapy. J Dent Res. 2005;84(12):1093-103.
357. Lin CY, Chang YH, Lin KJ, Yen TC, Tai CL, Chen CY, et al. The healing of critical-sized femoral segmental bone defects in rabbits using baculovirus-engineered mesenchymal stem cells. Biomaterials. 2010 Apr;31(12):3222-30.
358. Luo T, Zhang W, Shi B, Cheng X, Zhang Y. Enhanced bone regeneration around dental implant with bone morphogenetic protein 2 gene and vascular endothelial growth factor protein delivery. Clin Oral Implants Res. 2012;23(4):467-73.
359. Fischer S, Wagnera A, Kosd A, Aschrafid A, Handricka R, Hannemanna J, et al. Breaking limitations of complex culture media: Functional non-viral

miRNA delivery into pharmaceutical production cell lines. J. Biotechnol. 2013;168(4):589-600.
360. Liu SQ. Bioregenerative Engineering:Principles and Applications [Book]. Hoboken, New Jersey: Wiley; 2007.
361. Pinto OA, Tabakovic A, Goff TM, Liu Y, Adair JH. Calcium Phosphate and Calcium Phosphosilicate Mediated Drug Delivery and Imaging. In: Prokop A, editor. Intracellular Delivery:Fundamentals and Applications [Book]. Dordrecht-Heidelberg-London-New York: Springer Science & Business Media; 2011. p. 713-44.
362. Mentink A, Hulsman M, Groen N, Licht R, Dechering KJ, van der Stok J, et al. Predicting the therapeutic efficacy of MSC in bone tissue engineering using the molecular marker CADM1. Biomaterials. 2013;34(19):4592-601.
363. Duffy GP, Ahsan T, O'Brien T, Barry F, Nerem RM. Bone marrow-derived mesenchymal stem cells promote angiogenic processes in a time- and dose-dependent manner in vitro. Tissue Eng., Part A. 2009;15(9):2459-70.
364. Murphy JM, Fink DJ, Hunziker EB, Barry FP. Stem cell therapy in a caprine model of osteoarthritis. Arthritis Rheum. 2003;48(12):3464-74.
365. Cimmino A, Calin GA, Fabbri M, Iorio MV, Ferracin M, Shimizu M, et al. miR-15 and miR-16 induce apoptosis by targeting BCL2. P N A S. 2005;102(39):13944-9.
366. Adair JH, Parette MP, Altinoglu EI, Kester M. Nanoparticulate alternatives for drug delivery. ACS Nano. 2010;4(9):4967-70.
367. Kapoor M, Burgess DJ. Efficient and safe delivery of siRNA using anionic lipids: Formulation optimization studies. Int. J. Pharm. 2012;432(1-2):80-90.
368. Huang J, Zhao L, Xing L, Chen D. MicroRNA-204 regulates Runx2 protein expression and mesenchymal progenitor cell differentiation. Stem Cells. 2010;28(2):357-64.
369. Eskildsen T, Taipaleenmaki H, Stenvang J, Abdallah BM, Ditzel N, Nossent AY, et al. MicroRNA-138 regulates osteogenic differentiation of human stromal (mesenchymal) stem cells in vivo. P N A S. 2011;108(15):6139-44.
370. Yang X, Walboomers XF, van den Dolder J, Yang F, Bian Z, Fan M, et al. Non-viral bone morphogenetic protein 2 transfection of rat dental pulp stem cells using calcium phosphate nanoparticles as carriers. Tissue Eng.,Part A. 2008;14(1):71-81.

371. Liu Y, Wang T, He F, Liu Q, Zhang D, Xiang S, et al. An efficient calcium phosphate nanoparticle-based nonviral vector for gene delivery. Int J Nanomed. 2011;6:721-7.
372. Suhorutsenko J, Oskolkov N, Arukuusk P, Kurrikoff K, Eriste E, Copolovici DM, et al. Cell-penetrating peptides, PepFects, show no evidence of toxicity and immunogenicity in vitro and in vivo. Bioconjug Chem. 2011 16;22(11):2255-62.
373. Li J, Yang Y, Huang L. Calcium phosphate nanoparticles with an asymmetric lipid bilayer coating for siRNA delivery to the tumor. J Control Release. 2012;158(1):108-14.
374. Zhang P, Wu H, Lu Z, Deng C, Hong Z, Jing X, et al. RGD-conjugated copolymer incorporated into composite of poly(lactide-co-glycotide) and poly(L-lactide)-grafted nanohydroxyapatite for bone tissue engineering. Biomacromolecules. 2011;12(7):2667-80.
375. Luzi E, Marini F, Sala SC, Tognarini I, Galli G, Brandi ML. Osteogenic differentiation of human adipose tissue-derived stem cells is modulated by the miR-26a targeting of the SMAD1 transcription factor. J Bone Mineral Res. 2008;23(2):287-95.
376. Mizuno Y, Yagi K, Tokuzawa Y, Kanesaki-Yatsuka Y, Suda T, Katagiri T, et al. miR-125b inhibits osteoblastic differentiation by down-regulation of cell proliferation. Biochemical and biophysical research communications. 2008;368(2):267-72.
377. Kapinas K, Kessler CB, Delany AM. miR-29 suppression of osteonectin in osteoblasts: regulation during differentiation and by canonical Wnt signaling. J Cell Biochem. 2009;108(1):216-24.
378. Clark EA, Kalomoiris S, Nolta JA, Fierro FA. Concise Review: MicroRNA Function in Multipotent Mesenchymal Stromal Cells. Stem Cells. 2014;32:1074–82.
379. Kim KM, Lim S-K. Role of miRNAs in bone and their potential as therapeutic targets. Current Opinion in Pharmacology. 2014;16:133–41.
380. Takeshita F, Patrawala L, Osaki M, Takahashi RU, Yamamoto Y, Kosaka N, et al. Systemic delivery of synthetic microRNA-16 inhibits the growth of metastatic prostate tumors via downregulation of multiple cell-cycle genes. Mol Ther. 2010;18(1):181-7.

381. Selbach M, Schwanhausser B, Thierfelder N, Fang Z, Khanin R, Rajewsky N. Widespread changes in protein synthesis induced by microRNAs. Nature. 2008;455(7209):58-63.
382. TargetScan Release 6.2. Cambridge, MA: © 2006-2012 Whitehead Institute for Biomedical Research; 2012 [cited 2014 February]; Available from: http://www.targetscan.org/.
383. Fasanaro P, D'Alessandra Y, Di Stefano V, Melchionna R, Romani S, Pompilio G, et al. MicroRNA-210 modulates endothelial cell response to hypoxia and inhibits the receptor tyrosine kinase ligand Ephrin-A3. The Journal of biological chemistry. 2008;283(23):15878-83.
384. cBio. MicroRNA.org. New York: Memorial Sloan-Kettering Cancer Center ™; 2010 [cited 2014 February]; Available from: http://www.microrna.org.
385. ISBLab. miRTarBase: the experimentally validated microRNA-target interactions database. Hsinchu, Taiwan © ISBLab; 2013 [cited 2014 February]; Available from: http://mirtarbase.mbc.nctu.edu.tw/.
386. Hassan MQ, Maeda Y, Taipaleenmaki H, Zhang W, Jafferji M, Gordon JA, et al. miR-218 Directs a Wnt Signaling Circuit to Promote Differentiation of Osteoblasts and Osteomimicry of Metastatic Cancer Cells. J Biol. Chem. 2012;287(50):42084-92.
387. Liao XB, Zhang ZY, Yuan K, Liu Y, Feng X, Cui RR, et al. MiR-133a Modulates Osteogenic Differentiation of Vascular Smooth Muscle Cells. Endocrinology. 2013;154(9):3344-52.
388. Thomson DW, Bracken CP, Szubert JM, Goodall GJ. On Measuring miRNAs after Transient Transfection of Mimics or Antisense Inhibitors. PloS one. 2013;8(1):e55214.
389. Guo H, Ingolia NT, Weissman JS, Bartel DP. Mammalian microRNAs predominantly act to decrease target mRNA levels. Nature. 2010;466(7308):835-40.
390. Lim LP, Lau NC, Garrett-Engele P, Grimson A, Schelter JM, Castle J, et al. Microarray analysis shows that some microRNAs downregulate large numbers of target mRNAs. Nature. 2005;433(7027):769-73.
391. Flynt AS, Lai EC. Biological principles of microRNA-mediated regulation: shared themes amid diversity. Nat. Rev. Genet. 2008;9(11):831-42.

392. BLAST: Basic Local alignment Search Tool [database on the Internet] [cited 12/05/2015]. Available from: http://blast.ncbi.nlm.nih.gov/Blast.cgi.
393. Wu K, Song W, Zhao L, Liu M, Yan J, Andersen MO, et al. MicroRNA functionalized microporous titanium oxide surface by lyophilization with enhanced osteogenic activity. ACS Appl Mater Interf. 2013;5(7):2733-44.
394. Tierney EG, Duffy GP, Hibbitts AJ, Cryan SA, O'Brien FJ. The development of non-viral gene-activated matrices for bone regeneration using polyethyleneimine (PEI) and collagen-based scaffolds. J Control Release. 2011;158(2):304-11.
395. Deng Y, Zhou H, Zou D, Xie Q, Bi X, Gu P, et al. The role of miR-31-modified adipose tissue-derived stem cells in repairing rat critical-sized calvarial defects. Biomaterials. 2013;34(28):6717-28.
396. Sorrell JM, Baber MA, Caplan AI. Influence of adult mesenchymal stem cells on in vitro vascular formation. Tissue Eng., Part A. 2009;15(7):1751-61.
397. Hung SC, Pochampally RR, Chen SC, Hsu SC, Prockop DJ. Angiogenic effects of human multipotent stromal cell conditioned medium activate the PI3K-Akt pathway in hypoxic endothelial cells to inhibit apoptosis, increase survival, and stimulate angiogenesis. Stem Cells. 2007;25(9):2363-70.
398. Clarkin CE, Gerstenfeld LC. VEGF and bone cell signalling: an essential vessel for communication? Cell Biochem Funct. 2013;31(1):1-11.
399. Caplan AI. All MSCs are pericytes? Cell Stem Cell. 2008;3(3):229-30.
400. Carmeliet P, Ferreira V, Breier G, Pollefeyt S, Kieckens L, Gertsenstein M, et al. Abnormal blood vessel development and lethality in embryos lacking a single VEGF allele. Nature. 1996;380(6573):435-9.
401. Ferrara N, Carver-Moore K, Chen H, Dowd M, Lu L, O'Shea KS, et al. Heterozygous embryonic lethality induced by targeted inactivation of the VEGF gene. Nature. 1996;380(6573):439-42.
402. Mayr-Wohlfart U, Waltenberger J, Hausser H, Kessler S, Gunther KP, Dehio C, et al. Vascular endothelial growth factor stimulates chemotactic migration of primary human osteoblasts. Bone. 2002;30(3):472-7.
403. Orlandini M, Spreafico A, Bardelli M, Rocchigiani M, Salameh A, Nucciotti S, et al. Vascular endothelial growth factor-D activates VEGFR-3 expressed in osteoblasts inducing their differentiation. The Journal of biological chemistry. 2006;281(26):17961-7.

404. Gerber HP, Vu TH, Ryan AM, Kowalski J, Werb Z, Ferrara N. VEGF couples hypertrophic cartilage remodeling, ossification and angiogenesis during endochondral bone formation. Nat Med. 1999;5(6):623-8.
405. Gerber HP, Ferrara N. Angiogenesis and bone growth. Trends Cardiovasc Med. 2000;10(5):223-8.
406. Hsiong SX, Mooney DJ. Regeneration of vascularized bone. Periodontol 2000. 2006;41:109-22.
407. Suarez Y, Sessa WC. MicroRNAs as novel regulators of angiogenesis. Circulation research. 2009;104(4):442-54.
408. Poliseno L, Tuccoli A, Mariani L, Evangelista M, Citti L, Woods K, et al. MicroRNAs modulate the angiogenic properties of HUVECs. Blood. 2006;108(9):3068-71.
409. Suarez Y, Fernandez-Hernando C, Pober JS, Sessa WC. Dicer dependent microRNAs regulate gene expression and functions in human endothelial cells. Circulation research. 2007;100(8):1164-73.
410. Fish JE, Santoro MM, Morton SU, Yu S, Yeh RF, Wythe JD, et al. miR-126 regulates angiogenic signaling and vascular integrity. Developmental cell. [Research Support, N.I.H., Extramural
Research Support, Non-U.S. Gov't]. 2008 Aug;15(2):272-84.
411. Wang S, Aurora AB, Johnson BA, Qi X, McAnally J, Hill JA, et al. The endothelial-specific microRNA miR-126 governs vascular integrity and angiogenesis. Developmental cell. 2008;15(2):261-71.
412. Harris TA, Yamakuchi M, Ferlito M, Mendell JT, Lowenstein CJ. MicroRNA-126 regulates endothelial expression of vascular cell adhesion molecule 1. Proceedings of the National Academy of Sciences of the United States of America. 2008;105(5):1516-21.
413. van Rooij E. Introduction to the series on microRNAs in the cardiovascular system. Circulation research. 2012;110(3):481-2.
414. McArthur K, Feng B, Wu Y, Chen S, Chakrabarti S. MicroRNA-200b regulates vascular endothelial growth factor-mediated alterations in diabetic retinopathy. Diabetes. 2011;60(4):1314-23.
415. Feng B, Chen S, McArthur K, Wu Y, Sen S, Ding Q, et al. miR-146a-Mediated extracellular matrix protein production in chronic diabetes complications. Diabetes. 2011;60(11):2975-84.

416. Nunes DN, Dias-Neto E, Cardo-Vila M, Edwards JK, Dobroff AS, Giordano RJ, et al. Synchronous down-modulation of miR-17 family members is an early causative event in the retinal angiogenic switch. P N A S. 2015;112(12):3770-5.
417. Ma L, Young J, Prabhala H, Pan E, Mestdagh P, Muth D, et al. miR-9, a MYC/MYCN-activated microRNA, regulates E-cadherin and cancer metastasis. Nature cell biology. 2010;12(3):247-56.
418. Alaiti MA, Ishikawa M, Masuda H, Simon DI, Jain MK, Asahara T, et al. Up-regulation of miR-210 by vascular endothelial growth factor in ex vivo expanded CD34+ cells enhances cell-mediated angiogenesis. J Cell Mol Med. 2012;16(10):2413-21.
419. Kuijper S, Turner CJ, Adams RH. Regulation of Angiogenesis by Eph–Ephrin Interactions. Trends in Cardiovascular Medicine. 2007;17(5):145-51.
420. Shoji T, Nakasa T, Yamasaki K, Kodama A, Miyaki S, Niimoto T, et al. The Effect of Intra-articular Injection of MicroRNA-210 on Ligament Healing in a Rat Model. American J Sports Med. 2012;40(11):2470-8.
421. Samee M, Kasugai S, Kondo H, Ohya K, Shimokawa H, Kuroda S. Bone morphogenetic protein-2 (BMP-2) and vascular endothelial growth factor (VEGF) transfection to human periosteal cells enhances osteoblast differentiation and bone formation. J Pharmacol Sci. 2008;108(1):18-31.
422. Peng H, Wright V, Usas A, Gearhart B, Shen HC, Cummins J, et al. Synergistic enhancement of bone formation and healing by stem cell-expressed VEGF and bone morphogenetic protein-4. J Clin. Invest. 2002;110(6):751-9.
423. Shi S, Han L, Deng L, Zhang Y, Shen H, Gong T, et al. Dual drugs (microRNA-34a and paclitaxel)-loaded functional solid lipid nanoparticles for synergistic cancer cell suppression. J Control Release. 2014;194:228-37.
424. Schindelin J, Arganda-Carreras I, Frise E, Kaynig V, Longair M, Pietzsch T, et al. Fiji: an open-source platform for biological-image analysis. Nat. Methods. 2012;9(7):676-82.
425. Jazayeri M, Allameh A, Soleimani M, Jazayeri SH, Piryaei A, Kazemnejad S. Molecular and ultrastructural characterization of endothelial cells differentiated from human bone marrow mesenchymal stem cells. Cell Biol Int. 2008;32(10):1183-92.

426. Oswald J, Boxberger S, Jorgensen B, Feldmann S, Ehninger G, Bornhauser M, et al. Mesenchymal stem cells can be differentiated into endothelial cells in vitro. Stem Cells. 2004;22(3):377-84.
427. Rousseau S, Houle F, Huot J. Integrating the VEGF Signals Leading to Actin-Based Motility in Vascular Endothelial Cells. Trends Cardiovasc. Med. 2000;10(8):321-7.
428. Kim HW, Haider HK, Jiang S, Ashraf M. Ischemic preconditioning augments survival of stem cells via miR-210 expression by targeting caspase-8-associated protein 2. J Biol Chem. 2009;284(48):33161-8.
429. Chio CC, Lin JW, Cheng HA, Chiu WT, Wang YH, Wang JJ, et al. MicroRNA-210 targets antiapoptotic Bcl-2 expression and mediates hypoxia-induced apoptosis of neuroblastoma cells. Arch. Toxicol. 2013;87(3):459-68.
430. Yamasaki K, Nakasa T, Miyaki S, Yamasaki T, Yasunaga Y, Ochi M. Angiogenic microRNA-210 is present in cells surrounding osteonecrosis. J Orthop Res. 2012;30(8):1263-70.
431. Springer IN, Niehoff P, Acil Y, Marget M, Lange A, Warnke PH, et al. BMP-2 and bFGF in an irradiated bone model. J Craniomaxillofac Surg. 2008;36(4):210-7.
432. O'Donnell KA, Wentzel EA, Zeller KI, Dang CV, Mendell JT. c-Myc-regulated microRNAs modulate E2F1 expression. Nature. 2005;435(7043):839-43.
433. Zhang R, Ma J, Yao J. Molecular mechanisms of the cartilage-specific microRNA-140 in osteoarthritis. Inflamm Res. 2013;62(10):871-7.
434. Stappert L, Borghese L, Roese-Koerner B, Weinhold S, Koch P, Terstegge S, et al. MicroRNA-based promotion of human neuronal differentiation and subtype specification. PloS one. 2013;8(3):e59011.
435. Wang Y, Huang C, Reddy Chintagari N, Bhaskaran M, Weng T, Guo Y, et al. miR-375 regulates rat alveolar epithelial cell trans-differentiation by inhibiting Wnt/beta-catenin pathway. Nucl. Acids Res. 201;41(6):3833-44.
436. Fitzgerald KA, Malhotra M, Curtin CM, O'Brien FJ, O'Driscoll CM. Life in 3D is Never Flat: 3D Models to Optimise Drug Delivery. J Control Release. 2015; 215:39-54.